Laboratory Medicine

March 2022 Vol 53 No 2 Pgs 107–221

labmedicine.com

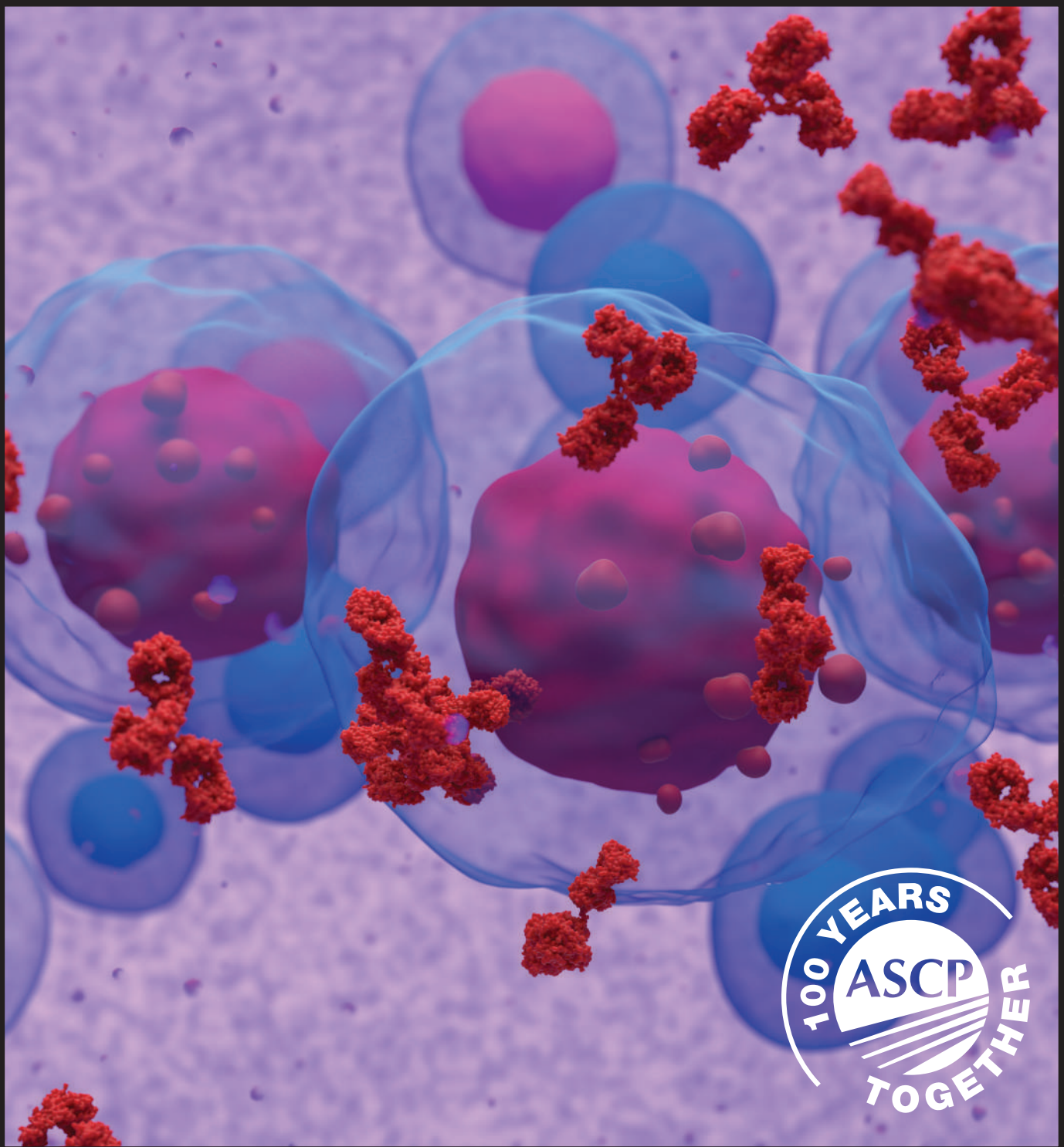

Laboratory Medicine

March 2022
Vol 53, No 2
p 107-221

SCIENCE

CASE STUDY

IN MEMORIAM

REVIEWERS LIST

The following are online-only papers that are available as part of Issue 53(2) online.

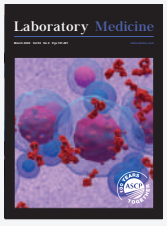

ON THE COVER: Multiple myeloma (MM) is a plasma cell dyscrasia characterized by proliferation of a monoclonal B cell population and consequent overproduction of a monoclonal antibody (M-protein) that can be detected and identified by serum protein electrophoresis (SPE) and immunoelectrophoresis, respectively. MM accounts for 10% of hematological malignancies, with approximately 160,000 cases worldwide. The 5-year survival rate for MM is a mere 54%. MM may be preceded by a slowly progressing monoclonal gammopathy, so laboratory monitoring of the disease is essential for clinical management. In this issue of *Laboratory Medicine*, two papers by Professor Gurmkh Singh and colleagues at Medical College of Georgia examine aspects of laboratory monitoring of MM. In one paper [insert page #], he proposes a method for quantitating M-spikes that comigrate with beta globulins on SPE. In his other paper [insert page #], Professor Singh correlates impaired renal function and decreased survival in patients with light chain-predominant MM.

Laboratory Medicine (ISSN 0007-5027), is published 6 times per year (bimonthly). Periodicals Postage paid at Chicago, IL and additional mailing offices. POSTMASTER: Send address changes to *Laboratory Medicine*, Journals Customer Service Department, Oxford University Press, 2001 Evans Road, Cary, NC 27513-2009.

SUBSCRIPTION INFORMATION: Annually for North America, $173 (electronic) or $225 (electronic and print); single issues for individuals are $29 and for institutions $64. Annually for Rest of World, £112/€159 (electronic) or £144/€206 (electronic and print); single issues for individuals are £19/€27 and for institutions £40/€57. All inquiries about subscriptions should be sent to Journals Customer Service Department, Oxford Journals, Great Clarendon Street, Oxford OX2 6DP, UK, Tel: +44 (0) 1865-35-3907, e-mail: jnls.cust.serv@oup.com. In the Americas, please contact Journals Customer Service Department, Oxford Journals, 2001 Evans Road, Cary, NC 27513. Tel: 800-852-7323 (toll-free in USA/Canada) or 919-677-0977, e-mail: jnlorders@oup.com.

MEMBERSHIP INFORMATION: The ASCP membership fees for pathologists are as follows: fellow membership is $349; fellow membership plus 1-year unlimited online CE is $519; 2-year fellow membership is $675; and 2-year fellow membership plus 2-year unlimited online CE is $1,015. The ASCP membership fees for laboratory professionals are as follows: newly certified membership is $49; annual membership is $99; annual membership plus 1-year unlimited online CE is $129; 3-year membership is $349. All inquiries about membership should be sent to American Society for Clinical Pathology, 33 West Monroe Street, Suite 1600, Chicago, IL 60603, Tel: 312-541-4999, e-mail: ascp@ascp.org.

CLAIMS: Publisher must be notified of claims within four months of dispatch/ order date (whichever is later). Subscriptions in the EEC may be subject to European VAT. Claims should be made to Laboratory Medicine, Journals Customer Service Department, Oxford University Press, 2001 Evans Road, Cary, NC 27513, Tel: 800-852-7323 (toll-free in USA/Canada) or 919-677-0977, e-mail: jnlorders@oup.com.

Laboratory Medicine is published bimonthly by Oxford University Press (OUP), on behalf of the ASCP, a not-for-profit corporation organized exclusively for educational, scientific, and charitable purposes. Devoted to the continuing education of laboratory professionals, *Laboratory Medicine* features articles on the scientific, technical, managerial, and educational aspects ofthe clinical laboratory. Publication of an article, column, or other item does not constitute an endorsement by the ASCP of the thoughts expressed or the techniques, organizations, or products described therein. *Laboratory Medicine* is indexed in the following: MEDLINE/PubMed, Science Citation Index, Current Contents—Clinical Medicine, and the Cumulative Index to Nursing and Allied Health Literature.

Printed in the USA

ASCP
Laboratory Medicine
33 West Monroe Street, Suite 1600
Chicago, IL 60603

T: 312-541-4999
F: 312-541-4750

Laboratory Medicine

March 2022
Vol 53, No 2
p 107-221

SCIENCE

CASE STUDY

IN MEMORIAM

REVIEWERS LIST

The following are online-only papers that are available as part of Issue 53(2) online.

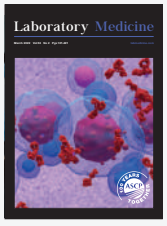

ON THE COVER: Multiple myeloma (MM) is a plasma cell dyscrasia characterized by proliferation of a monoclonal B cell population and consequent overproduction of a monoclonal antibody (M-protein) that can be detected and identified by serum protein electrophoresis (SPE) and immunoelectrophoresis, respectively. MM accounts for 10% of hematological malignancies, with approximately 160,000 cases worldwide. The 5-year survival rate for MM is a mere 54%. MM may be preceded by a slowly progressing monoclonal gammopathy, so laboratory monitoring of the disease is essential for clinical management. In this issue of *Laboratory Medicine*, two papers by Professor Gurmkh Singh and colleagues at Medical College of Georgia examine aspects of laboratory monitoring of MM. In one paper [insert page #], he proposes a method for quantitating M-spikes that comigrate with beta globulins on SPE. In his other paper [insert page #], Professor Singh correlates impaired renal function and decreased survival in patients with light chain-predominant MM.

SCIENCE

Whole-Exome Sequencing Identifies a Recurrent Small In-Frame Deletion in *MYO15A* Causing Autosomal Recessive Nonsyndromic Hearing Loss in 3 Iranian Pedigrees

Samane Nasrniya, PhD,[1] Paniz Miar, MSc,[1] Sina Narrei, MSc,[2] Mahsa Sepehrnejad, MSc,[6] Mohammad Hussein Nilforoush, MSc,[6] Hamidreza Abtahi, MD,[3,5] Mohammad Amin Tabatabaiefar, PhD[1,2,4,]*

[1]Department of Genetics and Molecular Biology, School of Medicine, Isfahan University of Medical Sciences, Isfahan, Iran; [2]Erythron Pathobiology and Genetics lab, Isfahan, Iran; [3]Department of Otolaryngology, Al-Zahra Hospital, Isfahan University of Medical Sciences, Isfahan, Iran; [4]Pediatric Inherited Diseases Research Center, Research Institute for Primordial Prevention of Noncommunicable Disease, Isfahan University of Medical Sciences, Isfahan, Iran; [5]Department of Ear, Nose & Throat, and Head & Neck Surgery, School of Medicine, Isfahan University of Medical Sciences, Isfahan, Iran; [6]Department of Audiology, School of Rehabilitation Sciences, Isfahan University of Medical Sciences University of Medical Sciences, Isfahan, Iran; *To whom correspondence should be addressed. Tabatabaiefar@med.mui.ac.ir

Keywords: hearing loss, *MYO15A*, whole-exome sequencing, small in-frame deletion, cochlear implantation, Iranian population

Abbreviations: HL, hearing loss; ARNSHL, autosomal recessive nonsyndromic hearing loss; NGS, next-generation sequencing; CIs, cochlear implants; WES, whole-exome sequencing; TEs/DPOAEs, transient emissions/distortion-product optoacoustics; ABR, auditory brainstem response; ASSR, auditory steady-state response; CAP, Categories of Auditory Performance; SIR, Speech Intelligibility Rating; Hg19, Human Genome Build 19; gnomAD, Genome Aggregation Database; dbSNP, Single Nucleotide Polymorphism Database; I-TASSER, Iterative Threading ASSEmbly Refinement; ACMG, American College of Medical Genetics and Genomics; ESP, Exome Sequencing Project; TGP, 1000 Genomes project; ExAC, Exome Aggregation Consortium; PND, prenatal diagnostic test; PGD, preimplantation genetic diagnosis; IGV, Integrative Genomics Viewer; NA, information not available; … , nonapplicable

Laboratory Medicine 2022;53:111–122; https://doi.org/10.1093/labmed/lmab047

ABSTRACT

Background: Hearing loss (HL) is the most prevalent and genetically heterogeneous sensory disabilities in humans throughout the world.

Methods: In this study, we used whole-exome sequencing (WES) to determine the variant causing autosomal recessive nonsyndromic hearing loss (ARNSHL) segregating in 3 separate Iranian consanguineous families (with 3 different ethnicities: Azeri, Persian, and Lur), followed by cosegregation analysis, computational analysis, and structural modeling using the I-TASSER (Iterative Threading ASSEmbly Refinement) server. Also, we used speech-perception tests to measure cochlear implant (CI) performance in patients.

Results: One small in-frame deletion variant (*MYO15A* c.8309_8311del (p.Glu2770del)), resulting in deletion of a single amino-acid residue was identified. We found it to be cosegregating with the disease in the studied families. We provide some evidence suggesting the pathogenesis of this variant in HL based on the American College of Medical Genetics (ACMG) and Genomics guidelines. Evaluation of auditory and speech performance indicated favorable outcome after cochlear implantation in our patients.

Conclusions: The findings of this study demonstrate the utility of WES in genetic diagnostics of HL.

Hereditary hearing loss (HL), as the most frequent neurosensory disorder, affects millions of people worldwide. The prevalence of HL in Iran is 2 to 3 times higher than in most other parts of the world due to consanguineous marriage.[1] Genetic factors are the main reason for HL, with more than 50% of cases having a genetic etiology.[2] Monogenic inheritance accounts for 70% of all congenital HL with all Mendelian inheritance patterns. However, autosomal recessive nonsyndromic HL (ARNSHL) is the most frequent hereditary pattern, for which more than 74 genes have been identified (The Hereditary Hearing Loss Homepage: http://hereditaryhearingloss.org/).

The *MYO15A* gene (OMIM no. 602666) with 71-kb length and 66 exons on chromosome 17p11.2 (chr17:18,012,020-18,083,116; hg19 assembly), also known as DFNB3, was described in 1995 in the literature for the first time.[3] Since then, hundreds of variants have been identified in this gene that cause ARNSHL. Pathogenic/likely pathogenic variants of *MYO15A* in Iran, as in other ethnic groups, are considered the third-most-common cause of ARNSHL.[4]

Myosin XVA, or unconventional myosin XV, is a protein with 3530 residues in its longest form (MYO15_HUMAN, Q9UKN7, and NP_057323.3). There are 2 alternatively spliced transcripts according to

the presence or lack of exon 2, isoform classes 1 and 2, respectively.[5] The long isoform of the human myosin XVA consists of an N-terminal domain (aa 1–1223), an ATPase motor-head domain (aa 1224–1899); the neck region contains 2 light chain–binding motifs (IQ; aa 1909–1942), the tail region contains 2 MyTH4 (myosin tail homology 4) domains (aa 2066–2174 and 3051–3161), 2 FERM (band 4.1, ezrin, radixin, and moesin) domains (aa 2687–2867 and 3217–3497), a SH3 (src homology 3) domain (aa 2865–2959), and a C-terminal class I PDZ-binding motif.[6,7]

Myosin XVA is essential for elongation and maintenance of stereocilia, the mechanosensory sound-transducing organelles in the inner-ear hair cells.[8–11] Pathogenic variants of the MyTH4-FERM domain of the myosin XVA are frequently reported to be associated with HL. Thus, it is among the most prevalent genetic causes of ARNSHL.[4]

To date, more than 900 variants have been reported in *MYO15A* worldwide, which encompass a wide range of missense/nonsense, splicing, deletion, insertions, and complex mutations (https://www.ncbi.nlm.nih.gov/clinvar). So far, only 41 pathogenic or likely pathogenic variants have been reported in this gene from the Iranian population.

Genetic diagnosis of HL, as one of the most genetically heterogeneous disorders, based on Sanger sequencing, is cumbersome. Except for *GJB2,* as the most common cause of ARNSHL with 1 coding exon, direct sequencing of other common deafness genes is not cost-effective due to the large size/number of exons. This idea has also been emphasized by the ACMG guideline for hearing loss,[12] in which it has been recommended for ARNSHL to jump to next-generation sequencing (NGS) after only excluding *GJB2/GJB6* pathogenic variants. We note that *GJB6* pathogenic variants have near-0 frequencies in Iran, based on the findings of many investigations. The advent of NGS facilitates genetic diagnosis by sequencing massive amounts of DNA simultaneously, and reduces time and cost of sequencing by several orders of magnitude.

Cochlear implants (CIs) bypass cochlear hair cells and directly stimulate the hearing nerves. Also, pathogenic variants in different deafness genes have different pathological effects. As a result, the findings of recent physiological studies, such as Eppsteinter et al,[13] suggest that the site of the genetic defect might impact outcomes of cochlear implantation.

In this study, as a part of a larger study, we report on 3 consanguineous Iranian families with a history of profound sensorineural HL compatible with ARNSHL. We applied whole-exome sequencing (WES) to clarify the etiology of HL in the studied families and identified 1 pathogenic homozygous small nonframeshifting deletion in *MYO15A* (c.8309_8311del [p.Glu2770del]), resulting in the deletion of a single amino-acid residue.

Material and Methods

Study Participants and Clinical Evaluations

This study is a part of a larger study on genetics of HL in several provinces of Iran. The study families involved 3 consanguineous Iranian families with 3 different ethnicities, namely, Azeri, Persian, and Lur. Written informed consent was obtained from all of the participants in the study, and written consent to participate was obtained from the parents of patients younger than age 16 years. Written informed consent for publication of clinical details and clinical images was obtained from all of the participants and from the parents of the patients younger than 18 years.

Comprehensive family history, physical examination, and audiological testing consisting of play audiometry, tympanometry, acoustic stapedial reflex, transient emissions/distortion-product otoacoustic emissions (TEs/DPOAEs), auditory brainstem response (ABR), and auditory steady-state response (ASSR) was performed. The case individuals had received a CI 3 years ago (the first individual at the age of 1 year and 10 months, the second at 2 years and 5 months, and the third one at 3 years and 6 months).

Auditory and speech performance were evaluated using the Categories of Auditory Performance (CAP)[14] and Speech Intelligibility Rating (SIR)[15] after cochlear implantation. CAP consists of 8 categories, ranging from complete deafness: "no awareness of environment" (CAP score 0) to good verbal communication: "use of telephone with known users" (CAP score 7). SIR consists of 5 categories that range from "unintelligible speech" (SIR score 1) to "speech intelligible to all listeners" (SIR score 5). All 3 families signed written informed-consent forms.

DNA Extraction and Mutation Screening via NGS

Genomic DNA was extracted from peripheral blood of the patients and their family members using QIAamp DNA Blood Mini kit (QIAGEN), according to the manufacturer-provided instructions. We assessed quality and quantity of DNA using agarose gel and the Nanodrop 2000 instrument (Thermo Fisher Scientific Inc.), respectively. Sanger sequencing was performed, to exclude pathogenic/likely pathogenic variants in exon 2 of the *GJB2* as the most common deafness gene. For this purpose, the forward and reverse primers were used, as described previously.[16] After making sure there was no pathogenic/likely pathogenic variant in the *GJB2*, patient specimens were subjected to WES.

DNA libraries were generated from fragmented genomic DNA and subjected to the enrichment of coding exons and flanking intronic sequences using the SureSelect Human All Exon 50 Mb kit (Agilent Technologies, Inc.). The enriched DNA was sequenced using NextSeq 500 with the 90bp pair-end reads. The sequencing yielded an average sequencing depth of 100× per specimen, with at least 90% of the targeted region covered at 10×. Sequence alignment was performed by Burrows Wheeler Alignment software using Human Genome Build 19 (Hg19) as the reference, and variant filtering steps were performed using GATK software,[17] by excluding noncoding regions variants, exonic synonymous variants, and variants with an MAF greater than 0.01. We based these values on the contents of public databases, including the 1000 Genomes Project (http://www.1000genomes.org),the Genome Aggregation Database (gnomAD) (gnomad.broadinstitute.org/), the Single Nucleotide Polymorphism Database (dbSNP), the Iranome database (www.iranome.com, which is an online variant frequency database consisting of genome data of 800 healthy Iranians from 8 ethnic groups in Iran), and the GTaC database (our own locally developed database consisting of 1500 exomes, followed by annotation for conservation [phyloP, phastCons] and pathogenicity [MutationTaster,[18] PROVEAN,[19] SIFT indel,[20] and DDIG-in [21]).

The 3-D Structure of the MYO15A Protein

We used the I-TASSER (Iterative Threading ASSEmbly Refinement)[22] server to construct the 3D structure of the wild-type and mutant forms of the MYO15A tail. The PDB file of the generated protein model was used as the input for visualized by PyMOL software.

Cosegregation Study and Pathogenicity Examination

We performed Sanger sequencing to confirm the variant reported via NGS, to examine cosegregation of the genotype and HL phe-

notype among family members. A set of primers were designed via Primer 3 software (F: 5′ -AGGGAGACTGAGGCTGACAA-3′ and R: 5′-CACAGCTAGGAGCTGCACAC-3′) to amplify the region of the small deletion in exon 46 of all family members. Then, the amplicon was used for bidirectional Sanger sequencing using an ABI 3130 automated sequencer (Thermo Fisher Scientific Inc.). The sequences were compared with the *MYO15A* gene reference sequence. Based on the criteria introduced by the American College of Medical Genetics and Genomics (ACMG) and HL-specific ACMG/AMP guidelines,[12,23] the pathogenicity of the variant in *MYO15A* was examined.

FIGURE 1. The electropherogram analysis shows wild-type (D), homozygote (E), and heterozygote (F) variants (*MYO15A* c.8309_8311del (p.Glu2770del)) in 3 pedigrees. The lower panel indicate the integrative genomics viewer (IGV) illustration of the identified variant. A, Family HL-CI 10. B, Family HL-CI 3. C, Family HL-CI 19.

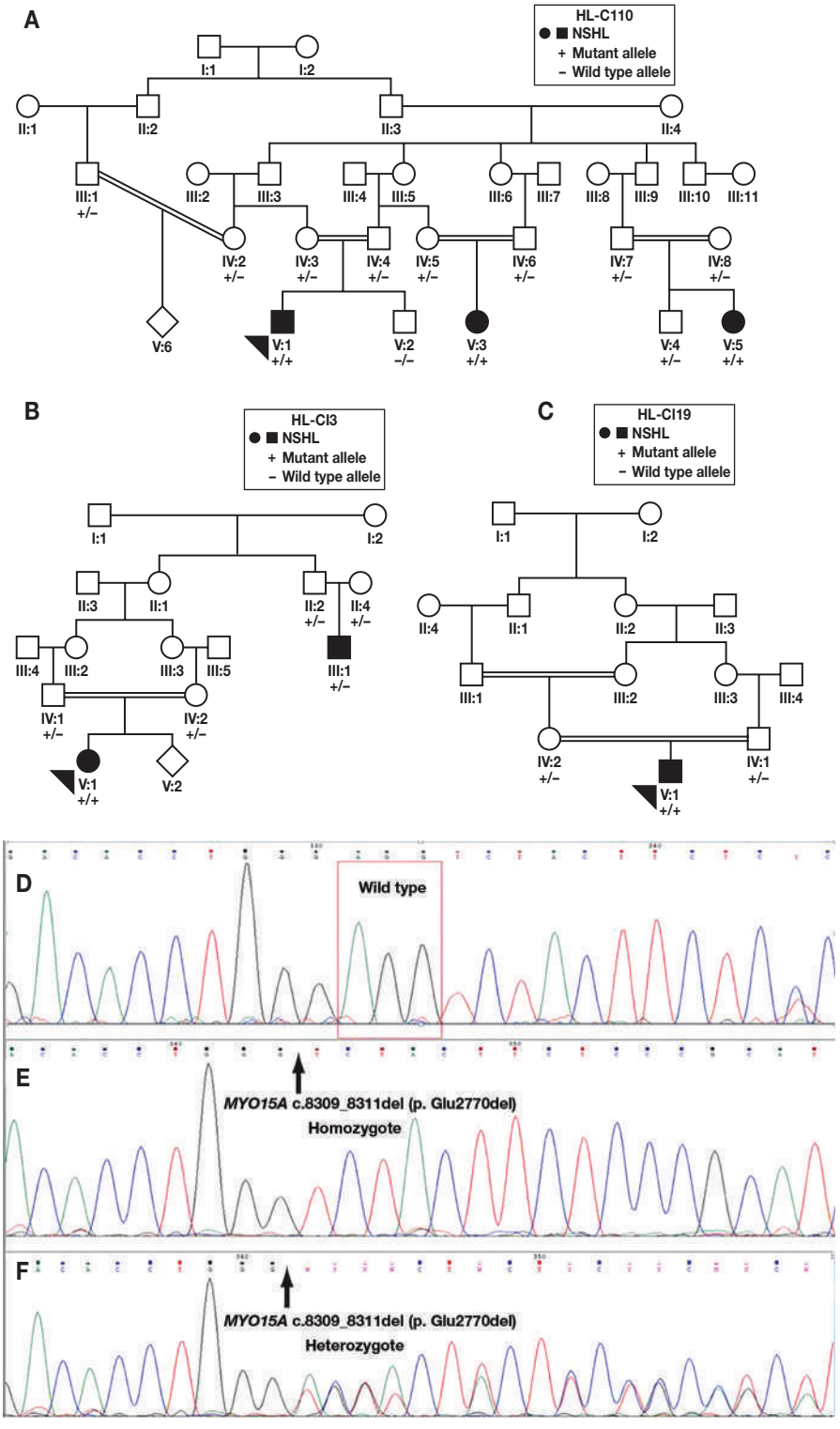

FIGURE 1. Continued

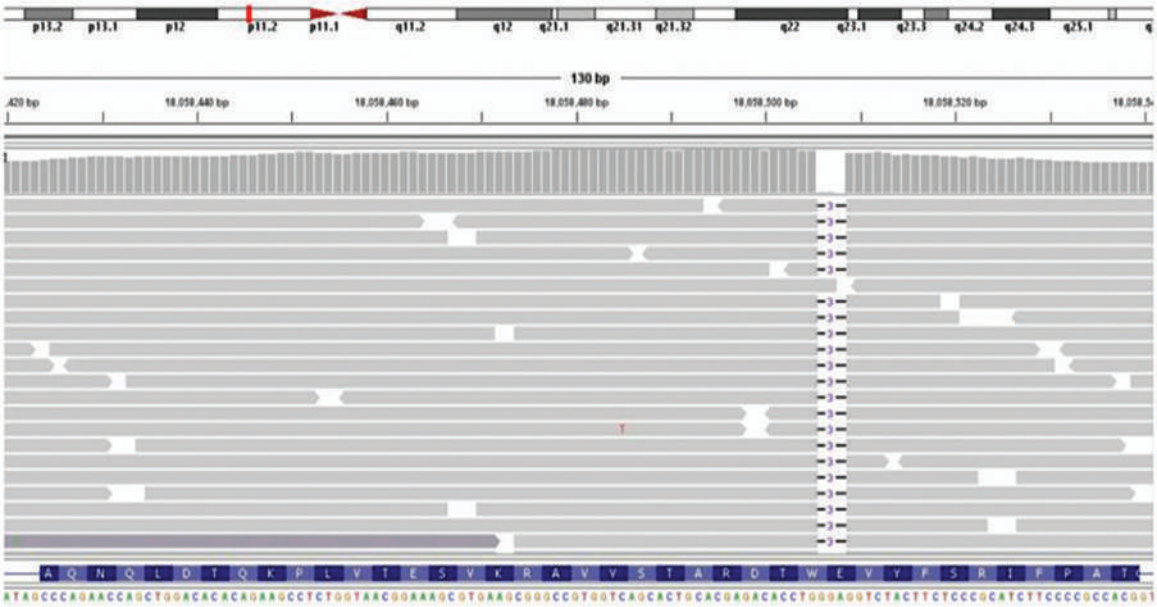

Results

In the first family (HL-CI 10) (**FIGURE 1A**), a 35 year old pregnant woman (IV2) was referred to our genetics laboratory with a positive family history for ARNSHL. The couples were consanguineous. After taking history and drawing the pedigree, the nephew of that woman (V1: a 5 year old boy) underwent WES after Sanger sequencing of *GJB2*.

The second family (HL-CI 3) (**FIGURE 1B**) referred to our genetics laboratory had a girl child (V1), aged 5 years, with congenital HL. Clinical evaluation suggested it to be a result of ARNSHL. The parents were first cousins and had a family history of HL; the mother was pregnant and was worried about whether her embryo would be affected. Her affected daughter, underwent genetic testing.

The third family (HL-CI 19) (**FIGURE 1C**) referred to our laboratory had a 6 year old boy with HL that had been diagnosed at age 1 year. He was the only deaf person in the family. His parents were first cousins and were worried about the possibility of HL in their next pregnancy. After ensuring there was no pathogenic/likely pathogenic variant in the *GJB2* gene, WES was performed for probands of HL-CI 10, HL-CI 3, and HL-CI 19 families.

Several filtering steps were used to analyze patient variants. The total number of variants in patients (HL-CI 10-V1, HL-CI3-IV1, and HL-CI 19-IV1) after alignment and SNV calling were 82096, 67072, and 46690, respectively. By applying several exclusion processes, such as function (ie, exonic/intronic variants), frequency in dbSNP, 1000 Genomes Project, ESP, and gnomAD databases (among others) and quality filtering, the number of variants in patients was reduced to 1023, 1302, and 923, respectively.

The variants were prioritized based on the comparisons with known deafness genes; eventually, regarding the inheritance pattern in pedigrees, only 1 relevant variant was identified. No significant pathogenic incidental findings were observed in any probands. As the result, a homozygous nonframeshift deletion variant was detected in *MYO15A* (*MYO15A*:NM_016239: exon 46: c.8309_8311del (p.Glu2770del) in the all 3 families. Based on the data provided in the NCBI Clinvar database, this homozygous deletion variant had been categorized as likely pathogenic without providing any evidence (Variation ID: 493209). Therefore, in these study findings, the pathogenicity status of the variant is established.

FIGURE 2. The typical downsloping audiogram at the time of diagnosis, which was similar in the patients.

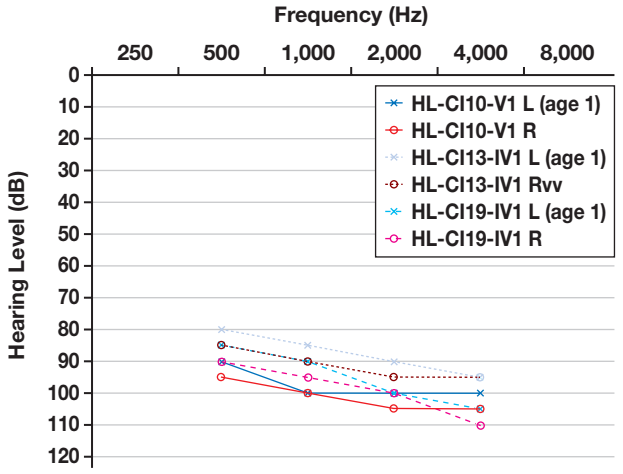

Based on audiological reports and clinical manifestations, all 3 cases showed bilateral profound nonsyndromic sensorineural HL (**FIGURE 2**). CAP and SIR scaling were used to assess auditory and speech performance after cochlear implantation. These scales, as a reliable instrument for measuring the outcome of cochlear implantation, are approved.[24,25]

Results of auditory and speech performance indicated favorable outcome of cochlear implantation in all cases after 3 years (the first patient had a CAP score of 5 (understanding of common phrases without lip reading) and a SIR score of 5 (speech is intelligible to all listeners). The second patient had a CAP score of 6 (understanding conversation without lip reading) and a SIR score of 5 (speech is intelligible to all listeners). The third patient had a CAP score of 6 and a SIR score of 4 (speech is in-

FIGURE 3. Schematic structure of Myosin XVa and conservation analysis. Human *MYO15A* domains consist of N-terminal domain (aa 1–1223), an ATPase motor head domain (aa 1224–1899). The neck region contains 2 light chain–binding motifs (IQ; aa 1909–1942), and the tail region contains 2 MyTH4 domains (aa 2066–2174 and 3051–3161), 2 FERM domains (aa 2687–2867 and 3217–3497), 1 SH3 domain (aa 2865–2959), and a C-terminal class I PDZ-binding motif. Protein alignment by Clustal Omega showed evolutionary conservation of residue E2770 in *MYO15A*.

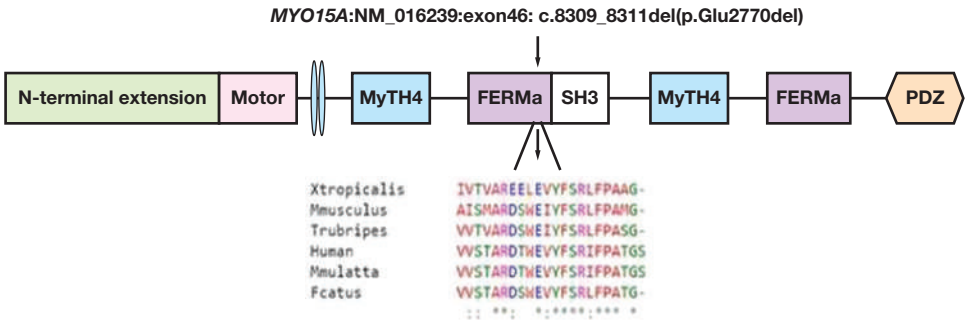

TABLE 1. In Silico Analysis of the Identified Variant in *MYO15A*

Transcript	ENST00000647165.2 NM_016239.4
Variant	c.8309_8311del p.Glu2770del
Alteration (physical location)	chr17:18058506_18058508delGGA
dbSNP rsID	rs1555546699
Associated disease	Deafness, autosomal recessive
OMIM ID	#602666
1000 Genomes MAF	…
PhastCons score	1
PhyloP	5.89
Zygosity	Homo
DDIG-in	Disease
SIFT indel	Damaging
MutationTaster	Disease-causing
PROVEAN	Deleterious
ACMG Classification	Pathogenic
Segregates in the family	yes

… , nonapplicable; ACMG, American College of Medical Genetics and Genomics.

telligible to listeners with little experience of the speech of deaf people), respectively.

Sanger sequencing on family members confirmed that the variant was cosegregating with HL (homozygote in patients and heterozygote in parents) (**FIGURES 1D-1F**). Comparison of the sequence of the MYO15A protein with multiple species proved that p.Glu2770 is evolutionarily conserved and, thus, suggested its importance in the proper protein function (**FIGURE 3**).

According to the ACMG and HL-specific ACMG/AMP guidelines, this variant c.8309_8311del (p.Glu2770del) is classified as pathogenic, based on some lines of evidence. The *moderate (PM2)* variant is absent from the controls of the Exome Sequencing Project (ESP), 1000 Genomes Project (TGP), Exome Aggregation Consortium (ExAC), Iranome, and GTaC databases. *Moderate (PM3):* 0.5 point awarded from tables 6A and 6B of the ACMG/AMP guidelines to each of the probands (total score of 1.5 for homozygous occurrence due to consanguinity in a total of 6 patients).

Moderate (PM4): Protein length is changed as a result of small in-frame deletion (1 amino acid) in a nonrepeating region of the protein. *Strong (PP1):* the cosegregation study using the Sanger sequencing method reveals that the variant is cosegregating with the disease in all 3 families.

The greatest strength level, *PP1*, was identified in the HL-CI10 pedigree, with 3 affected and 2 unaffected siblings, based on table 4 of the ACMG/AMP guideline. The LOD score was 2.06, suggesting a strong cosegregation with the disease. *Supporting (PP3):* multiple lines of computational evidence support the deleterious effect of this variant (evolutionary conservation, pathogenicity prediction, protein structure) (**TABLE 1**). *Supporting (PP5):* this variant is reported as likely pathogenic in 2 separate studies;[26,27] however, no evidence has been provided.

The 3D structure of *MYO15A* and its mutant model was constructed using the I-TASSER online server. The results showed that this protein has missed 1 negatively charged amino acid in an α-helix structure of the second FERM domain due to *MYO15A*:NM_016239:exon46: c.8309_8311del (p.Glu2770del) (**FIGURE 4**). Using modeling, we showed that noncovalent interaction between Glu2770 and Ser 2774 is missed due to deletion of Glu and the resultant disruption of the α-helix structure (**FIGURE 4**). Because there are 3.6 residues per turn in every α-helix, deletion of glutamate as a residue with negative charge could lead a considerable shift in side chains of the remaining residues in the disrupted α-helix and may consequently negatively affect the protein folding.

After elucidating the pathogenicity of the variant, during the next pregnancy, 2 of the studied families requested a prenatal diagnosis. In family HL-CI 10, the father (III1) was not a carrier for the *MYO15A* c.8309_8311del (p.Glu2770del) variant. Because the risk of deafness due to compound heterozygous pathogenic variants in the fetus was expected to be low because of consanguinity, the parents choose not to pursue prenatal diagnostic testing (PND). In family HL-CI 3, performing PND by amniotic fluid sampling at the 14th week of gestation showed the fetus is heterozygous for *MYO15A* c.8309_8311del (p.Glu2770del).

FIGURE 4. Structure of the *MYO15A* tail with MyTH4-FERM domains. A, The affected amino acid is located in an α-helical region in the FERMa domain and is highlighted in red. Ribbon representation of the wild-type protein and noncovalent interaction between Glu2770 (B) and Ser 2774 (C). D, Analysis of the variant at the molecular level reveals how the deletion might lead to loss of the noncovalent interaction and so contribute to disruption of the α-helix structure.

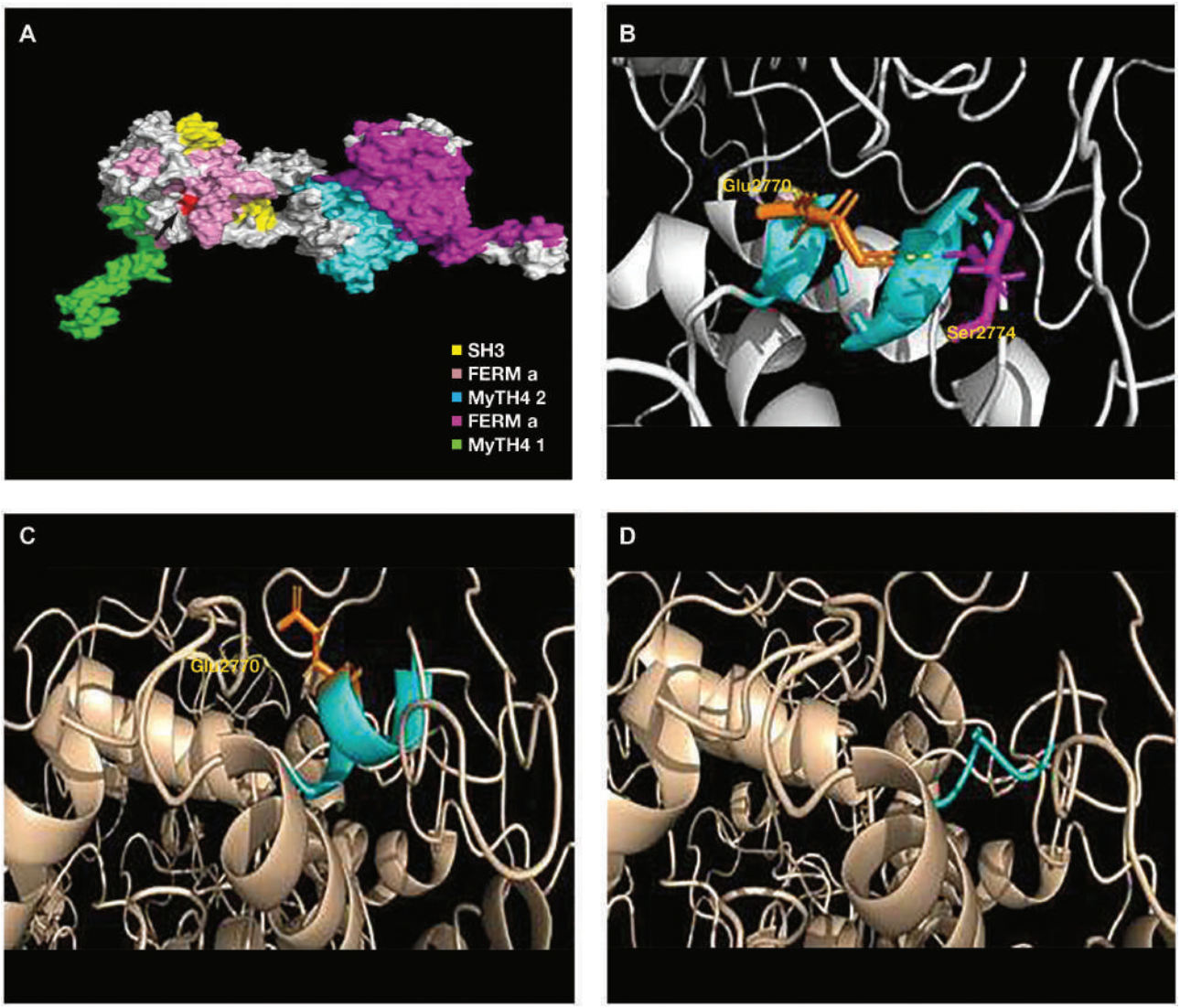

Thus, both fetuses (HL-CI 10-V6 and HL-CI 3-V2) were predicted to be unaffected for *MYO15A*-related hearing loss. Our predictions were confirmed after the birth of both infants. In the case of the third family (HL-CI 19), they were told that they could benefit from PND or PGD (preimplantation genetic diagnosis) testing in the next pregnancy to have a child without hearing impairment.

Discussion

MYO15A variants are documented as one of the most prevalent genetic causes of ARNSHL worldwide.[4] This type of variant is recognized as a common cause of HL, in third place after the *GJB2* and *SLC26A4* variants in the Iranian population.[27–30]

According to the information provided in the ClinVar online archive, more than 900 variants have been reported in *MYO15A* worldwide. However, the results of professional HGMD indicated that 343 of these variants were associated with HL. They involve a wide spectrum of variant types, including missense/nonsense (n = 220), splicing (n = 51), small deletion (n = 39), small insertion (n = 26), small indel (n = 2), gross deletion (n = 4), and complex mutation (n = 1). Until now, 41 pathogenic or likely pathogenic variants have been reported in this gene from the Iranian population, including 16 missense, 13 small insertion or deletion, 7 splice site, and 5 nonsense variant (**TABLE 2**).

In this study report, we have identified and investigated the effect of 1 small in-frame deletion in *MYO15A* in 3 separate consanguineous Iranian families. We applied NGS to the molecular diagnosis and identified 1 homozygous small nonframeshifting deletion in *MYO15A* (c.8309_8311del [p.Glu2770del]), which was classified as pathogenic based on the ACMG and HL-specific ACMG/AMP guidelines. It results in the deletion of 1 glutamate from an α-helical region in the FERM domain of unconventional myosin-15.

Small insertions/deletions are the second-most-abundant type of variants in the human genome after single nucleotide variants; in-frame indels account for 50% of these variants.[31] Indels present a unique chal-

TABLE 2. ***MYO15A*** **Pathogenic and Likely Pathogenic Variants Reported in the Iranian Population**

Nucleotide Change NM_016239.4 _	Amino-Acid Change	Protein Region	Exon/ Intron No.	Variant Type	Severity	No. of Individuals Harboring the Variant	Cosegregation	Allele Frequency in Iranome	Genomic Location (NC_000017.10) (GRCh37) ACMG Classification	Reference
c.284dupA	p.Lys96GlufsTer132	N-terminal extension	2	Frameshift	Profound	2	Pending	…	g.18022398dup Pathogenic	Sloan-Heggen et al[30]
c.855dupT	p.Pro286SerfsTer15	N-terminal extension	2	Frameshift	Severe to profound	1	Yes	…	g.18022969dup Pathogenic	Sloan-Heggen et al[30]
c.1047C > A	p.Tyr349Ter	N-terminal extension	2	Nonsense	Severe	2	Yes	…	g.18023161C > A Pathogenic	Asgharzadeh et al[36]
c.2280delC	p.Ser761LeufsTer20	N-terminal domain	2	Frameshift	NA	2	No	…	g.18024393del Likely pathogenic	Yan et al[37]
c.2516delC	p.Pro839fsTer24	N-terminal extension	2	Frameshift	Severe to profound	4	Yes	…	g.18024630del Pathogenic	Sloan-Heggen et al[30]
c.2759G > A	p.Trp920Ter	N-terminal extension	2	Nonsense	Moderate to profound	2	Pending	…	g.18024873G > A Pathogenic	Sloan-Heggen et al[30]
c.4142 + 1G > T		Motor domain	9	Splice site	Severe to profound	3	Yes	…	g.18034657G > T Pathogenic	Sloan-Heggen et al[30]
c.4176C > A	p.Tyr1392Ter	Motor domain	10	Nonsense	Severe to profound	5	Yes	0.000625	g.18034815C > A Pathogenic	Sloan-Heggen et al[30]
c.4519C > T	p.Arg1507Ter	Motor domain	13	Nonsense	Profound	1	Yes	…	g.18039061C > T Pathogenic	Sarmadi et al[38]
c.4596 + 1G > A		Motor domain	Intron 13	Splice site	NA	2	Yes	…	g.18039139G > A Pathogenic	Motavaf et al[39]
c.4655 + 1G > A		Motor domain	Intron 14	Splice site	Severe to profound	1	Yes	…	g.18039790G > A Pathogenic	Sloan-Heggen et al[30]
c.4909_4911delGAG	p.Glu1637del	Motor domain	17	Nonframeshift	Profound	2	No	…	g.18041462-18041464 Likely pathogenic	Fattahi et al[40] Sloan-Heggen et al[30]
c.5087dupT	p.Pro1697AlafsTer2	Motor domain	18	Frameshift	Severe to profound	1	Yes	…	g.18042204dup Pathogenic	Sloan-Heggen et al[30]
c.5305A > G	p.Thr1769Ala	Motor domain	20	Missense	Severe to profound	2	Yes	…	g. 18043924A > G Likely pathogenic	Sloan-Heggen et al[30] Fattahi et al[40]

TABLE 2. Continued

Nucleotide Change NM_016239.4 _	Amino-Acid Change	Protein Region	Exon/ Intron No.	Variant Type	Severity	No. of Individuals Harboring the Variant	Cosegregation	Allele Frequency in Iranome	Genomic Location (NC_000017.10) (GRCh37) ACMG Classification	Reference
c.5421delT	p.Phe1807LeufsTer6	Motor domain	22	Frameshift	Severe to profound	2	Yes	…	g.18044345del Pathogenic	Sloan-Heggen et al[30] Fattahi et al[40]
c.5810G > A	p.Arg1937His	IQ motif	24	Missense	Severe Severe to profound	1	Yes	…	g.18045553G > A Likely pathogenic	Sloan-Heggen et al[30] Fattahi et al[40]
c.5910 + 1G > T		IQ motif	Intron 25	Splice site	Severe to profound	2	Yes	…	g.18046155G > TPathogenic	Sloan-Heggen et al[0]
c.6273 + 1G > A		MyTh4 domain	Intron 29	Splice site	NA	2	No	…	g. 18047907G > A Pathogenic	Yan et al[37]
c.6341T > G	p.Val2114Gly	MyTh4 domain	30	Missense	Profound	2	Yes	…	g.18049253T > G Likely pathogenic	Sloan-Heggen et al[30]
c.6371G > A	p.Arg2124Gln	MyTh4 domain	30	Missense	Severe to profound	2	Yes	…	g.18049283G > A Likely pathogenic	Sloan-Heggen et al[30] Noman et al[41] Shearer et al[42]
c.6436C > T MyTH4 1	p.Arg2146Trp	MyTh4 domain	30	Missense	Profound	2	Yes	…	g.18049348C > T Likely pathogenic	Mehregan et al[43] Zhang J et al[45]
c.6437G > A	p.Arg2146Gln	MyTh4 domain	30	Missense	Severe	1	Yes	…	g.18049349G > A Likely pathogenic	Sloan-Heggen et al[30] Woo et al[46]
c.6442T > A	p.Trp2148Arg	MyTh4 domain	30	Missense	Severe to profound	2	Yes	…	g. 18049354 T > A Likely pathogenic	Reiisi et al[47] Khatami et al[44]
c.6893G > A	p.Arg2298Gln	MyTh4 domain	33	Missense	Profound	2	Yes	…	g.18052203G > > A Likely pathogenic	Sloan-Heggen et al[30] Abu Rayyan et al[48] Sloan-Heggen et al[27]
c.7047delG	p.Tyr2350ThrfsTer67	MyTh4 domain	34	Frameshift	NA	1	Yes	…	g.18052620del Likely pathogenic	Sloan-Heggen et al[30]

TABLE 2. Continued

Nucleotide Change NM_016239.4 _	Amino-Acid Change	Protein Region	Exon/ Intron No.	Variant Type	Severity	No. of Individuals Harboring the Variant	Cosegregation	Allele Frequency in Iranome	Genomic Location (NC_000017.10) (GRCh37) ACMG Classification	Reference
c.7395 + 1G > A		MyTh4 domain	Intron 37	Splice site	Severe to profound	2	Yes	-	g.18054080G > A Pathogenic	Sloan-Heggen et al[30]
c.7720C > T	p.Gln2574Ter	MyTh4 domain	40	Nonsense	Profound	2	Yes	…	g.18054774C > T Pathogenic	Zarepour[49]
c.8309_8311del I	p.Glu2770del	FERM domain	46	Nonframeshift	Profound	1	Yes	…	g.18058508_18058510del Pathogenic	Sloan-Heggen et al[30] This study
c.8446_8449delCTGC	p.Leu2816ValfsTer11	FERM domain	47	Frameshift	Profound	1	Yes	…	g.18058733-18058736delPathogenic	Sarmadi et al[38]
c.8467G > A	p.Asp2823Asn	FERM domain	48	Missense	Moderate	2	Yes	-	g.18059516G > A Pathogenic	Sloan-Heggen et al[30] Brownstein et al[50] Fattahi et al[40]
c.8601 + 2T > G		SH3	Intron 48	Splice site	Profound	2	Yes	…	g.18059652T > G Pathogenic	Sloan-Heggen et al[30]
c.8638_8641delCCTG	p.Pro2880ArgfsTer19	SH3	49	Frameshift	NA	2		…	g.18060300-18060303del Pathogenic	Bademci et al[26]
c.8725G > A	p.Gly2909Ser	SH3	50	Missense	Profound	1	Yes	…	g.18060481G > A Likely pathogenic	Sloan-Heggen et al[30]
c.9534C > G	p.Cys3178Trp	MyTH4 2	58	Missense	NA	1	Yes	…	g. 18065915C > G Likely pathogenic	Sloan-Heggen et al[30]
c.9572G > A	p.Arg3191His	MyTH4 2	58	Missense	Profound	2	Yes	…	g. 18065953G > A Pathogenic	Sloan-Heggen et al[30]
c.9584C > G	p.Pro3195Arg	MyTH4 2	58	Missense	Moderate to sever	2	No	…	g. 18065965C > G Likely pathogenic	Mehregan et al[43]
c.9698T > G	p.Leu3233Ala	FERM -2	60	Missense	NA	2	Yes	0.000625	g.18067063T > G Likely pathogenic	Talebi[51]

TABLE 2. Continued

Nucleotide Change NM_016239.4 _	Amino-Acid Change	Protein Region	Exon/ Intron No.	Variant Type	Severity	No. of Individuals Harboring the Variant	Cosegregation	Allele Frequency in Iranome	Genomic Location (NC_000017.10) (GRCh37) ACMG Classification	Reference
c.9611_9612 + 8delTGGTGAGCAT	p.Leu3204CysfsTer17	FERM -2	58	Frameshift	NA	2	Yes	…	g.18066543-18066552del Likely pathogenic	Akbariazar et al[52]
c.10266G > T	p.Gln3422His	FERM -2	64	Missense	Profound	2	No	…	g.18075520G > T Likely pathogenic	Mehregan et al[43]
c.6442T > A	p.Trp2148Arg	MyTH4	30	Missense	Profound	2	Yes	…	g.18049354T > A Likely pathogenic	Khatami et al[44]
c.10504dupT	p.Cys3502ValfsTer16	I PDZ-binding motif	66	Frameshift	Profound	2	Yes	…	g.18082093dup Pathogenic	Khatami et al[44]

NA, information not available; … , nonapplicable.

lenge because they alter protein primary structure, and also, they are highly prevalent in healthy populations.[32]

The variant found in our study has been reported previously in 1 Iranian and 1 Turkish family and has been categorized as likely pathogenic in the NCBI Clinvar database. However, no cosegregation or bioinformatics analyses had been performed on it.[26,27] In this study report, we provide further evidence of the pathogenicity of the variant. We have performed a cosegregation analysis along with computational analysis and structural modeling to improve our diagnostic value. This deletion is predicted by MutationTaster, SIFT-indel, PROVEAN, and DDG-in to be deleterious.

Structural analysis of the mutant protein in this study suggests that the absence of a single residue in an α-helical region affects amino-acid interaction and helical stability. Because there are 3.6 residues per turn in every α-helix, deletion of 1 hydrophilic amino acid with a negative charge (Glu2770) shifts the position of the remaining residues. This action might affect protein structure by changing in the stability of protein folding. However, structural modeling is speculative, and experimentally determined structure, obtained by structural biology techniques such as X-ray crystallography, is needed to elucidate the exact structure of the MYO15A protein. Our result indicates that an abnormal phenotype can occur through change in the structure of the protein and, ultimately, disruption of the protein function, which is necessary for the mechanosensory activity of hair cells in the inner ear.

The findings from recent studies, such as Eppsteiner et al,[13] suggest that pathogenic/likely pathogenic variants in different deafness genes lead to different pathologies and, thus, affect the outcome of postoperative cochlear implantation. Our results are in line with those from previous studies,[31,33–35] suggesting that patients with *MYO15A* pathogenic variants show favorable auditory performance after CI surgery. However, a comprehensive study in a group with larger sample sizes is required to correlate the genetic findings to CI performance.

Conclusions

Our results, which indicate the pathogenicity of *MYO15A* (c.8309_8311del [p.Glu2770del]) in affected patients from 3 separate families of different ethnicities, could be used in cascade screening of consanguineous marriage in extended families. Also, our finding of a small recurrent in-frame deletion variant in *MYO15A* causing ARNSHL has implications for genetic diagnosis of HL in Iran.

Acknowledgments

The study was approved by the Review Board of Isfahan University of Medical Sciences. This work was financially supported by Isfahan University of Medical Sciences (grant NO.396133). The authors declare no conflict of interest.

NGS working group: Samane Nasrniya, Paniz Miar, Sina Narrei, Mohammad Amin Tabatabaiefar. Clinical Working Group: Mahsa Sepehrnejad, Mohammad Hussein Nilforoush, Hamidreza Abtahi.

REFERENCES

1. Mahdieh N, Rabbani B, Wiley S, Akbari MT, Zeinali S. Genetic causes of nonsyndromic hearing loss in Iran in comparison with other populations. *J Hum Genet.* 2010;55(10):639–648.

2. Zhang Y, Malekpour M, Al-Madani N, et al. Sensorineural deafness and male infertility: a contiguous gene deletion syndrome. *J Med Genet.* 2007;44(4):233–240.
3. Friedman TB, Liang Y, Weber JL, et al. A gene for congenital, recessive deafness DFNB3 maps to the pericentromeric region of chromosome 17. *Nat Genet.* 1995;9(1):86–91.
4. Hilgert N, Smith RJH, Van Camp G. Forty-six genes causing nonsyndromic hearing impairment: which ones should be analyzed in DNA diagnostics? *Mutat Res.* 2009;681(2-3):189–196.
5. Liang Y, Wang A, Belyantseva IA, et al. Characterization of the human and mouse unconventional myosin XV genes responsible for hereditary deafness *DFNB3* and shaker 2. *Genomics.* 1999;61(3):243–258.
6. García-Alvarez B, de Pereda JM, Calderwood DA, et al. Structural determinants of integrin recognition by talin. *Mol Cell.* 2003;11(1):49–58.
7. Kalay E, Uzumcu A, Krieger E, et al. *MYO15A* (*DFNB3*) mutations in Turkish hearing loss families and functional modeling of a novel motor domain mutation. *Am J Med Genet A.* 2007;143A(20):2382–2389.
8. Wang A, Liang Y, Fridell RA, et al. Association of unconventional myosin *MYO15* mutations with human nonsyndromic deafness *DFNB3*. *Science.* 1998;280(5368):1447–1451.
9. Anderson DW, Probst FJ, Belyantseva IA, et al. The motor and tail regions of myosin XV are critical for normal structure and function of auditory and vestibular hair cells. *Hum Mol Genet.* 2000;9(12):1729–1738.
10. Probst FJ, Fridell RA, Raphael Y, et al. Correction of deafness in *shaker-2* mice by an unconventional myosin in a BAC transgene. *Science.* 1998;280(5368):1444–1447.
11. Belyantseva IA, Boger ET, Friedman TB. Myosin XVa localizes to the tips of inner ear sensory cell stereocilia and is essential for staircase formation of the hair bundle. *Proc Natl Acad Sci U S A.* 2003;100(24):13958–13963.
12. Oza AM, DiStefano MT, Hemphill SE, et al; ClinGen Hearing Loss Clinical Domain Working Group. Expert specification of the ACMG/AMP variant interpretation guidelines for genetic hearing loss. *Hum Mutat.* 2018;39(11):1593–1613.
13. Eppsteiner RW, Shearer AE, Hildebrand MS, et al. Prediction of cochlear implant performance by genetic mutation: the spiral ganglion hypothesis. *Hear Res.* 2012;292(1–2):51–58.
14. Wu C-C, Liu T-C, Wang S-H, Hsu C-J, Wu C-M. Genetic characteristics in children with cochlear implants and the corresponding auditory performance. *Laryngoscope.* 2011;121(6):1287–1293.
15. Fang H-Y, Ko H-C, Wang N-M, et al. Auditory performance and speech intelligibility of Mandarin-speaking children implanted before age 5. *Int J Pediatr Otorhinolaryngol.* 2014;78(5):799–803.
16. Tabatabaiefar M, Alasti F, Zohour MM, et al. Genetic linkage analysis of 15 DFNB loci in a group of Iranian families with autosomal recessive hearing loss. *Iran J Public Health.* 2011;40(2):34–48.
17. Li H, Durbin R. Fast and accurate short read alignment with Burrows-Wheeler transform. *Bioinformatics.* 2009;25(14):1754–1760.
18. Schwarz JM, Rödelsperger C, Schuelke M, Seelow D. MutationTaster evaluates disease-causing potential of sequence alterations. *Nat Methods.* 2010;7(8):575–576.
19. Choi Y, Chan AP. PROVEAN web server: a tool to predict the functional effect of amino acid substitutions and indels. *Bioinformatics.* 2015;31(16):2745–2747.
20. Hu J, Ng PC. SIFT Indel: predictions for the functional effects of amino acid insertions/deletions in proteins. *PLoS One.* 2013;8(10):e77940.
21. Zhao H, Yang Y, Lin H, et al. DDIG-in: discriminating between disease-associated and neutral non-frameshifting micro-indels. *Genome Biol.* 2013;14(3):R23.
22. Yang J, Yan R, Roy A, Xu D, Poisson J, Zhang Y. The I-TASSER Suite: protein structure and function prediction. *Nat Methods.* 2015;12(1):7–8.
23. Richards S, Aziz N, Bale S, et al; ACMG Laboratory Quality Assurance Committee. Standards and guidelines for the interpretation of sequence variants: a joint consensus recommendation of the American College of Medical Genetics and Genomics and the Association for Molecular Pathology. *Genet Med.* 2015;17(5):405–424.
24. Archbold S, Lutman ME, Nikolopoulos T. Categories of auditory performance: inter-user reliability. *Br J Audiol.* 1998;32(1):7–12.
25. Allen C, Nikolopoulos TP, Dyar D, O'Donoghue GM. Reliability of a rating scale for measuring speech intelligibility after pediatric cochlear implantation. *Otol Neurotol.* 2001;22(5):631–633.
26. Bademci G, Foster J 2nd, Mahdieh N, et al. Comprehensive analysis via exome sequencing uncovers genetic etiology in autosomal recessive nonsyndromic deafness in a large multiethnic cohort. *Genet Med.* 2016;18(4):364–371.
27. Sloan-Heggen CM, Bierer AO, Shearer AE, et al. Comprehensive genetic testing in the clinical evaluation of 1119 patients with hearing loss. *Hum Genet.* 2016;135(4):441–450.
28. Koohiyan M, Hashemzadeh-Chaleshtori M, Salehi M, et al. *GJB2* mutations causing autosomal recessive non-syndromic hearing loss (ARNSHL) in two Iranian populations: report of two novel variants. *Int J Pediatr Otorhinolaryngol.* 2018;107:121–126.
29. Azadegan-Dehkordi F, Ahmadi R, Koohiyan M, et al. Update of spectrum c. 35delG and c.-23+ 1G > A mutations on the GJB2 gene in individuals with autosomal recessive nonsyndromic hearing loss. *Ann Hum Genet*. 2019;83(1):1–10.
30. Sloan-Heggen CM, Babanejad M, Beheshtian M, et al. Characterising the spectrum of autosomal recessive hereditary hearing loss in Iran. *J Med Genet.* 2015;52(12):823–829.
31. The 1000 Genomes Project Consortium. A global reference for human genetic variation. *Nature*. 2015;526(7571):68–74.
32. The 1000 Genomes Project Consortium. A map of human genome variation from population-scale sequencing. *Nature*. 2010;467(7319):1061–1073.
33. Miyagawa M, Nishio SY, Ikeda T, Fukushima K, Usami S. Massively parallel DNA sequencing successfully identifies new causative mutations in deafness genes in patients with cochlear implantation and EAS. *PLoS One.* 2013;8(10):e75793.
34. Miyagawa M, Nishio SY, Ikeda T, Fukushima K, Usami S. Massively parallel DNA sequencing successfully identifies new causative mutations in deafness genes in patients with cochlear implantation and EAS. *PLoS One.* 2013;8(10):e75793.
35. Miyagawa M, Nishio S-Y, Hattori M, et al. Mutations in the *MYO15A* gene are a significant cause of nonsyndromic hearing loss: massively parallel DNA sequencing–based analysis. *Ann Otol, Rhinol Laryngol*. 2015;124(1_suppl):158S–68S.
36. Asgharzade S, Chaleshtori MH, Tabatabaifar MA, et al. Mutation in second exon of myo15a gene cause of nonsyndromic hearing loss and its association in the Arab population in Iran. *Genetika*. 2016;48(2):587–96.
37. Yan D, Tekin D, Bademci G, et al. Spectrum of DNA variants for nonsyndromic deafness in a large cohort from multiple continents. *Hum Genet.* 2016;135(8):953–961.
38. Sarmadi A, Nasrniya S, Narrei S, Nouri Z, Abtahi H, Tabatabaiefar MA. Whole exome sequencing identifies novel compound heterozygous pathogenic variants in the *MYO15A* gene leading to autosomal recessive non-syndromic hearing loss. *Mol Biol Rep.* 2020;47(7):5355–5364.
39. Motavaf M, Soveizi M, Maleki M, Mahdieh N. MYO15A splicing mutations in hearing loss: A review literature and report of a novel mutation. *Int J Pediatr Otorhinolaryngol.* 2017;96:35–38.
40. Fattahi Z, Shearer AE, Babanejad M, et al. Screening for *MYO15A* gene mutations in autosomal recessive nonsyndromic, *GJB2* negative Iranian deaf population. *Am J Med Genet A.* 2012;158A(8):1857–1864.
41. Noman M, Ishaq R, Bukhari SA, Ahmed AM, Riazuddin S. Delineation of homozygous variants associated with prelingual sensorineural hearing loss in Pakistani families. *Genes*. 2019;10(12):1031.
42. Shearer AE, Hildebrand MS, Webster JA, et al. Mutations in the first MyTH4 domain of *MYO15A* are a common cause of DFNB3 hearing loss. *Laryngoscope.* 2009;119(4):727–733.

43. Mehregan H, Mohseni M, Jalalvand K, et al. Novel mutations in MYTH4-FERM domains of myosin 15 are associated with autosomal recessive nonsyndromic hearing loss. *Int J Pediatr Otorhinolaryngol.* 2019;117:115–126.
44. Khatami S, Askari M, Bahreini F, Hashemzadeh-Chaleshtori M, Hematian S, Asgharzade S. Novel MYO15A variants are associated with hearing loss in the two Iranian pedigrees. *BMC Med Genet.* 2020;21(1):226.
45. Zhang J, Guan J, Wang H, et al. Genotype-phenotype correlation analysis of *MYO15A* variants in autosomal recessive non-syndromic hearing loss. *BMC Med Genet.* 2019;20(1):60.
46. Woo H-M, Park H-J, Baek J-I, et al. Whole-exome sequencing identifies *MYO15A* mutations as a cause of autosomal recessive nonsyndromic hearing loss in Korean families. *BMC Med Genet.* 2013;14:72.
47. Reiisi S, Tabatabaiefar MA, Sanati MH, Chaleshtori MH. Screening of DFNB3 in Iranian families with autosomal recessive non-syndromic hearing loss reveals a novel pathogenic mutation in the MyTh4 domain of the MYO15A gene in a linked family. *Iran J Basic Med Sci.* 2016;19(7):772–778.
48. Abu Rayyan A, Kamal L, Casadei S, et al. Genomic analysis of inherited hearing loss in the Palestinian population. *Proc Natl Acad Sci U S A.* 2020;117(33):20070–20076.
49. Zarepour N, Koohiyan M, Taghipour-Sheshdeh A, et al. Identification and clinical implications of a novel MYO15A variant in a consanguineous Iranian family by targeted exome sequencing. *Audiol Neurotol.* 2019;24(1):25–31.
50. Brownstein Z, Abu-Rayyan A, Karfunkel-Doron D, et al. Novel myosin mutations for hereditary hearing loss revealed by targeted genomic capture and massively parallel sequencing. *Eur J Hum Genet.* 2014;22(6):768–775.
51. Talebi F. Novel homozygous mutation in the MYO15A gene in autosomal recessive hearing loss. *Zahedan J Res Med Sci*. 2016;18(10):e4256.
52. Akbariazar E, Vahabi A, Abdi Rad I. Report of a novel splicing mutation in the *MYO15A* gene in a patient with sensorineural hearing loss and spectrum of the *MYO15A* mutations. *Clin Med Insights Case Rep.* 2019;12:1179547619871907.

Interleukin-6 and Serum/Fecal Calprotectin as Useful Specific Markers for Monitoring Rheumatic Diseases: A Pilot Study

Margherita Scapaticci, PhD,[1,] Andrea Bartolini, MD,[1] Marta Biscaro, MD,[2] Renzo Biscaro, MD,[2] Giorgio Da Rin, MD[3]*

[1]Unified Metropolitan Laboratory, AUSL Bologna, Bologna, Italy; [2]Rheumatology Department, San Camillo Hospital, Treviso, Italy; [3]Laboratory Medicine, IRCCS Policlinico San Martino Hospital, Genova, Italy; *To whom correspondence should be addressed. margherita.scapaticci@ausl.bologna.it

Keywords:autoimmune rheumatoid diseases, calprotectin, interleukin-6, gastrointestinal diseases, DMARDs, DAS28-PCR

Abbreviations: ESR, erythrocyte sedimentation rate; CRP, C-reactive protein; IL-6, interleukin-6

Laboratory Medicine 2022;53:123–127; https://doi.org/10.1093/labmed/lmab034

ABSTRACT

Objective: Some conventional laboratory tests are routinely used for the prediction of systemic autoimmune disease activity, such as the erythrocyte sedimentation rate (ESR) and C-reactive protein (CRP); however, they can give false-negative results, pointing out the need to identify more specific markers.

Methods: We evaluated biomarkers in 21 Italian patients naïve to treatment with a diagnosis of autoimmune rheumatic disease according to the 2010 American College of Rheumatology/European League Against Rheumatism Classification Criteria for Rheumatoid Arthritis during 6 months of therapeutic treatments.

Results: We found a significant difference in interleukin-6 (IL-6), CRP, ESR, platelet count, and fecal calprotectin in diagnosed patients compared with healthy participants and a significant decrease in these values during follow-up, except for IL-6 and platelet count.

Conclusion: We found that CRP, ESR, and fecal calprotectin seemed to be related to autoimmune rheumatic disorders and to be associated with therapy, whereas serum calprotectin and IL-6 did not seem to be associated with disease improvement after the start of treatment, along with leukocyte count and platelet count.

Rheumatic diseases include more than 150 different disorders affecting more than 5 million of people worldwide, and this number is expected to increase because of the aging of the population. However, these pathologies are still undervalued by most affected individuals, who erroneously believe that the pain is caused by age. For these reasons, too many diagnoses are formulated belatedly, and clinicians are often forced to intervene when the situation has already evolved. The rheumatic diseases are quite different from each other, both the symptoms and the causes that determine them. They mainly affect the joints, the skeleton, and the muscular apparatus, but sometimes they also involve internal organs and other tissues. Inflammation is often the consequence of an abnormal response of the immune system, in that it happens in many "autoimmune" rheumatic diseases, that can gradually lead to disability conditions if not treated.[1]

Rheumatoid arthritis (RA) is the most common chronic immune-mediated inflammatory joint disease. It has a progressive evolution that compromises articular function with a high invalidating risk.[2] The treatment of RA has improved greatly over the last 15 years, especially with the introduction of biologic therapies and treat-to-target strategies.

Polymyalgia rheumatica (PMR) is a systemic inflammatory disease that occurs in patients older than age 50 years. It mostly affects women and is characterized by an elevated erythrocyte sedimentation rate (ESR), proximal extremity pain, morning stiffness, and rapid relief with the administration of corticosteroids; however, some patients may take longer to come to clinical attention because of a persistently "normal" ESR. In these patients, a measurement of C-reactive protein (CRP) may be useful, even if it is not considered part of the published diagnostic criteria.[3]

Psoriatic arthritis (PsA) is a heterogeneous condition with musculoskeletal involvement, including arthritis, enthesitis, dactylitis, and axial involvement and potential nails and skin disease.[4] In patients with severe cases, there is a risk that the joints will become permanently damaged or deformed, requiring a surgical treatment. Early diagnosis and appropriate treatment are important to slow down the progression of the condition and to minimize or prevent permanent damage to the joints.[5,6]

In clinical practice, some laboratory tests are commonly used for the prediction of systemic autoimmune disease activity including ESR, CRP, and leukocyte and platelet (PLT) counts, which are considered generic

inflammatory-disease biological markers and are usually elevated in patients with RA.

In fact, even though PLTs are primarily recognized for their role in the prevention of bleeding, because of their large number of receptors, they respond promptly to complement and damage-associated molecular patterns, representing a great reservoir of immunomodulatory molecules in the circulation and confirming their role in immune responses and inflammation.[7]

Regarding the association between leukocytosis and rheumatic diseases, data from the literature are controversial: Intermittent or persistent leukocytosis seem to be common in patients with RA receiving low-dose oral steroid therapy; moreover, a higher white blood cell (WBC) count has been found in patients with more active disease.[8] On the other hand, hemolytic anemia, leukopenia, lymphopenia, and immune-mediated thrombocytopenia are frequently seen in patients with systemic lupus erythematosus.[9]

However, some studies have shown that these nonspecific markers can give false-negative results.[10,11] For this reason, in recent years, there has been a constant search for specific markers that reflect the inflammatory status of patients with autoimmune disease and that may predict responsiveness to treatment.[12]

Calprotectin is a calcium-binding leukocyte protein consisting of the heterodimers of the proteins S100A8 and S100A9 (myeloid-related protein, MRP8/MRP14) that is mainly expressed in early-stage differentiated monocytes and neutrophil granulocytes[13,14] and is released predominantly at sites of inflammation. In contrast to CRP, calprotectin regulates the maturation of inflammatory cells, facilitating further inflammation; it is secreted from these cells and for this reason its plasma concentration reflects both the number of inflammatory cells and their activity.[15] This protein can actually be measured in body fluids, and several studies have shown that elevated concentrations of calprotectin in serum and/or synovial fluid are present in various rheumatic diseases[14] and that high levels of calprotectin predict methotrexate (MTX) responsiveness.[12-16] Moreover, its concentration in stool is proportional to the presence of neutrophils and inflammation in the gut. Because some studies show a correlation between inflammatory rheumatic diseases and a variety of gastrointestinal manifestations, fecal calprotectin has been used in our work to assess subclinical gut inflammation in patients who are rheumatic without symptoms.

In addition to calprotectin, data from the literature indicate that cytokines are also important components of inflammatory response in rheumatic diseases. Among them, interleukin (IL)-6 serum concentration is significantly elevated in patients with RA and decreases with medical treatment, proposing a potential role for the IL-6 family of cytokines in the pathogenesis of RA.[17-19]

Pharmacological treatments for autoimmune rheumatic diseases include nonsteroidal anti-inflammatory drugs, glucocorticoids (GCs), and other disease-modifying anti-rheumatoid drugs (DMARDs), which may be synthetic (either conventional [csDMARDs] or targeted) or biologic.[20] In many patients, DMARDs allow them to achieve a good remission, especially when used efficaciously and in combination.[21] Among the csDMARDs, the most used are hydroxychloroquine (HCQ), MTX, and sulfasalazine.[22-24]

The objectives of the present study were (i) to indirectly investigate the prevalence of subclinical intestinal inflammation in naïve patients (patients that started pharmacological treatment for the first time) affected by autoimmune rheumatic disease according to the 2010 American College of Rheumatology/European League Against Rheumatism (ACR/EULAR) Classification Criteria for Rheumatoid Arthritis,[25] without intestinal symptoms and before starting any therapy, by measuring their fecal calprotectin concentrations at recruitment and comparing these values to those of healthy participants; (ii) to assess the patients' serum calprotectin levels, exploring their possible associations with those of fecal calprotectin, before and during 6 months of pharmacological csDMARDs and/or GC treatment; and (iii) to compare patients' concentrations of fecal calprotectin, serum calprotectin, and serum IL-6 to those of the most common used unspecific inflammatory markers (ESR, CRP, PLT count, and leukocyte count) at the time of recruitment and after 1, 3, and 6 months from the start of therapy, also evaluating the changes in rheumatic symptoms, disease activity parameters, and organ manifestations.

Materials and Methods

Between April 2016 and May 2017, a total of 245 outpatients came to the rheumatology department of San Camillo Hospital in Treviso, Italy for the first time and, among them, 21 patients—14 women and 7 men (mean age 63.3 years; standard deviation [SD] 9.2)—were consecutively recruited for this prospective study under the following criteria: a new diagnosis of autoimmune rheumatic disease according to the 2010 ACR/EULAR Classification Criteria for Rheumatoid Arthritis,[25] without gastrointestinal manifestations at recruitment. Patients presenting with inflammatory bowel disease, acute or chronic kidney and liver disease, any form of current acute or chronic infection, or any hematological disease, and patients receiving antibiotic therapy and/or corticosteroid and estrogenic therapy were excluded. Patients' disease activity was evaluated by the Disease Activity Score 28-PCR (DAS28-PCR),[26] which was calculated using 4 measures: the number of swollen joints out of the 28 considered, the number of tender joints out of the 28 considered, CRP, and a "global assessment of health" of the patient using a visual analogue scale in a complex mathematical formula to produce the overall activity score of the disease. A DAS28-PCR >5.1 implies active disease, a value between 5.1 and 3.2 indicates moderate disease activity, <3.2 indicates low disease activity, and <2.6 indicates remission.

All the enrolled patients—4 with RA, 7 with PMR, and 10 with PsA—started the therapy with GCs or at least 1 of the csDMARDs associated with a GC immediately after recruitment; next, symptoms and fecal and serum biomarkers were evaluated at diagnosis and after one, 3, and 6 months from the start of treatment. The same laboratory tests, except for serum IL-6 and serum calprotectin, were also performed on the control group, which included 21 age- and sex-matched healthy participants (mean age 63.6 years; SD 13.7; $P = .999$).

CRP, ESR, leukocyte (WBC) counts, and PLT counts were analyzed immediately after blood collection using routine procedures in the laboratory department of San Camillo Hospital: CRP was determined by serum specimen using the immunoturbidimetric method (high-sensivity CRP assay) on a Dimension EXL with an LM analyzer (Siemens Healthcare Diagnostics Inc.), with an assay range of 0.1 to 50 mg/L. The ESR, WBC count, and PLT count were measured in blood specimens anticoagulated with K3EDTA. The ESR was measured using spectrophotometric assay (Alifax test-1 THL, 950 nm; Alifax, Polverara, Italy), reference range 0 to 20 mm/hour, and WBC and PLT counts were measured using a Siemens hematology analyzer (ADVIA 2120i System, with analytical ranges, respectively, of 0.02 to 400 × 10^3/μL and 5.0 to 3500 × 10^3/μL and a reference range from 4.8 × 10^3/μL to 10.5 × 10^3/μL for WBC and from 130 to 400 × 10^3/μL for PLT).

Fecal calprotectin was immediately evaluated by fluoroenzyme immunoassay for calprotectin determination on the instrument Phadia 100 with the EliA Calprotectin (Thermo Scientific) kit for both patients and healthy control participants. Stool extraction was performed using the EliA Stool Extraction Kit, according to manufacturer instructions. When the EliA Calprotectin test could not be performed immediately after specimen extraction, the extract was frozen at –20°C until the analysis was performed. The extract is stable for a maximum of 3 months at ≤20°C. The reportable range (detection limit, upper limit) for EliA Calprotectin is from 15.0 to ≥ 3000 mg/kg, reference range < 50 mg/Kg.

Blood for calprotectin and IL-6 measurements was collected from patients using a serum separator tube. The specimens were allowed to clot for 2 hours at room temperature and then were centrifuged for 20 minutes at 1000 g; the serum was separated and kept frozen immediately at a temperature of –80°C until the analyses were performed. The IL-6 and calprotectin serum concentrations were measured in batches using commercial enzyme-linked immunosorbent assay (ELISA) kits (Cloud-Clone Corp.,) on a GDMS Micro Plate Read ELISA microplate analyzer (Gentaur/GDMS Belgium). The intra-assay coefficients of variation (CVs) of the 2 kits were <10%, and the interassay CVs were <12%. The lower limit of detection was 13.3 ng/L for serum calprotectin and 3.2 ng/L for IL-6 with a reportable range of 7.8 to 500 pg/mL for IL-6 and 125 to 2000 pg/mL for calprotectin. Accuracy (as a percentage of recovery) in serum ranged from 83% to 98% for IL-6 and from 81% to 96% for calprotectin. Both the assays were executed according to the manufacturer's instructions.

The study was performed according to the guidelines of the Declaration of Helsinki and was approved by the local ethics committee of the institute. All the included individuals gave their informed written consent before being enrolled for the study.

Statistical Analysis

A Kolmogorov-Smirnov test of normality was performed for all variables. Then, to analyze the differences between groups of interest, statistical significance was calculated using a Mann-Whitney *U* test (nonparametric)[27] or an independent-sample Student's *t*-test (parametric). A *P* value of <.05 was considered significant. The overall test used was the nonparametric Friedman test or analysis of variance (parametric alternative) for repeated measures. Where results were deemed significant, the comparison between 2 results was evaluated using a paired Student's *t*-test (parametric) or Wilcoxon test (nonparametric). The *P* values were finally adjusted according to the Bonferroni correction.

Results

As shown in **TABLE 1**, at the time of diagnosis, a significant increase in fecal calprotectin and serum IL-6 and of ESR, CRP, and PLT counts (P <.05) was observed in patients who had not begun therapy, compared to healthy participants. Conversely, no significant difference was found for the leukocyte count. When we compared patients' serum and fecal biomarker concentrations during the 6 months after diagnosis (**TABLE 2**), we found no significant difference in PLT and leukocyte counts, whereas ESR and CRP had a significant reduction in their concentrations during the entire follow-up period. In addition, fecal calprotectin showed a significant decrease after 1 and 3 months from the start of treatment with GCs or GCs with MTX or HCQ but increased again at the last follow-up. Furthermore, contrary to what we expected, there was an increase of IL-6 and serum calprotectin concentrations from recruitment to the first follow-up, followed by a progressive significant overall decrease in the median values at third and fourth controls, respectively after 3 and 6 months. Finally, regarding the DAS28-PCR score, a significant decrease was noted in all patients from diagnosis to the last follow-up date (P < .001), indicating an overall good response to the therapy. In fact, because the DAS28-PCR score is a strong predictor of disability and radiological progression,[28] based on the score ranges, we found that at recruitment 19% of patients showed high disease activity (score >5.1), 67% showed moderate activity (score between 3.2 and ≤5.1), and 14% showed low activity (score between 2.6 and <3.2), whereas after 6 months of treatment, no patient showed a DAS28-PCR score corresponding to high disease activity, 5% presented a low disease activity score, 76% presented a moderate disease activity score, and 19% showed remission (score between 0 and <2.6).

Discussion

Some acute-phase laboratory tests routinely used in clinical practice, such as the ESR and CRP levels, may be elevated in several inflammatory illnesses, providing important information about a current patient's disease activity and inflammatory state. Nevertheless, data from the literature report that approximately one-half and even more of individuals affected by RA have a normal ESR or CRP level.[10,29] Further, it has been shown that a reduction of these parameters reflects a clinical improvement in most but not all patients with RA.[30]

Our prospective study, involving 21 patients with a new diagnosis of autoimmune rheumatic disease according to the 2010 ACR/EULAR Classification Criteria for Rheumatoid Arthritis,[25] showed that fecal calprotectin, CRP, ESR, IL-6, and PLT counts were significantly increased

TABLE 1. Laboratory Test Results Compared Between Patients at Diagnosis and Control Participants

Parameter	Patients (n = 21), Median, IQR	Control Group (n = 21), Median, IQR	*P* Value
Leukocyte count, × 10^9/L	7.32, 1.19	5.93, 1.57	.164
ESR, mm/h	27.5, 26.0	8.0, 7.5	**<.001**
CRP, mg/L	1.21, 1.46	0.24, 0.10	**<.001**
Platelet count, × 10^9/L	260.50, 45.25	236.50, 46.25	**.015**
IL-6	28.1, 16.9	3.9, 4.5	**<.001**
Fecal calprotectin, mg/kg	60.36, 48.25	5.00, 6.50	**<.001**

CRP, C-reactive protein (extended range); ESR, erythrocyte sedimentation rate; IL-6, interleukin-6; IQR, interquartile range. Significant values in bold.

TABLE 2. Variation in Patients' Laboratory Test During GC Use or GC Use Associated with csDMARD Pharmacological Treatment

Parameter (unit)	At Recruitment, Median, IQR	After 1 Mo, Median, IQR	After 3 Mo, Median, IQR	After 6 Mo, Median, IQR	*P* Value
Serum calprotectin (ng/L)	1101.1, 592.9	1647.0, 617.6	1395.0, 786.9	1212.9, 605.55	.700
Fecal calprotectin (mg/kg)	60.36, 48.25	25.57, 5.00	12.00, 4.75	51.64, 32.50	**.002**
IL-6 (ng/L)	28.1, 16.9	35.6, 16.9	32.8, 7.2	41.3, 7.8	.310
WBC count ($\times 10^9$/L)	7.32, 1.19	7.30, 1.45	7.10 2.81	6.30, 2.64	.150
CRP (mg/L)	1.21, 1.46	0.37, 0.88	0.36, 0.21	0.53, 0.70	**.024**
PLTs ($\times 10^9$/L)	260.50, 45.25	266.00, 54.00	281.00, 41.25	275.0, 67.25	.061
ESR (mm/h)	27.5, 19.0	21.0, 19.0	18.5, 10.8	16.0, 15.0	**<.001**
DAS28-PCR	4.17, 1.24	3.08, 0.97	3.02, 1.31	3.49, 1.01	**<.001**

CRP, C-reactive protein; DAS28-PCR, Disease Activity Score 28-PCR; ESR, erythrocyte sedimentation rate; IL-6, interleukin-6; IQR, interquartile range; PLTs, platelets; WBCs, white blood cells. Significant values in bold.

in patients at recruitment compared to those of healthy participants, confirming the potential role of these biomarkers in helping to diagnose autoimmune rheumatic diseases.

Our aim was also to understand whether these specific markers could provide more information about the prognosis rather than the most common inflammatory markers. For this reason, we compared the concentration of all parameters investigated during 6 months of therapy, including serum calprotectin, that were not tested in healthy participants. The fact that in our study IL-6 and serum calprotectin did not decrease after 1 month of treatment but rather increased significantly at the first follow-up and began to decrease only after 3 and 6 months of treatment suggests that these parameters cannot be considered as such good prognostic markers but rather that they could be useful to evaluate the efficacy of long-term therapy during treatment, offering a current, static indication of the patient's overall condition. Therefore, these markers do not currently provide any additional value to the less-specific markers and scores already used. On the other hand, some authors have observed that freeze-thawing resulted in a higher variability of calprotectin levels in serum than in EDTA plasma, which could be a further cause of variable results.[31]

Probably the most interesting observation in this study was that even though all the patients were enrolled without gastrointestinal symptoms, the high levels of fecal calprotectin found at recruitment suggest that they likely had some subclinical gastrointestinal conditions, possibly because of the concomitant rheumatic disease, indicating a probable involvement of the intestine in the generalized inflammation status of these patients and, consequently, a potential role of fecal calprotectin as a noninvasive marker with "predictive" value of gastrointestinal disease in individuals affected by autoimmune rheumatic illnesses. In fact, because fecal calprotectin increases in patients with inflammatory bowel disease and its concentration in stool correlates with the infiltration of the intestinal mucosa by polymorphonuclear neutrophils and, consequently, with the clinical and histopathological activity of this disease, it can be used to detect subclinical inflammatory gastrointestinal activity in asymptomatic disease.[32,33]

To support our hypothesis, a recent study evaluated the relationship between patients with PsA and fecal calprotectin, showing that it was higher in patients with high skin disease activity and suggesting a potential therapeutic implication of gut inflammation in this kind of pathology.[34] However, it remains to be clarified why the decrease in the fecal calprotectin concentration did not persist after 6 months of therapy but that after this period its concentration seemed to increase again. This apparently contradictory behavior could probably be explained by the fact that at the last control after 6 months, three of the 21 enrolled patients reported that they had discontinued GC and DMARD therapy after the third medical checkup regardless of the therapist's opinion, 2 because of an improvement in painful symptoms, the other one because of the onset of pneumonia. As a result, these patients showed a high increase in serum and fecal calprotectin and in their DAS28-PCR score, with concomitant worsening of painful symptoms. Moreover, 4 of the 18 patients who followed the therapy correctly had a substantial increase in their serum calprotectin concentration at the 6-month medical checkup, referencing a persistent or substantial worsening in joint pain. The *P* value was confirmed as not significant ($P > .05$), also excluding from the calculations the patients who had stopped the therapy.

Our data note that CRP, ESR, and fecal calprotectin had a good correlation with the response to DMARDs and or GC treatment in patients with systemic autoimmune rheumatic disorders and, contrary to what we expected, that serum calprotectin and IL-6 were not good markers of disease improvement after the start of pharmacological treatment. However, to date, IL-6 and serum calprotectin are not routinely available in most clinical laboratories worldwide because the methods currently used for its detection are still not standardized. In any event, the poor significance results of serum calprotectin at the 6-month follow-up need more in-depth studies, involving a larger number of patients, to find an efficient explanation.

Although a weakness of this study is the relatively small sample size of patients, note that they were recruited in a rigorous manner as regards the diagnosis, therapy, and exclusion criteria; however, some confounding factors such as smoking and diet that also may have an important role in the development of inflammatory conditions were not taken into consideration.[12,35]

Conclusion

Certainly, more substantial studies, involving a larger number of individuals and using standardized methods, are needed to confirm our

results and clarify the benefit of the routine use of calprotectin and IL-6 as inflammatory markers for patients affected by inflammatory rheumatic diseases.

REFERENCES

1. Clunie G, Wilkinson N, Nikiphorou E, et al. *Oxford Handbook of Rheumatology*. 4 ed. 2018.
2. Smolen JS, Aletaha D, McInnes IB. Rheumatoid arthritis. *Lancet.* 2016;388(10055):2023–2038.
3. Ramírez J, Narváez JA, Ruiz-Esquide V, et al. Clinical and sonographic biomarkers of structural damage progression in RA patients in clinical remission: a prospective study with 12 months follow-up. *Semin Arthritis Rheum.* 2017;47(3):303–309.
4. Coatels LC, Helliwell P. Psoriatic arthritis: state of the art view. *Clin Med.* 2017;1:65–70.
5. Longo DL, Ritchlin CT, Robert A, et al. Psoriatic arthritis. *N Engl J Med.* 2017;376:957–970.
6. National Health Service. Psoriatric arthritis. https://www.nhs.uk/conditions/psoriatic-arthritis. Accessed July 20, 2021.
7. Linge P, Fortin PR, Lood C, Bengtsson AA, Boilard E. The non-haemostatic role of platelets in systemic lupus erythematosus. *Nat Rev Rheumatol.* 2018;14(4):195–213.
8. Syed KM, Pinals RS. Leukocytosis in rheumatoid arthritis. *J Clin Rheumatol.* 1996;2(4):197–202.
9. Kleina A, Moladb Y. Hematological manifestations among patients with rheumatic diseases. *Acta Haematol.* Published online November 20, 2020. doi: 10.1159/000511759.
10. Sokka T, Pincus T. Erythrocyte sedimentation rate, C-reactive protein, or rheumatoid factor are normal at presentation in 35%–45% of patients with rheumatoid arthritis seen between 1980 and 2004: analyses from Finland and the United States. *J Rheumatol.* 2009;36(7):1387–1390.
11. Pincus T, Gibson KA, Shmerling RH. An evidence-based approach to laboratory tests in usual care of patients with rheumatoid arthritis. *Clin Exp Rheumatol.* 2014;32:S-23–S-28.
12. Nielsen UB, Bruhn LV, Ellingsen T, Stengaard-Pedersen K, Hornung N. Calprotectin in patients with chronic rheumatoid arthritis correlates with disease activity and responsiveness to methotrexate. *Scand J Clin Lab Invest.* 2018;78(1–2):62–67.
13. Youssef P, Roth J, Frosch M, et al. Expression of myeloid related proteins (MRP) 8 and 14 and the MRP8/14 heterodimer in rheumatoid arthritis synovial membrane. *J Rheumatol.* 1999;26(12):2523–2528.
14. Abildtrup M, Kingsley GH, Scott DL. Calprotectin as a biomarker for rheumatoid arthritis: a systematic review. *J Rheumatol.* 2015;42(5):760–770.
15. Jonsson MK, Sundlisæter NP, Nordal HH, et al. Calprotectin as a marker of inflammation in patients with early rheumatoid arthritis. *Ann Rheum Dis.* 2017;76(12):2031–2037.
16. Choi IY, Gerlag DM, Herenius MJ, et al. MRP8/14 serum levels as a strong predictor of response to biological treatments in patients with rheumatoid arthritis. *Ann Rheum Dis.* 2015;74(3):499–505.
17. Chung SJ, Kwon YJ, Park MC, Park YB, Lee SK. The correlation between increased serum concentrations of interleukin-6 family cytokines and disease activity in rheumatoid arthritis patients. *Yonsei Med J.* 2011;52(1):113–120.
18. Gaber W, Azkalany GS, Gheita TA, et al. Clinical significance of serum interleukin-6 and –174 G/C promoter polymorphism in rheumatoid arthritis patients. *Egypt Rheumatol*. 2013;35:107–113.
19. Narazaki M, Tanaka T, Kishimoto T. The role and therapeutic targeting of IL-6 in rheumatoid arthritis. *Expert Rev Clin Immunol.* 2017;13(6):535–551.
20. Gunasekera WMA, Kirwan JR. Rheumatoid arthritis: previously untreated early disease. *BMJ Clin Evid*. 2016;8:1124.
21. van Aken J, Lard LR, le Cessie S, Hazes JM, Breedveld FC, Huizinga TW. Radiological outcome after four years of early versus delayed treatment strategy in patients with recent onset rheumatoid arthritis. *Ann Rheum Dis.* 2004;63(3):274–279.
22. ter Wee MM, den Uyl D, Boers M, et al. Intensive combination treatment regimens, including prednisolone, are effective in treating patients with early rheumatoid arthritis regardless of additional etanercept: 1-year results of the COBRA-light open-label, randomised, non-inferiority trial. *Ann Rheum Dis.* 2015;74(6):1233–1240.
23. Konijn NPC, van Tuyl LHD, Boers M, et al. Similar efficacy and safety of initial COBRA-light and COBRA therapy in rheumatoid arthritis: 4-year results from the COBRA-light trial. *Rheumatology (Oxford).* 2017;56(9):1586–1596.
24. Smole JS, Landewe R, Bijlsma J, et al. EULAR recommendations for the management of rheumatoid arthritis with synthetic and biological disease-modifying antirheumatic drugs: 2016 update. *Ann Rheum Dis.* 2017;76:960–977.
25. Aletaha D, Neogi T, Silman AJ, et al. 2010 rheumatoid arthritis classification criteria: an American College of Rheumatology/European League Against Rheumatism collaborative initiative. *Arthritis Rheum.* 2010;62(9):2569–2581.
26. Prevoo ML, van 't Hof MA, Kuper HH, van Leeuwen MA, van de Putte LB, van Riel PL. Modified disease activity scores that include twenty-eight-joint counts. Development and validation in a prospective longitudinal study of patients with rheumatoid arthritis. *Arthritis Rheum.* 1995;38(1):44–48.
27. Marx A, Backes C, Meese E, Lenhof HP, Keller A. EDISON-WMW: Exact Dynamic Programing Solution of the Wilcoxon-Mann-Whitney test. *Genomics Proteomics Bioinformatics.* 2016;14(1):55–61.
28. van der Heijde DM, van Leeuwen MA, van Riel PL, et al. Biannual radiographic assessments of hands and feet in a three-year prospective followup of patients with early rheumatoid arthritis. *Arthritis Rheum.* 1992;35(1):26–34.
29. Hurnakova J, Hulejova H, Zavada J, et al. Serum calprotectin may reflect inflammatory activity in patients with active rheumatoid arthritis despite normal to low C-reactive protein. *Clin Rheumatol.* 2018;37(8):2055–2062.
30. Felson DT, Smolen JS, Wells G, et al.; American College of Rheumatology; European League Against Rheumatism. American College of Rheumatology/European League Against Rheumatism provisional definition of remission in rheumatoid arthritis for clinical trials. *Arthritis Rheum.* 2011;63(3):573–586.
31. Van Hoovels L, Vander Cruyssen B, Bogaert L, Van den Bremt S, Bossuyt X. Pre-analytical and analytical confounders of serum calprotectin as a biomarker in rheumatoid arthritis. *Clin Chem Lab Med.* 2019;58(1):40–49.
32. Manceau H, Chicha-Cattoir V, Puy H, Peoc'h K. Fecal calprotectin in inflammatory bowel diseases: update and perspectives. *Clin Chem Lab Med.* 2017;55(4):474–483.
33. Schoepfer AM, Beglinger C, Straumann A, et al. Fecal calprotectin correlates more closely with the Simple Endoscopic Score for Crohn's Disease (SES-CD) than CRP, blood leukocytes, and the CDAI. *Am J Gastroenterol.* 2010;105(1):162–169.
34. Adarsh MB, Dogra S, Vaiphei K, Vaishnavi C, Sinha SK, Sharma A. Evaluation of subclinical gut inflammation using faecal calprotectin levels and colonic mucosal biopsy in patients with psoriasis and psoriatic arthritis. *Br J Dermatol.* 2019;181(2):401–402.
35. Ertugrul AS, Sahin H. The effect of smoking on myeloid-related protein-8 and myeloid-related protein-14. *Braz Oral Res*. 2016;30:e51.

Mass Spectrometry–Based Detection of Beta Lactam Hydrolysis Enables Rapid Detection of Beta Lactamase Mediated Antibiotic Resistance

Raymond T. Suhandynata, PhD,[1] Kyle Lund, PhD,[1] Andrés M. Caraballo-Rodríguez, PhD,[2] Sharon L. Reed, MD,[1] Pieter C. Dorrestein, PhD,[2] Robert L. Fitzgerald, PhD,[1] Nicholas J. Bevins, MD, PhD[1,]*

[1]Department of Pathology, UC San Diego Health, San Diego, California, US; [2]Collaborative Mass Spectrometry Innovation Center, Skaggs School of Pharmacy and Pharmaceutical Sciences, University of California, San Diego, La Jolla, California, US; *To whom correspondence should be addressed. nbevins@health.ucsd.edu

Keywords: antibiotic resistance, beta lactamase, ESBL, beta lactam hydrolysis, mass-spectrometry, urinary tract infection, antibiotic resistance testing

Abbreviations: ESBL, extended spectrum beta lactamase; MALDI-TOF, matrix-assisted laser desorption ionization-time of flight; CFU, colony forming unit; DFU, drug-free urine; IS, internal standard; LC, liquid chromatography; MS, mass spectrometry; QTOF, quadrupole time of flight; ACN, acetonitrile; EIC, extracted ion chromatogram; CTX-IS ratio, ceftriaxone-internal standard ratio; CCO, ceftriaxone, cefazolin, oxacillin; UTI, urinary tract infection; RT, room temperature; CDC, Centers for Disease Control and Prevention.

Laboratory Medicine 2022;53:128–137; https://doi.org/10.1093/labmed/lmab068

ABSTRACT

Objective: Antibiotic resistance by beta lactamase expression is a serious and growing threat. We aimed to determine whether beta-lactamase activity is detectable in urine specimens to enable faster identification of resistance.

Methods: Urine specimens from patients with extended spectrum beta lactamase (ESBL)-expressing urinary infections were incubated with beta lactam antibiotics. Beta lactam hydrolysis was determined by mass spectrometry methods.

Results: Ceftriaxone hydrolysis was observed in 45 of 45 ESBL-containing specimens from patients not treated with a beta lactamase inhibitor before specimen collection. Ceftriaxone hydrolysis was not observed in 108 of 108 non-ESBL-containing specimens. Spiking studies show that beta lactam hydrolysis can be observed within 30 minutes. Beta lactam hydrolysis is evidenced by mass spectrometry preceded by either liquid chromatography or matrix-assisted laser desorption ionization specimen processing methods.

Conclusion: Clinically significant beta lactamase activity is detectable directly from urine specimens. The described methods would enable the detection of beta lactam resistance 24 to 48 hours sooner than culture based methods.

The beta lactam class of antibiotics is a key component of the antimicrobial arsenal. The archetypal beta lactam is penicillin, which is naturally derived from penicillium mold and is synthetically manufactured for frequent human use.[1] Since the discovery of penicillin, many other beta lactam antibiotics (all containing a beta lactam ring) have been developed to improve pharmacologic properties (eg, oral availability) and microbicidal properties (eg, targeting a broader spectrum of organisms).[2] This class of antibiotics comprises 19 of 40 spots on the World Health Organization list of essential antibiotics and accounts for more than half of all antibiotics used globally.[2-4]

The beta lactam ring that defines the beta lactam class of drugs mimics the d-alanyl-d-alanine structure that nearly all bacterial species require for the composition of their cell wall.[5] Beta lactam drugs irreversibly bind to cell-wall synthesis enzymes, leading to structural degradation and bacterial death. Resistance to beta lactams can be acquired by 3 mechanisms: (i) mutation of the beta lactam binding enzymes to prevent beta lactam binding, (ii) acquisition of a beta lactam efflux pump that prevents the drugs from entering the cell, and (iii) acquisition of a beta lactamase enzyme that hydrolyzes the beta lactam ring, rendering the molecule ineffective.[6-8] The first 2 mechanisms of resistance are slow to be acquired and have a negative impact on the overall fitness of an organism.[9] In contrast, the acquisition of a beta lactamase enzyme is fast because the gene encoding the enzyme can be transferred between bacteria (even those of different species) and production of the enzyme in sufficient quantities to confer resistance presents minimal metabolic cost to the organism.[6,9]

The evolution and spread of beta lactamase enzymes has led to a substantial health care burden. The rise and spread of extended spectrum beta lactamase (ESBL)-expressing *Enterobacteriaceae* have led to approx-

imately 197,400 infections, 9,100 deaths, and $1.2 billion in estimated attributable health care costs annually in the United States.[10,11] New beta lactamase enzymes are continuing to emerge and spread, presenting a serious public health threat.[12,13]

The typical workflow in a clinical microbiology laboratory leading to identification of antibiotic-resistant organisms consists of (1) specimen plating and mixed growth, (ii) pathogen isolation and growth, (iii) identification of the organism by biochemical tests or matrix-assisted laser desorption ionization-time of flight (MALDI-TOF), and (iv) observed growth in antibiotic-containing media to determine antibiotic susceptibility/resistance patterns.[14-17] This workflow requires 36 to 72 hours, involves multiple manual steps, and may not detect inducible resistance.[18] While awaiting results, most patients are empirically treated, and when susceptibility results are available the treatment strategy is adjusted.[19] Inevitable delays in providing appropriate antibiotic treatment lead to higher patient morbidity and mortality and contribute to the spread of resistant organisms.[20,21]

Given the clinical challenges that beta lactamase expressing pathogens present, there is a clear need for faster identification to both enable effective treatment and enact isolation precautions preventing the further spread of resistant organisms. Resistant bacteria typically express high levels of beta lactamase to effectively counteract therapeutic doses of beta lactam antibiotics.[22] We sought to determine whether beta lactamase activity could be sensitively and specifically detected in unprocessed clinical specimens to quickly (within hours) detect the presence of beta lactamase expressing organisms. Our approach used mass spectrometry to show beta lactamase activity directly in biological specimens by measuring the hydrolysis of target antibiotics through the disappearance of protonated molecular ions in the presence of resistant organisms.

Methods

Specimen Preparation

Residual urine specimens collected during routine clinical care were used for this study. The study was approved by the University of California, San Diego Institutional Review Board with a waiver of informed consent (protocol number 181656XL).

Urine specimens were collected in Becton Dickinson Biosciences vacutainer culture and susceptibility preservative tubes containing 2.63 mg/mL boric acid, 3.95 mg/mL sodium borate, and 1.65 mg/mL sodium formate to prevent bacterial overgrowth (Becton, Dickinson, and Company, Franklin Lakes, NJ) as part of routine clinical practice. All specimens tested were excess clinical specimens stored at 4°C for 7 days or less. Colony forming units (CFUs) were determined by colony counting after the application of specimens using a 0.001-mL loop. Specimens were centrifuged and reconstituted in drug-free urine (DFU) to remove preservatives, which inhibit hydrolysis activity. Next, 400 µL of the specimen was centrifuged at 21,000 g in a fixed-angle rotor for 10 minutes in 1.7 mL Eppendorf tubes. After centrifugation, the supernatant was aspirated off using an air-displacement pipette and discarded. The aspiration of supernatant was conducted in such a manner as to leave behind any pellet, regardless of whether it as visible to the naked eye. Next, 200 µL of certified DFU (UTAK Catalog #88121-CDF) containing 500 µg/mL of ceftriaxone was added to each specimen and mixed by vortexing for 1 minute. Specimens were then incubated at 37°C for at least 4 hours. After incubation, specimens were centrifuged at 13,000 g in a fixed-angle rotor for 5 minutes. In addition, 100 µL of the supernatant was diluted using 300 µL of 95% deionized H_2O, 5% methanol containing internal standard (IS; 50 ng/mL amphetamine-d5). Isotopically labeled beta lactam was not used as an internal standard to prevent (i) ESBL-mediated hydrolysis of the internal standard or (ii) an internal standard acting as an inhibitor of ESBL-mediated hydrolysis. Finally, 20 µL of the diluted specimen was injected using a full-loop injection on a liquid chromatography (LC) quadrupole TOF mass spectrometer (MS) system (Waters ultra performance liquid chromatography, Waters Xevo quadrupole time-of-flight [QTOF]).

For multidrug analysis, specimen preparation was performed as above with the exception that specimens were incubated for 12 hours at 37°C and that 200 µL of certified DFU containing 500 µg/mL of each drug (ceftriaxone, cefazolin, and oxacillin or ceftriaxone, cefazolin, oxacillin, and meropenem) was added to each specimen. The kinetics of ceftriaxone hydrolysis and identification of its hydrolysis products were performed as stated above, with the exception that certified DFU containing 300 µg/mL of ceftriaxone was used. Incubation times were 5 minutes, 30 minutes, and 20 hours, with specimens being immediately injected into the LC-MS system after centrifugation and specimen dilution.

LC

For ceftriaxone analysis, LC was performed using a Waters BEH-C18 column (1.7 µm) on a Waters Acquity UPLC system. Mobile phase A was 5 mM ammonium formate, 0.1% formic acid, and 99.9% deionized H_2O (buffer A). Mobile phase B was 0.1% formic acid and 99.9% acetonitrile (ACN). The LC method spanned a total of 8 minutes and is described in Supplemental Table 1. Specimens were injected using an autosampler with a full loop injection of 20 µL.

For multidrug analysis (ceftriaxone, cefazolin, oxacillin, meropenem), LC was performed with the same buffers, column, and injection parameters as above. The LC method spanned a total of 8 minutes and is described in Supplementary Table 1.

For ceftriaxone hydrolysis product analysis, LC was performed with the same buffers, column, and injection parameters as above. The LC method spanned a total of 15 minutes and is described in Supplementary Table 1.

QTOF-MS

Data for MS were acquired on a Waters Xevo G2 TOF MS. Mass spectra were acquired in a scanning mode across an m/z range (50–900 m/z) at a rate of 1 scan per 0.5 seconds in continuum mode. The total MS method spanned 6.5 minutes and was run in positive polarity with the analyzer in sensitivity mode. Electrospray ionization was used as the ionization method with a cone voltage of 25 volts and a fixed collision energy value of 6 volts.

Qualitative Matrix Interference Studies

Qualitative assessment of matrix interference was performed by injecting 5 unspiked ESBL-containing urine specimens and 5 unspiked ESBL-negative urine specimens while simultaneously infusing a solution containing 50 µg/mL of ceftriaxone reconstituted in 50% ACN:50% deionized H_2O.

Extracted ion chromatograms (EICs) of ceftriaxone were overlaid with the expected ceftriaxone peak for all 10 patient urine specimens.

MALDI-TOF

MALDI-TOF MS was performed on a Bruker Microflex MALDI-TOF mass spectrometer equipped with an N2 laser. Spectra were acquired in reflectron-positive mode, with 100 μm raster spot and roughly 80% laser power, 200 shots (random walk, 20 shots) detection gain 40×, and a range of 100–1000 m/z. Specimens were prepared as above and mixed 1:1 with 10 mg/mL α-cyano-4-hydroxycinnamic acid. Using the dried drop method, 2 μL of the mixture was spotted on a Bruker MSP 96 target ground steel plate. Calibration was performed using a ceftriaxone standard at 555.0533 m/z before data acquisition.

MS Data Processing

The LC-MS data were processed in MassLynx (Waters) using the integration parameters described in Supplemental Table 2. All traces were smoothed with 1 iteration using the mean of 2 adjacent scans. The MALDI-TOF data were processed using Flex Analysis 4.2 (Bruker Daltronics). Peak areas described throughout are measured in arbitrary units correlated to the quantity of ions colliding with the ion detector.

Data Analysis and Graphing

Data analysis was performed with R studio (rstudio.com). Graphs were created using the ggplot function within the tidyverse package (cran.r-project.org/web/packages/tidyverse).

Results

Hydrolysis of Ceftriaxone in Urine Specimens

The ESBL hydrolysis of ceftriaxone was evaluated by examining EICs of ceftriaxone (500 μg/mL) and IS in DFU (control) after 4 hours of incubation at 37°C in the presence or absence of an ESBL-containing patient urine specimen (**FIGURE 1**). In DFU alone, peak areas of ceftriaxone and IS were 76,484 and 4,073, respectively. However, a discernible ceftriaxone peak was not observed after incubation with an ESBL, whereas a similar peak area for the IS was observed (4,957). It is clear when comparing **FIGURE 1A** with **FIGURE 1B** that ceftriaxone was hydrolyzed by the ESBL-containing specimen because the protonated molecular ion of ceftriaxone is not discernible in **FIGURE 1B**. The IS is easily seen in both **FIGURE 1A** and **1B** and helps rule out a matrix effect that could potentially suppress the ceftriaxone signal in **FIGURE 1B**. Boxplots illustrating the median ratios of ceftriaxone area counts and IS area counts (CTX/IS ratio) after incubation with DFU, ESBL-containing patient specimens, ESBL-containing specimens from patients treated with a beta lactamase inhibitor (tazobactam or meropenem), and non-ESBL-containing patient specimens are shown in **FIGURE 1C**. Strikingly, there was at least a 10-fold difference in the median CTX/IS ratio between ESBL-containing specimens and specimens lacking ESBL activity. A cutoff of the CTX/IS of anywhere between 0.77 and 5.4 would allow perfect discrimination. To confirm the discriminatory utility of the hydrolysis assay, we tested 94 specimens in a blinded manner (**FIGURE 1D**). Two specimens showed clear evidence of hydrolysis (filled arrow), and these 2 specimens were confirmed to contain ESBLs.

During a 12-month period from December 2019 to December 2020, the University of California, San Diego Clinical Microbiology Laboratory performed 37,731 urine cultures. Of these cultures, gram negative rods were observed in 11,560 (30.6%). In addition, ESBL-expressing organisms were observed in 1,283 cultures (3.4% of total cultures, 11.2% of gram negative rods). All ESBL-expressing organisms were gram negative rods: 987 (76.9%) were *Escherichia coli,* 280 (21.8%) were *Klebsiella pneumoniae,* and 16 (1.3%) were *Klebsiella oxytoca*. Thus, our finding that 2 out of 94 culture specimens contained ESBL organisms is consistent with the overall prevalence of ESBLs in our institution's tested population.

Discrimination between ESBL- and non-ESBL-containing specimens was robust under conditions intended to simulate decreased analytical sensitivity or detect potential interferences. The robust identification of ESBL-containing specimens was also apparent when data were analyzed at unit resolution (Supplemental Figure 1), simulating the performance of an instrument with lower mass accuracy. To determine whether bacterial overgrowth or matrix effects could lead to false positives or false negatives, 5 specimens with ESBL and 5 specimens without ESBL, all with visible turbidity and/or discoloration, were analyzed on 5 nonconsecutive days in both a qualitative and a quantitative matrix effect study. The CTX/IS ratios were separated by at least an order of magnitude on all days, although some degradation of hydrolysis activity was observed (Supplemental Figure 2). An infusion of 50 μg/mL of ceftriaxone performed during an injection of urine specimens from the same set of 10 specimens revealed no significant ion suppression or enhancement across the ceftriaxone peak observed (Supplementary Figure 3).

Collective Hydrolysis of Ceftriaxone, Cefazolin, and Oxacillin in Urine Specimens

To show the generalizability of our approach, we looked for ESBL hydrolysis of a mixture of 3 beta lactam antibiotics (ceftriaxone, cefazolin, oxacillin [CCO]) by observing the EICs of ceftriaxone (500 μg/mL), cefazolin (500 μ g/mL), and oxacillin (500 μ g/mL), and the EIC of the IS in DFU were evaluated after 12 hours of incubation at 37°C, in the presence or absence of an ESBL (**FIGURE 2**). As expected, robust peak areas for the molecular ions corresponding to ceftriaxone (99,907), cefazolin (66,619), oxacillin (36,612), and IS (2,511) were observed in the absence of an ESBL (**FIGURE 2A**). Except for the IS, these peaks disappeared after incubation with an ESBL-containing specimen, indicating robust hydrolysis of all 3 beta lactam antibiotics (**FIGURE 2B**). Boxplots illustrating the median ratios of ceftriaxone/IS, cefazolin/IS, and oxacillin/IS after incubation with (n = 10) or without (n = 3) an ESBL-containing specimen are shown in **FIGURE 2C**. As seen with the hydrolysis of ceftriaxone alone, there was at least a 10-fold difference in the median ratios between ESBL-containing specimens and specimens lacking ESBL activity for the CCO mixture, with all beta lactam antibiotics being hydrolyzed in a similar fashion.

CCO Hydrolysis Inhibited by Meropenem in Noncultured Urine Specimens

Because a subpopulation of patients with suspected urinary tract infections (UTIs) take antibiotics or inhibitors that prevent ESBL activity, we monitored the hydrolysis of a CCO mixture in the presence of meropenem. The EICs for the protonated molecular ions of CCO, meropenem, and IS are shown in DFU after 12 hours of incubation at 37°C (**FIGURE 3A**). Peak areas of ceftriaxone (500 μg/mL), cefazolin

FIGURE 1. Evaluation of ESBL Hydrolysis of Ceftriaxone: (A) EICs of the protonated molecular ions (exact m/z) of ceftriaxone (*top*) and IS (*bottom*) after 4 hours of incubation with a sample not containing an extended spectrum beta lactamase (-ESBL) expressing pathogen. (B) EICs of the protonated molecular ions of ceftriaxone (*top*) and IS (*bottom*) after 4 hours of incubation with an ESBL containing specimen (+ESBL). Expected retention times for each compound are indicated to illustrate the loss of a peak. % ion intensity (indicated at top left of each EIC) is plotted on the Y-axis and Time (min) is plotted on the X-axis. (C) Boxplots of median ratios of ceftriaxone/IS after incubation with: Control DFU –drug free urine (n = 12), ESBL containing urine specimens (n = 45), ESBL containing urine specimens from patients receiving beta-lactamase inhibitor treatment (n = 6), and non-ESBL containing specimens (n = 108). Wilcoxon P-values are displayed. (D) Scatterplot illustrating ratios of ceftriaxone/IS plotted on log scale for 94 random urine culture specimens after incubation. Closed arrow indicates two samples with ESBL identified by urine culture and susceptibility assays. Open arrow indicates a non-ESBL containing specimen.

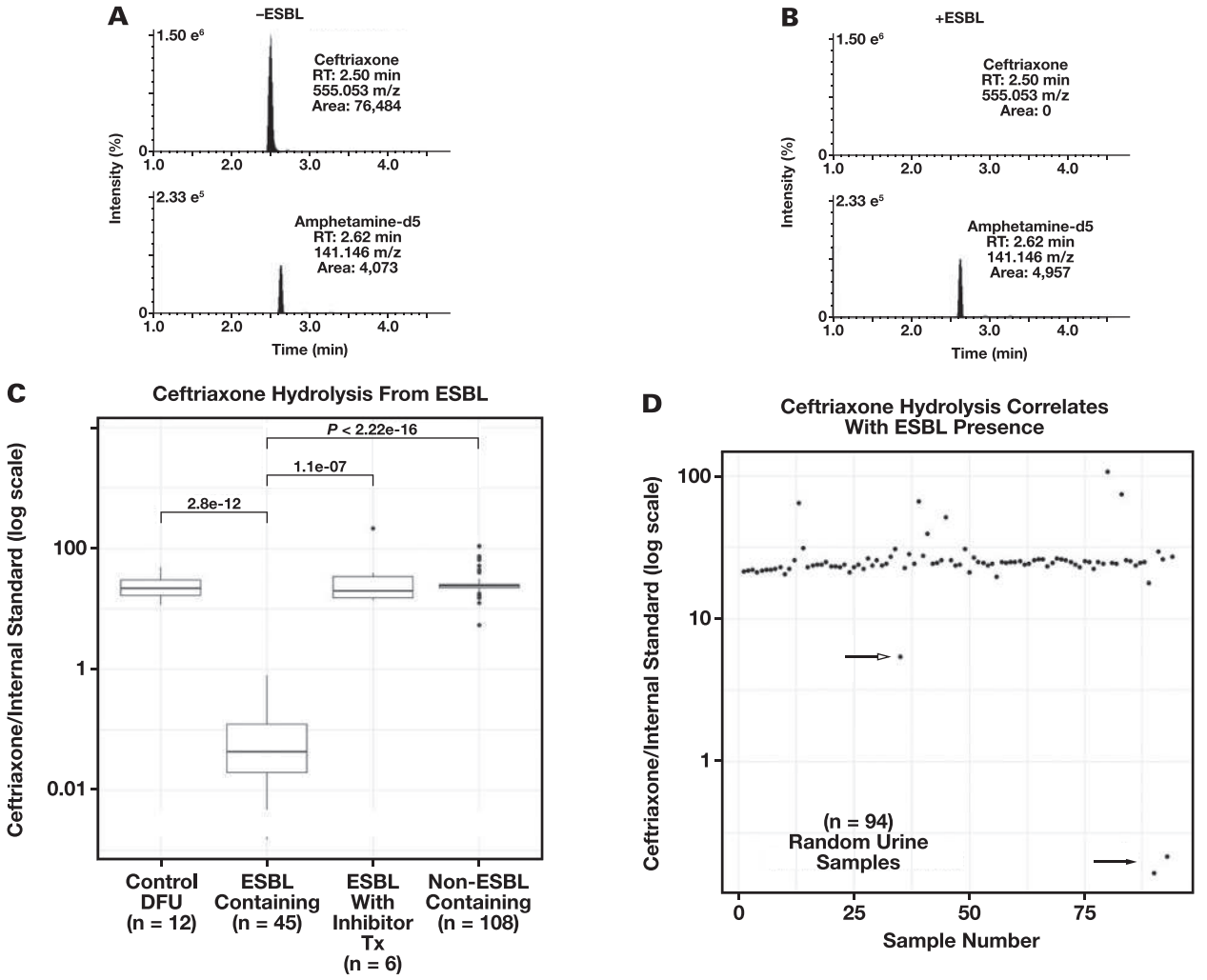

(500 µg/mL), oxacillin (500 µg/mL), meropenem (500 µg/mL), and IS were 87,072; 66,190; 28,882; 225,280; and 1,524, respectively. As expected, these peak areas were essentially unchanged after a parallel incubation with an ESBL-containing specimen, indicating that meropenem inhibits the ESBL hydrolysis of CCO (**FIGURE 3B**). Boxplots illustrating the median ratios of ceftriaxone/IS, cefazolin/IS, oxacillin/IS, and meropenem/IS after incubation with (n = 10) or without (n = 3) an ESBL-containing specimen are shown in **FIGURE 3C**.

Kinetics of ESBL Ceftriaxone Hydrolysis and Identification of Hydrolysis Products

The kinetics of ceftriaxone hydrolysis by ESBL-containing specimens was evaluated by incubating ceftriaxone in the presence or absence of an ESBL-containing specimen for 5 minutes and 30 minutes at room temperature (RT). At the 5-minute time point, ceftriaxone peak areas were 15,166 in the absence of an ESBL and 10,574 in the presence of an ESBL (**FIGURE 4A**), an approximate 30% reduction in raw area counts. Hydrolysis was essentially complete by the 30-minute time point; the ceftriaxone peak area was 15,391 in the absence of an ESBL and was not observed in the presence of an ESBL (**FIGURE 4B**). The correlation of the CTX/IS ratios with the CFUs of the specimens showed no correlation (Supplemental Figure 4), suggesting that hydrolysis kinetics were substrate limited.

The presence of a ceftriaxone hydrolysis product was evaluated by monitoring the EICs of the protonated molecular ion of ceftriaxone after the loss of its triazine-ylthiol group (414.05 m/z).[23] In the presence of an ESBL, a peak at 3.41 minutes was observed with an integrated area

FIGURE 2. **Evaluation of ESBL Hydrolysis of CCO: (A) EICs of the protonated molecular ions of ceftriaxone, cefazolin, oxacillin, and IS are shown after incubation with a sample not containing extended spectrum beta lactamase (-ESBL) expressing pathogen. Exact m/z of the protonated molecular ion for each compound is indicated. (B) EICs of the protonated molecular ions of ceftriaxone, cefazolin, oxacillin, and IS are shown after incubation with a sample containing an ESBL containing specimen (-ESBL). Expected retention times of the protonated molecular ions for each compound are indicated to illustrate the loss of a peak. % ion intensity (indicated at top left of each EIC) is plotted on the Y-axis and Time (min) is plotted on the X-axis. (C) Boxplots plotted on a log scale of individual median ratios of CCO/IS after incubation with: Control DFU –drug free urine (n = 3) or ESBL containing urine specimens (n = 10). Dotted line indicates a ceftriaxone/IS ratio of 1.**

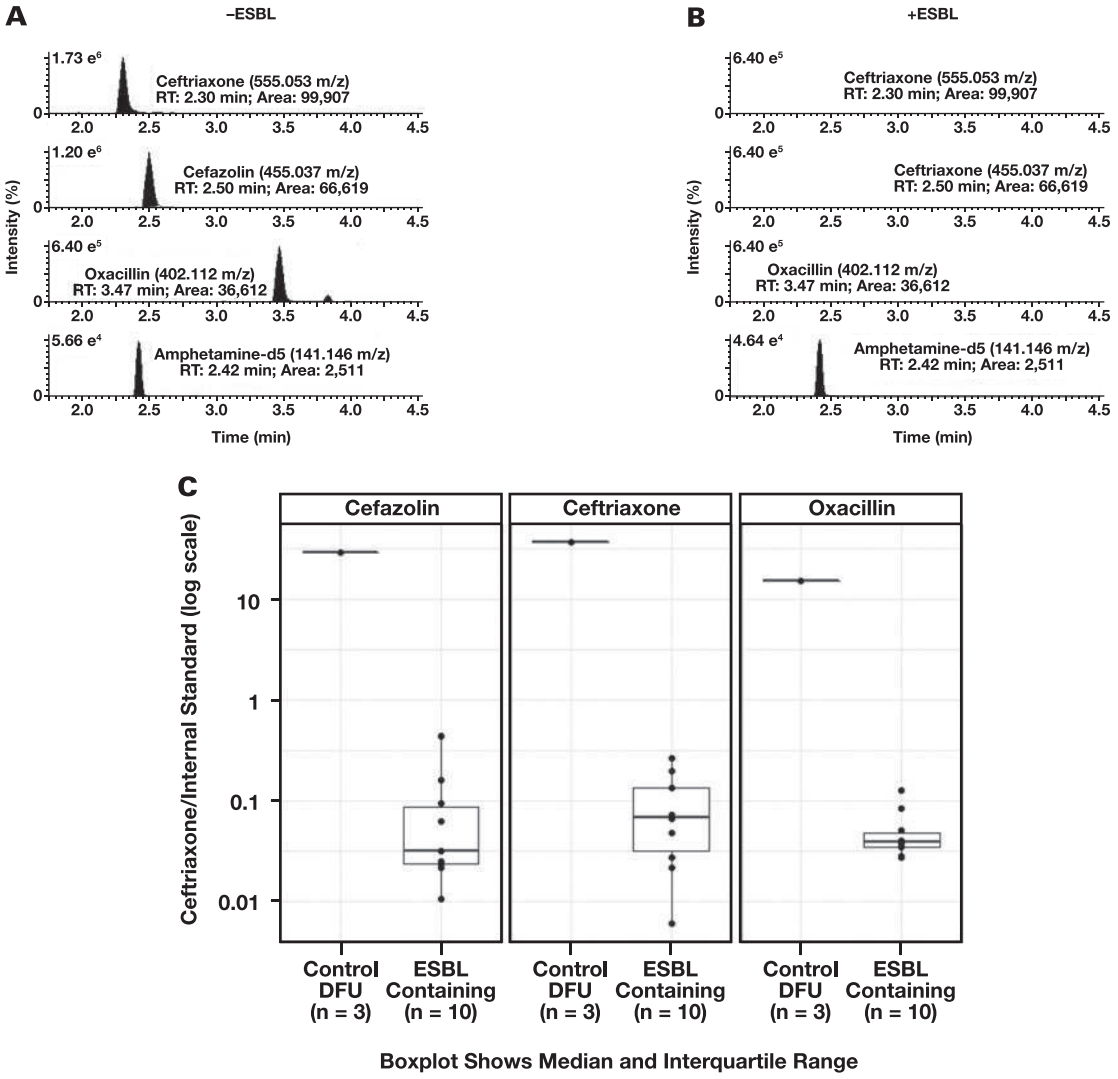

of 858. After 30 minutes, the peak at 3.41 minutes had an increased peak area of 1247 (**FIGURE 4D**). This peak was no longer observed after a 20-hour incubation at RT (Supplemental Figure 5), indicating that this hydrolysis product was likely unstable and unsuitable for end-point analysis.

Monitoring of Ceftriaxone Hydrolysis by MALDI-TOF MS

Because many clinical microbiology laboratories are equipped with MALDI-TOF MS instruments, we evaluated ceftriaxone hydrolysis using a Bruker Microflex MALDI-TOF MS (**FIGURE 5**). Using the same specimen preparation used for LC-MS analysis, the protonated molecular ion of ceftriaxone was clearly observed at 555.0533 m/z in both the control and ESBL-negative specimens (**FIGURE 5A** and **5B**). In contrast, this peak was absent in the ESBL-positive specimens, indicating ceftriaxone hydrolysis by ESBL (**FIGURE 5C**). Boxplots representing the median area counts for the protonated molecular ion of ceftriaxone are shown for controls (n = 2), ESBL-containing specimens (n = 14), ESBL-containing specimens from patients treated with a beta lactamase inhibitor (n = 1), and non-ESBL-containing specimens (n = 13; **FIGURE 5D**). The median ceftriaxone area counts for the controls, ESBL positives from patients treated with a beta lactamase inhibitor, and ESBL-negative specimens were at least 100-fold greater than the median area counts observed in ESBL-positive specimens.

Discussion

The evolution and spread of antibiotic resistance among human pathogens represents a serious public health threat.[11] Faster identifi-

FIGURE 3. **Meropenem Inhibits ESBL CCO Hydrolysis: (A) EICs of the protonated molecular ions of ceftriaxone, cefazolin, oxacillin, meropenem and IS are shown after incubation with a sample not containing extended spectrum beta lactamase (-ESBL) expressing pathogen. Exact m/z of the protonated molecular ion for each compound is indicated. (B) EICs of the protonated molecular ions of ceftriaxone, cefazolin, oxacillin, meropenem, and IS are shown after incubation with a sample containing an ESBL containing specimen (-ESBL). Expected retention times of the protonated molecular ions for each compound are indicated to illustrate the loss of a peak. % ion intensity (indicated at top left of each EIC) is plotted on the Y-axis and Time (min) is plotted on the X-axis. (C) Boxplots plotted on a log scale of individual median ratios of CCO and meropenem/IS after incubation with: Control DFU –drug free urine (n = 3) or ESBL containing urine specimens (n = 10).**

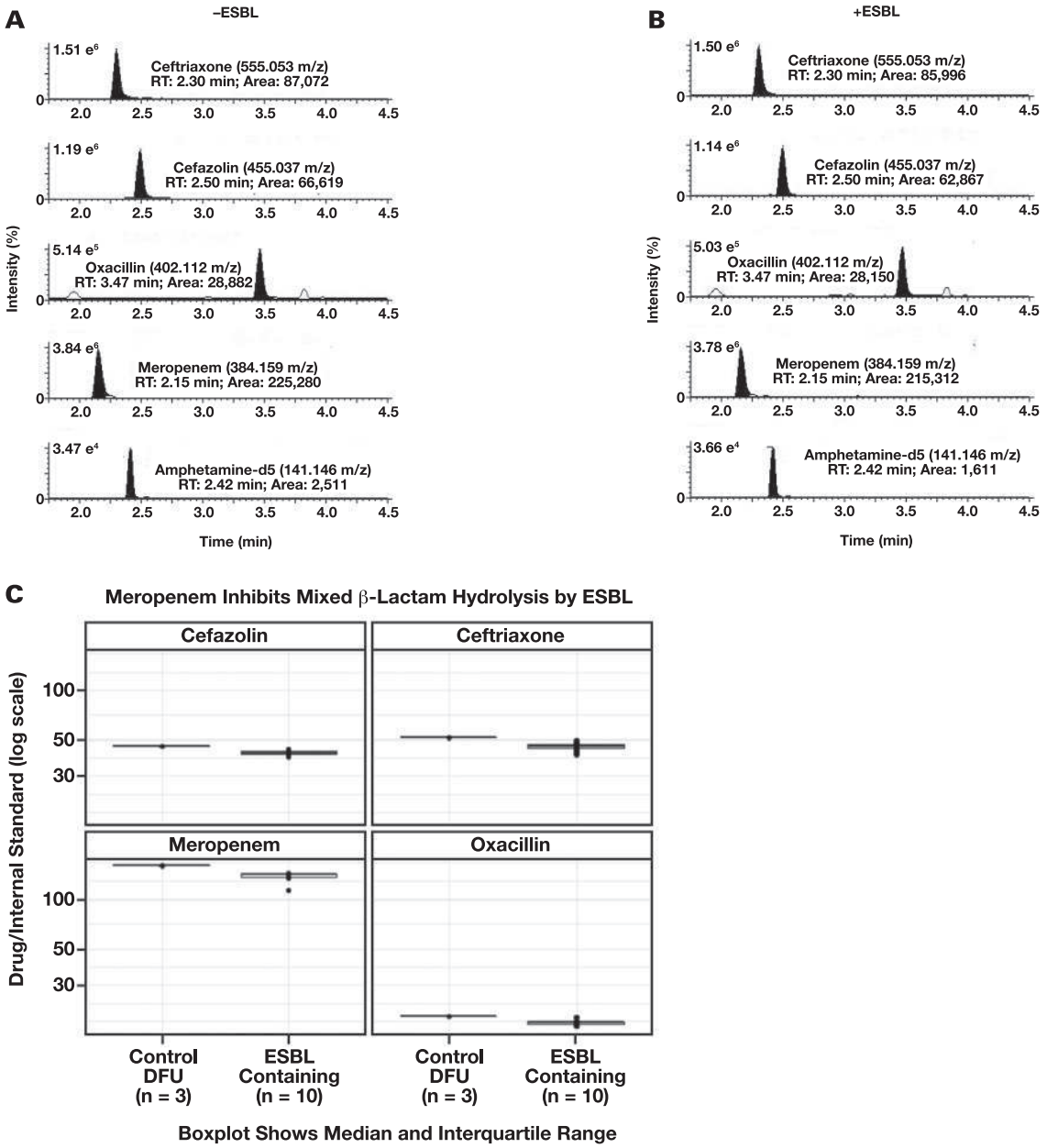

cation of the presence of antibiotic-resistant organisms is a key component in the effort to reduce the spread of antibiotic resistance, as evidenced by the inclusion of diagnostic development in the Centers for Disease Control and Prevention's (CDC) national strategy to combat antibiotic resistance.[24] Our findings indicate that beta lactamase activity from resistant organisms can be detected in clinical urine specimens. This finding enables a diagnostic strategy that could provide same-day detection of beta lactamase expressing organisms as compared with the several days required for traditional culture and susceptibility methods.

Same-day identification of beta lactamase expressing organisms could provide both clinical and infection control benefits. Timely treatment with effective antibiotics leads to improved clinical outcomes and decreased costs for individual patients.[25] Infection control measures for patients with antibiotic-resistant organisms (eg, use of personal protective equipment) can prevent the nosocomial spread of resistant infections

FIGURE 4. **Kinetics of Ceftriaxone Hydrolysis: Peak intensity of ceftriaxone after 5 minutes (A) and 30 minutes (B) of incubation with (+ESBL) or without (-ESBL) an ESBL containing specimen. The predicted hydrolysis product due to the loss of the ceftriaxone's triazine-ylthiol group at 414.05 m/z (RT: 3.40 min) appears after 5 minutes (C) and 30 minutes (D) of incubation only in the presence of ESBL expressing bacteria. % ion intensity (indicated at top left of each EIC) is plotted on the Y-axis and Time (min) is plotted on the X-axis.**

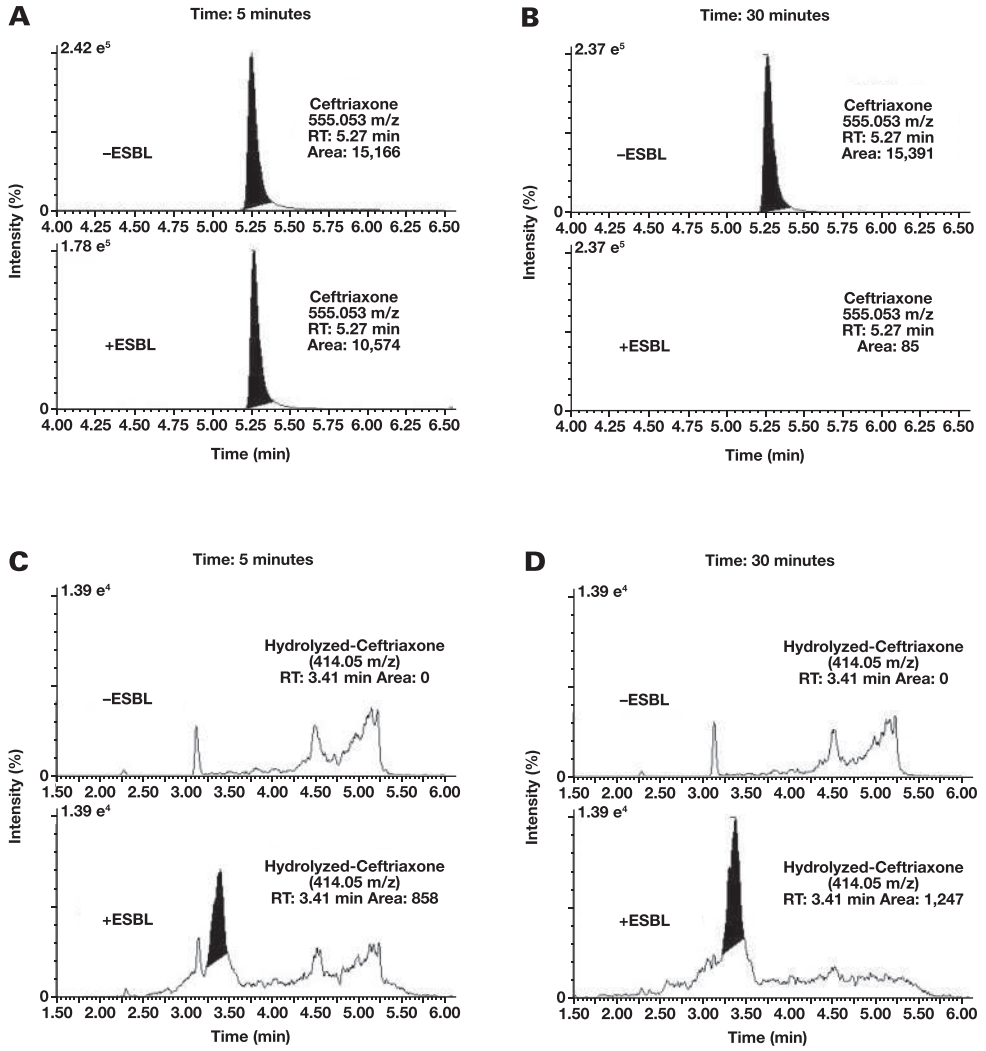

if implemented in a timely manner.[26] In addition, our method may be useful for public health or agricultural monitoring for ESBL.[27] Our data, and that from other centers, suggest that ESBL-expressing organisms account for 3% to 23% of all UTIs and are likely to increase as antibiotic resistance spreads.[24,28-30] According to chart reviews of our small and randomly selected population of ESBL-expressing *E. coli* UTIs, 6 of 34 patients were empirically treated with ineffective cephalosporins (ceftriaxone or cefazolin). These patients may have had shorter lengths of infection had they been treated with effective antibiotics earlier. Furthermore, ESBL-expressing *E. coli* was discovered in one of these patients 48 hours after being discharged to a long-term care facility with an ineffective oral antibiotic regimen, a scenario associated with the continued spread of antibiotic-resistant organisms. Consistent with our findings, an observational study of hospitalized patients with ESBL pyelonephritis showed that ~65% of patients received ineffective antibiotic coverage.[31] Direct detection of ESBL activity in urine specimens could be used to rule out empirical treatment for Gram-negative UTIs (eg, ceftriaxone or cefazolin).

Significant effort has gone into the detection of antibiotic-resistant organisms given the clinical need for faster identification. Primarily, breakthroughs have occurred in identifying the sequence of the genes responsible for resistance.[32,33] Specifically, molecular identification of the *mecA* gene creating methicillin-resistant *Staphylococcus aureus* has shown clinical utility.[34] However, the diversity of known beta lactamase genes (hundreds have been identified) and the emergence of novel genes limits the utility of this approach.[32,33] Identification of ESBL enzyme activity from clinical specimens utilizing a chromogenic substrate has shown promise, but the reagents necessary are not readily available.[35,36]

Our findings show, for the first time, that the activity of ESBL enzyme present in a centrifuged urine specimen is sufficient for robust detection, using LC-MS, before the required culture and isolation of pathogenic organisms. Such direct detection of beta lactamase activity enables the fast detection of resistance in clinical scenarios involving other pathogens, clinical specimens, or beta lactam drugs. For example, detecting the presence of carbapenemase activity in sputum specimens

FIGURE 5. **Evaluation of Ceftriaxone hydrolysis by MALDI-TOF MS. Protonated molecular ion of ceftriaxone after incubation with DFU (n = 2) (A), patient specimens (n = 8) without an ESBL (B), and patient specimens with an ESBL (n = 14) (C). The expected m/z of the protonated ceftriaxone molecular ion (555.0533 m/z) is indicated in each plot with a dotted line and each plot is shown using the same X and Y axis scale. (D) Box plots of the median area counts of ceftriaxone after incubation with DFU, ESBL +, ESBL + w/Inhibitor Treatment, and ESBL – specimens as measured by MALDI-TOF MS. Whiskers are up to but no greater than 1.5 times the inter-quartile range.**

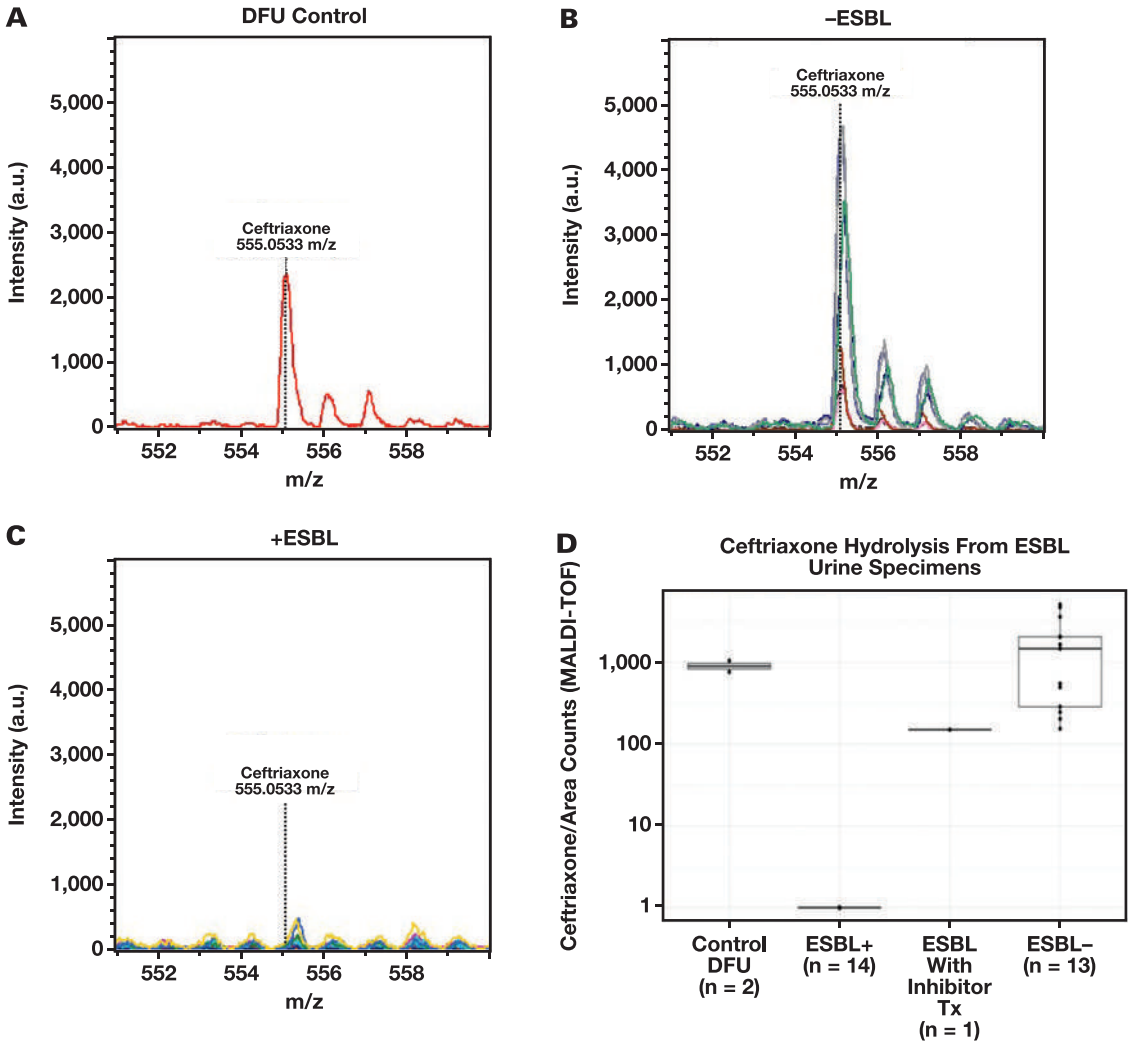

from patients with suspected *Acinetobacter* infections could indicate the presence of carbapenemase expressing *Acinetobacter* infections, another class of antibiotic-resistant organisms classified as an urgent threat by the CDC.[11] Additional studies need to be conducted to show that direct detection of beta lactamase activity could be used to differentiate a pathogenic infection from non-disease-causing colonization with a resistant organism, a common diagnostic challenge.[37]

Our data was primarily generated using LC-based separation methods followed by MS detection of parent beta lactam ions because of analytical sensitivity and ease of data interpretation. Because we did not rely on high-resolution data for identifying beta lactamase activity, this technique is generalizable to LC combined with most quadrupole mass spectrometers. In addition, we have shown that beta lactamase detection can be performed using MALDI techniques. The MALDI-TOF technology is utilized for organism identification in many clinical microbiology laboratories. Notably, the specific instrument type and matrix we used for our experiments is the same as those used for clinical specimens in our institution's microbiology laboratory. The ready availability of both quadrupole and MALDI-TOF technology in clinical laboratories would enable the utilization of our described diagnostic approach with minimal additional instrumentation required.

Clinically administered beta lactamase inhibitors are a potential interferent of the described diagnostic strategy. As we observed, patients who received tazobactam or meropenem before specimen collection did not have appreciable beta lactamase activity in their urine. It should be noted that specimens intended for microbiology testing are ideally collected from patients before they receive treatment because antibiotics can also interfere with most culture, identification, and susceptibility testing methods. Thus, the potential for interference in the described method of beta lactamase activity assessment would not present an excessive burden compared to standard methods. Both tazobactam and meropenem have been shown to inhibit beta lactamase activity in vitro.[38,39]

Conclusion

Further development (eg, identifying optimal buffers and matrices, and the most stable hydrolysis products) of the described diagnostic strategy will be needed to improve turnaround time, which could be reduced to 30 minutes or less based on estimates of beta lactamase enzyme kinetics.[40] Larger studies including unique clinical scenarios must be performed to understand sensitivity, specificity, optimal cutoffs, and concordance with traditional culture and susceptibility analysis for relevant pathogen, specimen, and antibiotic combinations.

Supplementary Data

Supplemental figures and tables can be found in the online version of this article at www.labmedicine.com.

Acknowledgments

We sincerely thank the staff of the clinical microbiology laboratory for assistance with data and specimen acquisition, especially Olympia Alverez and Janet Stagnaro.

This work was primarily funded using laboratory discretionary funds. A.M.C.R. and P.C.D. were supported by the National Science Foundation grant IOS-1656481 and National Institutes of Health grant number 1DP2GM137413-01. P.C.D. was supported by the Gordon and Betty Moore Foundation through grant GBMF7622 and the National Institutes of Health (P41 GM103484, R03 CA211211, R01 GM107550).

Raymond Suhandynata, Robert Fitzgerald, and Nicholas Bevins are listed as coinventors on a provisional patent application involving this work.

REFERENCES

1. Zaffiri L, Gardner J, Toledo-Pereyra LH. History of antibiotics. From salvarsan to cephalosporins. *J Invest Surg.* 2012;25(2):67–77.
2. Bush K, Bradford PA. β-Lactams and β-lactamase inhibitors: an overview. *Cold Spring Harb Perspect Med.* 2016;6(8):a025247.
3. Elander RP. Industrial production of beta-lactam antibiotics. *Appl Microbiol Biotechnol.* 2003;61(5–6):385–392.
4. Wirtz VJ, Hogerzeil HV, Gray AL, et al. Essential medicines for universal health coverage. *Lancet.* 2017;389(10067):403–476.
5. Yocum RR, Rasmussen JR, Strominger JL. The mechanism of action of penicillin. Penicillin acylates the active site of Bacillus stearothermophilus D-alanine carboxypeptidase. *J Biol Chem.* 1980;255(9):3977–3986.
6. Essack SY. The development of beta-lactam antibiotics in response to the evolution of beta-lactamases. *Pharm Res.* 2001;18(10):1391–1399.
7. Fani F, Leprohon P, Zhanel GG, Bergeron MG, Ouellette M. Genomic analyses of DNA transformation and penicillin resistance in Streptococcus pneumoniae clinical isolates. *Antimicrob Agents Chemother.* 2014;58(3):1397–1403.
8. Fuda CC, Fisher JF, Mobashery S. Beta-lactam resistance in Staphylococcus aureus: the adaptive resistance of a plastic genome. *Cell Mol Life Sci.* 2005;62(22):2617–2633.
9. Autiero I, Costantini S, Colonna G. Modeling of the bacterial mechanism of methicillin-resistance by a systems biology approach. *PLoS One.* 2009;4(7):e6226.
10. Jernigan JA, Hatfield KM, Wolford H, et al. Multidrug-resistant bacterial infections in U.S. hospitalized patients, 2012–2017. *N Engl J Med.* 2020;382:1309–1319.
11. Centers for Disease Control and Prevention. *Antibiotic resistance threats in the United States, 2019*. https://www.cdc.gov/drugresistance/pdf/threats-report/2019-ar-threats-report-508.pdf. Accessed July 21, 2021.
12. De Angelis G, Del Giacomo P, Posteraro B, Sanguinetti M, Tumbarello M. Molecular mechanisms, epidemiology, and clinical importance of β-lactam resistance in Enterobacteriaceae. *Int J Mol Sci.* 2020;21(14):5090.
13. Pitout JDD, Peirano G, Kock MM, Strydom KA, Matsumura Y. The global ascendency of OXA-48-type carbapenemases. *Clin Microbiol Rev.* 2019;33(1):e00102-19.
14. Processing, isolation, detection, and interpretation of aerobic bacteriology cultures. In: Leber AL, ed. *Clinical Microbiology Procedures Handbook*. Vol. 1–3, 4th ed. American Society for Microbiology; 2016: 3.3.1.1–3.3.2.15.
15. Beta-lactamase tests. In: Leber AL, ed. *Clinical Microbiology Procedures Handbook*. Vol. 1–3, 4th ed. American Society for Microbiology; 2016: 5.5.1–5.5.8.
16. Extended-spectrum beta-lactamase testing for Escherichia coli, Klebsiella pneumoniae, Klebsiella oxytoca, and Proteus mirabilis. In: Leber AL, ed. *Clinical Microbiology Procedures Handbook*. Vol. 1–3, 4th ed. American Society for Microbiology; 2016: 5.12.1–5.12.7.
17. Minimum bactericidal concentration testing. In: Leber AL, ed. *Clinical Microbiology Procedures Handbook*. Vol. 1–3, 4th ed. American Society for Microbiology; 2016: 5.14.1.1–5.14.3.6.
18. Harada S, Ishii Y, Yamaguchi K. Extended-spectrum β-lactamases: implications for the clinical laboratory and therapy. *Korean J Lab Med.* 2008;28(6):401–412.
19. Leekha S, Terrell CL, Edson RS. General principles of antimicrobial therapy. *Mayo Clin Proc.* 2011;86(2):156–167.
20. Bengtsson-Palme J, Kristiansson E, Larsson DGJ. Environmental factors influencing the development and spread of antibiotic resistance. *FEMS Microbiol Rev.* 2018;42(1):fux053.
21. San Millan A. Evolution of plasmid-mediated antibiotic resistance in the clinical context. *Trends Microbiol.* 2018;26(12):978–985.
22. Livermore DM. Beta-lactamases: quantity and resistance. *Clin Microbiol Infect.* 1997;3(Suppl 4):S10–S19.
23. Oviaño M, Gómara M, Barba MJ, Revillo MJ, Barbeyto LP, Bou G. Towards the early detection of β-lactamase-producing Enterobacteriaceae by MALDI-TOF MS analysis. *J Antimicrob Chemother.* 2017;72(8):2259–2262.
24. Centers for Disease Control and Prevention. U.S. action to combat antibiotic resistance: a national priority. https://www.cdc.gov/drugresistance/us-activities.html. AccessedJuly 21, 2021.
25. Bonine NG, Berger A, Altincatal A, et al. Impact of delayed appropriate antibiotic therapy on patient outcomes by antibiotic resistance status from serious Gram-negative bacterial infections. *Am J Med Sci.* 2019;357(2):103–110.
26. Kluytmans-van den Bergh MFQ, Bruijning-Verhagen PCJ, Vandenbroucke-Grauls CMJE, et al.; SoM Study Group. Contact precautions in single-bed or multiple-bed rooms for patients with extended-spectrum β-lactamase-producing Enterobacteriaceae in Dutch hospitals: a cluster-randomised, crossover, non-inferiority study. *Lancet Infect Dis.* 2019;19(10):1069–1079.
27. Kim YA, Kim H, Seo YH, Park GE, Lee H, Lee K. Prevalence and molecular epidemiology of extended-spectrum-β-lactamase (ESBL)-producing Escherichia coli from multiple sectors of the swine

industry in Korea: a Korean nationwide monitoring program for a one health approach to combat antimicrobial resistance. *Ann Lab Med.* 2021;41(3):285–292.

28. Flokas ME, Detsis M, Alevizakos M, Mylonakis E. Prevalence of ESBL-producing Enterobacteriaceae in paediatric urinary tract infections: a systematic review and meta-analysis. *J Infect.* 2016;73(6):547–557.
29. Lee DS, Lee CB, Lee SJ. Prevalence and risk factors for extended spectrum beta-lactamase-producing uropathogens in patients with urinary tract infection. *Korean J Urol.* 2010;51(7):492–497.
30. Baek YJ, Kim YA, Kim D, et al. Risk factors for extended-spectrum-β-lactamase-producing Escherichia coli in community-onset bloodstream infection: impact on long-term care hospitals in Korea. *Ann Lab Med.* 2021;41(5):455–462.
31. Talan DA, Takhar SS, Krishnadasan A, et al. Fluoroquinolone-resistant and extended-spectrum β-lactamase-producing Escherichia coli infections in patients with pyelonephritis, United States. *Emerg Infect Dis.* 2016;22(9):1594–1603.
32. De Angelis G, Grossi A, Menchinelli G, Boccia S, Sanguinetti M, Posteraro B. Rapid molecular tests for detection of antimicrobial resistance determinants in Gram-negative organisms from positive blood cultures: a systematic review and meta-analysis. *Clin Microbiol Infect.* 2020;26(3):271–280.
33. Burnham CD, Leeds J, Nordmann P, O'Grady J, Patel J. Diagnosing antimicrobial resistance. *Nat Rev Microbiol.* 2017;15(11):697–703.
34. Hiramatsu K, Ito T, Tsubakishita S, et al. Genomic basis for methicillin resistance in Staphylococcus aureus. *Infect Chemother.* 2013;45(2):117–136.
35. Gallah S, Decré D, Genel N, Arlet G. The β-lacta test for direct detection of extended-spectrum-β-lactamase-producing Enterobacteriaceae in urine. *J Clin Microbiol.* 2014;52(10):3792–3794.
36. Nordmann P, Dortet L, Poirel L. Rapid detection of extended-spectrum-β-lactamase-producing Enterobacteriaceae. *J Clin Microbiol.* 2012;50(9):3016–3022.
37. Bajaj P, Singh NS, Virdi JS. Escherichia coli β-lactamases: what really matters. *Front Microbiol.* 2016;7:417.
38. Bonomo RA, Rudin SA, Shlaes DM. Tazobactam is a potent inactivator of selected inhibitor-resistant class A beta-lactamases. *FEMS Microbiol Lett.* 1997;148(1):59–62.
39. Nukaga M, Bethel CR, Thomson JM, et al. Inhibition of class A beta-lactamases by carbapenems: crystallographic observation of two conformations of meropenem in SHV-1. *J Am Chem Soc.* 2008;130(38):12656–12662.
40. Page MG. Extended-spectrum beta-lactamases: structure and kinetic mechanism. *Clin Microbiol Infect.* 2008;14(Suppl 1):63–74.

Accurate Quantification of Monoclonal Immunoglobulins Migrating in the Beta Region on Protein Electrophoresis

Nivin Omar, MD,[1] Kiran Madwani, MD,[1] Pramila Moideen, MD,[1] David M. Manthei, MD, PhD,[2] David F. Keren, MD,[2] Gurmukh Singh, MD, PhD, MBA[1,]*

Department of Pathology; [1]Medical College of Georgia at Augusta University, Augusta, Georgia, and; [2]University of Michigan, Ann Arbor, Michigan; *To whom correspondence should be addressed. gurmukhsinghmdphd@yahoo.com

Keywords: clinical pathology, clinical chemistry, immunology, immunopathology, monoclonal gammopathy, light chain–predominant multiple myeloma

Abbreviations: MGUS, monoclonal gammopathy of undetermined significance; SMM, smoldering/asymptomatic multiple myeloma; MM, plasma cell/multiple myeloma; Ig, immunoglobulin; LCPMM, light chain–predominant multiple myeloma; SFLC, serum free light chain; SPEP, serum protein electrophoresis; CE, capillary electrophoresis; ISUB, immunosubtraction; IMWG, International Myeloma Working Group; MASS FIX, immunoglobulin enrichment coupled with MALDI-TOF mass spectrometry; SIFE, serum protein immunofixation

Laboratory Medicine 2022;53:138–144; https://doi.org/10.1093/labmed/lmab055

ABSTRACT

Background: The concentration of monoclonal immunoglobulins (Igs) in neoplastic monoclonal gammopathic manifestations is generally measured by densitometric scanning of the monoclonal peaks on gel or by measuring absorbance at 210 nm in capillary electrophoresis (CE). For monoclonal Igs migrating in the beta region, measurement is complicated by the major beta-region proteins, namely, transferrin and C3.

Methods: C3 interference in densitometry was eliminated by heat treatment of serum, and monoclonal Igs were quantified by densitometry of the residual band. The immunochemical measurement of transferrin was converted to its equivalent densitometric quantity. For monoclonal Ig migrating with transferrin, the contribution of the latter was removed by subtracting the converted transferrin concentration from the combined densitometric quantification of the band. With CE, monoclonal Ig was measured by using immunosubtraction (ISUB) to guide demarcation.

Results: The results obtained using the C3 depletion and transferrin subtraction method were lower and yet comparable to the results derived from using CE measurement guided by ISUB. As we expected, the results from both methods were lower than those derived from a perpendicular drop measurement of the peak or via nephelometric assay of the involved isotype.

Discussion: Accurate measurement of monoclonal Igs is important for the diagnosis and monitoring of monoclonal gammopathic manifestations. Determination of serum free light chain concentration per gram of monoclonal Ig is an essential measure for the diagnosis of light chain–predominant multiple myeloma. The method described herein improves accuracy of measurements for monoclonal Igs migrating in the beta region, without the need for special reagents or equipment.

The diagnosis of monoclonal gammopathy of undetermined significance (MGUS), smoldering/asymptomatic multiple myeloma (SMM), and plasma cell/multiple myeloma (MM) is based, partly, on the serum concentration of monoclonal immunoglobulin (Ig).[1–6] For light chain–predominant multiple myeloma (LCPMM), a newly described variant of MM, diagnosis is based partly on the involved serum free light chain (SFLC) concentration per gram of intact monoclonal Ig.[7] LCPMM constitutes approximately 18% of total intact Ig-producing MM and has an adverse prognosis.[7] Accurate measurement of beta-region monoclonal Igs is essential for correct diagnosis of LCPMM and was the impetus for this investigation. Beyond the initial diagnosis, accurate determination of the concentration of monoclonal Igs is essential for monitoring the course of disease in these neoplastic monoclonal gammopathic manifestations.[6]

The concentration of monoclonal Ig is generally determined by densitometric scanning of the peak observed on serum protein electrophoresis (SPEP). This measurement is affected by many factors, including variations in dye binding by different proteins, the background of polyclonal Igs, and interference by other normal proteins, especially in the case of monoclonal Igs migrating outside the gamma region.[8,9] Differences in gel-based protein and capillary electrophoresis (CE), use of perpendicular drop or tangent skimming, and the subjectivity of demarcation all compound variability in measurements of monoclonal-Ig concentration.[8,9] Within a laboratory, the densitometric measurement of monoclonal Igs in the gamma region is generally reliable and provides clinically useful results, although these variables do not permit easy comparison of results among laboratories.[9]

A fraction of the monoclonal Igs, usually IgA in particular, migrate in the beta region, where the monoclonal peak may overlap the native transferrin and/or C3 bands. In rare instances, monoclonal Igs migrate in the alpha region; however, for the purpose of this research, we restricted ourselves to improving the accuracy of measurement of monoclonal Ig migrating in the beta region.

CE may be used with immunosubtraction (ISUB) for identification of monoclonal Igs. Also, CE with ISUB allows estimation of the protein concentration specific to monoclonal Ig versus the contribution by background Igs and other normal proteins, such as transferrin and C3.[8]

Because normal beta-region components interfere with measurement of beta-migrating monoclonal Igs, the International Myeloma Working Group (IMWG) recommended using immunochemical determination of total IgA to follow patients with IgA monoclonal Igs migrating in the beta region.[10] Because this measurement includes polyclonal IgA and the monoclonal molecules, the use of Hevylite measurements has been proposed to decrease interference from polyclonal IgA molecules of the uninvolved light-chain isotype.[11] However, as with assays for SFLC, the Hevylite method is not specific for monoclonal Igs.[11–13]

Despite the appeal of this method, it has not been adopted by the laboratory community, partly because the method provides little advantage over measuring total IgA.[14] A more recent assay, MASS FIX (Ig enrichment coupled with MALDI-TOF mass spectrometry), may provide better estimation of monoclonal Ig, as and when it is configured to provide quantitative results. However, it is available from only 1 reference laboratory. Also, given the need for special reagents, equipment, and expertise, the method may be suitable only for high-volume reference laboratories.[15]

For improving the accuracy of measurement of monoclonal Igs migrating in the beta region, we considered the following processes: ISUB of transferrin and C3 proteins; heat degradation of C3 followed by densitometric measurement of residual band in case of monoclonal Ig comigrating with C3; subtraction of transferrin and/or C3 protein concentration, as determined by immunochemical measurement, from the densitometric concentration of the combined band; and a combination of these techniques.

Methods

This study was performed on 32 serum specimens available after routine testing performed at a tertiary-care, medical school–affiliated medical center in the southeastern United States. The protocol was reviewed and approved by the institutional review board. SPEP, serum protein immunofixation (SIFE), and densitometric measurements were conducted using the SPIFE Touch instrument from Helena Laboratories Corporation, as described earlier in the literature.[16,17]

CE was carried out at the University of Michigan. Deidentified specimens were submitted for ISUB quantification of monoclonal Igs migrating in the beta region based on gel electrophoresis. Serum specimens were analyzed according to manufacturer recommendations on a CAPILLARYS 2 Flex Piercing instrument (Sebia SA) using PROTEIN(E) and IMMUNOTYPING programs for CE and ISUB, respectively. Total serum protein concentrations were used in determining monoclonal-protein concentrations by CE, and total Ig levels were used to select the appropriate ISUB parameters. Determining the concentration of monoclonal protein was estimated by perpendicular drop or tangent skim methods on the CE, based on which method better estimated the output of the ISUB, as determined by 2 independent pathologist interpretations.[8]

Heat inactivation of C3: C3 is a labile protein that degrades at room temperature storage for a few days. Initially, inactivation of C3 was performed by heating serum at 56°C. Due to degradation of Igs and other proteins in these conditions, serum specimens were incubated at 37°C for 24 hours.

Immunochemical measurement of transferrin: We compared immunochemical and densitometric measurements of transferrin concentration in specimens without monoclonal immunoglobulins in the beta region. Transferrin was quantified by routine immunoassay using Beckman-Coulter Inc. AU 5800 equipment. Also, concentration of transferrin was estimated by densitometric measurement of the beta 1 band on SPEP. Immunochemical measurements of transferrin were converted to their densitometric equivalent by using the regression equation presented in the Results section of this article. This derived value was subtracted from the combined, densitometric protein concentration of monoclonal Igs and transferrin, in cases of monoclonal Igs migrating in the beta 1 position. In cases of monoclonal Ig overlapping the C3 and transferrin bands, a combination of the 2 processes was used.

We attempted ISUB of transferrin by incubation of serum with antiserum to human transferrin. We tried 2 antiserum concentrations: 10 µL of serum plus 10 µL saline plus 10 µL antiserum, and 10 µL serum plus 50 µL antiserum. The mixtures were incubated overnight at 4°C and centrifuged at 16,600*g* for 5 minutes before protein electrophoresis.[18]

Heat inactivation of C3 was sufficiently effective in eliminating the interference by C3. Therefore, we did not attempt antibody-mediated immune elimination for C3 or subtraction of immunochemically determined concentration of C3.

Results

In 20 of 32 cases, the monoclonal Ig overlapped C3; in 10 of 32 cases, it overlapped the transferrin band; and in 2 cases, the monoclonal Ig overlapped both bands. In 21 of 32 cases, CE results determined that the quantity of monoclonal Ig was less than 1.0 g/dL.

Heat inactivation of C3: Heat treatment of normal serum at 56°C for 30 minutes eliminated the C3 peak/band on SPEP (**FIGURE 1**). However, this treatment denatured other proteins, including Igs, particularly monoclonal IgM and monoclonal IgG and IgA when present at higher concentrations (**FIGURE 2**). Therefore, we used only 37°C treatment for elimination of interference by C3. Incubation of serum with monoclonal Igs comigrating with C3 at 37°C for 24 hours yielded mainly monoclonal Igs on SPEP. The peak/band specific to the monoclonal Ig was measured by perpendicular drop of the densitometric scan. Heat treatment, especially at 37°C, did not transform the C3 mobility area to the baseline becuase other proteins, including other complement components and normal Igs, also migrate in the same region. Data showing pre–heat treatment concentration of monoclonal Ig, along with C3 and post-treatment concentration of monoclonal Ig, as well as total concentration of involved Igs, are presented in **TABLE 1**. Similarly, densitometric quantification of beta 1 peaks before correction for transferrin levels are also included in the pretreatment values.

Immunosubtraction of transferrin: ISUB of transferrin with antibody specific to transferrin was unsuccessful. At the concentrations used, the antibody not only failed to deplete transferrin but also interfered with

FIGURE 1. Normal serum specimens from 2 patients were subjected to serum protein electrophoresis (SPEP) in their native state, after 56°C treatment for 30 minutes and incubation at 37°C for 24 hours. Both treatments eliminated the peak due to C3 at the beta 2 position. However, treatment at 56°C induced more artefacts than 37°C treatment. A small residual peak at the C3 site in specimens treated at 37°C could be complement that did not get degraded or it could be due to other proteins present at the same location. The lack of such a small peak in 56°C-treated specimens could be due to denaturation of the other proteins normally present in that location.

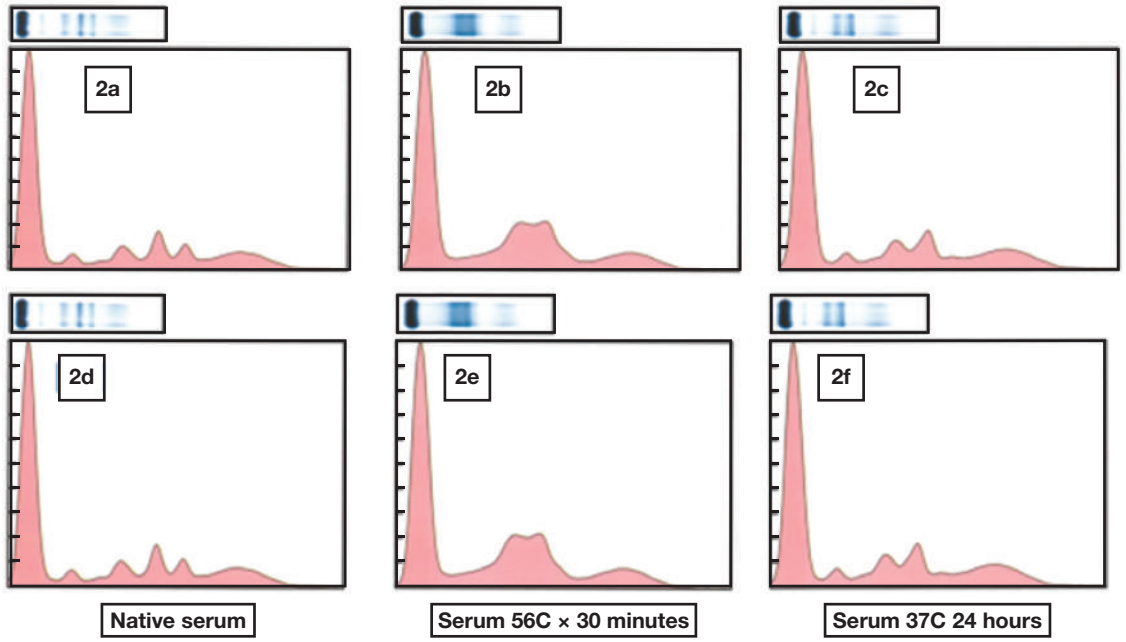

FIGURE 2. Scans of serum protein electrophoresis (SPEP). Serum specimens from 2 patients with monoclonal immunoglobulins (Igs) in the beta 2 location were subjected to heat treatment at 56°C and 37°C, respectively. Although treatment at 56°C was effective in eliminating the C3 peak/band, it caused distortion of monoclonal Ig bands and was replaced by incubation of the specimens at 37°C for 24 hours. The estimate of monoclonal Ig in 56°C specimens was markedly lower than that for 37°C treatment. Arrows indicate the monoclonal Ig peak. A, Untreated serum specimen showing monoclonal Ig and C3 at beta 2 site. B, Serum specimen treated at 56°C showing residual peak at beta 2 site. C, Serum specimen treated at 37°C showing residual peak at beta 2 site. D, Untreated serum specimen showing monoclonal Ig and C3 at beta 2 site. E, Serum specimen treated at 56°C showing residual peak at beta 2 site. F, Serum specimen treated at 37°C showing residual peak at beta 2 site.

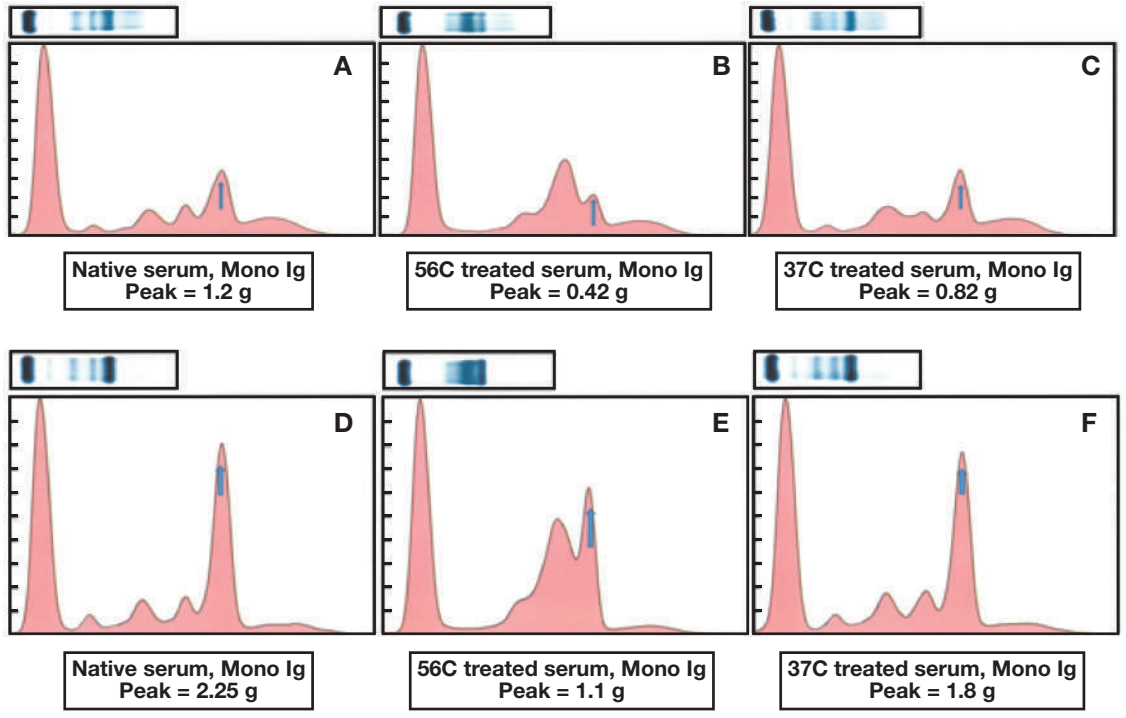

2022;53;138–144 | https://doi.org/10.1093/labmed/lmab055

monoclonal Ig measurement due to the addition of reagent antibody. ISUB of transferrin did not yield satisfactory results, so we did not pursue it further.

Comparison of the immunochemical measurement of transferrin and densitometric quantification of the protein is shown in **FIGURE 3**. To adjust for the difference in the values of transferrin by immunochemical measurement, compared with densitometric scanning of the beta 1 band, a regression analysis of the 2 values yielded the following equation when immunochemical measurement was designated as the independent measurement: Y = 0.77848X + 0.08914. The correlation coefficient for the 2 methods is 0.73. Densitometric measurement results were approximately 11% higher than those obtained by immunochemical quantification. This difference was statistically significant by the Student t test ($P = .02$).

The results for monoclonal immunoglobulins migrating in a beta 2 position were estimated by perpendicular drop on the densitometric scan of the band/spike after C3 depletion by heat treatment. The immunochemically measured transferrin values were converted to their densitometric equivalent by using the equation given earlier herein. This value was subtracted from the densitometric scan–measured concentration of beta 1 migrating monoclonal Igs. These values will be collectively referred to as *beta-depleted values*.

TABLE 1. Comparison of CE with Beta Region Measurement Before and After Depletion of C3 and Transferrin[a]

Specimen ID	M Protein	Beta Site[b]	g/dL			
			CE Quant[c]	Beta dep[d]	Beta Pre-dep[e]	Total Involved Ig[f]
1	IgG kappa	2	0.1	0.13	0.33	1.25
2	IgA kappa	1	0.1	0.12	0.35	0.31
3	IgM lambda	2	0.1	0.086	0.34	0.34
4	IgA kappa	1	0.1	0.18	0.23	0.28
5	IgG kappa	1	0.8	0.96	1.11	1.86
6	IgA lambda	2	0.5	0.18	0.26	0.34
7	IgA lambda	2	0.3	0.19	0.36	0.46
8	IgG lambda	2	2.3	1.8	2.25	2.83
9	IgA kappa	2	0.2	0.3	0.85	0.54
10	IgA kappa	1	0.1	0.07	0.33	0.28
11	IgA kappa	2	0.5	0.31	0.58	0.88
12	IgG kappa	2	0.1	0.19	0.24	0.79
13	IgG kappa	2	2.7	2.04	2.11	2.5
14	IgA kappa	1	0.2	0.26	0.44	1.45
15	IgA kappa	2	0.4	0.32	0.39	0.42
16	IgA lambda	1	0.1	0.11	0.26	0.18
17	Ig A kappa	2	0.1	0.17	0.22	0.25
18	IgM kappa	2	5	3.4	3.8	6.4
19	IgG lambda	2	2.8	1.9	2	2.9
20	IgA kappa	1	1.2	0.54	1.24	1.5
21	IgA kappa	2	1.3	1.4	1.54	2.12
22	IgG lambda	2	1.1	0.82	1.19	2.53
23	IgA lambda	1	0.1	0.11	0.23	0.06
24	IgA kappa	1	0.6	0.59	1.27	0.99
25	IgA lambda	1	0.3	0.18	0.33	0.49
26	IgA lambda	2	0.1	0.17	0.3	0.31
27	IgG lambda	2	3.1	2.39	2.7	3.49
28	IgA kappa	2	0.1	0.17	0.28	0.34
29	IgA lambda	2	3.6	2.53	2.63	3.4
30	IgA lambda	2	0.5	0.43	0.45	1.01
31	IgA kappa	Both	1.1	0.93	1.2	1.08
32	IgA kappa	Both	2	1.76	2.03	2.26

CE, capillary electrophoresis; Ig, immunoglobulin; ISUB, immunosubtraction.
[a]The results of beta depletion are insignificantly lower than those measured via by CE (P = .43) the correlation coefficient between the 2 methods is 0.98.
[b]Beta site: Beta 1 or beta 2 location of the monoclonal immunoglobulin peak based on gel electrophoresis and which correction technique was utilized. In 2 cases the monoclonal immunoglobulin overlapped C3 and transferrin, and both corrections were applied to these specimens.
*[c]CE quant: CE measurement of M protein based on ISUB pattern (for example, see **FIGURE 4**).*
[d]Beta dep: Beta measurement results after C3 and/or transferrin depletion.
[e]Beta Pre-dep: Densitometric quantity of beta peak measurement before C3 or transferrin depletion.
[f]Total Involved Ig: Nephelometric measurement of the involved isotype (IgG, IgA, or IgM).

FIGURE 3. Plot of results of immunochemical measurement of transferrin (X-axis) and densitometric readings of the beta 1 band (Y-axis) on serum protein electrophoreses of specimens without monoclonal immunoglobulins in the beta region. The trend line and regression equation for estimating densitometric equivalent of immunochemical measurement of transferrin are displayed. The correlation coefficient is 0.73. AQ18

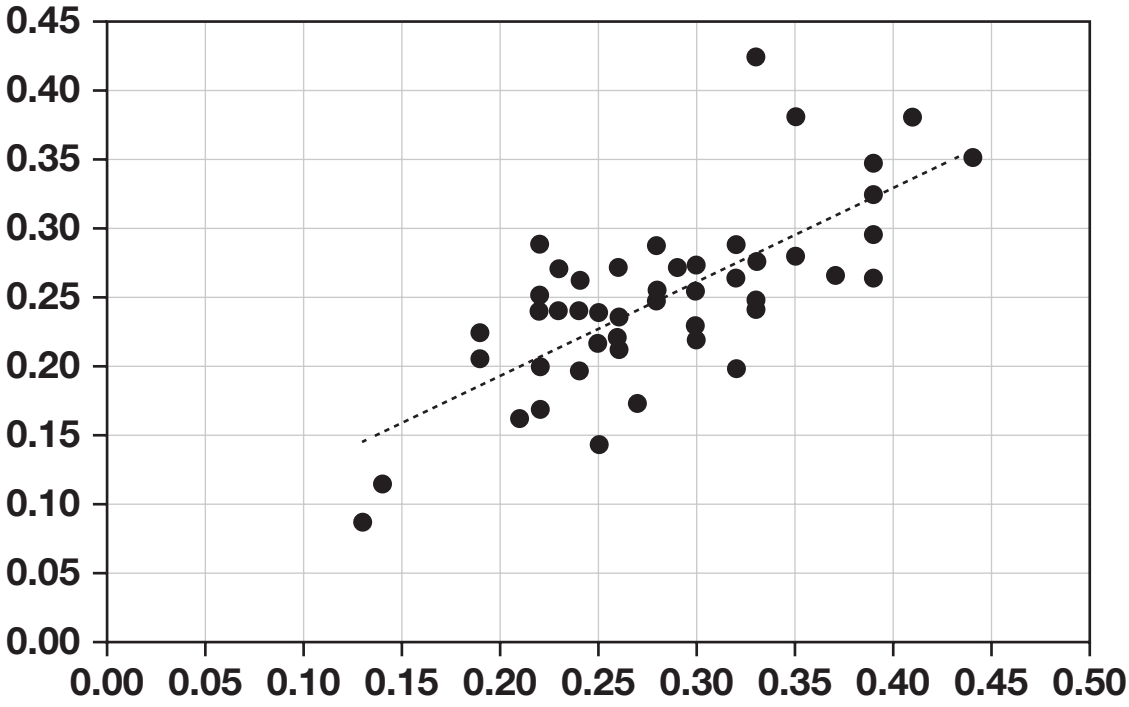

Measurement of the beta-migrating M-protein was performed by CE using the results from the ISUB to guide the demarcation positions (**FIGURE 4**). Results of CE estimation of the beta-migrating monoclonal Igs are included in **TABLE 1**. Compared with CE results, the results from beta depletion were lower, but the difference was statistically nonsignificant (P = .43). As expected, the results from CE and beta depletion were, on average, lower than those estimated by densitometric scanning of the monoclonal band/spike in native serum and the concentration of involved Ig (**TABLE 1**).

Discussion

Accurate determination of the concentrations of monoclonal Igs is important in distinguishing between the diagnosis of MGUS and SMM, and in establishing a baseline level of the M-spike for patients with MM.[2,4] This information is critical for monitoring the change in the concentration of monoclonal Igs in response to treatment and for monitoring the course of treatment in MM.[19] In a given patient, the concentration of the monoclonal Igs reflects the tumor burden and is a valid tumor marker.[19,20] The monoclonal Igs migrating in the gamma region can be quantified reasonably well by densitometric scanning. Variations in marking the area occupied by the monoclonal peak affect the quantification and has been addressed elsewhere.[8,9] The major factors affecting the accuracy of quantification of monoclonal Igs in the gamma region are the non-neoplastic background Igs. The latter issue is further aggravated by the polyclonal increase in background Igs and oligoclonal pattern, as observed in patients treated with hematopoietic stem-cell transplants.[6,21]

Quantification of monoclonal Igs migrating in the beta region is more significantly impacted by other proteins and Igs migrating in the same location. Normal IgA, IgM, and IgG all exhibit migration in the beta region to varying degrees, with IgA being the dominant Ig in the beta region.[22] The primary non-Ig proteins are transferrin and C3. When SPEP is performed in gels capable of resolving the beta 1 and beta 2 proteins, transferrin results in an easily recognizable band in the beta 1 region, and C3 produces a recognizable peak in the beta 2 region. Both of these proteins can be quantified by densitometric scanning, although immunoassays are generally used for measurement of these proteins. Other, lower concentration proteins migrating in the beta region include C4, C5, and factor B components of the complement system, antithrombin 3, and hemopexin.[22] None of these proteins result in a measureable band on usual SPEP.[23]

Quantification of monoclonal Igs in the beta region may be approximated by measuring the total amount of involved Igs, measuring Hevylite combination of relevant heavy and light chains, and using ISUB to guide measurement by CE.[24] Although the latter helps to exclude nonmonoclonal proteins, it is subjective and not in common use, as more laboratories employ gel-based assays for SPEP and SIFE.[14] MASS-FIX has not yet been adopted in routine clinical practice.

The method described in this article approximates the results obtained by CE with ISUB without the need for special equipment and reagents. In general, densitometric measurement of the peak produced by monoclonal Igs, even when it includes normal beta-region proteins, is generally suitable for monitoring the progress of a patient.[6] However, more accurate measurement of beta-migrating monoclonal Igs is essential for diagnosis of patients with LCPMM, a subgroup with a higher risk of renal damage and shorter survival than patients with typical MM.[7] Thus, accurate estimation of the quantity of monoclonal Igs migrating in the beta region acquires greater importance. The concentration of intact monoclonal Ig in

FIGURE 4. Immunosubtraction (ISUB) and capillary electrophoresis (CE) tangent skim measurement of involved isotype: ISUB and monoclonal protein estimation by CE. An example of monoclonal protein identification and size determination is shown for specimen 24, which by perpendicular drop measured via gel electrophoresis is 1.27 g/dL before removal of C3 and transferrin but corrects to 0.59 g/dL after removal matching the CE measurement of 0.6 g/dL. A, ISUB in gamma depletion. B, ISUB in kappa depletion. C, ISUB in alpha depletion. D, ISUB in lambda depletion. E, ISUB in mu depletion. The correspondingly labeled component is diminished in the blue tracing, compared with the black baseline tracing. The dominant monoclonal protein in the beta region is subtracted by immunoglobulin (Ig)A and kappa (arrows in parts B and C), yet shows a baseline even with the IgA and kappa subtracted. This visualization is used to guide estimation of the area on CE by the tangent skim method for measurement (F). If a perpendicular drop had been were used, the estimate would rise from 0.6 g/dL to 0.8 g/dL. Two small free kappa bands also are present at the cathodal end of the gamma region in part F.

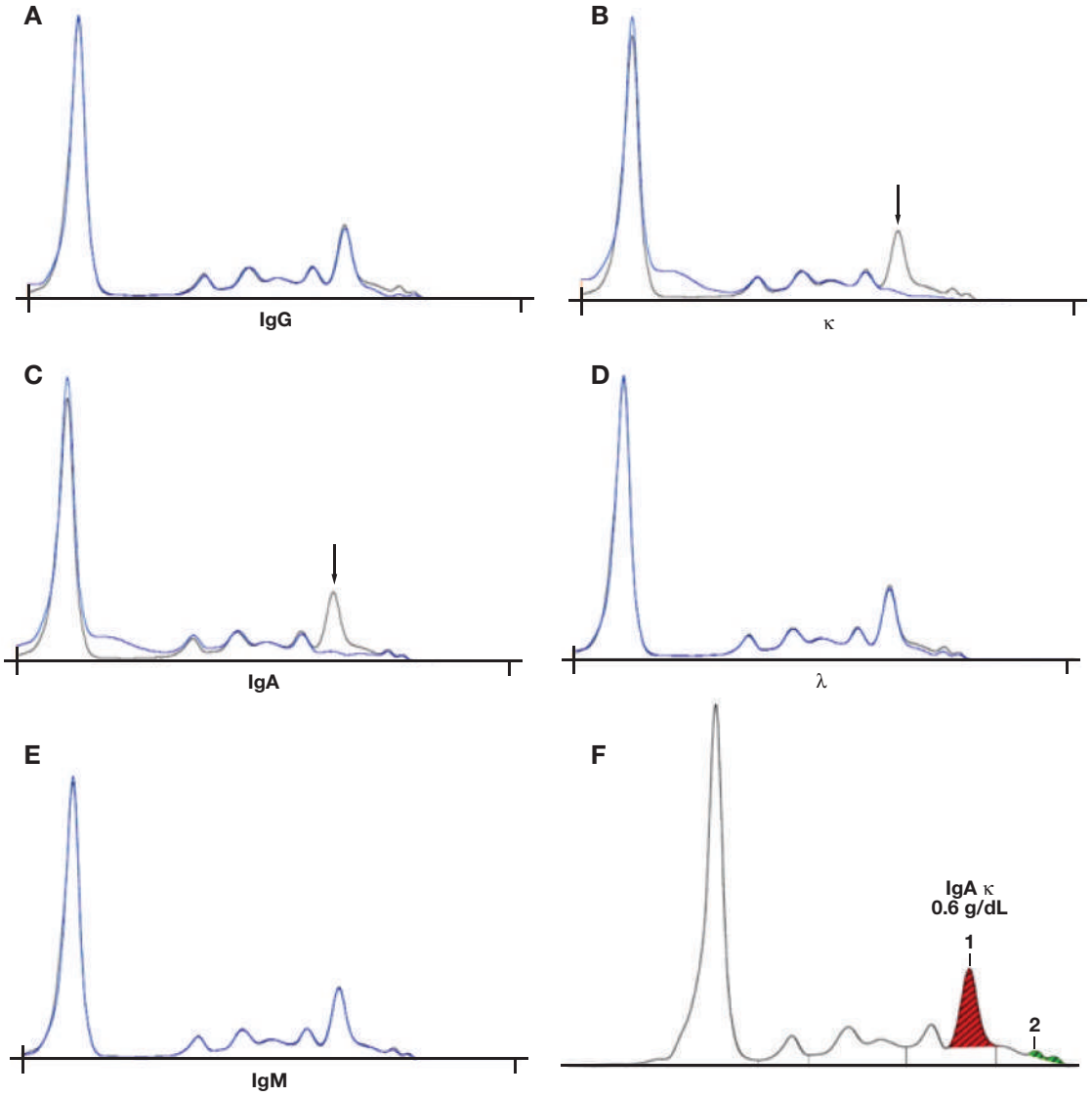

LCPMM is generally low and is subject to overestimation if correction for comigrating proteins in the beta region is not implemented. The error for measuring monoclonal Igs is higher at lower concentrations, and this fact is especially important in the diagnostic criteria for LCPMM.

The estimation of monoclonal Igs overlapping the transferrin band is complicated by the need to immunochemically measure transferrin and then convert the value to its densitometric equivalent. However, nearly two-thirds of the monoclonal Igs migrating in the beta region overlapped C3, and elimination of C3 is easily accomplished by incubating at 37°C. Even if only C3 abrogation were adopted, that would address approximately two-thirds of the cases with monoclonal Ig migrating in the beta region.

AQ21

The lack of a gold standard method for quantification of monoclonal Igs in general, and those migrating in the beta region in particular, is a weakness in this field. If purified preparations of monoclonal IgA and IgG migrating in the beta region were available, these could be used to assess the accuracy of the method described herein. Similarly, longitudinal comparisons in patients with progressive disease or responding to therapy could demonstrate how each evaluated measurement compares over a range of values, although this finding might lack generalizability.

We recognize the modest number of specimens analyzed in this study; however, the close agreement with ISUB CE measurement lends credence to the assay. As we expected, all quantification results were lower than the untreated peak and the concentration of involved Ig.

In brief, the beta-depletion method described in this report adds to the accuracy of measurement of monoclonal Igs migrating in the beta region, without the need for special reagents, equipment, or expertise. This improvement is particularly important in accurate diagnosis of LCPMM because of the adverse prognosis associated with this disease entity.

Personal and Professional Conflicts of Interest

Dr Singh serves as a consultant for Diazyme Inc. and HealthTap.

REFERENCES

1. Dimopoulos M, Kyle R, Fermand J-P, et al; International Myeloma Workshop Consensus Panel 3. Consensus recommendations for standard investigative workup: report of the International Myeloma Workshop Consensus Panel 3. *Blood.* 2011;117(18):4701–4705.
2. Rajkumar SV, Dimopoulos MA, Palumbo A, et al. International Myeloma Working Group updated criteria for the diagnosis of multiple myeloma. *Lancet Oncol.* 2014;15(12):e538–e548.
3. Kyle RA, Therneau TM, Rajkumar SV, et al. Prevalence of monoclonal gammopathy of undetermined significance. *N Engl J Med.* 2006;354(13):1362–1369.
4. Kyle RA, Larson DR, Therneau TM, et al. Long-term follow-up of monoclonal gammopathy of undetermined significance. *N Engl J Med.* 2018;378(3):241–249.
5. Kyle RA, Remstein ED, Therneau TM, et al. Clinical course and prognosis of smoldering (asymptomatic) multiple myeloma. *N Engl J Med.* 2007;356(25):2582–2590.
6. Singh G. Serum and urine protein electrophoresis and serum free light chain assays in the diagnosis and monitoring of monoclonal gammopathies. *J Applied Lab Med.* 2020;5(6):1358–1371.
7. Singh G, Xu H. Light chain predominant intact immunoglobulin monoclonal gammopathy disorders: shorter survival in light chain predominant multiple myelomas. *Lab Med*. 2021;52(4):390–398.
8. Keren DF, Schroeder L. Challenges of measuring monoclonal proteins in serum. *Clin Chem Lab Med.* 2016;54(6):947–961.
9. Clavijo A, Ryan N, Xu H, Singh G. Measurement of monoclonal immunoglobulin protein concentration in serum protein electrophoresis: comparison of automated vs manual/human readings. *Lab Med.* 2020;51(3):252–258.
10. Ludwig H, Miguel JS, Dimopoulos MA, et al. International Myeloma Working Group recommendations for global myeloma care. *Leukemia.* 2014;28(5):981–992.
11. Ting HY, Sthaneshwar P, Bee PC, Shanmugam H, Lim M. Heavy/light chain assay in the monitoring of multiple myeloma. *Pathology.* 2019;51(5):507–511.
12. Katzmann JA, Willrich MAV, Kohlhagen MC, et al. Monitoring IgA multiple myeloma: immunoglobulin heavy/light chain assays. *Clin Chem.* 2015;61(2):360–367.
13. Jacobs JFM, Haagen I-A, Lodder A, et al. Analytical validation of the Hevylite assays for M-protein quantification. *Clin Chem Lab Med.* 2018;56(7):1169–1175.
14. Beaumont-Epinette M-P, Moreau C, Besnard S, et al. Heavy/light chain specific immunoglobulin ratio provides no additional information than serum protein electrophoresis and immunofixation for the diagnosis and follow-up of intact immunoglobulin multiple myeloma patients. *Pathol Biol*. 2015;63(4-5):215–221.
15. Kohlhagen M, Dasari S, Willrich M, et al. Automation and validation of a MALDI-TOF MS (Mass-Fix) replacement of immunofixation electrophoresis in the clinical lab. *Clin Chem Lab Med.* 2020;59(1):155–163.
16. Singh G. Serum free light chain assay and κ/λ ratio: performance in patients without monoclonal gammopathies: high false-positive rate. *Am J Clin Pathol*. 2016;146(2):207–214.
17. Singh G. Serum free light chain assay and κ/λ ratio: performance in patients with monoclonal gammopathy-high false negative rate for κ/λ ratio. *J Clin Med Res.* 2017;9(1):46–57.
18. Aguzzi F, Poggi N. "Immunosubtraction" electrophoresis: a simple method for identifying specific proteins producing the cellulose acetate electrophoretogram. *Boll Ist Sieroter Milan.* 1977;56(3):212–216.
19. Kumar S, Paiva B, Anderson KC, et al. International Myeloma Working Group consensus criteria for response and minimal residual disease assessment in multiple myeloma. *Lancet Oncol.* 2016;17(8):e328–e346.
20. Paiva B, Martinez-Lopez J, Vidriales M-B, et al. Comparison of immunofixation, serum free light chain, and immunophenotyping for response evaluation and prognostication in multiple myeloma. *J Clin Oncol.* 2011;29(12):1627–1633.
21. Singh G. Oligoclonal pattern/abnormal protein bands in post-treatment plasma cell myeloma patients: implications for protein electrophoresis and serum free light chain assay results. *J Clin Med Res.* 2017;9(8):671–679.
22. Narayan S, Lujan MG, Baskin LB, Devaraj S, Rutherford C, Jialal I. Measurement of beta1- and beta2-globulins improves detection of M-spikes on high-resolution electrophoresis. *Clin Chem.* 2003;49(4):676–678.
23. McPherson RA. Specific proteins. In: RA McPherson, MR Pincus, eds. *Henry's Clinical Diagnosis and Management by Laboratory Methods. Chapter 19*. Elsevier; 2017.
24. Jacobs JFM, Turner KA, Graziani MS, et al. An international multicenter serum protein electrophoresis accuracy and M-protein isotyping study. Part II: limit of detection and follow-up of patients with small M-proteins. *Clin Chem Lab Med.* 2020;58(4):547–559.

Light Chain–Predominant Multiple Myeloma Subgroup: Impaired Renal Function Correlates with Decreased Survival

Gurmukh Singh, MD,[1,] Natasha M. Savage, MD,[1] Anand P. Jillella, MD,[2] Roni J. Bollag, MD[1]*

[1]Division of Clinical Pathology, Department of Pathology, Medical College of Georgia at Augusta University, Augusta, Georgia, US; [2]Division of Hematology/Oncology, Department of Medicine, Medical College of Georgia at Augusta University, Augusta, Georgia, US; *To whom correspondence should be addressed. gurmukhsinghmdphd@yahoo.com

Keywords: multiple myeloma, serum free light chains, cast nephropathy, light chain–predominant multiple myeloma, eGFR, survival

Abbreviations: MGUS, monoclonal gammopathy of undetermined significance; SMM, smoldering multiple myeloma; MM, multiple myeloma; ASCT, autologous stem cell transplantation; SFLC, serum free light chain; LCPMM, light chain–predominant multiple myeloma; SIFE, serum immunofixation electrophoresis; ESRD, end-stage renal disease; eGFR, estimated glomerular filtration rate; ALT, alanine transaminase; COPD, chronic obstructive pulmonary disease; DVT, deep vein thrombosis; PE, pulmonary embolism; BMI, body mass index.

Laboratory Medicine 2022;53:145–148; https://doi.org/10.1093/labmed/lmab054

ABSTRACT

Objective: Patients with light chain–predominant multiple myeloma have been shown to exhibit shorter survival. Retrospective comparison of clinical and laboratory data was undertaken to ascertain the likely cause(s) of this observation.

Methods: Records of patients with multiple myeloma seen at 1 institution revealed 316 patients with conventional and 71 patients with light chain–predominant multiple myelomas with secretion of intact immunoglobulins. Laboratory and clinical findings in the 2 groups were compared.

Results: Patients with light chain–predominant multiple myeloma had a significantly higher death rate, a higher rate of chronic dialysis, a lower estimated glomerular filtration rate and serum albumin, a significantly higher urine protein concentration, and a significantly higher prevalence of hypertension and blood transfusion requirements. Other clinical and laboratory parameters surveyed were not significantly different between the 2 groups.

Conclusion: The shorter survival of patients with light chain–predominant multiple myeloma is clearly associated with renal damage caused by excess free immunoglobulin light chains. Renal damage may be ameliorated by early aggressive treatment with chemotherapy, plasmapheresis, and dialysis; a multi-institutional prospective controlled trial would be needed to test this hypothesis.

Neoplastic disorders of plasma cells include, in order of severity of pathology, the premalignant entities of monoclonal gammopathy of undetermined significance (MGUS) and smoldering or asymptomatic myeloma (SMM) and the malignant entity of plasma cell myeloma/multiple myeloma (MM).[1-4] Research has shown that MM is the most common hematologic malignancy in adults in the United States.[5] The disease is treatable but for the most part not curable. Advances in chemotherapy, precision medicine, and perhaps the implementation of autologous hematopoietic stem cell transplantation (ASCT) have improved outcomes in this malignancy.[6-9]

Studies have shown that MMs generally produce and secrete monoclonal immunoglobulins that can be detected in serum and urine and provide diagnostic information and an estimate of tumor burden to monitor the effects of treatment. Approximately 85% of MM lesions secrete intact immunoglobulins, and approximately 13% secrete light chains only; the balance is composed of bi- or triclonal lesions and nonsecretory myelomas.[10] Although stoichiometrically the standard immunoglobulin consists of 2 heavy chains covalently bound to 2 light chains, both normal and neoplastic plasma cells may produce more light chains than heavy chains. The excess free light chains can be measured in serum and urine.[11] An assay for serum free light chains (SFLCs) selectively measures free light chains, albeit it is not specific for monoclonal light chains.[12]

There is wide variation in the amount of SFLCs produced by myelomas. Some lesions, especially those associated with lambda light chains, do not produce detectable excess SFLCs, whereas at the other extreme are lesions that produce only light chains.[10,13] Among approximately 85% of myelomas that produce intact immunoglobulins, a subgroup constituting close to 18% of these lesions has been shown to produce a marked excess of SFLCs. This subgroup has been designated as light chain–predominant multiple myeloma (LCPMM), which produces an intact monoclonal immunoglobulin in serum

and has increased levels of SFLCs. The specific diagnostic criteria for LCPMM lesions are based on levels of SFLCs and include (i) SFLC concentrations of ≥35.2 mg/L (kappa) or ≥36.8 mg/L (lambda), (ii) a ratio of involved to uninvolved SFLCs of ≥44.9 (regardless of light chain specificity), (iii) an SFLC concentration in mg/L/concentration of monoclonal immunoglobulin in g/dL of ≥67 mg/g (kappa) and ≥43.5 mg/g (lambda), and (iv) a ratio of involved to uninvolved SFLC concentration to monoclonal immunoglobulin of ≥68.4 g/dL (kappa) or ≥51.6 g/dL (lambda) (**TABLE 1**). All 4 criteria need to be met or exceeded for the lesion to be classified as LCPMM. It has been shown that patients with LCPMM have significantly shorter survival, by nearly 2 years.[14] This study was undertaken to further assess the extent and degree of adverse outcomes and to ascertain the likely cause of adverse outcomes in patients with LCPMM.

Methods

This retrospective, observational investigation was conducted at a 480-bed tertiary care, medical school–affiliated medical center in the southeastern United States. The study protocol was reviewed and approved by the institutional review board. Methods for serum and urine protein electrophoreses, serum immunofixation electrophoresis (SIFE) and urine immunofixation electrophoresis, and SFLC measurement have been described in earlier research.[10,11]

Records of all patients undergoing SIFE at this institution, from January 2010 through August 2020, were reviewed. Some of the results of the studies from these reviews have been published, including a recent study that categorized the subgroup of LCPMM and showed significantly shorter survival in this subgroup.[13,14] Of the 624 patients with MM in the records at this institution, sufficient data were available for 387 patients for evaluation of the various parameters examined in the study. The patients not included in the study were those who were examined and treated elsewhere and were referred for evaluation for hematopoietic stem cell transplantation, and their record was limited to 1 visit. No patients in whom required data were available were excluded. Laboratory and clinical data were examined to ascertain the likely pathophysiology responsible for shorter survival in LCPMM. The various parameters examined are listed in **TABLE 2**.

Patient deaths were ascertained from the medical records, including notifications by next of kin through phone calls. Only patients with end-stage renal disease (ESRD) on chronic dialysis were recorded as receiving dialysis. Patients refusing dialysis despite having ESRD were not included. The estimated glomerular filtration rate (eGFR) was calculated using the CKD-Epi equation.[15] Creatinine values at the date of last contact with the patient were used for the eGFR estimation, as were the values for serum albumin, alanine transaminase (ALT), and total bilirubin. For urine protein, the highest recorded urine protein concentration was noted, although this information was not available for 26.6% of patients with conventional MM and 19.7% of patients with LCPMM. Hypertension, diabetes, heart disease, hypothyroidism, pathologic fractures, tobacco use, occurrence of plasmacytomas, chronic obstructive pulmonary disease (COPD), and malignancy (other than MM) were recorded as present or not present based on annotation in the medical record. Transfusion was recorded as positive for any transfusion reported in the host electronic medical records, with the caveat that patients not receiving transfusions at this institution may have been transfused elsewhere. Because the host institution is a tertiary care center, many patients were referred for consideration of hematopoietic stem cell transplantation after treatment at other medical centers. Patients were recorded as being positive for deep vein thrombosis (DVT) if there was a history of DVT and/or pulmonary embolism (PE). The highest recorded body mass index (BMI) for each individual was used in the study. Finally, ASCT was recorded whether it was performed at this institution or elsewhere, as noted in the medical records.

Continuous variables were compared by Student's *t*-test between patients with conventional MM and those with LCPMM. A 2-tailed comparison with an assumption of unequal variances was employed in the Student's *t*-test to ensure conservative estimates of the *P* value. The chi-square test was used for discrete variables. A correction to the *P* value for the number of comparisons was not applied to the display in **TABLE 1**, although the key parameters of higher death rate, higher rate of dialysis, and lower eGFR and higher urine protein levels in LCPMM did maintain statistical significance when the Bonferroni correction was applied for the 25 issues compared between the 2 groups.

TABLE 1. Diagnostic Criteria for LCPMM

Diagnostic Criteria for LCPMM Subgroup		
	Kappa	Lambda
SFLC, mg/L	≥35.2	≥36.8
Involved SFLC/uninvolved SFLC, mg/L	≥44.9	≥44.9
SFLC/monoclonal immunoglobulin, g/dL	≥67	≥43.5
(involved SFLC/uninvolved SFLC)/monoclonal immunoglobulin, g/dL	≥68.4	≥51.6

LCPMM, light chain–predominant multiple myeloma; SFLC, serum free light chain.
Highest levels of the parameters listed in the table were used for the LCPMM designation.

Results

Out of a total of 624 patients with MM patients evaluated, 387 patients with intact immunoglobulin-producing MM had sufficient data available for classification into 316 patients with conventional intact immunoglobulin MM and 71 patients with LCPMM. Comparative laboratory and clinical data for the 2 groups along with the statistical analysis are presented in **TABLE 2**. Mortality was significantly higher for patients with LCPMM and was nearly 3 times higher than that for patients with conventional MM. Kidney function as assessed by eGFR was lower by a mean of 23 mL in patients with LCPMM. When patients on chronic dialysis were excluded, the eGFR was lower by 19 mL in patients with LCPMM, although the difference was still highly significant at *P* <.00001. More patients with LCPMM (18.3%) were on chronic dialysis than patients with conventional MM (3.5%). Mean urine protein concentration was significantly higher in patients with LCPMM, at 239 mg/dL, compared to 76 mg/dL in conventional MM. Serum albumin levels were significantly lower in LCPMM, at a mean of 3.4 g/dL, compared to 3.7 g/dL in conventional MM. Hypertension was prevalent at a significantly higher frequency of 87% in patients with LCPMM compared to 72% in patients with conventional MM. Requirement for blood transfusion was more frequent in patients with LCPMM.

The following parameters were not significantly different between the 2 groups: age, age at diagnosis, race, sex, BMI, ALT, total bilirubin, presence of plasmacytomas, pathologic fractures, diabetes, COPD,

TABLE 2. Comparison of Laboratory and Clinical Findings in Conventional MM vs LCPMM.

	MM	LCPMM	*P* Value
Number of patients	316	71	
Death (%)	43 (13.6)	25 (35.2)	.00001
Dialysis (%)	11 (3.5)	13 (18.3)	.00001
eGFR, mL (SD) [median]	69.4 (29.3) [73]	46.3(32.4) [46]	.0000003
Urine protein, mg/dL (SD) [median]	75.9 (288.3) [16]	238.8 (332.9) [96]	.001
Hypertension (%)	227 (71.8)	62 (87.3)	.007
Albumin, g/dL (SD) [median]	3.7 (0.62) [3.8]	3.44 (0.71) [3.5]	.005
Transfusion (%)	224 (70.9)	59 (83.1)	.05
ASCT (%)	205 (64.9)	37 (52.1)	.06
Age, y (SD) [median]	66.9(10.3) [66]	67.4 (11.8) [68]	.74
Age at diagnosis, y (SD) [median]	61.0(10.4) [62]	63.0 (12) [60]	.20
Sex: male–female (%)	183 (57.9)—133 (42.1)	44 (62.0)—27 (38)	.53
Race, White (%)	134 (42.4)	31 (43.7)	.95
Race, Black (%)	176 (55.7)	40 (56.3)	…
Race, Hispanic (%)	2 (0.6)	0	…
Race, Other (%)	4 (1.3)	0	…
Tobacco use (%)	49 (15.5)	13 (18.3)	.56
BMI (SD) [median]	31.2 (6.5) [30]	31.4 (7.8) [29.6]	.88
ALT, U/L (SD) [median]	31.1 (87.8) [17]	34 (66.9) [16]	.75
Total bilirubin, mg/dL (SD) [median]	0.8 (2.5) [0.5]	0.7 (0.6) [0.5]	.52
Plasmacytoma (%)	39 (12.3)	11 (15.5)	.47
Diabetes (%)	89 (38.2)	20 (28.2)	1.00
COPD (%)	53 (16.8)	10 (14.1)	.58
Malignancy (%)	50 (15.8)	12 (16.9)	.82
Heart disease (%)	95 (30.1)	25 (35.2)	.40
Hypothyroidism (%)	40 (12.7)	5 (7.0)	.18
Fracture	100 (31.74)	19 (26.8)	.42
DVT/PE (%)	59 (18.7)	16 (22.5)	.46
CVA (%)	21 (6.6)	6 (8.5)	.59

ALT, alanine transaminase; ASCT, autologous stem cell transplantation; BMI, body mass index; COPD, chronic obstructive pulmonary disease; CVA, cerebrovascular accident; DVT, deep vein thrombosis; eGFR, estimated glomerular filtration rate; LCPMM, light chain–predominant multiple myeloma; MM, multiple myeloma; PE, pulmonary embolism; SD, standard deviation.
Patients with LCPMM had significantly higher death rate, prevalence of chronic dialysis, proteinuria, hypertension, and transfusion rate along with significantly lower eGFR and serum albumin levels. The adverse outcomes in LCPMM can be attributed to renal damage caused by excess free light chains.

additional malignancy, heart disease, hypothyroidism, DVT/PE, cerebrovascular disease including transient ischemic attacks, and tobacco use. The frequency of treatment with ASCT was similar in the 2 groups, albeit marginally lower in patients with LCPMM.

In 35 patients in the conventional MM group, 3 of the 4 change point criteria were met for designation as LCPMM. In 31 of these 35 patients, the criterion not meeting the change point target was light chain per g of monoclonal Ig. The eGFR in this group of 35 patients was 72.5 mL and was not significantly different from that in the other 281 patients with conventional MM, who had an eGFR of 74.1 mL. The eGFR in the patients with LCPMM (49.1 mL) was significantly lower than that of the the entire conventional MM group (ie, the 35 patients who met 3 of the 4 change point criteria and the 281 patients in whom fewer than 3 change point criteria were met).

The key parameters were not significantly different between kappa and lambda chain–associated lesions. The *P* values for the LCPMM groups with kappa and lambda light chains were .23 and .95 for length of survival and eGFR, respectively.

Discussion

The higher death rate and shorter survival in patients with LCPMM are clearly associated with greater disease burden in the form of excess SFLCs compromising renal function. Significantly lower eGFR, a significantly higher prevalence of chronic dialysis, a higher prevalence of hypertension, and a greater extent of proteinuria with resultant hypoalbuminemia are all indicative of more severe renal pathology in patients with LCPMM. The greater extent of renal failure can also explain the higher frequency of blood transfusions in patients with LCPMM, and the greater disease burden of renal insufficiency likely explains the strikingly higher mortality in these patients. It was not feasible to ascertain whether the higher prevalence of hypertension caused worse re-

nal function or if the renal damage by free immunoglobulin light chains resulted in a higher prevalence of hypertension in the LCPMM group.

Excess free immunoglobulin light chains are a known risk factor for renal disease, with light chain cast nephropathy being the usual pathogenetic mechanism for renal damage. Addressing the free light chain burden early in the course of illness in patients with LCPMM may help mitigate or reverse renal pathology. The pathogenic burden of SFLCs could be ameliorated by chemotherapy, plasmapheresis, and dialysis with a higher-molecular-weight pore size membrane.[16] Rigorously testing this hypothesis would require a multisite prospective randomized controlled clinical trial. The present study has the usual drawbacks of a retrospective observational study; nevertheless, it documents the likely explanation for lower survival in the newly described LCPMM subgroup as renal damage mediated by excess free immunoglobulin light chains.

The marginally lower rate of ASCT in patients with LCPMM likely reflects fewer patients with LCPMM being suitable candidates for ASCT because of poorer baseline functional status. Although low serum albumin is a general marker of poor health, the hypoalbuminemia was more likely the result of renal protein loss rather than hepatic hypofunction because the liver function markers of ALT and bilirubin were not different between the patients with MM and those with LCPMM.

With additional data and harmonization of light chain quantification methods, it may be feasible to devise a single criterion, for each light chain type, to identify patients with LCPMM. The light chain concentration/g of monoclonal Ig is the single criterion most likely to meet the requirement for this diagnostic marker.

In brief, LCPMM has higher mortality than conventional MM. The adverse outcomes in LCPMM seem to be mediated by renal damage caused by excess free light chains. Prospective controlled trials designed to aggressively lower SFLC concentrations to improve outcomes are warranted.

Conclusion

Tumors in a subset (approximately 18%) of patients with MM secrete distinctly higher amounts of free immunoglobulin light chains. The excess free light chains are clearly associated with renal damage, resulting in renal failure and significantly shorter survival in the affected patients. Effectiveness of early and aggressive treatment aimed at reducing SFLCs needs to be ascertained through clinical trials.

Acknowledgments

Dr. Singh serves as a consultant to Diazyme Inc. and HealthTap.

REFERENCES

1. Kyle RA, Therneau TM, Rajkumar SV, et al. Prevalence of monoclonal gammopathy of undetermined significance. *N Engl J Med.* 2006;354(13):1362–1369.
2. Kyle RA, Larson DR, Therneau TM, et al. Long-term follow-up of monoclonal gammopathy of undetermined significance. *N Engl J Med.* 2018;378(3):241–249.
3. Kyle RA, Remstein ED, Therneau TM, et al. Clinical course and prognosis of smoldering (asymptomatic) multiple myeloma. *N Engl J Med.* 2007;356(25):2582–2590.
4. Palumbo A, Anderson K. Multiple myeloma. *N Engl J Med.* 2011;364(11):1046–1060.
5. Michels TC, Petersen KE. Multiple myeloma: diagnosis and treatment. *Am Fam Physician.* 2017;95(6):373–383.
6. Pawlyn C, Davies FE. Toward personalized treatment in multiple myeloma based on molecular characteristics. *Blood.* 2019;133(7):660–675.
7. Durie BGM, Hoering A, Abidi MH, et al. Bortezomib with lenalidomide and dexamethasone versus lenalidomide and dexamethasone alone in patients with newly diagnosed myeloma without intent for immediate autologous stem-cell transplant (SWOG S0777): a randomised, open-label, phase 3 trial. *Lancet.* 2017;389(10068):519–527.
8. Lauwers-Cances AM, Hulin C, Leleu X, Caillot D, Escoffre M, Arnulf B, et al. Lenalidomide, bortezomib, and dexamethasone with transplantation for myeloma. *N Engl J Med*. 2017;376:1311–1320.
9. Dhakal B, Szabo A, Chhabra S, et al. Autologous transplantation for newly diagnosed multiple myeloma in the era of novel agent induction: a systematic review and meta-analysis. *JAMA Oncol.* 2018;4(3):343–350.
10. Singh G. Serum free light chain assay and κ/λ ratio: performance in patients with monoclonal gammopathy-high false negative rate for κ/λ ratio. *J Clin Med Res.* 2017;9(1):46–57.
11. Singh G. Serum free light chain assay and κ/λ ratio: performance in patients without monoclonal gammopathies—high false positive rate. *Am J Clin Pathol.* 2016;146:207–214.
12. Bradwell AR. *Serum Free Light Chain Analysis: Plus Hevylite.* 7th ed. Birmingham, UK: The Binding Site Limited; 2015.
13. Singh G. Serum and urine protein electrophoresis and serum-free light chain assays in the diagnosis and monitoring of monoclonal gammopathies. *J Appl Lab Med.* 2020;5(6):1358–1371.
14. Singh G, Xu H. Light chain predominant intact immunoglobulin monoclonal gammopathy disorders: shorter survival in light chain-predominant multiple myelomas. *Lab Med.* 2021;52(4):390–398.
15. Levey AS. CKD-EPI equations for glomerular filtration rate (GFR). MDCalc. https://www.mdcalc.com/ckd-epi-equations-glomerular-filtration-rate-gfr. Accessed July 26, 2021.
16. Finkel KW, Cohen EP, Shirali A, Abudayyeh A; American Society of Nephrology Onco-Nephrology Forum. Paraprotein-related kidney disease: evaluation and treatment of myeloma cast nephropathy. *Clin J Am Soc Nephrol.* 2016;11(12):2273–2279.

Serum IL-6 and TNF-α Levels Are Correlated with Disease Severity in Patients with Ankylosing Spondylitis

Jing Du, PhD[1,#] Jinxia Sun, PhD,[3,#,✉] Zhanpeng Wen, BS,[1] Zhicheng Wu, BS,[1] Qian Li, BS,[1] Yuhao Xia, BS,[1] Qiannan Yang, BS,[4] Chao Yang, PhD[2,]*

[1]Department of Laboratory Medicine, Peking University Shenzhen Hospital, Shenzhen, P.R. China; [2]Department of Surgery, Shenzhen People's Hospital, Shenzhen, P.R. China;[3]Shenzhen GenTarGet Biotherapeutics Co., Ltd., Shenzhen, P.R. China; [4]Department of Biology, Case Western Reserve University, Cleveland, Ohio, US; [#]These authors contributed equally to this work. *To whom correspondence should be addressed. djchaoyang@163.com

Keywords: ankylosing spondylitis, interleukin-6, tumor necrosis factor-α, Bath Ankylosing Spondylitis Disease Activity Index, C-reactive protein, erythrocyte sedimentation rate

Abbreviations: AS, ankylosing spondylitis; IL, interleukin; TNF-α, tumor necrosis factor-α; HCs, healthy control patients; BASDAI, Bath Ankylosing Spondylitis Disease Activity Index; CT, computed tomography; NSAIDs, nonsteroidal anti-inflammatory drugs; CRP, C-reactive protein; ESR, erythrocyte sedimentation rate; HLA-B27, human leukocyte antigen-B27; CH50, total hemolytic complement; MMP, matrix metalloproteinase.

Laboratory Medicine 2022;53:149–155; https://doi.org/10.1093/labmed/lmab029

ABSTRACT

Objective: Previous studies have shown that a number of cytokines participate in the regulation of ankylosing spondylitis (AS). To investigate the potential role of interleukin (IL)-6 and tumor necrosis factor- α (TNF-α) in AS pathogenesis, this study examined the serum levels of IL-6 and TNF-α in patients with AS and its clinical association with disease activity.

Materials and Methods: The serum concentrations of IL-6 and TNF-α from 80 patients with AS and 46 healthy control patients (HCs) were examined by electrochemiluminescence immunoassay. The correlations between the serum IL-6 and TNF-α levels and the Bath Ankylosing Spondylitis Disease Activity Index (BASDAI), computed tomography (CT) imaging-based classification, and laboratory indicators were analyzed using the Spearman correlation test.

Results: Compared to HCs, patients with AS showed higher levels of IL-6 and TNF-α. There was also a positive correlation between the serum IL-6 and TNF-α levels and the BASDAI, the progression of AS, and the CT imaging–based classification. The serum levels of IL-6 correlated closely with C-reactive protein and the erythrocyte sedimentation rate. More important, patients with AS with hip joint involvement exhibited a significant elevation of serum levels of TNF-α, and higher IL-6 was detected in patients with the involvement of joints other than the hip and sacroiliac joints.

Conclusion: The serum levels of IL-6 and TNF-α can function as important indicators for auxiliary diagnosis and disease activity evaluation of AS.

Ankylosing spondylitis (AS) is an immune-mediated chronic inflammatory disorder that primarily affects the sacroiliac joints, the axial skeleton, and the peripheral joints and eventually leads to spinal deformity and stiffness.[1,2] Chronic back pain and progressive spinal stiffness are the most common features of the disease.[3-5] Many patients with AS suffer a severe loss of mobility and lose their ability to work as a consequence.[6] As an insidiously progressive and debilitating form of arthritis, AS has an estimated prevalence in the global population of 0.7% to 3.2%.[7,8] The disorder typically starts during the second or third decade of life and develops in young adult men with a sex ratio of approximately 3:1 (male:female).[9,10] It is a lifelong condition with an unpredictable disease course that eventually severely affects the quality of life of individual patients.[11,12]

The pharmacological treatment for AS involves nonsteroidal anti-inflammatory medications (NSAIDs) and tumor necrosis factor--α (TNF-α) inhibitors. In general, NSAIDs are first-line treatments for patients with active AS and TNF-α inhibitors are advised for patients with high disease activity. Additional biologic drugs for patients who fail to respond to TNF-α inhibitors or who develop tolerability issues include interleukin (IL)-17 inhibitors, IL-12/23 inhibitors, and antibodies against $CD20^+$ B cells.[13]

The early diagnosis and timely treatment of AS are important for improving clinical outcomes. The clinical Bath Ankyosing Spondylitis Disease Activity Index (BASDAI) is widely used to evaluate disease activity in patients with AS and includes self-reported feelings expressed by patients that are evaluated from the patient questionnaire.[14,15] C-reactive protein (CRP) and the erythrocyte sedimentation rate (ESR) are 2 laboratory acute-phase reactants that are classically used to assess the presence of inflammation in patients with AS.[16,17] However, just 45% to 50% of patients with AS show elevated ESR and CRP levels. There is a poor correlation between clinical disease activity and the ESR in AS. Patients with spondylitis may have a normal ESR, and an elevated ESR is often seen in patients with a clinically

quiescent condition. The ESR is also a nonspecific test that is influenced by a large number of factors unrelated to inflammation.[16,18-20] Therefore, there is a clear and urgent need for more sensitive and specific disease activity markers for the measurement of disease activity to guide the diagnosis and treatment of AS.

Although the mechanisms underlying this disease are not fully understood, and the treatment options for AS are limited, a number of studies have clearly shown that the cytokine network plays an immunopathological role in AS.[21] Increasing attention has focused on the roles of cytokines in the inflammatory process of autoimmune diseases and the correlation between cytokines and clinical disease activity. Many studies have indicated that TNF-α and IL-6 play pivotal roles in the pathogenesis of AS. Currently, TNF-α inhibitors are increasingly used for patients with AS with active disease when other treatment options have proven ineffective. In fact, TNF-α inhibitors are effective in reducing pain and stiffness and improving the function of patients with AS.[22,23] It remains unclear why some patients with AS achieve significant improvement after TNF-α inhibitor treatment whereas others do not respond to the same treatment. Furthermore, IL-6 is a pleiotropic cytokine that participates in the development of AS, but whether it can be used to assess disease activity remains controversial.[24]

The current study examined the serum levels of IL-6 and TNF-α in patients with AS to clarify the correlation of these levels with imaging classification of the sacroiliac joint, clinical parameters, and laboratory indicators, which will provide a theoretical basis for their clinical implications.

Materials and Methods

Participants

Eighty hospitalized patients with AS with radiographic axial spondyloarthritis were invited to enroll in our research from March 2018 to September 2018 at the Peking University Shenzhen Hospital, Shenzhen, People's Republic of China. Patients were excluded according to the following criteria: acute inflammatory diseases, heart failure, blood system diseases, and endocrine diseases. All patients with AS were individually diagnosed according to the modified New York criteria[25] and the Assessment of SpondyloArthritis International Society classification criteria. An additional set of 46 age- and sex-matched healthy volunteers served as the healthy control patients (HCs) who had no previous history of arthritis, back pain, or chronic diseases such as diabetes. The clinical characteristics of patients with AS and HCs are summarized in **TABLE 1**. The regional ethics committee of Peking University Shenzhen Hospital approved the research. Written informed consents were obtained from all participants.

Measurement of IL-6 and TNF-α

Peripheral blood specimens were obtained from patients with AS and HCs. All serum specimens were taken at different time points and stored at –80℃ until cytokines were determined. The serum levels of IL-6 and TNF-α were determined using a Cobas E601 automatic electrochemical luminescence immune analyzer (Roche Diagnostics) and a DPC immulite 1000 immunoassay analyzer (Siemens), respectively. According to the manufacturer, the assay range for IL-6 is 1.5 to 5000 pg/mL and the assay limit is 1.5 pg/mL, whereas the assay range and limit for TNF-α are 1.7 to 1000 pg/mL and 1.7 pg/mL. The normal reference ranges of IL-6 and TNF-α are ≤7.0 pg/mL and ≤8.1 pg/mL, respectively.

BASDAI Assessment

The BASDAI reflects disease activity in AS and includes fatigue, spinal pain, joint pain/swelling, areas of localized tenderness, and morning stiffness. The possible BASDAI score ranges from 0 to 10. A score of 1 to 4 suggests inactive disease, and a score of 4 to 6 indicates that a combination of laboratory indicators is required to determine whether the disease is active. Scores of 6 to 10 are suggestive of active disease.

Assessment of Laboratory Indicators

All laboratory indicators were measured by independent researchers who were blinded to the clinical characteristics of the patients. The surface expression of human leukocyte antigen-B27 (HLA-B27) was analyzed using a Cytomics FC500 flow cytometer (Beckman). The CRP and total hemolytic complement (CH50) were measured according to the immune turbidity method using the Beckman Coulter AU5800 biochemical analyzer. The ESR was determined using the Westergren method according to the manufacturer's instructions. The normal reference range of CRP is ≤10 mg/dL, that of the ESR is ≤20 mm/h, and that of CH50 is 23 to 46 U/mL.

Computed Tomography Imaging-Based Classification

Computed tomography (CT) scans were performed to evaluate sacroiliac arthritis. The clinical evaluation of sacroiliac arthritis was graded from I to III as follows: I, blurring of articular surface, minor bone cortex destruction; II, bone cortex sclerosis, rough articular surface, but no change in joint space; and III, articular surface erosions or sclerosis, irregular and narrow joint space or nonuniform width.

Statistical Analysis

The results are expressed as the mean ± standard deviation. Statistical analyses were performed using SPSS software version 25.0 and GraphPad Prism software version 6.0. Statistical comparisons of the 2 groups were performed using a 2-tailed Student's *t*-test. The Spearman nonparametric correlation analysis was used to evaluate the associations between the serum cytokine levels and disease activity

TABLE 1. Clinical and Laboratory Characteristics in Patients with AS and HCs

Characteristics	AS	HC
Number of participants	80	46
Female, n (%)	17 (21%)	10 (22%)
Male, n (%)	63 (79%)	36 (78%)
Age, y (range)	32.6 ± 10.8	32.7 ± 10.9
Disease duration (y)	7.2 ± 5.9	…
BASDAI	5.1 ± 1.8	…
HLA-B27-positive, n (%)	69 (86%)	…
CH50 (U/mL)	42.6 ± 6.3	35.1 ± 4.7
ESR (mm/h) (mean ± SD)	26.8 ± 19.2	10.5 ± 8.2
CRP (mg/L) (mean ± SD)	16 ± 16.7	1.9 ± 1.9

AS, ankylosing spondylitis; BASDAI, Bath Ankylosing Spondylitis Disease Activity Index; CH50, total hemolytic complement; CRP, C-reactive protein; ESR, erythrocyte sedimentation rate; HCs, healthy control patients; HLA-B27, human leukocyte antigen-B27; SD, standard deviation.
Values are expressed as mean ± SD. There were no significant differences between patients with AS and HCs in terms of age and sex.

parameters. Differences with *P <.05, **P <.01, and ***P <.001 were considered to be significant.

Results

Serum Levels of IL-6 and TNF-α in AS

To investigate the correlations between the serum IL-6 and TNF-α levels with the BASDAI, we first compared the levels of IL-6 and TNF-α in the serum from 80 patients with AS with the levels of IL-6 and TNF-α in the serum from 46 HCs. As shown in **FIGURE 1**, serum IL-6 and TNF-α levels were markedly higher in the specimens from patients with AS than in those from the HCs.

Serum Levels of IL-6 and TNF-α in AS with Different Clinical Characteristics

Twenty-seven of the 80 patients with AS had fever. Forty-seven patients with AS exhibited hip joint involvement, and 19 patients had other joint involvement such as in the knee joints and the cervical vertebra beside the sacroiliac joints. There were 6 patients with complications, such as ophthalmia, intestinal inflammation, or vasculitis, and 69 patients were HLA-B27-positive. We compared the serum levels of IL-6 and TNF-α in each group. As shown in **FIGURE 2**, serum levels of IL-6 were significantly increased in patients with AS with other joint involvement, and obviously enhanced serum levels of TNF-α were found only in patients with AS with hip joint involvement.

Correlations Between Serum IL-6 and TNF-α Levels and Imaging Classification

The inflammation and injury of the sacroiliac joint in patients with AS were classified into 3 levels using imaging, and the differences between the serum levels of IL-6 and TNF-α were compared between groups. As shown in **FIGURE 3**, the Spearman nonparametric correlation analysis showed that the serum levels of IL-6 increased gradually with sacroiliac arthritis progression, but that serum levels of TNF-α did not show any significant correlation with the imaging classification of the sacroiliac joint.

FIGURE 1. Expression of IL-6 and TNF-α in patients with AS and HCs. Comparison of IL-6 (A) and TNF-α (B) protein expression by automatic electrochemical luminescence immune analyzer or enzyme-linked immunosorbent assay in sera from patients with AS (n = 80) or HCs (n = 46). Data are shown as mean ± SD. **P <.01; Student's t-test. AS, ankylosing spondylitis; HCs, healthy control patients; IL-6, interleukin-6; TNF-α, tumor necrosis factor-α.

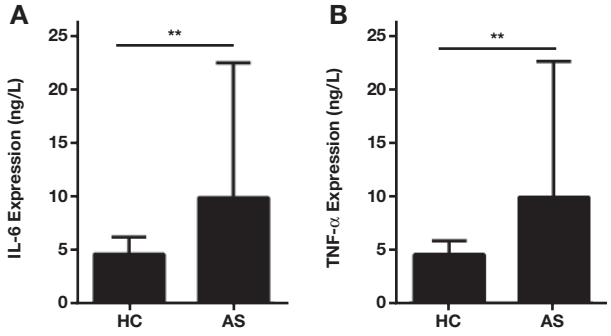

Correlations Between Serum IL-6 and TNF-α Levels with Clinical Parameters and Laboratory Indicators

A Spearman nonparametric correlation analysis was also performed between the serum IL-6 and TNF-α levels and the clinical parameters and laboratory indicators. A statistically significant positive correlation was observed between the serum levels of IL-6 and the BASDAI, disease duration, CH50, CRP, and ESR in the patients with AS (**FIGURE 4**). However, the serum levels of TNF-α positively correlated with the BASDAI and disease duration but did not correlate with the CH50, CRP, or ESR levels.

Discussion

Although the exact etiology of AS remains unclear, genetic predisposition and innate immune aspects in combination with environmental factors are considered to be essential for disease development.[13] Previous studies have confirmed obvious genetic and familial tendencies in the onset of AS.[26,27] The major histocompatibility complex haplotype HLA-B27 is a major predisposing factor that plays a major role in the evaluation, pathogenesis, and prognosis of AS.[28,29] Mechanistically, HLA-B27 contributes to the pathogenesis of AS mainly via 3 pathways: peptide presentation to CD8 T cells, abnormal forms of the HLA-B27 heavy chain and their recognition by leukocyte immunoglobulin-like receptors on immune effector cells, and HLA-B27 heavy chain misfolding and intrinsic biological effects on affected cells.[30,31] Although most patients with AS in the general population are HLA-B27-positive, the presence of the HLA-B27 genotype is not sufficient for AS pathogenesis.[32,33] In this study, we revealed that 87% of patients were positive for HLA-B27. However, we failed to detect a significant correlation between the IL-6 and TNF-α levels with HLA-B27, which suggests that HLA-B27 does not affect the expression of IL-6 or TNF-α.

Various cell types produce IL-6, such as monocytes, fibroblasts, and endothelial cells, and IL-6 was originally identified as a B-cell differentiation factor. Furthermore, IL-6 is a multifunctional proinflammatory cytokine with significant functions in the regulation of the immune system. It also exerts its biological activities via its unique receptor system. Numerous preclinical and clinical studies have revealed that IL-6 plays a pathological role in inflammation, autoimmunity, and cancer. Increased levels of IL-6 are detected in several human inflammatory diseases. Moreover, many studies have shown that IL-6 is also critically involved in the pathogenesis of autoimmune diseases.[34,35]

Research has shown that CRP, an acute-phase protein produced in the liver, is a powerful marker for disease activity in infectious and inflammatory diseases, and IL-6 contributes to the expression and release of CRP. Rising CRP concentrations furthermore activate neutrophils and monocytes to secrete IL-6.[36] Thus, IL-6 and CRP are the 2 most commonly assayed biomarkers of inflammation. Recently, research in immunology has shown that IL-6 and CRP are more than inflammatory biomarkers. Specifically, IL-6 is a pleiotropic cytokine with proinflammatory, anti-inflammatory, and endocrine functions. Similarly, CRP is involved in inflammation but also in many other processes related to tissue maintenance, and it plays both proinflammatory and anti-inflammatory roles within the immune system.[37]

A previous study suggested that the persistent proinflammatory environment in AS is suitable for the differentiation of Th17 and Th1 cells.[38] The balance of IL-17-induced Th17 cells and regulatory

FIGURE 2. **Expression of IL-6 and TNF-α in patients with AS with different clinical characteristics. Comparison of IL-6 (A) and TNF-α (B) protein expression in patients with AS with or without fever, hip joint involvement, other joint involvement, complications, and positive HLA-B27, respectively. Data are shown as mean ± SD. *P <.05; Student's t-test. AS, ankylosing spondylitis; HLA-B27, human leukocyte antigen-B27; ns, no significant difference; SD, standard deviation; TNF-α, tumor necrosis factor-α.**

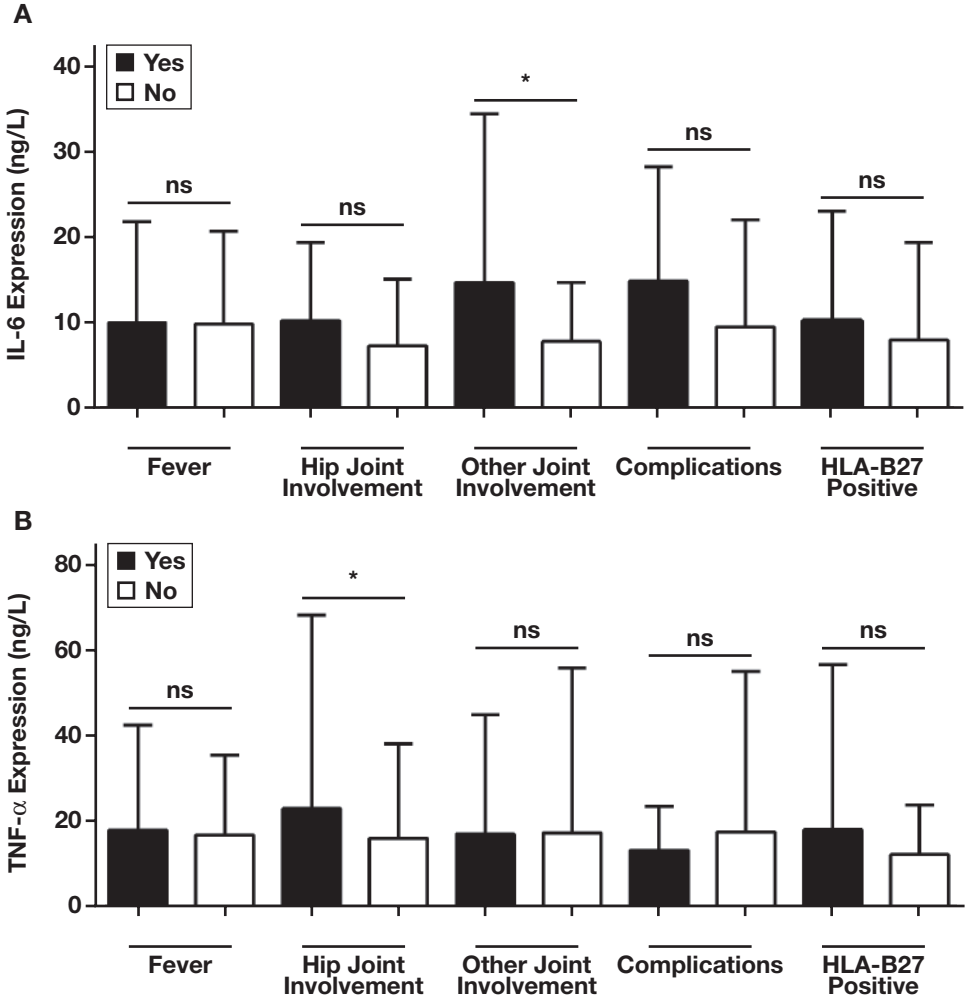

Treg cells serves an important role in the pathogenesis of AS.[39] Evidence from animal models has suggested that anti-IL-6 increases Th17 and decreases Treg cell differentiation.[40] In the present study, serum levels of IL-6 were substantially higher in patients with AS than in HCs. Notably, our experiments also showed that serum IL-6 positively correlated with the BASDAI and laboratory values, such as CRP and the ESR. Taken together, these observations suggest that IL-6 probably plays an important role in the disease evaluation of AS.

Studies have shown that IL-6 signaling-enhanced expression of matrix-degrading enzymes, such as matrix metalloproteinase (MMP)-1 and MMP-3, contributes to cartilage destruction in rheumatoid arthritis.[41] Furthermore, fibroblast- or macrophage-secreted IL-6 and IL-1β induces bone damage by promoting the differentiation of precursor cells to mature osteoclasts and eventually causes irreversible damage to joints and bones in osteoporosis.[38] We found that the levels of serum IL-6 positively correlated with CT imaging classification of sacroiliac arthritis, which suggests that IL-6 plays an important role in the progression of bone damage in AS. Notably, we confirmed high IL-6 levels in serum from patients with AS with sacroiliac arthritis and other joint involvement, such as the knee joints and cervical vertebrae. Therefore, high IL-6 levels likely represent severe sacroiliac joint involvement and active disease and predict other joints that are frequently involved and poor prognosis of the disease. In another words, the elevated levels of IL-6 are closely related to disease activity and participate in AS occurrence and development.

The pleiotropic cytokine TNF-α is produced by activated mononuclear macrophages, natural killer cells, and T cells.[42] The TNF-α pathway plays pivotal roles in the pathogenesis of AS, in which TNF-α stimulates the inflammatory immune response and accelerates AS development and progression via the activation of immune cells to produce cytokines, including IL-1, IL-6, and IL-37.[43] The expression of TNF-α may be significantly elevated at local inflammatory sites in patients with AS. For example, sacroiliac joint biopsy specimens and atrial water from patients with uveitis exhibit increased levels of TNF-α, and this enhanced expression positively correlates with ESR levels and disease activity.[44-46] The underlying mechanisms of TNF-α participation in pathogenesis

FIGURE 3. Correlations between the serum IL-6 and TNF-α levels and imaging classification of the sacroiliac joint. Comparison of IL-6 (A) and TNF-α (C) protein expression and Spearman nonparametric correlation analysis of the serum levels of IL-6 (B) and TNF-α (D) in patients with AS grouped by sacroiliac joint imaging. Data are shown as mean ± SD. *P <.05; ** P <.01; Student's t-test; Spearman nonparametric test. AS, ankylosing spondylitis; IL-6, interleukin-6; ns, no significant difference; r, Spearman correlation coefficient; SD, standard deviation; TNF-α, tumor necrosis factor-α.

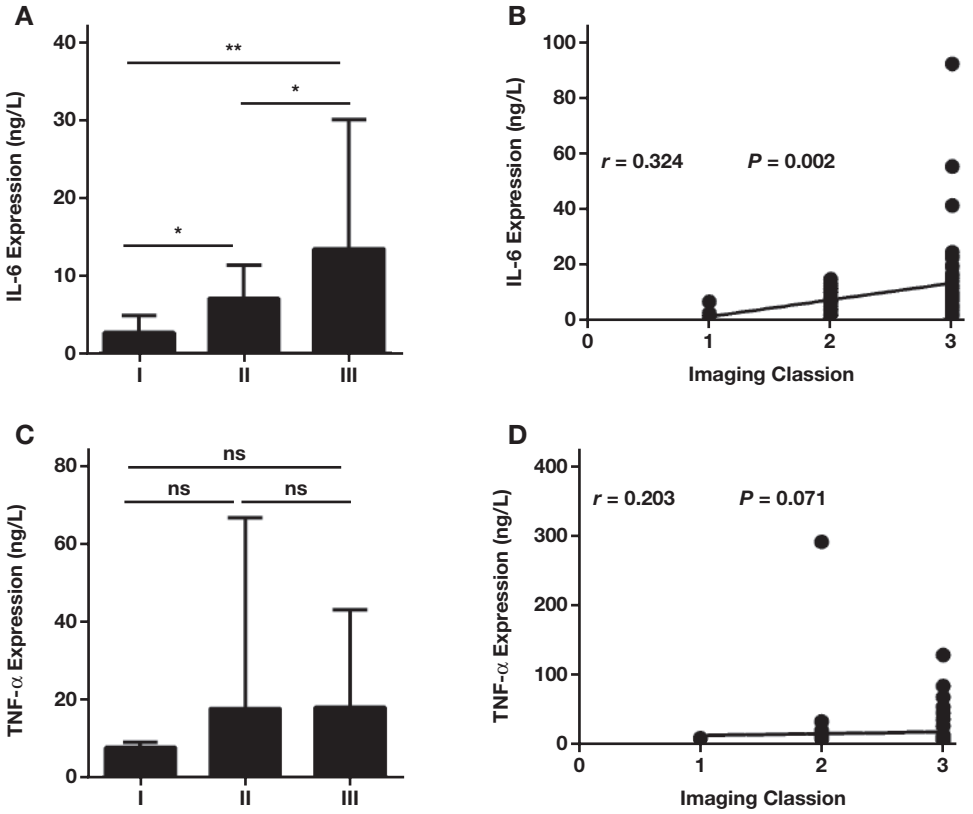

may be the promotion of IL-1β expression in chondrocytes, and TNF-α and IL-1β eventually result in the synergistic disruption of cartilage homeostasis because of the faster decomposition than synthesis of cartilage.[47]

Currently, anti-TNF-α-blocking therapy is increasingly used for patients with AS with active disease when other treatment options have proven ineffective. In fact, TNF-α inhibitors are effective in reducing pain and stiffness and improving the function of patients with AS.[22,23] It is remain unclear why some patients achieve significant improvement after anti-TNF-α treatment whereas others do not respond to the same treatment.

The results of this study showed that the serum levels of TNF-α of patients with AS were significantly higher than those of HCs. These results positively correlated with the BASDAI and disease duration. Therefore, our findings suggest that serum TNF-α levels reflect the degree of AS disease to a certain extent. Unlike serum levels of IL-6, we did not find any significant differences in the serum levels of TNF-α and CRP or the ESR. Taken together, these results indicate that TNF-α and IL-6 participate in pathogenesis likely by 2 different mechanisms, and IL-6 better reflects the degree of damage in sacroiliac arthritis.

Involvement of the sacroiliac joints is the first symptom of AS, which is the basis of diagnosis of this disease. Hip involvement is a common extraspinal arthritic manifestation in AS, which is associated with a worse functional outcome and may seriously worsen the prognosis of the disease.[48] Herein, the serum levels of TNF-α were markedly enhanced in patients with AS with hip joint involvement, which suggests that increased levels of TNF-α are associated with hip injury. Taken together, the inconsistent expression pattern of TNF-α and IL-6 showed the complex network of cytokine signaling pathways in AS that participate together in regulating the development of AS.

However, some limitations remain in this study. For example, it is unclear why serum levels of TNF-α did not correlate with the imaging classification of the sacroiliac joint; why serum levels of IL-6 were increased in patients with AS with other joint involvement, whereas serum levels of TNF-α were found only in patients with AS with hip joint involvement; and why serum levels of TNF-α were associated with the BASDAI and disease duration but did not correlate with the imaging classification of sacroiliac arthritis, CH50, CRP, or ESR levels. It will be necessary to conduct further studies to clarify these questions and further elucidate the mechanism of AS.

Conclusion

Taken together, our findings showed that the increased serum levels of IL-6 and TNF-α were closely related to the damage of the sacroiliac joint, hip joint, and other joints and were positively correlated with measures of disease activity, such as the BASDAI and disease duration, respectively. Therefore, these data suggest that IL-6 and TNF-α function as important indicators for the auxiliary diagnosis and evaluation of the disease activity of AS.

FIGURE 4. Correlations between the serum IL-6 and TNF-α levels and clinical parameters and laboratory results. Spearman nonparametric correlation analysis between serum levels of IL-6 (A–E) and TNF-α (F–J) with the BASDAI, disease duration, CH50, CRP, and ESR in patients with AS. AS, ankylosing spondylitis; BASDAI, Bath Ankylosing Spondylitis Disease Activity Index; CH50, total hemolytic complement; CRP, C-reactive protein; ESR, erythrocyte sedimentation rate; IL-6, interleukin-6; r, Spearman correlation coefficient; SD, standard deviation; TNF-α, tumor necrosis factor-α.

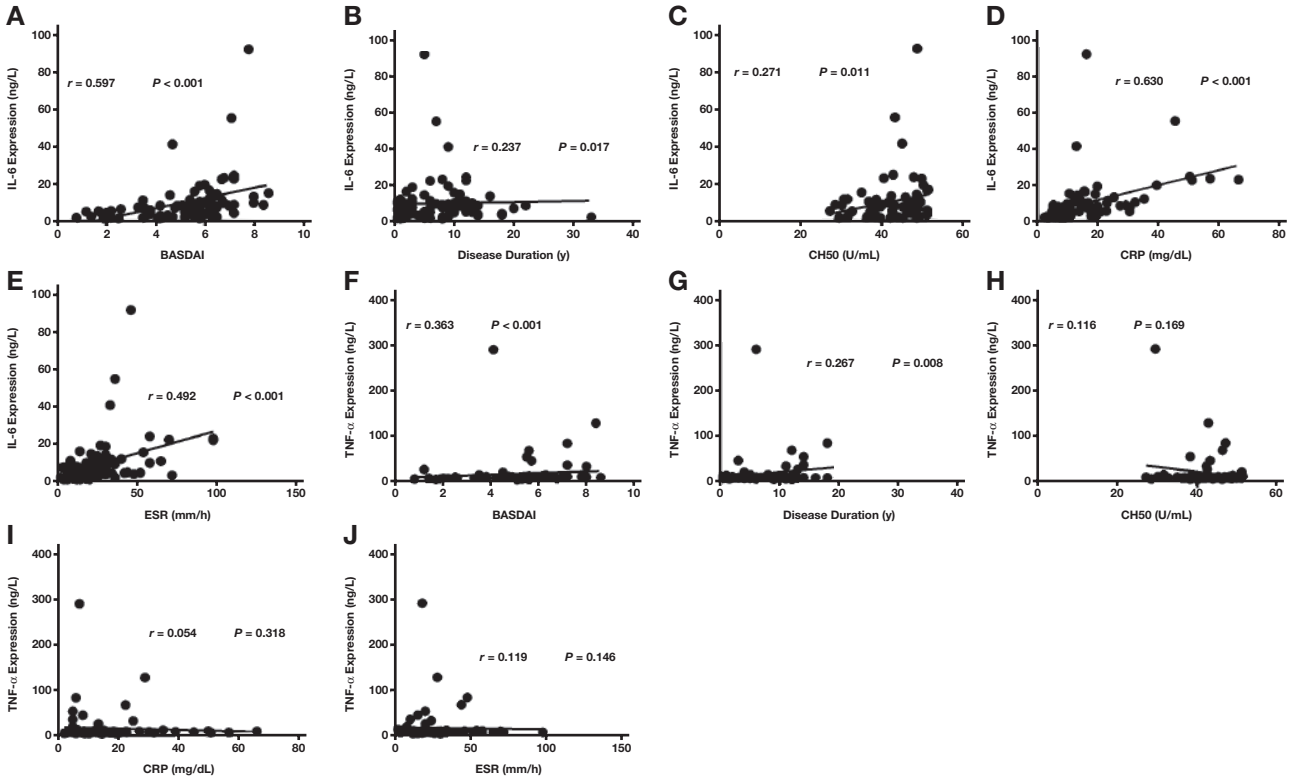

Acknowledgments

The authors thank the patients for donating specimens to the study. In addition, the authors thank the staff of Peking University Shenzhen Hospital for assistance with the collection of clinical specimens, members of the laboratory for help with specimen processing, and clinical data competing interests. Jing Du and Jinxia Sun designed and performed the experiments and helped with the preparation of manuscript; Zhanpeng Wen, Zhicheng Wu, Qian Li, and Qiannan Yang performed the experiments and helped with the writing of the manuscript; and Chao Yang conceived and supervised the study and prepared the manuscript.

This material is to be used for non–life science journals.

This work was supported by grants from the Special Program of Construction National Innovative City of Shenzhen (grant JCYJ20190809151205630).

REFERENCES

1. Sieper J, Braun J, Rudwaleit M, Boonen A, Zink A. Ankylosing spondylitis: an overview. *Ann Rheum Dis.* 2002;61(Suppl 3):iii8–iii18.
2. Amor B, Dougados M, Mijiyawa M. Criteria of the classification of spondylarthropathies. Article published in French. *Rev Rhum Mal Osteoartic.* 1990;57(2):85–89.
3. Khan MA. Ankylosing spondylitis: introductory comments on its diagnosis and treatment. *Ann Rheum Dis.* 2002;61(Suppl 3):iii3–iii7.
4. Braun J, Sieper J. Ankylosing spondylitis. *Lancet.* 2007;369(9570):1379–1390.
5. Taurog JD, Chhabra A, Colbert RA. Ankylosing spondylitis and axial spondyloarthritis. *N Engl J Med.* 2016;374(26):2563–2574.
6. van der Heijde D, Landewé R, Einstein S, et al. Radiographic progression of ankylosing spondylitis after up to two years of treatment with etanercept. *Arthritis Rheum.* 2008;58(5):1324–1331.
7. Saraux A, Guedes C, Allain J, et al. Prevalence of rheumatoid arthritis and spondyloarthropathy in Brittany, France. Société de Rhumatologie de l'Ouest. *J Rheumatol.* 1999;26(12):2622–2627.
8. Ranganathan V, Gracey E, Brown MA, Inman RD, Haroon N. Pathogenesis of ankylosing spondylitis—recent advances and future directions. *Nat Rev Rheumatol.* 2017;13(6):359–367.
9. Gran JT, Husby G, Hordvik M. Prevalence of ankylosing spondylitis in males and females in a young middle-aged population of Tromsø, Northern Norway. *Ann Rheum Dis.* 1985;44(6):359–367.
10. Dekker-Saeys BJ, Meuwissen SG, Van Den Berg-Loonen EM, De Haas WH, Agenant D, Tytgat GN. Ankylosing spondylitis and inflammatory bowel disease. II. Prevalence of peripheral arthritis, sacroiliitis, and ankylosing spondylitis in patients suffering from inflammatory bowel disease. *Ann Rheum Dis.* 1978;37(1):33–35.
11. Feldtkeller E, Khan MA, van der Heijde D, van der Linden S, Braun J. Age at disease onset and diagnosis delay in HLA-B27 negative vs. positive patients with ankylosing spondylitis. *Rheumatol Int.* 2003;23(2):61–66.
12. Franke LC, Ament AJ, van de Laar MA, Boonen A, Severens JL. Cost-of-illness of rheumatoid arthritis and ankylosing spondylitis. *Clin Exp Rheumatol.* 2009;27(4 Suppl 55):S118–S123.
13. Zhu W, He X, Cheng K, et al. Ankylosing spondylitis: etiology, pathogenesis, and treatments. *Bone Res.* 2019;7:22.
14. Fallahi S, Jamshidi AR, Gharibdoost F, et al. Urolithiasis in ankylosing spondylitis: correlation with Bath Ankylosing Spondylitis Disease Activity Index (BASDAI), Bath Ankylosing Spondylitis Functional Index

(BASFI) and Bath Ankylosing Spondylitis Metrology Index (BASMI). *Caspian J Intern Med.* 2012;3(4):508–513.

15. Garrett S, Jenkinson T, Kennedy LG, Whitelock H, Gaisford P, Calin A. A new approach to defining disease status in ankylosing spondylitis: the Bath Ankylosing Spondylitis Disease Activity Index. *J Rheumatol.* 1994;21(12):2286–2291.
16. Laurent MR, Panayi GS. Acute-phase proteins and serum immunoglobulins in ankylosing spondylitis. *Ann Rheum Dis.* 1983;42(5):524–528.
17. McVeigh CM, Cairns AP. Diagnosis and management of ankylosing spondylitis. *BMJ.* 2006;333(7568):581–585.
18. de Vlam K. Soluble and tissue biomarkers in ankylosing spondylitis. *Best Pract Res Clin Rheumatol.* 2010;24(5):671–682.
19. Estrores IM, Harrington A, Banovac K. C-reactive protein and erythrocyte sedimentation rate in patients with heterotopic ossification after spinal cord injury. *J Spinal Cord Med.* 2004;27(5):434–437.
20. Wu Y, Potempa LA, El Kebir D, Filep JG. C-reactive protein and inflammation: conformational changes affect function. *Biol Chem.* 2015;396(11):1181–1197.
21. Chen CH, Chen HA, Liao HT, Liu CH, Tsai CY, Chou CT. Suppressors of cytokine signalling in ankylosing spondylitis and their associations with disease severity, acute-phase reactants and serum cytokines. *Clin Exp Rheumatol.* 2016;34(1):100–105.
22. Sieper J, Poddubnyy D. New evidence on the management of spondyloarthritis. *Nat Rev Rheumatol.* 2016;12(5):282–295.
23. Maxwell LJ, et al. TNF-alpha inhibitors for ankylosing spondylitis. *Cochrane Database Syst Rev.* 2015;4:CD005468.
24. International Genetics of Ankylosing Spondylitis Consortium (IGASC); Cortes A, Hadler J, Pointon JP, et al. Identification of multiple risk variants for ankylosing spondylitis through high-density genotyping of immune-related loci. *Nat Genet.* 45(7):730–738.
25. van der Linden S, Valkenburg HA, Cats A. Evaluation of diagnostic criteria for ankylosing spondylitis. A proposal for modification of the New York criteria. *Arthritis Rheum.* 1984;27(4):361–368.
26. Robinson PC, Brown MA. Genetics of ankylosing spondylitis. *Mol Immunol.* 2014;57(1):2–11.
27. Tsui FW, Tsui HW, Akram A, Haroon N, Inman RD. The genetic basis of ankylosing spondylitis: new insights into disease pathogenesis. *Appl Clin Genet.* 2014;7:105–115.
28. Trull A, Ebringer A, Panayi G, Ebringer R, James DC. HLA-B27 and the immune response to enterobacterial antigens in ankylosing spondylitis. *Clin Exp Immunol.* 1984;55(1):74–80.
29. Thomas GP, Brown MA. Genetics and genomics of ankylosing spondylitis. *Immunol Rev.* 2010;233(1):162–180.
30. Colbert RA, Tran TM, Layh-Schmitt G. HLA-B27 misfolding and ankylosing spondylitis. *Mol Immunol.* 2014;57(1):44–51.
31. Colbert RA, Navid F, Gill T. The role of HLA-B*27 in spondyloarthritis. *Best Pract Res Clin Rheumatol.* 2017;31(6):797–815.
32. Brewerton DA, Hart FD, Nicholls A, Caffrey M, James DC, Sturrock RD. Ankylosing spondylitis and HL-A 27. *Lancet.* 1973;1(7809):904–907.
33. Reveille JD. An update on the contribution of the MHC to AS susceptibility. *Clin Rheumatol.* 2014;33(6):749–757.
34. Gratacós J, Collado A, Filella X, et al. Serum cytokines (IL-6, TNF-alpha, IL-1 beta and IFN-gamma) in ankylosing spondylitis: a close correlation between serum IL-6 and disease activity and severity. *Br J Rheumatol.* 1994;33(10):927–931.
35. Londono J, Romero-Sanchez MC, Torres VG, et al. The association between serum levels of potential biomarkers with the presence of factors related to the clinical activity and poor prognosis in spondyloarthritis. *Rev Bras Reumatol.* 2012;52(4):536–544.
36. Eklund CM. Proinflammatory cytokines in CRP baseline regulation. *Adv Clin Chem.* 2009;48:111–136.
37. Del Giudice M, Gangestad SW. Rethinking IL-6 and CRP: why they are more than inflammatory biomarkers, and why it matters. *Brain Behav Immun.* 2018;70:61–75.
38. Liu W, Wu YH, Zhang L, et al. Elevated serum levels of IL-6 and IL-17 may associate with the development of ankylosing spondylitis. *Int J Clin Exp Med.* 2015;8(10):17362–17376.
39. Kimura A, Kishimoto T. IL-6: regulator of Treg/Th17 balance. *Eur J Immunol.* 2010;40(7):1830–1835.
40. Nistala K, Wedderburn LR. Th17 and regulatory T cells: rebalancing pro- and anti-inflammatory forces in autoimmune arthritis. *Rheumatology.* 2009;48(6):602–606.
41. Araki Y, Tsuzuki Wada T, Aizaki Y, et al. Histone methylation and STAT-3 differentially regulate interleukin-6-induced matrix metalloproteinase gene activation in rheumatoid arthritis synovial fibroblasts. *Arthritis Rheumatol.* 2016;68(5):1111–1123.
42. Guzik TJ, Skiba DS, Touyz RM, Harrison DG. The role of infiltrating immune cells in dysfunctional adipose tissue. *Cardiovasc Res.* 2017;113(9):1009–1023.
43. Rezaiemanesh A, Abdolmaleki M, Abdolmohammadi K, et al. Immune cells involved in the pathogenesis of ankylosing spondylitis. *Biomed Pharmacother.* 2018;100:198–204.
44. Sharma SM, Jackson D. Uveitis and spondyloarthropathies. *Best Pract Res Clin Rheumatol.* 2017;31(6):846–862.
45. Jones A, Ciurtin C, Ismajli M, Leandro M, Sengupta R, Machado PM. Biologics for treating axial spondyloarthritis. *Expert Opin Biol Ther.* 2018;18(6):641–652.
46. Hu H, Du F, Zhang S, Zhang W. Serum calprotectin correlates with risk and disease severity of ankylosing spondylitis and its change during first month might predict favorable response to treatment. *Mod Rheumatol.* 2019;29(5):836–842.
47. Lories RJ. Advances in understanding the pathophysiology of spondyloarthritis. *Best Pract Res Clin Rheumatol.* 2018;32(3): 331–341.
48. Younes M, Jalled A, Aydi Z, et al. Socioeconomic impact of ankylosing spondylitis in Tunisia. *Joint Bone Spine.* 2010;77(1):41–46.

Anti-Golgi Antibody as a Potential Indicator for Rheumatoid Arthritis

Jianzhao Zhai, MM,[1,¶] Jing Liao, MM,[1,¶] Minjin Wang, MM,[1] Zhuochun Huang, MD,[1] Jing Hu, BS,[1] Huan Xu, MM,[1] Qibing Xie, MD,[2] Bin Ma, MD,[3] Carla C. Baan, MD,[4] Yongkang Wu, MD[1,5,]*

[1]West China School of Medicine/Department of Laboratory Medicine, West China Hospital, Sichuan University, Chengdu, China; [2]Department of Rheumatology, West China Hospital, Sichuan University, Chengdu, China; [3]School of Veterinary and Life Sciences, Murdoch University, Murdoch, Australia; [4]Department of Internal Medicine, Sector of Nephrology & Transplantation, Erasmus MC, Rotterdam, Netherlands; [5]Department of Outpatient and National Clinical Research Center for Geriatrics, West China Hospital of Sichuan University, Chengdu, China; *To whom correspondence should be addressed.vipwyk@163.com ¶Coauthors Zhai and Liao contributed equally to this work.

Keywords: anti-Golgi antibody, antinuclear antibodies, rheumatoid arthritis, autoimmune diseases, antibody titer, disease progression

Abbreviations: AID, autoimmune diseases; IIF, indirect immunofluorescence; ANAs, antinuclear antibodies; AGA, anti-Golgi antibody; SS, Sjögren syndrome; AKA, antikeratin antibody; anti-CCP, anti–cyclic citrullinated peptide; RF, rheumatoid factor; LIA, line immunoblot assay; ENAs, extractable nuclear antigens; CTDs, connective-tissue diseases; SLE, systemic lupus erythematosus; PSS, progressive systemic sclerosis; PM/DM, polymyositis/dermatomyositis; anti-SSB, anti–Sjögren syndrome antigen B; anti-RNP, antiribonucleoprotein; anti–Scl-70, antiscleroderma 70/antitopoisomerase I antibodies; anti–Jo-1, anti–histidyl-tRNA synthetase antibody; anti-Sm, anti–Chistosoma mansoni antibody; anti–Rib-P, anti–ribosomal P protein antibody

Laboratory Medicine 2022;53:156–160; https://doi.org/10.1093/labmed/lmab046

ABSTRACT

Objective: To reveal the relationship between anti-Golgi antibody (AGA) and clinical diseases through retrospective analysis.

Methods: The clinical data of 584 cases testing positive for AGA in the past 11 years were collected and retrospectively analyzed.

Results: AGA pattern accounted for .2% of positive ANA results. In total, 35.0% of diagnosed patients had autoimmune diseases (AID), mainly rheumatoid arthritis (RA). High-titer AGA (≧1:1000) was common in AID. In nondiagnosed patients with clinical symptoms, joint pain/muscle pain was the most common.

Conclusions: Positive AGA with high titer was closely related to RA. Joint pain/muscle pain was the most common symptom in patients who tested AGA positive. Therefore, AGA may be a key indicator of RA in the Chinese population.

Autoantibodies can be found in most autoimmune diseases (AID),[1] and their detection is greatly value for diagnosis, classification, and disease-activity monitoring.[2,3] Some specific autoantibodies have become serological markers of AID.[4] Indirect immunofluorescence (IIF) is the most common method to detect antinuclear antibodies (ANAs).[5,6] In 1982, it was first reported that anti-Golgi antibody (AGA) was found in a patient with Sjögren syndrome (SS) and lymphoma.[7] Since then, AGA has been described in patients with diverse conditions, such as viral infectious diseases and neurological diseases.[1,8] AGA recognizes autoantigens including giantin/macrogolgin/GCP372, golgin-245/p230, golgin-160/GCP170, golgin-95/gm130, golgin-97, and golgin-67. Moreover, the immunoreactivity was related to the molecular mass of the Golgi.[9,10] It has been suggested that even if there are no clinical symptoms, the persistent high titer of AGA can constitute an early sign of systemic autoimmune disorder[1]; however, some researchers think it is not very specific for autoimmune diseases.[11] Until now, the relationship between AGA and clinical diseases has been obscure. Therefore, we collected and retrospectively analyzed the information of patients at West China Hospital who had tested positive for AGA in the past 11 years, to determine the correlation between AGA and specific diseases, and to assist and guide clinical decision and treatment.

Material and Methods

Case Individuals and Specimens

From 2007 to 2018, a total of 283,845 patients who tested ANA positive and had various diseases were recruited from West China Hospital, Chengdu, China. Among them, 584 case individuals had tested AGA positive; these cases do not include the same patients. The male-to-female ratio was 1:1.97. These patients were aged 12 years to 91 years when tested for AGA, with an average age of 52.0 ± 16.2 years. According to whether they had received a clear diagnosis, the patients were divided into 2 groups: the diagnosis group (277/584) and the nondiagnosis group (307/584). The diagnosis group included patients with AID

(97/277) and patients without AID (180/277). In the nondiagnosis group, 240 patients lacked clinical information, and the other 67 had certain clinical symptoms. To further study the effect of AGA in RA, we compared 2 groups of RA patients: 30 patients with a positive AGA result and the other 45 with a negative AGA result. We tried to keep the other variables consistent. The authors had access to information that could identify individual participants during or after data collection. Our research gained ethical approval from Ethics Committee of West China Hospital of Sichuan University, and all experiments were conducted in accordance with Declaration of Helsinki.

Test Methods

ANA testing was performed on HEp-2 cell substrate by IIF, and antikeratin antibody (AKA) testing was performed on primate esophagus using the same method. In this study, we used 5 levels, namely, 1:100, 1:320, 1:1000, 1:3200, and 1:10000 to evaluate the titer of ANA. Anti–cyclic citrullinated peptide (anti-CCP) antibody was tested via the electrochemiluminescence method. The rate-scattering turbidimetric method was used to assess rheumatoid factor (RF). Line immunoblot assay (LIA) method was used for antibodies against extractable nuclear antigens (ENA), including anti-Sm, anti-SSA, anti-SSB anti-RNP, anti-Scl-70, anti–Jo-1, and anti–Rib-P antibodies. Serum CRP was determined using nephelometry. RBC was analyzed using automatic blood analyzer. Blood biochemical detected by spectrophotometry such as ALT, AST, ALP, and serum urea.

Statistical Analysis

Mean, median, and mean (SD) values were used for data description. χ^2 testing was used for comparison of the composition ratio between groups. Because the antibody titer and the results of indicators were not normally distributed, and the variances were not uniform, we used rank-sum testing to analyze the differences. *P* values less than .05 were considered statistically significant. All analyses were performed using SPSS software, version 24.0 (IBM Corporation).

Results

The fluorescence pattern of AGA was shown in **FIGURE 1**; this caplike coarse granular staining on one side of the cytoplasm is characteristic of AGAs. In our study, the positive proportion of AGA in patients with a positive test result for ANA was .21% (584/283,845). Among these patients, 412 cases had the anti-Golgi pattern only, and the remaining 172 cases had a mixed ANA pattern. The most common mixed pattern was speckled (n = 90 cases), followed by homogeneous (n = 18 cases). A total of 35.02% patients had AID, mainly in the form of RA (30.9%), connective-tissue diseases (CTDs; 16.5%), and systemic lupus erythematosus (SLE; 15.5%). The ratio of RA was significantly different from other diseases (P <.05).

Comparing the proportion of AID and non-AID with different titers, we discovered that high-titer results (≥1:1000) appeared more often in AID, and with the increase of AGA titer, the proportion of patients with AID gradually increased (**FIGURE 2**). The disease distribution and titer values for the patients are listed in **TABLE 1**.

There were 67 patients without a clear diagnosis but with definite clinical symptoms. Among these patients the most common clinical symptom was joint pain/muscle pain (38.8%), followed by headache (14.9%). The results are shown in **TABLE 2**. The median AGA titer for each kind of symptom was 1:100.

Compared with other items, the positive rates of anti-CCP, RF, and AKA antibodies in patients who had tested AGA positive were higher—31.1%, 21.2%, and 20.3%, respectively. The relationship between AGA and other items is listed in **TABLE 3**.

RA was the disease most closely related to AGA. Some indicators were analyzed to compare the differences caused by AGA in patients with RA, including 30 patients with RA who tested AGA positiveand 45 patients with RA testing AGA negative. There were no statistically significant differences in age (P = .08) or sex (P = .80) between the 2 groups of patients. We compared CRP representing the disease activity; ALT, AST, and ALP, showing the hepatic function; serum urea, displaying the renal function, and RBCs to investigate the condition of the blood system. Also, the differences in RF, anti-CCP, and AKA between the 2 groups of patients were analyzed. Among these indicators, CRP was obviously different between the groups (**TABLE 4**).

Discussion

AGA is a kind of anticytoplasmic antibody with a unique staining pattern.[12,13] Its pathogenic effect, clinical utility, and diagnostic value were obscure until now. We retrospectively analyzed the clinical information and laboratory tests data of 584 patients with an AGA-positive test result who had been treated in West China Hospital in the past 11 years, aiming to explore the clinical significance of AGA in the Chinese population.

AGA has a low positivity rate in ANA testing.[14] In this study that rate was .21%, which was almost consistent with the known results. Hence, it can easily be overlooked, and clinicians may be misled by the negative results of ANA tests. In the diagnosis group, patients with AID had a median titer of 1:320, and patients without AID had a median titer of 1:100. Also, high-titer AGA (≥1:1000) was mainly found in patients with AID, and the cut-off point was approximately 1:1000 (**FIGURE 2**). In other words, low-titer, transient AGA was more related to non-AID diseases. AGA was associated with rheumatic diseases, the most common of which was RA (30.9%; **TABLE 1**). Therefore, AGA may have strong correlation with RA.[15]

FIGURE 1. Specific anti-Golgi antibody (AGA) pattern.

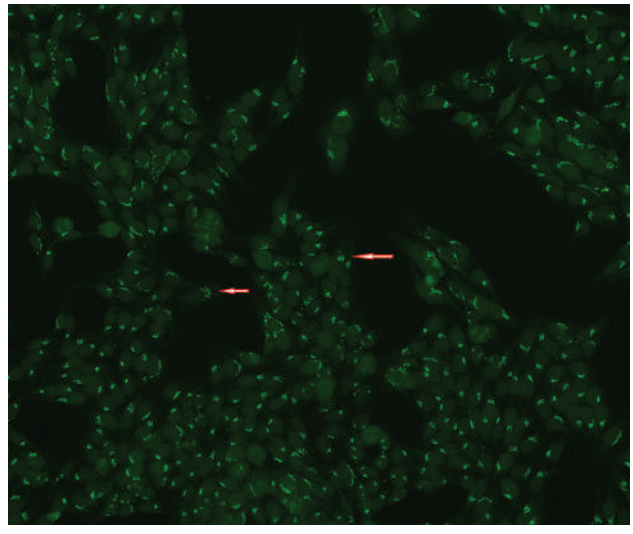

In the non-AID group, multiple systems can be involved—mostly, the pulmonary, renal, cardiovascular, and cerebrovascular systems. Among the 97 patients with AID, some people also have lung disease (13.4%) and renal disease (11.3%). However, most of the lung diseases were pneumonia, which may be related to immunosuppressive therapy, and the renal diseases were caused by autoimmune disease, such as lupus nephritis and ANCA-associated glomerulonephritis. Also, a total of 23 cases (12.8%) of patients without AID who have a positive AGA result contracted cancer, such as lung, liver, and gastric cancer. The findings of relevant studies[16–18] exposed that certain autoantibodies have been found in patients with cancer, suggesting that the proteins related to cancer-cell division or proliferation may be the corresponding targets of these autoantibodies.

FIGURE 2. The trend of anti-Golgi antibody (AGA) titer in patients with or without autoimmune disease (AID).

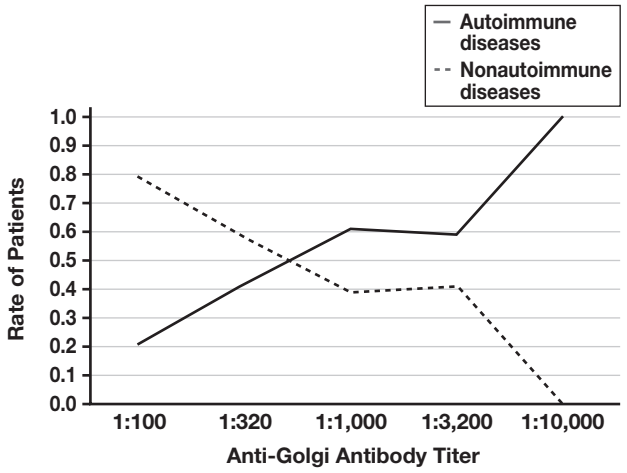

Besides, multiple clinical symptoms were displayed in patients testing AGA positive who had no clear diagnosis (**TABLE 2**), such as joint pain/muscle pain, headache, thrombocytopenia, and anemia. The most common symptom was joint pain/muscle pain (38.8%); the patients in this category could check the immune system–related items regularly to exclude AID. Patients who have tested AGA positive and have these symptoms may further progress to AID, and the titer may increase. This possibility can be researched through follow-up studies.

Apart from AGA, some other autoantibodies also can be detected in these patients (**TABLE 3**). After analyzing other indicators of all patients testing AGA positive, we found that anti-CCP, RF, and AKA antibodies had higher positivity rates, which are all characteristic and diagnostic antibodies of RA. However, there was no difference in these indicators between patients testing AGA positive and those testing AGA negative, among patients with RA. Our findings confirmed that AGA may be closely related to RA in the Chinese population. In the 317 cases of ENA detection, there were 31 anti-SSA, 6 anti-SSB, 6 anti-RNP, 3 anti–Scl-70, 1 anti–Jo-1, anti-Sm, and anti–Rib-P, respectively. Whether the aforementioned autoantibodies were related to AID itself or AGA requires further analysis.

To further study the influence of AGA in RA, we analyzed the indicators of 2 groups of patients with RA—those who had tested positive for AGA and those who had tested negative for it. Among the indicators, CRP was significantly different between the groups (**TABLE 4**). The CRP of patients testing positive for AGA was 3.77 times that of patients testing negative for AGA. This finding suggested that AGA may affect the activity and severity of RA.

Despite these findings, according to the reports, we noticed that some Golgi antigens were found to be related to specific diseases. For instance, Golgi antigen with molecular masses of 64 kDa, 95 kDa, and 160 kDa is related to SLE and 79 kDa to RA; further, some Golgi

TABLE 1. Disease Distribution and Titer of 277 Diagnosed Patients with an AGA-Positive Test Result

Diagnosis	No.	Frequency, %	Titer Range	Geometric Mean of Titer
AID[a]	97	35.0%	1:100–1:10000	1:320[b]
RA	30	30.9%	1:100–1:1000	1:320
CTDs	16	16.5%	1:100–1:10000	1:1000
SLE	15	15.5%	1:100–1:3200	1:320
SS	11	11.3%	1:100–1:3200	1:320
PSS	5	5.2%	1:100–1:1000	1:320
PM/DM	5	5.2%	1:100–1:3200	1:320
Others[c]	17	17.5%	1:100–1:3200	1:100
Non-AID[a]	180	65.0%	1:100–1:10000	1:100[b]
Pulmonary diseases	43	23.9%	1:100–1:3200	1:100
Renal diseases	37	20.6%	1:100–1:3200	1:100
Cancer	22	12.2%	1:100–1:3200	1:100
Cardiovascular- and cerebrovascular-system diseases	20	11.1%	1:100–1:1000	1:100
Hepatic diseases	15	8.3%	1:100–1:1000	1:100
Others[d]	52	28.9%	1:100–1:10000	1:100

AID, autoimmune disease; RA, rheumatoid arthritis; CTDs, connective-tissue diseases; SLE, systemic lupus erythematosus; SS, Sjögren syndrom; PSS, progressive systemic sclerosis; PM/DM, polymyositis/dermatomyositis.
[a]The AID group had 2 patients with mixed diagnoses—one had SS with RA; the other had CTDs with PM/DM; the non-AID group had 9 patients with mixed diagnoses—5 had pulmonary diseases with renal diseases, 3 had renal diseases with cancer, and 1 had pulmonary disease with cancer.
[b]T = 11,719; P <.001.
[c]Including myasthenia gravis, autoimmune hemolytic anemia, rheumatic heart diseases, etc.
[d]Including infection, thrombocytopenic purpura, gastritis, etc.

autoantigens with the same molecular masses can present in different diseases.[19] These findings can explain why AGA manifests itself in many diseases. Nevertheless, only when AGA that recognizes specific Golgi autoantigens appears and accumulates can we discover high-titer AGA and its specificity for diseases. There are study findings noting that during apoptosis, the Golgi were localized to a unique indentation of the nucleus, and antigenic fragments with distinctive characteristics were produced.[20] These results suggested that Golgi may play a role in sustaining autoantibody production in AID.

We emphasize that the relationship between AGA and disease has not reached general consensus. A few researchers believe that these entities are not related to AID.[11] However, according to our results, we considered that our findings may be related to the titer of AGA. Low-titer AGA might be transient and can present in non-AID, but high-titer AGA was related to AID, particularly RA.

TABLE 2. Symptoms Distribution and Titer of 67 Patients Testing AGA Positive[a]

Clinical Symptoms	No.	Frequency (%)	Titer Range
Joint pain/muscle pain	26	38.8%	1:100–1:1000
Headache	10	14.9%	1:100
Effusion	7	10.5%	1:100–1:1000
Thrombocytopenia	6	9.0%	1:100
Limb weakness	4	6.0%	1:100
Anemia	4	6.0%	1:100–1:320
Others[b]	16	26.9%	1:100–1:320

[a]Median titer for each = 1:100.
[b]Including swelling or deformity of the joints, cough and expectoration, proteinuria, etc.

Conclusions

Most patients with high-titer AGA (≥1:1000) had AID, particularly RA. Most patients with an AGA-positive test result were characterized as having high rates of joint pain/muscle pain and anti-CCP, RF, and AKA antibodies. So, in conclusion, the presence of high-titer AGA might be the key serological marker for RA in the Chinese population.

Acknowledgments

This work was supported by Project of Science and Technology Department of Sichuan (grant no. 2020YFS0125); Project of Science and Technology Bureau of Chengdu (grant no. 2019-GH02-00006-HZ, 2019-YF05-00463-SN) and the 1·3·5 Project for Disciplines of

TABLE 3. Relationship Between AGA and Other Test Items

Items	Test Cases, no.	Positive Results, no.	Positivity Rate, %	Main Corresponding Diseases	Main Diseases, no.
Anti-CCP	90	28	31.1%	RA	21
RF	292	62	21.2%	RA	17
AKA	69	14	20.3%	RA	11
Anti-SSA	317	31	9.8%	RA, SS	5 of each
Anti-SSB	317	6	1.9%	SS, PSS	2 of each
Anti-RNP	317	6	1.9%	CTD	5
Anti–Scl-70	317	3	1.0%	PSS	2
Anti–Jo-1	317	1	.3%	PM/DM	1
Anti-Sm	317	1	.3%	CTD	1
Anti–Rib-P	317	1	.3%	Pulmonary diseases	1

anti-CCP, anticyclic citrullinated peptide; RF, rheumatoid factor; AKA, antikeratin antibodies; anti-SSA, anti–Sjögren syndrome antigen A; anti-SSB, anti–Sjögren syndrome antigen B; anti-RNP, antiribonucleoprotein; anti–Scl-70, antiscleroderma 70/antitopoisomerase I antibodies; anti–Jo-1, anti–histidyl-tRNA synthetase antibody; anti-Sm, anti–Chistosoma mansoni antibody; anti–Rib-P, anti–ribosomal P protein antibody

TABLE 4. Comparison of Indicators Between Patients with RA Having AGA-Negative and AGA-Positive Test Results

Indicator	Reference Range	Median Value (Quartile Range)		*P* Value
		AGA-Positive Group (*n* = 30)	AGA-Negative Group (*n* = 45)	
CRP (mg/L)	0–5	23.4 (5.5–33.0)	6.2 (2.51–16.05)	.01
ALT (IU/L)	<50	18.0 (11.0–28.0)	17.0 (13.0–22.0)	.95
AST (IU/L)	<40	21.0 (16.0–28.0)	23.0 (19.0–29.0)	.27
ALP (IU/L)	51–160	84.0 (63.0–104.0)	80.5 (56.0–03.3)	.61
Serum urea (mmol/L)	3.2–7.79	5.2 (3.9–5.9)	4.7 (3.8–6.2)	.97
RBC (10^{12}/L)	4.3–5.8	4.3 (3.7–4.6)	4.2 (4.0–4.5)	.68
RF (IU/mL)	<20	78.1 (20.0–470.0)	45.5 (20.0–153.0)	.37
Anti-CCP (U/mL)	<7	111.9 (63.6–414.7)	385.4 (36.1–500)	.19
AKA	negative	50.0%	47.8%	.89

RF, rheumatoid factor; anti-CCP, anti–cyclic citrullinated peptide; AKA, antikeratin antibodies.

Excellence–Clinical Research Incubation Project, West China Hospital, Sichuan University (grant no. 2020HXFH038).

Personal and Professional Conflicts of Interest

None declared.

REFERENCES

1. Ma L, Zeng A, Chen Y, Chen B, Zhou R. Anti-golgi antibodies: Prevalence and disease association in Chinese population. *Clin Chim Acta.* 2019;496:121–124.
2. Kuret T, Lakota K, Hočevar A, Burja B, Čučnik S, Sodin-Semrl S. Evaluating the utility of autoantibodies for disease activity and relapse in giant cell arteritis. *J Biol Regul Homeost Agents.* 2018;32(2):313–319.
3. Tozzoli R, Villalta D, Bizzaro N. Challenges in the standardization of autoantibody testing: a comprehensive review. *Clin Rev Allergy Immunol.* 2017;53(1):68–77.
4. Aggarwal A. Role of autoantibody testing. *Best Pract Res Clin Rheumatol.* 2014;28(6):907–920.
5. Zhang Y, Xi Y, Fang J, Luo S, Wilson JJ, Huang RP. Identification and characterization of monoclonal antibodies against GP73 for use as a potential biomarker in liver cancer screening and diagnosis. *J Immunoassay Immunochem.* 2016;37(4):390–406.
6. Infantino M, Carbone T, Manfredi M, et al; Study Group on Autoimmune Diseases of the Italian Society of Clinical Pathology and Laboratory Medicine. A new diagnostic algorithm for pattern-oriented autoantibody testing according to the ICAP nomenclature: A pilot study. *Autoimmun Rev.* 2020;19(8):102588.
7. Rodríguez JL, Gelpi C, Thomson TM, Real FJ, Fernández J. Anti-golgi complex autoantibodies in a patient with Sjögren syndrome and lymphoma. *Clin Exp Immunol.* 1982;49(3):579–586.
8. Andrejevic S, Milenkovic B, Stojsic J, Stevic R, Bonaci-Nikolic B. Coexistence of autoantibodies against the golgi complex and Ro52 antigen in a patient with nonspecific interstitial pneumonia. *Intern Med.* 2016;55(3):273–278.
9. Van den Bergh K, Vercammen M, Regenass S, et al. Betaine homocysteine methyl transferase 1, a novel auto-antigen associated with anti-Golgi immune reactivity. *Clin Chim Acta.* 2012;413(1-2):105–108.
10. Nozawa K, Fritzler MJ, von Mühlen CA, Chan EK. Giantin is the major Golgi autoantigen in human anti-Golgi complex sera. *Arthritis Res Ther.* 2004;6(2):R95–102.
11. Vermeersch P, Van den Bergh K, Blockmans D, Westhovens R, Bossuyt X. Anti-Golgi autoantibodies are not clinically associated with systemic autoimmune diseases. *Ann Rheum Dis.* 2011;70(1):234–235.
12. Sener AG, Afsar I, Demirci M. Evaluation of antinuclear antibodies by indirect immunofluorescence and line immunoassay methods: four years' data from Turkey. *APMIS.* 2014;122(12):1167–1170.
13. Bertin D, Jourde-Chiche N, Bongrand P, Bardin N. Original approach for automated quantification of antinuclear autoantibodies by indirect immunofluorescence. *Clin Dev Immunol.* 2013;2013:182172.
14. Vermeersch P, Bossuyt X. Prevalence and clinical significance of rare antinuclear antibody patterns. *Autoimmun Rev.* 2013;12(10):998–1003.
15. Yang Y, Fujita J, Tokuda M, et al. Clinical features of several connective tissue diseases with anti-Golgi antibody. *Ann Rheum Dis.* 2001;60(10):986–987.
16. Dumstrei K, Chen H, Brenner H. A systematic review of serum autoantibodies as biomarkers for pancreatic cancer detection. *Oncotarget.* 2016;7(10):11151–11164.
17. Tang ZM, Ling ZG, Wang CM, Wu YB, Kong JL. Serum tumor-associated autoantibodies as diagnostic biomarkers for lung cancer: A systematic review and meta-analysis. *PLoS One.* 2017;12(7):e0182117.
18. Ebrahimnezhad S, Jazayeri M, Hassanian SM, Avan A. Current status and prospective regarding the therapeutic potential of natural autoantibodies in cancer therapy. *J Cell Physiol.* 2017;232(10):2649–2652.
19. Hong HS, Chung WH, Hung SI, Chen MJ, Lee SH, Yang LC. Clinical association of anti-golgi autoantibodies and their autoantigens. *Scand J Immunol.* 2004;59(1):79–87.
20. Nozawa K, Casiano CA, Hamel JC, Molinaro C, Fritzler MJ, Chan EK. Fragmentation of Golgi complex and Golgi autoantigens during apoptosis and necrosis. *Arthritis Res.* 2002;4(4):R3.

Estimation of Low-Density Lipoprotein Cholesterol Concentration Using Machine Learning

Hikmet Can Çubukçu, MD,[1,*] *Deniz İlhan Topcu, MD, PhD, CLP*[2]

[1]Ankara University Stem Cell Institute, Interdisciplinary Stem Cells and Regenerative Medicine, Ankara, Turkey; [2]Başkent University Faculty of Medicine, Department of Medical Biochemistry, Ankara, Turkey; *To whom correspondence should be addressed. hikmetcancubukcu@gmail.com; The authors contributed equally to this work.

The present study was performed in a Başkent University Faculty of Medicine clinical laboratory.

Keywords: low-density lipoproteins, cholesterol, lipids, artificial intelligence, machine learning, lipoproteins

Abbreviations: LDL-C, low-density lipoprotein cholesterol; TG, triglycerides; ANN, artificial neural network; ASCVD, atherosclerotic cardiovascular disease; TC, total cholesterol; HDL-C, high-density lipoprotein cholesterol; VLDL-C, very-low-density lipoprotein cholesterol; EAS, European Atherosclerosis Society; EFLM, European Federation of Clinical Chemistry and Laboratory Medicine; NCEP, National Cholesterol Education Program; ATP, Adult Treatment Panel; ML, machine learning; CLIA, Clinical Laboratory Improvement Amendments; CV, coefficient of variation; PPV, positive predictive value; AHA, American Heart Association; ACC, American College of Cardiology; KNN, K-nearest neighbors; MD, mean differences.

Laboratory Medicine 2022;53:161–171; https://doi.org/10.1093/labmed/lmab065

ABSTRACT

Objective: Low-density lipoprotein cholesterol (LDL-C) can be estimated using the Friedewald and Martin-Hopkins formulas. We developed LDL-C prediction models using multiple machine learning methods and investigated the validity of the new models along with the former formulas.

Methods: Laboratory data (n = 59,415) on measured LDL-C, high-density lipoprotein cholesterol, triglycerides (TG), and total cholesterol were partitioned into training and test data sets. Linear regression, gradient-boosted trees, and artificial neural network (ANN) models were formed based on the training data. Paired-group comparisons were performed using a *t*-test and the Wilcoxon signed-rank test. We considered *P* values <.001 with an effect size >.2 to be statistically significant.

Results: For TG ≥177 mg/dL, the Friedewald formula underestimated and the Martin-Hopkins formula overestimated the LDL-C (*P* <.001), which was more significant for LDL-C <70 mg/dL. The linear regression, gradient-boosted trees, and ANN models outperformed the aforementioned formulas for TG ≥177 mg/dL and LDL-C <70 mg/dL based on a comparison with a homogeneous assay (*P* >.001 vs. *P* <.001) and classification accuracy.

Conclusion: Linear regression, gradient-boosted trees, and ANN models offer more accurate alternatives to the aforementioned formulas, especially for TG 177 to 399 mg/dL and LDL-C <70 mg/dL.

Atherosclerotic cardiovascular disease (ASCVD) is one of the most common causes of mortality and morbidity globally. Low-density lipoprotein (LDL) is not only a risk factor for ASCVD but also a causal factor in its development. Further, the risk of cardiovascular events decreases with LDL cholesterol (LDL-C) reduction.[1]

Total cholesterol (TC), triglycerides (TG), HDL cholesterol (HDL-C), LDL-C, non-HDL-C, and calculated remnant particles (if LDL-C is measured directly) constitute a standard lipid profile. However, measuring TC, TG, and HDL-C along with LDL-C and non-HDL-C is considered to be a cost-efficient approach to obtaining a profile. Among the lipid profile components, LDL-C remains the factor providing the strongest evidence for cardiovascular risk management.[2] It can also aid in dyslipidemia characterization, the determination of treatment targets, and clinical decision-making.[2,3]

Beta-quantification, the standard reference method for LDL-C measurement, requires labor-intensive manual steps, such as precipitation and ultracentrifugation.[4] Direct homogeneous assays have thus come to the forefront for enabling the direct measurement of LDL-C with autoanalyzers.[5] Nevertheless, the Friedewald formula is also widely used for LDL-C estimation in clinical medicine.[3] However, the formula uses a fixed factor of 5 as a denominator of TG to calculate very-low-density lipoprotein cholesterol (VLDL-C) and was first developed based upon only 448 patient results.[6] Further, underestimated LDL-C results have been obtained when using the Friedewald formula, especially with a TG concentration >200 mg/dL.[4] The other most well-known LDL-C calculation method is the Martin-Hopkins formula, which is based on 180 adjustable factors for the TG/VLDL ratio based on TG and non-HDL-C concentrations ($LDLC = TC \;\; HDLC \;\; TG/adjustable\ factor$)[7].

The European Atherosclerosis Society (EAS) and the European Federation of Clinical Chemistry and Laboratory Medicine (EFLM) Joint Consensus Initiative found the Martin-Hopkins formula to be

preferable when LDL-C levels are <1.8 mmol/L (70 mg/dL) and/or when TG-C levels are between 2 and 4.5 mmol/L (177–399 mg/dL). For TG concentrations >4.5 mmol/L (399 mg/dL,) direct LDL-C measurement is recommended.[2] Further, direct homogeneous assays classify LDL-C better than the Friedewald formula in terms of the National Cholesterol Education Program (NCEP) Adult Treatment Panel (ATP) III cutoff points.[4]

Machine learning (ML) methods, including K-nearest neighbors,[8] artificial neural networks (ANNs),[9] linear regression, support vector machines, extreme gradient boosting,[10] and random forest[11] algorithms, have been investigated for LDL-C estimation. However, some of these studies lack information about the direction of misestimation[10] and classification performances[9] for clinically important LDL-C and TG concentrations concurrently. Moreover, no study has investigated the validity of ML models and the Friedewald and Martin-Hopkins formulas when used on the Turkish population.

The purpose of the present study is to develop alternative LDL-C estimation models using multiple ML techniques, including linear regression, gradient-boosted trees, and ANN models, and to investigate the validity of the Friedewald and Martin-Hopkins formulas and the new ML models by comparison with direct LDL-C measurement for clinically important LDL-C and TG concentrations in the Turkish population.

Materials and Methods

Study Population

This study was approved by the Başkent University Institutional Review Board (project number KA20/365). Data sets containing patients' age, sex, and directly measured laboratory test results on LDL-C, HDL-C, TG, and TC were retrospectively retrieved from laboratory information and management software. The data sets comprised 59,415 directly measured concomitant LDL-C, HDL-C, TG, and TC test results obtained from January 2011 to June 2020. The general features of the data are summarized in **TABLE 1**.

TABLE 1. Demographic Features and Biochemical Measurements of Patient Data

Characteristics	Unit	Measurement
N (train %–test %)	…	59.415 (80–20)
Sex, % (female–male)	…	49–51
Age,[a] y (female/male)	…	53.2 (20.6)/52.0 (19.6)
Outpatient %–inpatient %	…	77–23
Total cholesterol[a]	mmol/L	5.00 (1.29)
	mg/dL	193.50 (49.98)
LDL cholesterol[a]	mmol/L	3.05 (1.04)
	mg/dL	117.98 (4.03)
HDL cholesterol[a]	mmol/L	1.19 (0.35)
	mg/dL	45.99 (13.46)
Triglycerides[a]	mmol/L	1.68 (1.09)
	mg/dL	148.51 (96.52)

HDL, high-density lipoprotein; LDL, low-density lipoprotein.
[a]Mean (standard deviation).

LDL-C Measurement with Homogeneous Assay

The LDL-C, HDL-C, TC, and TG analyses were performed on Abbott Architect c and Abbott Alinity c series analyzers (Abbott Diagnostics). Internal quality control materials were run every 12 hours at 2 levels on the all clinical chemistry analyzers in our laboratory. Our laboratory also enrolled in an external quality control program (monthly) for all analytes. The total error values of LDL-C measurement were 9.3 and 10.7 for the Alinity c and Architect c analyzers, respectively, which met the specification limit defined by the 2019 Clinical Laboratory Improvement Amendments (CLIA; 20%) for both devices. The 2019 CLIA specification limits apply to model 3 of the proposed models from the 2015 EFLM strategic conference.[12]

Measurements of LDL-C, TC, and TG were performed using Sekisui-based reagents made by Abbott Diagnostics. The HDL-C was measured using reagents from Archem and Abbott Diagnostics. Direct LDL-C measurement was conducted using the homogeneous method with a liquid selective detergent. The LDL-C analysis took place in 2 phases. In the first phase, non-LDL particles were solubilized and then consumed by cholesterol esterase and cholesterol oxidase in a non-color-forming reaction. In the second phase, the remaining LDL was solubilized. The enzymatic reaction of LDL with a chromogenic coupler produced colored dye proportional to the LDL-C concentration. The HDL-C measurements were performed using the accelerator selective detergent methodology. We analyzed the TC levels using the enzymatic endpoint method and measured TG using the glycerol phosphate oxidase method.

For the Architect c analyzer, the analytical coefficients of variation (CVs) for the last 6-month period were as follows: LDL-C: 3.06% at 54 mg/dL and 3.4% at 76 mg/dL; TC: 1.31% at 102 mg/dL and 0.96% at 143 mg/dL; HDL-C: 3.9% at 31 mg/dL and 3.37% at 40 mg/dL; TG: 5.3% at 54 mg/dL and 3.8% at 153 mg/dL. For the Alinity c analyzer, the CVs for the 6-month period were as follows: LDL-C: 3.25% at 62 mg/dL and 3.9% at 95 mg/dL; TC: 1.42% at 106 mg/dL and 1.37% at 164 mg/dL; HDL-C: 2.16% at 39 mg/dL and 2.20% at 53 mg/dL; TG: 1.61% at 132 mg/dL and 1.32% at 215 mg/dL.

LDL-C Concentration Estimation by Formulas and ML Models

The LDL cholesterol calculation with the Friedewald formula was carried out as follows[6]:

$$\mathrm{LDLC} = 0.659 \times \mathrm{TC} + 0.182 \times \mathrm{HDLC} - 0.117 \times \mathrm{TG} + 18.03$$

The Martin-Hopkins formula used for LDL cholesterol calculation was applied using adjustable factors corresponding to 180 strata-specific medians for TG/VLDL ratios, as follows[7]:

$$\mathrm{LDLC\ (mg/dL)} = \mathrm{TC(mg/dL)} - \mathrm{HDLC\ (mg/dL)} - \mathrm{TG\ (mg/dL)/Factor}$$

Multivariate linear regression, gradient-boosted trees, and ANN models were used as ML models for more accurate LDL-C determination. First, the data sets were divided into 2 groups based on TG levels, depending on whether these were <400 mg/dL (n = 58,030) or ≥400 mg/dL (n = 1,385). Each group's data were partitioned into training and test data sets using 80% and 20% of the overall data, respectively, with

stratified sampling based on 6 essential LDL-C concentration ranges (<70 mg/dL, 70–99 mg/dL, 100–129 mg/dL, 130–159 mg/dL, 160–189 mg/dL, and ≥190 mg/dL[13]). The ML models were trained independently from 2 different training data sets based on the abovementioned division regarding TG values, as summarized in **FIGURE 1**. The HDL-C, TG, and TC concentrations were used as input variables for all models. The LDL-C results from direct measurement with homogeneous assay were utilized for training and performance evaluation of the models.

A multivariate linear regression model was used to determine a new formula that would apply better given the study population characteristics where HDL-C, TG, and TC results were regarded as independent variables and LDL-C as a dependent variable, as follows:

$$\mathrm{LDLC} = \beta 1 \times \mathrm{TC} + \beta 2 \times \mathrm{HDLC} + \beta 3 \times \mathrm{TG} + \beta 0$$

The gradient-boosted trees model, used to construct an ensemble of trees, was applied using a previously reported algorithm.[14] The algorithm uses simple regression trees to learn and boosting to construct an ensemble of them. One hundred decision trees with a 4-tree depth and a learning rate of 0.1 were used for the model build. The model's alpha value was set to 0.95, meaning that 95% of the data are not considered as outliers.

The ANN model was constructed with 2 hidden layers constructed of 10 and 5 nodes, respectively, with the rectified linear unit as an activation function, the root mean square propagation as an optimizer, the mean squared error as a loss function, and an output node with a linear activation function, as illustrated in Supplemental Figure 1. Before ANN model training, data sets were standardized using *z* score transformation with the scikit-learn 0.24.1 package. The ANN code can be downloaded from https://github.com/hikmetc/LDL_study.

The multivariate linear regression and gradient-boosted trees models were built using the KNIME Analytics Platform version 4.3.3 (Zurich, Switzerland), and the ANN model was built using Keras version 2.4.0.[15] Hyperparameter optimization was not performed for any model. There was no missing value, thus the data imputation was not performed.

Statistical Evaluation

Statistical evaluation was conducted using the test data set comprising 11,883 directly measured concomitant LDL-C, HDL-C, TG, and TC test results. The LDL-C results from the direct measurement with homogeneous assay were used as a comparator for the statistical evaluation. The *P* values <.001 with an effect size >.2 were considered statistically significant. Paired group comparison, correlation, and regression analysis of the LDL-C prediction models were carried out for 3 TG concentration ranges: <177 mg/dL, 177–399 mg/dL, and ≥400 mg/dL. Parametric assumptions were evaluated using the Kolmogorov-Smirnov test. Paired group comparisons were performed using a paired *t*-test and the Wilcoxon signed-rank test, depending on the parametric assumptions. The correlation between the LDL-C results of the prediction models and those of the homogeneous assay was evaluated using the Pearson and Spearman tests. A Passing-Bablok regression was carried out to determine the agreement between the prediction models and the homogeneous assay. Bland-Altman plots were used to assess systematic bias for different LDL-C concentrations. In the Bland-Altman plots, differences among the methods were plotted against direct LDL-C measurements, as previously suggested.[16]

Clinically significant differences between the prediction model results and the homogeneous assay results were evaluated based upon the 2019 CLIA acceptable limit (20%) for LDL-C, as was the percentage of estimated LDL-C results (the code can be downloaded from https://github.com/hikmetc/LDL_study).

The LDL-C classification performances of the formulas and ML models were evaluated independently using the test set with accuracy, sensitivity, specificity, positive predictive value (PPV), F-score values, and kappa statistics[17] for the 3 TG concentration ranges (<177 mg/dL, 177–399 mg/dL, and ≥400 mg/dL) and 6 essential LDL-C concentration ranges (<70 mg/dL, 70–99 mg/dL, 100–129 mg/dL, 130–159 mg/dL, 160–189 mg/dL, and ≥190 mg/dL) according to the NCEP/ATP III guidelines.[13] The F-score is the harmonized mean of the PPV and sensitivity ($2/(\mathrm{PPV}^{-1} + \mathrm{sensitivity}^{-1})$), which gives equal weight to PPV and sensitivity when representing classification performance.

Data processing, the implementation of ML models, and statistical analyses were performed using the KNIME Analytics Platform (Zurich, Switzerland),[18] R statistical software 3.6.0,[19] and Python 3.7.6.[20]

FIGURE 1. Study design. TG, triglycerides.

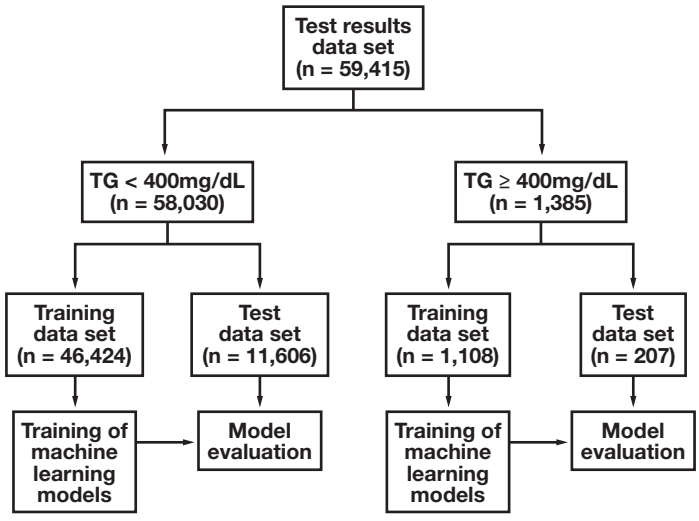

TABLE 2. Paired-Group Comparison, Correlation, and Regression Analysis of LDL-C Prediction Models and Formulas in Reference to LDL-C Homogeneous Assay

				Correlation Analysis		Passing-Bablok Regression Analysis		Comparison with Homogenous Assay			Results Within Specification Limits, %
TG, mg/dL	Model	Mean (SD)[a]	Median (IQR)[a]	*r*	*P* Value	Slope (CI)	Intercept (CI)	Difference	*P* Value	Effect Size	2019 CLIA
<177	Friedewald formula	115.37 (39.08)	111.80 (59.9)	0.968	<.001	1.01 (1.01–1.02)	0.156 (–0.44 to 0.76)	>	<.001	0.206	96.24
	Martin-Hopkins formula	115.78 (38.49)	112.18 (54.7)	0.971	<.001	1.00 (0.995–1.01)	2.24 (1.70–2.83)	>	<.001	0.262	96.54
	Multivariate linear regression	113.39 (36.76)	110.05 (55.0)	0.972	<.001	0.956 (0.951–0.961)	4.97 (4.43–5.54)	N/A	.977	0.0003	97.24
	Gradient-boosted trees	113.27 (36.65)	110.28 (53.9)	0.971	<.001	0.965 (0.960–0.971)	3.84 (3.26–4.38)	N/A	.185	0.014	97.37
	ANN	113.96 (37.39)	110.47 (55.6)	0.972	<.001	0.972 (0.967–0.977)	3.72 (3.17–4.27)	>	<.001	0.063	97.03
	Homogeneous assay	113.39 (38.35)	110.00 (54.4)	…	…	…	…	…	…	…	…
177–399	Friedewald formula	125.98 (45.68)	122.40 (50.5)	0.950	<.001	1.08 (1.06–1.09)	–15.4 (–16.8 to –13.7)	<	<.001	0.358	89.78
	Martin-Hopkins formula	135.87 (42.28)	132.07 (49.6)	0.956	<.001	0.985 (0.974–0.995)	5.75 (4.33–7.21)	>	<.001	0.396	91.21
	Multivariate linear regression	131.20 (42.24)	127.89 (47.4)	0.956	<.001	0.992 (0.982–1.00)	0.311 (–1.13 to 1.63)	N/A	.166	0.026	93.97
	Gradient-boosted trees	131.55 (40.62)	128.82 (48.9)	0.959	<.001	0.954 (0.944–0.964)	5.85 (4.52–7.15)	N/A	.002	0.057	94.42
	ANN	131.24 (42.43)	127.15 (48.2)	0.956	<.001	0.996 (0.985–1.01)	–0.135 (–1.52 to 1.22)	N/A	.115	0.029	93.97
	Homogeneous assay	130.87 (42.380)	128.00 (51.0)	…	…	…	…	…	…	…	…
≥400	Friedewald formula	102.19 (54.78)	94.30 (68.20)	0.817	<.001	1.183 (1.109–1.262)	–43.30 (–53.68 to –33.71)	<	<.001	0.771	50.18
	Martin-Hopkins formula	137.78 (47.95)	129.49 (53.4)	0.833	<.001	0.978 (0.912–1.045)	15.539 (8.20–24.07)	>	<.001	0.626	64.98
	Multivariate linear regression	121.70 (38.82)	117.79 (49.2)	0.880	<.001	0.822 (0.773–0.875)	20.573 (13.73–26.48)	N/A	.256	0.068	75.09
	Gradient-boosted trees	122.23 (39.66)	116.21 (49.8)	0.894	<.001	0.825 (0.772–0.876)	21.058 (14.69–27.37)	N/A	.433	0.047	75.45
	ANN	120.16 (39.80)	114.97 (50.8)	0.884	<.001	0.842 (0.790–0.895)	16.586 (10.30–22.52)	N/A	.020	0.140	75.45
	Homogeneous assay	123.22 (46.71)	115.00 (61.0)	…	…	…	…	…	…	…	…

ANN, artificial neural network; CI, 95% confidence interval; CLIA, Clinical Laboratory Improvement Amendments; IQR, interquartile range; LDL-C, low-density lipoprotein cholesterol; SD, standard deviation; TG, triglycerides.

P *values <.001 regarded as statistically significant.*

[a]*To convert mg/dL to mmol/L, multiply by 0.02586 for cholesterol and by 0.01129 for triglycerides. Cohen's* d *values with 0.2, 0.5, and 0.8 correspond to small, medium, and high effect sizes.*

TABLE 3. LDL-C Classification Performance of Prediction Models and Formulas in Reference to Homogeneous Assay

		NCEP Categories for LDL-C, mg/dL																				
		<70			70–99			100–129			130–159			160–189			≥190					Total Classification
TG, mg/dL	Model	PPV	Sen.	Spe.	PPV	Sen.	Spe.	PPV	Sen.	Spe.	PPV	Sen.	Spe.	PPV	Sen.	Spe.	PPV	Sen.	Spe.	Overall Accuracy	Cohen's Kappa	Correct	Incorrect
<177	Friedewald formula	84.94	80.25	98.28	81.48	78.72	92.99	76.69	76.71	89.79	71.41	72.72	93.00	63.21	68.25	96.45	68.17	80.00	98.83	76.29	0.693	6652	2067
	Martin-Hopkins formula	90.06	77.92	98.96	82.73	79.66	93.49	77.07	78.52	89.78	71.70	74.79	92.90	63.71	69.23	96.48	69.46	78.11	98.92	77.28	0.706	6738	1981
	Multivariate linear regression	88.13	80.36	98.69	81.30	83.82	92.45	77.76	81.27	89.83	75.02	73.91	94.08	68.75	64.62	97.38	80.00	66.42	99.48	78.64	0.721	6857	1862
	Gradient-boosted trees	86.70	83.01	98.46	81.63	82.80	92.71	77.66	79.62	89.98	74.09	74.79	93.71	68.49	66.57	97.26	81.16	63.40	99.54	78.38	0.719	6834	1885
	ANN	87.67	81.53	98.61	82.08	82.92	92.91	77.93	80.37	90.04	74.39	73.55	93.91	67.65	67.27	97.13	77.64	72.08	99.35	78.56	0.721	6850	1869
177–399	Friedewald formula	48.84	86.30	95.18	59.30	68.26	89.64	67.89	63.33	88.16	71.67	63.24	91.26	67.39	60.39	95.11	78.54	76.89	98.11	66.05	0.575	1907	980
	Martin-Hopkins formula	82.22	50.68	99.42	77.00	69.79	95.39	73.49	74.57	89.37	70.52	70.99	89.62	62.16	71.01	92.76	73.78	82.77	97.36	71.74	0.642	2071	816
	Multivariate linear regression	70.71	67.81	98.50	72.69	73.80	93.87	72.78	73.23	89.17	72.01	71.52	90.28	65.04	64.25	94.22	77.18	78.15	97.92	71.74	0.642	2071	816
	Gradient-boosted trees	83.65	59.59	99.38	73.43	78.20	93.74	73.87	73.96	89.66	71.65	73.66	89.81	65.54	65.70	94.22	80.27	75.21	98.34	72.84	0.655	2103	784
	ANN	73.33	67.81	98.69	72.76	76.10	93.70	73.25	72.98	89.46	72.17	70.72	90.46	64.56	64.25	94.10	76.73	78.99	97.85	71.94	0.645	2077	810
≥400	Friedewald formula	24.36	90.48	76.95	29.58	28.00	75.25	40.00	30.56	83.90	51.16	38.60	90.45	46.15	20.69	97.18	88.24	65.22	99.21	37.91	0.239	105	172
	Martin-Hopkins formula	60.00	14.29	99.22	58.49	41.33	89.11	41.67	48.61	76.10	40.91	47.37	82.27	41.30	65.52	89.11	73.91	73.91	97.64	47.65	0.341	132	145
	Multivariate linear regression	47.06	38.10	96.48	65.22	60.00	88.12	53.85	68.06	79.51	60.00	68.42	88.18	40.00	27.59	95.16	93.33	60.87	99.61	58.84	0.474	163	114
	Gradient-boosted trees	66.67	19,05	99.22	57.14	64.00	82.18	49.41	58.33	79.02	59.68	64.91	88.64	52.17	41.38	95.56	94.12	69.57	99.61	57.40	0.451	159	118
	ANN	40.00	28.57	96.48	60.98	66.67	84.16	53.57	62.50	80.98	60.66	64.91	89.09	42.11	27.59	95.56	93.75	65.22	99.61	58.12	0.463	161	116

ANN, artificial neural network; LDL-C, low-density lipoprotein cholesterol; NCEP, National Cholesterol Education Program; PPV, positive predictive value; Sen., sensitivity; Spe., specificity; TG, triglycerides concentration.

TABLE 4. LDL-C Classification Performance of Prediction Models and Formulas for LDL-C <70 mg/dL and TG 177–399 mg/dL

Model	True Positives	False Positives	True Negatives	False Negatives	PPV	Sensitivity	Specificity	F-Score
Friedewald formula	126	132	2609	20	48.84	86.30	95.18	62.38
Martin-Hopkins formula	74	16	2725	72	82.22	50.68	99.42	62.71
Multivariate linear regression	99	41	2700	47	70.71	67.81	98.50	69.23
Gradient-boosted trees	87	17	2724	59	83.65	59.59	99.38	69.60
ANN	99	36	2705	47	73.33	67.81	98.69	70.46

ANN, artificial neural network; LDL-C, low-density lipoprotein cholesterol; PPV, positive predictive value; TG, triglycerides concentration.

FIGURE 2. **Passing-Bablok regression plots between measured LDL-C and predicted LDL-C. A–E, TG levels <170 mg/dL. F–J, TG levels 170–399 mg/dL, K–O, TG levels >399 mg/dL. Identity lines are solid blue, regression lines are dashed blue, and confidence intervals are solid gray. LDL-C regression equations are given in the plots. The plots illustrate LDL-C levels <250 mg/dL. Plots including all data points are provided in the supplementary material (Supplemental Figure 2). LDL-C, low-density lipoprotein cholesterol; TG, triglycerides.**

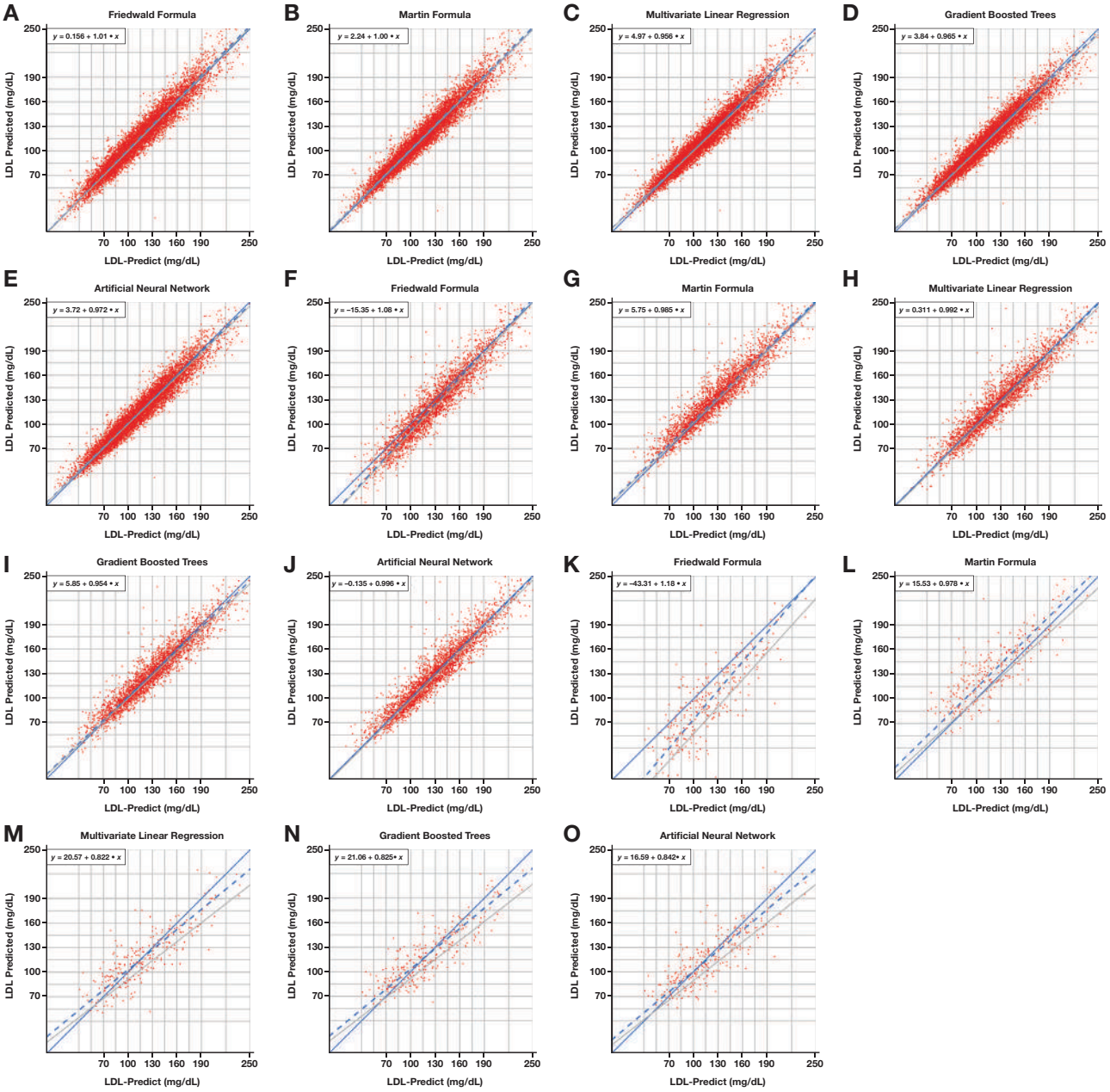

Results

The demographic features and biochemical parameters of the study population are summarized in **TABLE 1**. Paired group comparisons, correlations, and regression analyses of the LDL prediction models and formulas in reference to the homogeneous assay are provided in **TABLE 2**. The Passing-Bablok regression analysis and Bland-Altman plots are illustrated in **FIGURE 2** and **3**, respectively.

Our multivariate linear regression model revealed 2 simple formulas for LDL-C concentration estimation for TG values <400 and ≥400 mg/dL, respectively:

$$\mathrm{LDLC} = 0.927 \times \mathrm{TC} - 0.942 \times \mathrm{HDLC} - 0.126 \times \mathrm{TG} + 0.735$$

$$\mathrm{LDLC} = 0.659 \times \mathrm{TC} + 0.182 \times \mathrm{HDLC} - 0.117 \times \mathrm{TG} + 18.03$$

Although a paired-group comparison revealed statistically significant differences among the Friedewald formula and the Martin-Hopkins formula when TG levels were <177 mg/dL, at least 95% of the results were in agreement with the 2019 CLIA limit for LDL-C.

For TG levels between 177 and 399 mg/dL, the Friedewald formula results were significantly lower than those of the homogeneous as-

FIGURE 3. Bland-Altman plots between measured LDL-C and predicted LDL-C. A–E, TG levels <170 mg/dL. F–J, TG levels 170–399 mg/dL. K–O, TG levels >399 mg/dL. Line of equality are solid blue, mean differences are dashed cyan, mean differences ± 2 standard deviations are solid purple, and confidence intervals are solid gray. Mean differences between the 2 methods are given in the plots. The plots illustrate LDL-C levels <250 mg/dL. Plots including all data points are provided in the supplementary material (Supplemental Figure 3). LDL-C, low-density lipoprotein cholesterol; TG, triglycerides.

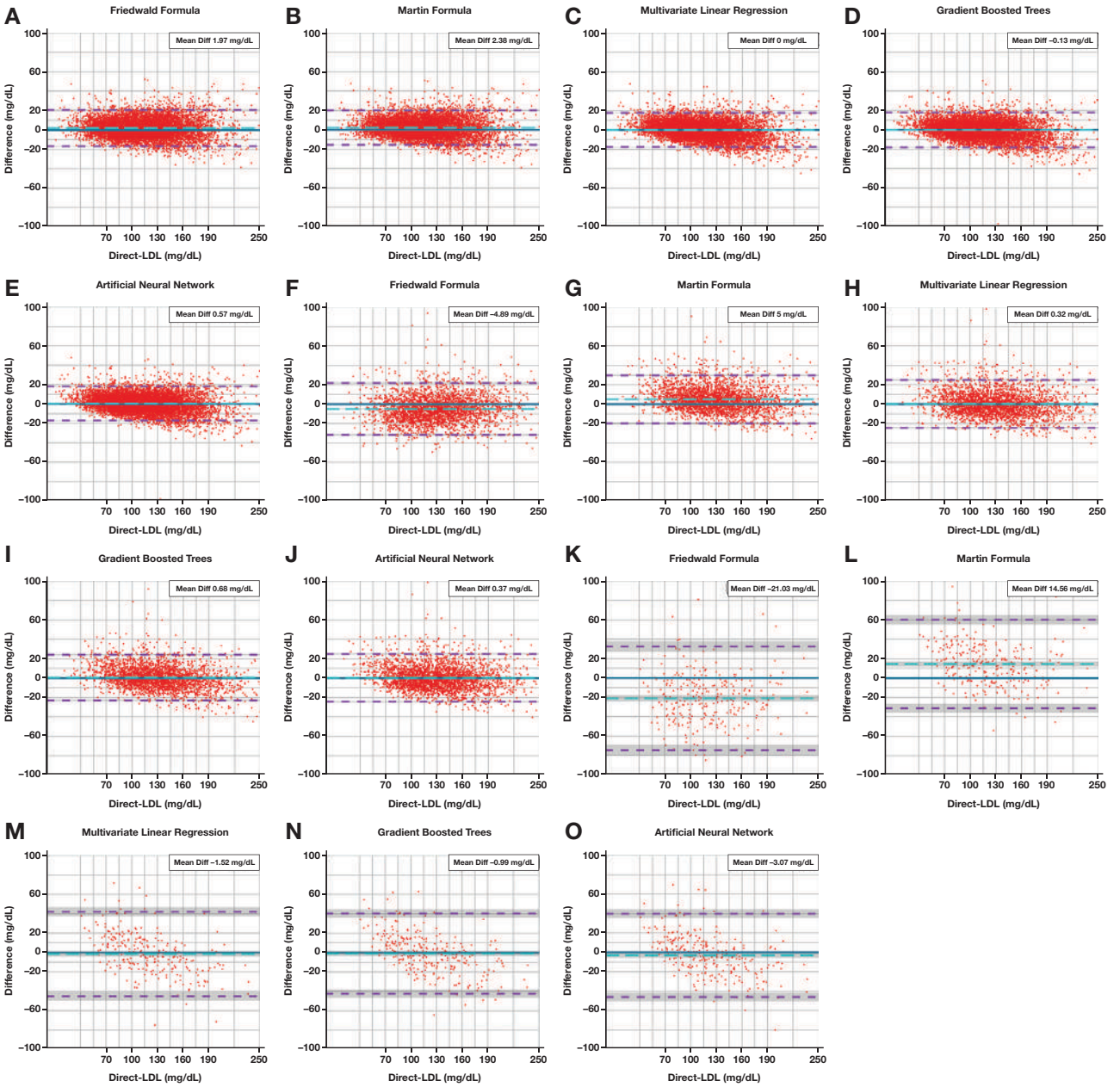

say (125.98 vs 130.87 mg/dL; P <.001). Similarly, the intercept value for the Passing-Bablok regression analysis was found to be –15.4. At the same time, the Martin-Hopkins formula results were significantly higher than those of the homogeneous assay (135.87 vs 130.87 mg/dL; P <.001).

For TG concentrations >399 mg/dL, the Friedewald and Martin-Hopkins formula results were found to be significantly lower and higher, respectively, than the homogeneous assay results. The formulas and ML models were not able to achieve 60% agreement with the 2019 CLIA limit.

The lowest correlations were found to be between the Friedewald formula and the homogeneous assay results for all TG groups. Multivariate linear regression, gradient-boosted trees, and ANN models had higher correlation coefficient values and were in better agreement with the 2019 CLIA limit than the Friedewald and Martin-Hopkins formulas.

TABLE 3 shows the LDL-C classification performance of the formulas and prediction models, taking the homogeneous assay as a reference. Substantial agreement (Cohen's kappa >0.6) was observed among all models when TG was <177 mg/dL. For TG concentrations ranging from 177 to 399 mg/dL, there was moderate and substantial

agreement among the Friedewald formula (Cohen's kappa = 0.575) and the other prediction models (Cohen's kappa >0.6), respectively. Although there was fair agreement between the Friedewald and Martin-Hopkins formulas (kappa = 0.239 and 0.341, respectively), the other prediction models showed moderate agreement (kappa >0.4) with directly measured LDL-C results for TG levels >399 mg/dL.

The LDL-C classification performance of the prediction models and formulas for LDL-C levels <70 mg/dL and TG concentrations ranging from 177 to 399 mg/dL are shown in **TABLE 4**. The F-scores were higher for the linear regression, gradient-boosted trees, and ANN models than for the Friedewald and Martin-Hopkins formulas, as a consequence of higher sensitivity and PPV.

Discussion

We investigated the validity of the Friedewald and Martin-Hopkins formulas for the Turkish population along with the performance of linear regression, gradient-boosted trees, and ANN models. For TG levels <177 mg/dL, the Friedewald and Martin-Hopkins formulas and the other models were in agreement with the homogeneous assay. However, the agreement was lower when the TG concentration was >177 mg/dL. Although the Friedewald formula seemed to be the worst LDL prediction model for TG levels >177 mg/dL, the linear regression, gradient-boosted trees, and ANN models outperformed both formulas.

We evaluated LDL prediction performances for 3 discrete TG concentration ranges regarding the EAS and EFLM Joint Consensus Initiative recommendations.[2] For TG concentrations <177 mg/dL, the Friedewald and Martin-Hopkins formulas and the ANN model revealed *P* values <.001. However, the effect sizes of these comparisons were quite small (0.206, 0.262, and 0.06, respectively). Thus, the *P* values that were <.001 may be attributed to the large sample size. Further, 95% of the results were within the 2019 CLIA limit (20%), so 95% of the estimated results were without a predetermined clinically significant difference, as shown in **TABLE 2**. Similarly, the clinical classification performances of the formulas and prediction models were in substantial agreement (Cohen's kappa >0.6) with the homogeneous assay, as shown in **TABLE 3**.

For TG levels between 177 and 399 mg/dL, the Friedewald formula results were significantly lower than those of the homogeneous assay (125.98 vs 130.87; *P* <.001; effect size = 0.358). In addition, the intercept value of the Passing-Bablok regression analysis was found to be –15.4, whereas the mean difference for the Friedewald formula in the Bland-Altman plot was –4.89 mg/dL (**FIGURE 3F**). There was also moderate agreement (Cohen's kappa = 0.575) between the Friedewald formula and the homogeneous assay results. The Friedewald formula underestimated the LDL-C levels, especially for concentrations close to 70 mg/dL, as illustrated in **FIGURE 2F**. The PPV of the Friedewald formula for the LDL-C results <70 mg/dL and between 70 and 99 mg/dL were found to be 48.84% and 59.30%, respectively, as shown in **TABLE 3**. In contrast, the Martin-Hopkins formula results were significantly higher than those of the homogeneous assay (135.87 vs 130.87; *P* <.001; effect size = 0.396). Further, the sensitivity of the Martin-Hopkins formula (50.68%) was lower than those of the other models for LDL-C levels <70 mg/dL because of overestimation compared with that of the homogeneous assay, as shown in **FIGURE 2G**.

At the same time, the LDL-C classification accuracy of the Martin-Hopkins formula was superior to that of the Friedewald formula (71.74% vs 66.05%) for this TG concentration range. Similarly, Lee, Jang, et al[21] showed that the Martin-Hopkins formula exhibited greater concordance with the homogeneous assay than the Friedewald formula. Meeusen et al[22] also noticed that the Friedewald formula underestimated and the Martin-Hopkins formula overestimated LDL-C concentrations compared with the beta-quantification method for TG levels <400 mg/dL. The discrepancies were found to be substantial for LDL-C concentrations <70 mg/dL. Likewise, Palmer et al[23] reported that the Martin-Hopkins formula calculated higher LDL-C levels than the Friedewald formula, especially for LDL-C levels <70 mg/dL, and the difference increased in those patients with greater TG concentrations. Similarly, in our study, the results of the Friedewald and Martin-Hopkins formulas were found to be lower and higher, respectively, than the homogeneous assay results for TG levels ranging from 177 to 399 mg/dL. However, for TG levels <177 mg/dL, the Friedewald and Martin-Hopkins formulas predicted LDL-C levels well with regard to classification performance and 2019 CLIA limit. It is therefore likely that the accuracy of the formulas decreases at the higher TG and lower LDL-C levels.

The accuracy values of the ML models and the formulas were between 76% and 78% for TG levels <177 mg/dL and showed a similar performance. Hence, all of the ML models and conventional formulas can be used at TG levels that are <177 mg/dL. The overall accuracy values of the linear regression (71.74%), gradient-boosted trees (72.84%), and ANN models (71.94%) were found to be similar and substantially in agreement with those of the homogeneous assay (Cohen's kappa >0.6) when TG was 177 to 399 mg/dL. However, the accuracy of the Friedewald formula was only 66.05% for TG that was 177 to 399 mg/dL. There was also no statistically significant difference detected between directly measured LDL-C results and ML models, as shown in **TABLE 2**. Further, 94% of the results of the ML models mentioned above were in agreement with the 2019 CLIA limit. Thus, the linear regression, gradient-boosted trees, and ANN models seem to be good alternatives to the Friedewald and Martin-Hopkins formulas for TG levels between 177 and 399 mg/dL. Furthermore, our linear regression model revealed the straightforward formula for TG levels <400 mg/dL. Our formula's performance was comparable to that of the gradient-boosted trees and ANN models and showed similar accuracy. Although the EAS and EFLM Joint Consensus Initiative recommends the Martin-Hopkins formula for TG concentrations ranging from 2.0 to 4.5 mmol/L (177–399 mg/dL),[2] our formulas' performance was found to be superior to the Friedewald and Martin-Hopkins formulas, considering the comparison with directly measured LDL-C levels (*P* >.001). Although the Martin-Hopkins formula uses 180 strata-specific medians for TG/VLDL ratios for LDL-C calculation, our formula is as simple as the Friedewald formula and therefore more applicable than the Martin-Hopkins formula.

The EAS and EFLM Joint Consensus Initiative recommends the Martin-Hopkins formula instead of the Friedewald formula for LDL-C levels <1.8 mmol/L (70 mg/dL).[2] At the same time, direct LDL-C measurement or modified LDL-C estimation was recommended in 2018 by the American Heart Association (AHA) and the American College of Cardiology (ACC) guideline on the management of blood cholesterol.[24] As shown in **TABLE 4**, the F-scores, which represent the harmonic mean of the PPV and sensitivity, were found to be 62.38, 62.71, 69.23, 69.60, and 70.46 for the Friedewald formula, the Martin-Hopkins formula, the linear regression model, the gradient-boosted trees model, and the ANN model, respectively, for LDL-C concentrations <70 mg/dL and TG levels in the range of 177 to 399 mg/dL.

In the 2019 ESC/EAS Guidelines for the Management of Dyslipidaemias[3] and the AHA/ACC guideline on the management of blood cholesterol,[24] an LDL-C threshold of 70 mg/dL was recommended for use in patients with both a high risk and a very high risk of ASCVD. Further, when LDL-C persists at levels >70 mg/dL during statin therapy, non-statins, such as ezetimibe and proprotein convertase subtilisin/kexin type 9, are recommended for use by the AHA/ACC guideline.[24] Although the underestimation of LDL-C concentration may lead to undertreatment, overestimation may result in the overtreatment of patients with ASCVD risk. Therefore, accurate LDL-C estimation, particularly for concentrations near 70 mg/dL, is crucial. The ML models represented in our study may serve as more accurate surrogates for widely used formulas regarding F-scores represented in **TABLE 3**.

One of the Friedewald formula's well-known limitations is its use of a fixed factor of 5 as a denominator of TG to calculate VLDL-C. When the TG level is >400 mg/dL, the ratio of TG to cholesterol in VLDL is greater than 5 because of the presence of chylomicrons, chylomicron remnants, or VLDL remnants. The resulting overestimation of VLDL-C will result in an underestimation of LDL-C.[25] Consistent with the literature, the Friedewald formula exhibited significantly lower results in our study than the homogeneous assay (102.194 vs 123.224 mg/dL; P <.001; effect size = 0.771) for TG levels >399 mg/dL, as illustrated in **FIGURE 3K**. Moreover, only 50.18% of the Friedewald formula results were found to be within the 2019 CLIA limit, and the classification accuracy of the Friedewald formula was 37.91%. In contrast, the Martin-Hopkins formula overestimated the LDL-C concentration compared with the homogeneous assay (137.781 vs 123.224 mg/dL; P < .001; effect size = 0.626) for TG levels >399 mg/dL. Further, the mean difference between the Martin-Hopkins formula results and the homogeneous assay results was 14.56 mg/dL, as shown in **FIGURE 3L**. The LDL-C classification accuracy of the Martin-Hopkins formula was found to be 47.65%, making it better than that of the Friedewald formula (37.91%). Similarly, the concordance between direct measurement and the Martin-Hopkins formula has previously been reported to be better than that with the Friedewald formula for TG levels >399 mg/dL.[7] However, Palmer et al[23] found the agreement between the Martin-Hopkins formula and beta-quantification to be poor for TG levels >400 mg/dL. Likewise, only 64.98% of the Martin-Hopkins formula results were within the 2019 CLIA limit, and the agreement between the homogeneous assay and the Martin-Hopkins formula was found to be fair (Cohen's kappa = 0.341) in the present study.

Although the Friedewald and Martin-Hopkins formulas exhibited fair agreement with the homogeneous assay for TG levels >399 mg/dL (kappa = 0.239 and 0.341, respectively), the ML prediction models showed moderate agreement (Cohen's kappa = 0.474, 0.451, 0.463, respectively). Further, there was no significant difference detected between directly measured LDL-C results and the ML models (P >.001). However, the aforementioned models' results had an approximately 75% agreement with the 2019 CLIA limit and their LDL-C classification accuracy values were <60%, as shown in **TABLE 2** and **3**. Further, as shown in **FIGURE 3**, the ML algorithms systematically underestimated LDL-C with increasing LDL-C concentrations for TG >399 mg/dL. The EAS and EFLM Joint Consensus Initiative recommends direct measurement of LDL-C for TG levels ≥4.5 mmol/L (≥399 mg/dL).[2] This recommendation is in accord with the present study, which indicates that the homogeneous assay is a more reliable method for TG concentrations >399 mg/dL.

Recently, ML methods have been shown to be candidate alternative LDL-C estimation models, especially for higher TG levels. Barakett-Hamade et al[8] compared the K-nearest neighbors (KNN) model with conventional formulas against the homogeneous assay method to elaborate the agreement of estimated LDL-C with direct LDL-C measurement. The KNN model had a higher intraclass correlation coefficient than the Friedewald formula and was more resistant to higher triglyceride levels, according to Bland-Altman analysis.[8] In the present study, Bland-Altman analysis revealed that mean differences (MD) of linear regression, gradient-boosted trees, and ANN models were only 0.32, 0.68, and 0.37 mg/dL for TG levels of 177 to 399 mg/dL; however, the Friedewald and Martin-Hopkins formulas had higher MD values (–4.89 mg/dL and 5 mg/dL, respectively; **FIGURE 3F–G**). Tsigalou et al[10] used ML methods including linear regression, support vector machines, extreme gradient boosting, and ANN algorithms to estimate LDL-C and found that classification accuracies were <85% for all models regarding NCEP/ATP III LDL-C ranges. However, the authors did not report each model's actual accuracies, and their study relied on a relatively small sample size (n = 4244).[10] On the other hand, we showed our models' accuracy for 6 discrete LDL-C concentration ranges and 3 different intervals (**TABLE 3**). None of the models' and conventional formulas' performance could exceed 79% classification accuracy (**TABLE 3**) even if the ML models' performances were superior to those of the Friedewald and Martin-Hopkins formulas. Moreover, the accuracies decreased in higher TG concentration ranges. Lee, Kim, et al[9] showed that their ANN model outperformed the Friedewald and Martin-Hopkins formulas based on squared error. However, they did not show the direction of the misestimation and classification performances for different LDL-C and TG concentration ranges.[9] In the present study, although the accuracy of our ANN model was higher than that of the Friedewald and Martin-Hopkins formulas for all LDL-C and TG ranges, the ANN model underestimated LDL-C at increasing LDL-C concentrations (**FIGURE 3O**), particularly when TG >399 mg/dL, in which direct measurement is recommended.

The ML models' success and generalizability are higher when they are developed from a larger data set.[26] Therefore, the present study was conducted using a suitably large dataset (n = 59,415) to show the validity of the Friedewald and Martin-Hopkins formulas in the Turkish population and develop novel ML models. The extensive performance evaluation carried out in the present study provides the most comprehensive assessment to date of the ML models and conventional formulas in the Turkish population used for LDL-C estimation. Furthermore, we found the new simple formula using multivariate linear regression and show its performance along with that of other ML models and conventional formulas. This is the first LDL-C estimation formula developed using Turkish population data that can be easily used after external validation studies.

One of the present study's limitations is that beta-quantification was not used as a reference method because of the labor-intensive manual steps it requires. Overall, more accurate results could be achieved with this method. However, LDL-C measurement was conducted by homogeneous assay using the Sekisui reagent, which has been shown to meet the NCEP's total error goals.[27] Another limitation of this study is that it used results from both fasting and nonfasting specimens. Research has shown that TG-enriched chylomicron concentrations are higher in nonfasting specimens than in fasting specimens, which may increase

the ratio of TG to cholesterol in VLDL.[28] Thus, the underestimation of LDL-C concentration when using the Friedewald formula may have been exaggerated because of the inclusion of nonfasting specimens. The Martin-Hopkins formula was shown to be more accurate than the Friedewald formula with nonfasting specimens.[29] At the same time, theoretically, homogeneous assays are only slightly (if at all) affected by the nonfasting state because one can detect LDL-C after eliminating non-LDL particles.[25] Furthermore, fasting specimens are no longer required for routine lipid profiles by the EAS and EFLM Joint Consensus Initiative.[2] Hence, the present study reflected current research.

Another limitation was that the study represented the validity of the formulas and models only on the Abbott platform. Thus, further multicentered research should be undertaken on different analyzer platforms to prove the present models' and formulas' external validity. Moreover, we developed the ML models by training them on our laboratory's data set. Therefore, the ML models given in the present study rely on our laboratory-specific data sets. Although the Friedewald and Martin-Hopkins formulas can have more general use in the data sets other than the ones they were derived from, it is not certain that our ML models could be used with confidence to estimate LDL-C levels from diverse populations without further validation.

Conclusion

In summary, the present study has shown that the Friedewald and Martin-Hopkins formulas are valid for TG levels <177 mg/dL. In addition, it has been shown that linear regression, gradient-boosted trees, and ANN models offer more accurate alternatives to the Friedewald and Martin-Hopkins formulas, especially for TG levels between 177 and 399 mg/dL and LDL-C levels <70 mg/dL.

Supplementary Data

Supplemental figures and tables can be found in the online version of this article at www.labmedicine.com.

Acknowledgments

The authors thank Prof. Nilüfer Bayraktar for providing laboratory data and Ayhan Parmaksız for statistical guidance.

REFERENCES

1. Ference BA, Ginsberg HN, Graham I, et al. Low-density lipoproteins cause atherosclerotic cardiovascular disease. 1. Evidence from genetic, epidemiologic, and clinical studies. A consensus statement from the European Atherosclerosis Society consensus panel. *Eur Heart J.* 2017;38(32):2459–2472.
2. Langlois MR, Nordestgaard BG, Langsted A, et al.; European Atherosclerosis Society (EAS) and the European Federation of Clinical Chemistry and Laboratory Medicine (EFLM) Joint Consensus Initiative. Quantifying atherogenic lipoproteins for lipid-lowering strategies: consensus-based recommendations from EAS and EFLM. *Clin Chem Lab Med.* 2020;58(4):496–517.
3. Mach F, Baigent C, Catapano AL, et al. 2019 ESC/EAS Guidelines for the management of dyslipidaemias: lipid modification to reduce cardiovascular risk. *Eur Heart J.* 2020;41(1):111–188.
4. Nauck M, Warnick GR, Rifai N. Methods for measurement of LDL-cholesterol: a critical assessment of direct measurement by homogeneous assays versus calculation. *Clin Chem.* 2002;48(2):236–254.
5. Miller WG, Myers GL, Sakurabayashi I, et al. Seven direct methods for measuring HDL and LDL cholesterol compared with ultracentrifugation reference measurement procedures. *Clin Chem.* 2010;56(6):977–986.
6. Friedewald WT, Levy RI, Fredrickson DS. Estimation of the concentration of low-density lipoprotein cholesterol in plasma, without use of the preparative ultracentrifuge. *Clin Chem.* 1972;18(6):499–502.
7. Martin SS, Blaha MJ, Elshazly MB, et al. Comparison of a novel method vs the Friedewald equation for estimating low-density lipoprotein cholesterol levels from the standard lipid profile. *JAMA.* 2013;310(19):2061–2068.
8. Barakett-Hamade V, Ghayad JP, Mchantaf G, Sleilaty G. Is machine learning-derived low-density lipoprotein cholesterol estimation more reliable than standard closed form equations? Insights from a laboratory database by comparison with a direct homogeneous assay. *Clin Chim Acta.* 2021;519:220–226.
9. Lee T, Kim J, Uh Y, Lee H. Deep neural network for estimating low density lipoprotein cholesterol. *Clin Chim Acta.* 2019;489:35–40.
10. Tsigalou C, Panopoulou M, Papadopoulos C, Karvelas A, Tsairidis D, Anagnostopoulos K. Estimation of low-density lipoprotein cholesterol by machine learning methods. *Clin Chim Acta.* 2021;517:108–116.
11. Singh G, Hussain Y, Xu Z, et al. Comparing a novel machine learning method to the Friedewald formula and Martin-Hopkins equation for low-density lipoprotein estimation. *PLoS One.* 2020;15(9):e0239934.
12. Sandberg S, Fraser CG, Horvath AR, et al. Defining analytical performance specifications: consensus statement from the 1st strategic conference of the European Federation of Clinical Chemistry and Laboratory Medicine. *Clin Chem Lab Med.* 2015;53(6):833–835.
13. Third report of the National Cholesterol Education Program (NCEP) Expert Panel on Detection, Evaluation, and Treatment of High Blood Cholesterol in Adults (Adult Treatment Panel III) final report. *Circulation*. 2002;106(25):3143-3143.
14. Friedman JH. Greedy function approximation: a gradient boosting machine. *Ann Statist*. 2001;29(5):1189–1232.
15. *Keras [computer program]*. GitHub, Inc. https://github.com/keras-team/keras. Accessed July 12, 2021.
16. Krouwer JS. Why Bland-Altman plots should use X, not (Y+X)/2 when X is a reference method. *Stat Med.* 2008;27(5):778–780.
17. McHugh ML. Interrater reliability: the kappa statistic. *Biochem Med.* 2012;22(3):276–282.
18. Berthold MR, Cebron N, Dill F, et al. KNIME—the Konstanz information miner: version 2.0 and beyond. *ACM SIGKDD Explor Newsl*. 2009;11(1):26–31.
19. *R: A language and environment for statistical computing [computer program]*. Vienna, Austria: R Foundation for Statistical Computing; 2010.
20. Van Rossum G, Drake FL. *Python 3 Reference Manual*. Scotts Valley, CA: CreateSpace; 2009.
21. Lee J, Jang S, Son H. Validation of the Martin method for estimating low-density lipoprotein cholesterol levels in Korean adults: findings from the Korea National Health and Nutrition Examination Survey, 2009–2011. *PLoS One*. 2016;11(1):e0148147.
22. Meeusen JW, Lueke AJ, Jaffe AS, Saenger AK. Validation of a proposed novel equation for estimating LDL cholesterol. *Clin Chem.* 2014;60(12):1519–1523.
23. Palmer MK, Barter PJ, Lundman P, Nicholls SJ, Toth PP, Karlson BW. Comparing a novel equation for calculating low-density lipoprotein cholesterol with the Friedewald equation: a VOYAGER analysis. *Clin Biochem.* 2019;64:24–29.
24. Grundy SM, Stone NJ, Bailey AL, et al. 2018 AHA/ACC/AACVPR/AAPA/ABC/ACPM/ADA/AGS/APhA/ASPC/NLA/PCNA Guideline on the management of blood cholesterol: a report of the American College of Cardiology/American Heart Associa-

tion Task Force on Clinical Practice Guidelines. *Circulation.* 2019;139(25):e1082–e1143.

25. Nordestgaard BG, Benn M. Fasting and nonfasting LDL cholesterol: to measure or calculate? *Clin Chem.* 2009;55(5):845–847.
26. Richardson A, Signor BM, Lidbury BA, Badrick T. Clinical chemistry in higher dimensions: machine-learning and enhanced prediction from routine clinical chemistry data. *Clin Biochem.* 2016;49(16-17):1213–1220.
27. Miller WG, Myers GL, Sakurabayashi I, et al. Seven direct methods for measuring HDL and LDL cholesterol compared with ultracentrifugation reference measurement procedures. *Clin Chem.* 2010;56(6):977–986.
28. Lund SS, Petersen M, Frandsen M, et al. Agreement between fasting and postprandial LDL cholesterol measured with 3 methods in patients with type 2 diabetes mellitus. *Clin Chem.* 2011;57(2):298–308.
29. Sathiyakumar V, Park J, Golozar A, et al. Fasting versus nonfasting and low-density lipoprotein cholesterol accuracy. *Circulation.* 2018;137(1):10–19.

Evaluation of the Preanalytical Interference of Hemoglobin, Bilirubin, or Lipids in Therapeutic Drug Monitoring Assays on Beckman Coulter AU Analyzers

Jieli Li, MD, PhD,[1,✉] Jacqua Rietschlin, BS,[1] Irene Miller, MS, MT(ASCP), CLS(NCA), BA,[1] Charlene Weber, BS,[1] Matt Scheidegger, BS,[1] Stephanie Barringer, BS, BA, MLT(ASCP),[1] Rae Kerlin, BS,[1] JoAnna Williams, MD[1,]*

[1]Department of Pathology, Wexner Medical Center, The Ohio State University, Columbus, Ohio, US; *To whom correspondence should be addressed. JoAnna.Williams@osumc.edu

Keywords: interference, hemolysis, icterus, lipemia, therapeutic drug monitoring, Beckman Coulter AU analyzers

Abbreviations: HIL, hemolysis, icterus, lipemia; TDM, therapeutic drug monitoring; QMS, quantitative microsphere system; AMIK, amikacin; Li, lithium; AMIKQ, quantitative microsphere system amikacin; AMIKE, enzyme multiplied immunoassay technique amikacin; ABN, abnormal; NAD, nicotinamide adenine dinucleotide; NADH, nicotinamide adenine dinucleotide plus hydrogen; RCV, reference change value.

Laboratory Medicine 2022;53:172–176; https://doi.org/10.1093/labmed/lmab048

ABSTRACT

Objective: The aim of this study was to evaluate the influence of hemolysis, icterus, and lipemia (HIL) interferences on 8 therapeutic drug monitoring (TDM) assays.

Methods: Amikacin, carbamazepine, digoxin, lidocaine, lithium, methotrexate, phenobarbital, and theophylline were spiked in specimen pools at the clinical decision cutoff values. The interferents were spiked in vitro in specimen pools. All analytes were tested on Beckman Coulter AU analyzers.

Results: Hemolysis interference was detected in quantitative microsphere system (QMS) amikacin at 55.59 μg/mL at a concentration of 500 mg/dL hemoglobin. Icterus interference was detected in enzyme multiplied immunoassay technique amikacin at 43.62 μg/mL and in QMS amikacin at 55.59 μg/mL, at a concentration of 20 mg/dL bilirubin.

Conclusion: Although the reference range value is recommended for clinical significance bias assessment for HIL interferences on most chemistry assays, an important investigation of the HIL interferences on TDM assays is to establish interferent thresholds at the clinical critical cutoff values.

Most therapeutic drug monitoring (TDM) assays are performed on automated systems in clinical laboratories. Immunoassays are most commonly used to evaluate TDMs in clinical laboratories. Most TDMs employ an immunoassay method in which the target analytes compete with a specific antibody. Signals generated from the reaction are converted into the analyte concentration. The TDM immunoassays can be homogeneous or heterogeneous. In the homogeneous format, the method is simpler and no separation is needed. In heterogeneous immunoassays, the bound labeled molecules are physically separated from the unbound labeled molecules and then the signal is measured. If plasma drug concentration measurements are to be of any value, then attention must be paid to preanalytical issues, such as the timing of blood sampling, the type of blood specimen, and interferences, such as hemolysis, icterus, and lipemia (HIL). Most of the interference from hemoglobin, bilirubin, or lipids occurs in the fluorimetric or photometric methods because of the properties of the interferents. Therefore, such interference happens more often in homogeneous than in heterogeneous assays. In competitive immunoassays, when the interference enhances the signal, such interference will generate false-negative results, because the signal is inversely proportional to the reported analyte concentration.

Lipids mostly cause interference by their turbidity; therefore, assays using turbidimetry are the most affected by lipid interference.[1] IntraLipid is a synthetically produced emulsion for intravenous administration as nutritional support. It mainly contains soybean oil and egg phospholipids, and some of the IntraLipid contains a small amount of triglycerides. Most manufacturers evaluate the lipids' interference by spiking IntraLipid into the specimens to simulate lipemic specimens. However, specimens spiked with IntraLipid do not necessarily represent lipemic specimens, because the various sizes, charges, and shapes of the particles affect their light-scattering capabilities.[2] In addition, in routine clinical practice, nonfasting is the major cause for lipemic specimens, which contain mostly triglycerides in chylomicron particles. High levels of triglycerides may interfere not only with turbidity but also with antigen binding, even when antibodies are linked to a solid support, resulting in erroneous results. The Beckman Coulter AU analyzers can measure the degree of hemolysis, icterus, and turbidity in the specimens. The degree of interference is noted as an index; however, the index for lipids is generated by spiking with IntraLipid and the lipid indices often do not correlate with the actual triglyceride levels,[3] as described earlier. Therefore, we used specimens spiked with

triglycerides to evaluate the lipids' interferences and the lipids' index as a guide for routine clinical practice in our institution.

One important aspect of this interference study is that many manufactured reagent package inserts often do not list information on what concentrations of analytes were tested, which thus offers limited information on interferences. In this study, the clinically significant interference was assessed by comparing the mean difference between specimens with and without interferents at the clinical decision cutoff values of each TDM assay.

Methods

This study was considered a quality assessment project and was therefore waived by the institutional review board. The study was conducted at the Critical Care Laboratory, Rapid Response Laboratory, and Toxicology Laboratory at The Ohio State University Wexner Medical Center. Based on the recommendation of the Clinical and Laboratory Standards Institute guideline C56, the screening (paired-difference) interference study was performed to guide routine clinical practice in our department.

Plasma/serum specimen pools containing a clinically important concentration of the analytes were spiked with the concentrations of the interferents (close to the threshold of system flags), and the assay results were compared with a control specimen (without a spiked interferent). To avoid drug-to-drug interaction or interference from other drugs, estimated concentrations of amikacin (AMIK), carbamazepine, digoxin, lidocaine, methotrexate, phenobarbital, and theophylline, of a maximum 1% volume, were individually spiked into each tube of patient specimen pools, which contained lithium (Li) heparin plasma. The Li was spiked in the serum specimen pools for the study. The estimated concentrations are from the clinical decision points practiced in our hospital and defined by pharmacists (listed in **TABLE 1**).

All the drugs were purchased from Sigma-Aldrich (St. Louis, MO); catalog numbers are listed in **TABLE 2**. The interferents of hemoglobin, conjugated bilirubin, and triglycerides were purchased from Sun Diagnostics, LLC (New Gloucester, ME) with known concentrations of each interferent (INT-01 ASSURANCE Interference Test Kit for Routine Interferents). The interferents of 10% volume were spiked to the patient specimen pools. Aliquots of these plasma/serum pools that were spiked with each drug but without the addition of interferents were used as the control group.

All the TDM assays were performed on Beckman Coulter AU 5800 or DxC700 analyzers (Beckman Coulter, Brea, CA) according to the manufacturer's specifications. The reagents, methodologies, and models are listed in **TABLE 2**. Each assay was performed twice on each analyzer. Indices were measured as recommended by the manufacturer. All statistical analyses and graphs were conducted using Microsoft Office Excel 2013. The acceptability criteria were defined according to the latest College of American Pathologists survey in 2020. Interference was judged as significant when the results of a spiked specimen were statistically different from those of the control specimen or the difference between the 2 means was beyond the defined acceptability criteria.

$$\text{Difference} = \text{Group spiked with interferents (mean)} - 0.9 * \text{control group (mean)}$$

$$\text{Difference \%} = \frac{\text{Group spiked with interferents (mean)} - 0.9 * \text{control group (mean)}}{0.9 * \text{control group (mean)}} \times 100$$

TABLE 1. List of Clinical Decision Points of Each Drug and Actual Concentration Measured After Spiking

Analyte	Unit	#1	#2	Clinical Decision Points
AMIKE	µg/mL	7.37	43.62	6.0 (trough), 60 (peak)
AMIKQ	µg/mL	8.15	55.59	6.0 (trough), 60 (peak)
CARB	µg/mL	2.98	8.03	4.0–12.0
DIG	ng/mL	1.18	2.60	1.0 and 2.0 (critical)
LIDO	µg/mL	1.30	5.35	1.5–5.0
Li	mmol/L	1.00	1.81	1.0, 2.0 (critical)
MTXA	µmol/L	0.62	NA	Various because of different protocols
MTXE	µmol/L	0.55	NA	Various because of different protocols
PBARB	µg/mL	13.00	38.90	15.0–40.0
THEO	µg/mL	17.35	31.95	10.0–20.0 (critical)

AMIKE, emit amikacin; AMIKQ, QMS amikacin; CARB, carbamazepine; DIG, digoxin; emit, enzyme multiplied immunoassay technique; Li, lithium; LIDO, lidocaine; MTXA, ARK methotrexate; MTXE, emit methotrexate; PBARB, phenobarbital; THEO, theophylline; TOB, tobramycin.

TABLE 2. Reagents and Methodology of Beckman Coulter AU Series and Catalog Number of Sigma-Aldrich Drugs

Analyte	Reagent	Methodology	Beckman Coulter AU	Sigma-Aldrich
AMIKE	Emit	Homogeneous enzyme immunoassay	DxC700	A1774
AMIKQ	QMS	Homogeneous particle-enhanced turbidimetric immunoassay	DxC700	A1774
CARB	Emit	Homogeneous enzyme immunoassay	5800	C-053
DIG	Emit	Homogeneous enzyme immunoassay	5800	D-029
LIDO	Emit	Homogeneous enzyme immunoassay	DxC700	L-018
Li	Infinity	Spectrophotometric method	5800	L7026
MTXE	Emit	Homogeneous enzyme immunoassay	DxC700	M-136
MTXA	ARK	Homogeneous enzyme immunoassay	DxC700	M-136
PBARB	Emit	Homogeneous enzyme immunoassay	5800	P-008
THEO	Emit	Homogeneous enzyme immunoassay	5800	IMPC-051-01

AMIKE, emit amikacin; AMIKQ, QMS amikacin; CARB, carbamazepine; DIG, digoxin; emit, enzyme multiplied immunoassay technique; Li, lithium; LIDO, lidocaine; MTXA, ARK methotrexate; MTXE, emit methotrexate; PBARB, phenobarbital; QMS, quantitative microsphere system; THEO, theophylline.

Results

The system flags measured on the analyzers are listed in **TABLE 3**. By using stored plasma/serum pools spiked with high or low critical levels of the TDM assays, we determined the results for hemolysis interference, presented in **TABLE 4**. Overall, the addition of hemoglobin within the threshold of flags from the analyzer did not significantly interfere with the results, except for QMS amikacin (AMIKQ) at 55.59 μg/mL with a concentration of 500 mg/dL hemoglobin. The difference caused by added hemoglobin in AMIKQ at 55.59 μg/mL was above the criterion of ±2.28 μg/mL, or 10%. The absolute or percentage of mean differences between the AMIKQ specimens at 55.59 μg/mL with or without hemoglobin 500 mg/dL did not support the data from the Beckman Coulter technical documents (threshold hemoglobin at 10,000 mg/dL, acceptability criteria 10%).

TABLE 3. System Flags Measured for Hemoglobin, Bilirubin, and Triglycerides on Beckman Coulter AU Series

Interferent	System Flag Index	Interferent Concentration (mg/dL)
Hemoglobin	+++	100–150
	++++	200–400
	ABN	>500
Conjugated bilirubin	0	15
	+	30–40
	++	45–60
Triglycerides	++	250–400
	+++	500–1200
	++++	1500

ABN, abnormal.

The conjugated bilirubin interference results are shown in **TABLE 5**. Increased bilirubin concentrations did cause significant interference in the results of enzyme multiplied immunoassay technique AMIK (AMIKE) at 43.62 μg/mL or those of AMIKQ at 55.59 μg/mL with a concentration of 20 mg/dL bilirubin, which had a difference of 7.15 μg/mL/18.06% or 5.19 μg/mL/10.37% compared with the control groups, respectively. The absolute or percentage of mean differences between the AMIKE specimens at 43.62 μg/mL with or without bilirubin 20 mg/dL did not support data from the Beckman Coulter technical documents (threshold bilirubin at 30 mg/dL, acceptability criteria 10%).

The interference caused by triglycerides is presented in **TABLE 6**. The addition of triglycerides within the threshold of flags from the analyzer did not cause significant interferences. Therefore, the results with respect to analyte levels showed that hemolysis interference in AMIKQ and icterus interference in AMIKE in this study were not in accordance with the manufacturer's claims. Furthermore, increasing icterus severity seemed to be correlated with increasing hemolysis and lipemia severity (**FIGURE 1A**). Increasing lipemia severity was correlated with increasing hemolysis and icterus severity (**FIGURE 1B**).

Discussion

The main findings of our study were the detection of hemolysis interference in the AMIKQ assay and the detection of icterus interferences in the AMIQ and AMIKE assays at clinically significant values. The hemoglobin, bilirubin, and turbidity in the specimens were spectrophotometrically assessed using HIL indices. The relationship between concentrations of hemoglobin, bilirubin, and triglycerides and the HIL indices were evaluated in this study. When the HIL indices were ≥5, the Beckman Coulter AU analyzers indicated "abnormal (ABN)." Therefore, according to our results, with a hemolysis in-

TABLE 4. Influence of Hemolysis on 8 Clinical TDM Tests According to Analyte Levels

Analyte	Hemoglobin (mg/dL)	Mean Difference	Mean Difference, %	Acceptability Criteria	Acceptable?
AMIKE-7.37	500	0.30 μg/mL	4.67	±5.79 μg/mL or 10%	Yes
AMIKE-43.62	500	3.16 μg/mL	8.07	±5.79 μg/mL or 10%	Yes
AMIKQ-8.15	500	0.71 μg/mL	9.84	±2.28 μg/mL or 10%	Yes
AMIKQ-55.59	500	5.28 μg/mL	10.56	±2.28 μg/mL or 10%	No
CARB-2.98	400	0.14 μg/mL	6.79	±25%	Yes
CARB-8.03	400	0.92 μg/mL	13.04	±25%	Yes
DIG-1.18	400	0.09 ng/mL	9.25	±0.2 ng/mL or 20%	Yes
DIG-2.60	400	0.07 ng/mL	3.44	±0.2 ng/mL or 20%	Yes
LIDO-1.30	400	0.08 μg/mL	7.14	±1.2 μg/mL or 10%	Yes
LIDO-5.35	400	0.54 μg/mL	11.17	±1.2 μg/mL or 10%	Yes
Li-1.00	300	0.01 mmol/L	0.78	±0.3 mmol/L or 20%	Yes
Li-1.81	300	0.01 mmol/L	0.62	±0.3 mmol/L or 20%	Yes
MTXE-0.55	500	0.05 μmol/L	10.10	±1.28 μmol/L or 10%	Yes
MTXA-0.62	500	–0.01 μmol/L	–2.34	±2.54 μmol/L or 10%	Yes
PBARB-13.00	400	–0.10 μg/mL	–0.86	±20%	Yes
PBARB-38.90	400	–0.38 μg/mL	–0.94	±20%	Yes
THEO-17.35	400	0.26 μg/mL	2.45	±25%	Yes
THEO-31.95	400	0.84 μg/mL	3.33	±25%	Yes

AMIKE, emit amikacin; AMIKQ, QMS amikacin; CARB, carbamazepine; DIG, digoxin; emit, enzyme multiplied immunoassay technique; Li, lithium; LIDO, lidocaine; MTXA, ARK methotrexate; MTXE, emit methotrexate; PBARB, phenobarbital; TDM, therapeutic drug monitoring; THEO, theophylline.

TABLE 5. Influence of Icterus on 8 Clinical TDM Tests According to Analyte Levels

Analyte	Bilirubin (mg/dL)	Mean Difference	Mean Difference, %	Acceptability Criteria	Acceptable?
AMIKE-7.37	20	0.46 µg/mL	6.96	±5.79 µg/mL or 10%	Yes
AMIKE-43.62	20	7.15 µg/mL	18.06	±5.79 µg/mL or 10%	No
AMIKQ-8.15	20	0.47 µg/mL	6.47	±2.28 µg/mL or 10%	Yes
AMIKQ-55.59	20	5.19 µg/mL	10.37	±2.28 µg/mL or 10%	No
CARB-2.98	45	-0.06 µg/mL	-2.13	±25%	Yes
CARB-8.03	45	0.40 µg/mL	5.48	±25%	Yes
DIG-1.18	45	0.07 ng/mL	7.97	±0.2 ng/mL or 20%	Yes
DIG-2.60	45	0.08 ng/mL	3.90	±0.2 ng/mL or 20%	Yes
LIDO-1.30	45	0.03 µg/mL	2.51	±1.2 µg/mL or 10%	Yes
LIDO-5.35	45	0.04 µg/mL	0.72	±1.2 µg/mL or 10%	Yes
Li-1.00	60	0.01 mmol/L	1.28	±0.3 mmol/L or 20%	Yes
Li-1.81	60	0.02 mmol/L	0.98	±0.3 mmol/L or 20%	Yes
MTXE-0.55	60	0.03 µmol/L	5.05	±1.28 µmol/L or 10%	Yes
MTXA-0.62	60	–0.06 µmol/L	–10.49	±2.54 µmol/L or 10%	Yes
PBARB-13.00	45	–0.08 µg/mL	–0.62	±20%	Yes
PBARB-38.90	45	–0.63 µg/mL	–1.71	±20%	Yes
THEO-17.35	45	–0.34 µg/mL	–1.34	±25%	Yes
THEO-31.95	45	0.22 µg/mL	1.39	±25%	Yes

AMIKE, emit amikacin; AMIKQ, QMS amikacin; CARB, carbamazepine; DIG, digoxin; emit, enzyme multiplied immunoassay technique; Li, lithium; LIDO, lidocaine; MTXA, ARK methotrexate; MTXE, emit methotrexate; PBARB, phenobarbital; TDM, therapeutic drug monitoring; THEO, theophylline.

TABLE 6. Influence of Lipemia on 8 Clinical TDM Tests According to Analyte Levels

Analytes	Triglycerides (mg/dL)	Mean Difference	Mean Difference, %	Acceptability Criteria	Acceptable?
AMIKE-7.37	1500	–0.03 µg/mL	–0.35	±5.79 µg/mL or 10%	Yes
AMIKE-43.62	1500	3.00 µg/mL	7.33	±5.79 µg/mL or 10%	Yes
AMIKQ-8.15	1500	0.02 µg/mL	0.47	±2.28 µg/mL or 10%	Yes
AMIKQ-55.59	1500	3.53 µg/mL	7.07	±2.28 µg/mL or 10%	Yes
CARB-2.98	1200	0.18 µg/mL	4.90	±25%	Yes
CARB-8.03	1200	0.74 µg/mL	8.82	±25%	Yes
DIG-1.18	1000	–0.18 ng/mL	–16.02	±0.2 ng/mL or 20%	Yes
DIG-2.60	1000	–0.31 ng/mL	–12.49	±0.2 ng/mL or 20%	Yes
LIDO-1.30	1500	–0.17 µg/mL	–14.02	±1.2 µg/mL or 10%	Yes
LIDO-5.35	1500	–0.22 µg/mL	–4.51	±1.2 µg/mL or 10%	Yes
Li-1.00	1500	0.03 mmol/L	2.60	±0.3 mmol/L or 20%	Yes
Li-1.81	1500	0.05 mmol/L	2.73	±0.3 mmol/L or 20%	Yes
MTXE-0.55	1200	0.02 µmol/L	3.03	±1.28 µmol/L or 10%	Yes
MTXA-0.62	1200	–0.01 µmol/L	–1.50	±2.54 µmol/L or 10%	Yes
PBARB-13.00	1200	0.47 µg/mL	2.92	±20%	Yes
PBARB-38.90	1200	2.22 µg/mL	4.20	±20%	Yes
THEO-17.35	1200	1.15 µg/mL	2.99	±25%	Yes
THEO-31.95	1200	1.88 µg/mL	4.83	±25%	Yes

AMIKE, emit amikacin; AMIKQ, QMS amikacin; CARB, carbamazepine; DIG, digoxin; emit, enzyme multiplied immunoassay technique; Li, lithium; LIDO, lidocaine; MTXA, ARK methotrexate; MTXE, emit methotrexate; PBARB, phenobarbital; TDM, therapeutic drug monitoring; THEO, theophylline.

dex of ABN, results should be suppressed and communication with providers may be needed for specimen recollection for AMIKQ measurement. With an icterus index of "+," results should be suppressed for AMIKQ and AMIKE measurement. This study will help clinicians evaluate HIL interferences on TDM analytes performed on Beckman Coulter AU analyzers.

The absorbance of hemoglobin is at 540 to 580 nm wavelengths. However, hemoglobin begins to absorb at approximately 340 nm, increasing in absorbance at 400 to 430 nm. Thus, methods of measuring nicotinamide adenine dinucleotide (NAD) or NAD plus hydrogen (NADH; 340 nm) may be affected by hemolysis. The AMIKQ assay is a homogeneous particle-enhanced turbidimetric immunoassay based on

FIGURE 1. **The relationship between (A) icterus and lipemia/hemolysis and (B) lipemia and icterus/hemolysis. All axes are plotted on HIL indices on Beckman Coulter AU analyzers. HIL, hemolysis, icterus, lipemia.**

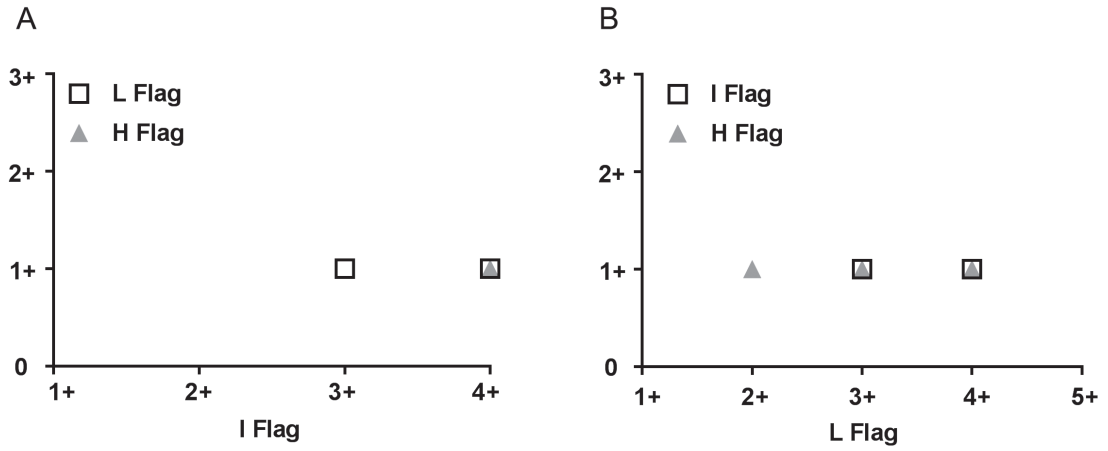

competition between the drug in the specimen and the drug coating a microparticle for antibody binding sites of the AMIK antibody reagent. The rate of absorbance change is measured photometrically, at a wavelength of 700 nm. From the results in our study, AMIKQ at 55.59 μg/mL spiked with 500 mg/dL of hemoglobin had a positive interference. If the interference was caused by the absorbance of hemoglobin, then theoretically a negative interference was expected. In addition, the wavelength of 700 nm for AMIKQ made the interference less likely to be caused by the absorbance of hemoglobin. However, hemoglobin interference occurred not only using the spectrophotometric methods but also from the chemical reaction with reagents.[4] Therefore, in this study, the chemical reaction with reagents was hypothesized as the possible reason for the positive interference caused by 500 mg/dL of hemoglobin.

The wavelength at which bilirubin absorbs is 450 to 460 nm. The AMIKE assay is a homogeneous enzyme immunoassay based on competition between the drug in the specimen and the drug labeled with the enzyme glucose-6-phosphate dehydrogenase for antibody binding sites. Enzyme activity decreases upon binding to the antibody, so the drug concentration in the specimen can be measured in terms of enzyme activity. The active enzyme converts oxidized NAD to NADH, resulting in an absorbance change that is measured spectrophotometrically at a wavelength of 340 nm. Bilirubin is less likely to interfere with the absorbance of NADH at 340 nm; however, the positive interference in the AMIKE may be interpreted as interference by bilirubin with the binding of NADH.[5] An alternative explanation could be the chemical reaction between bilirubin and the reagents,[6] which also helps explain the positive interference of bilirubin in AMIKQ.

Previous studies have reported that severely lipemic specimens are associated with increased hemolysis in serum/plasma specimens. Some highly lipemic body fluid specimens have also indicated more severe hemolysis, but this pattern was significantly more evident in serum/plasma specimens.[7,8] Our study observed similar scenarios in vitro by spiking high concentrations of triglycerides. In addition, we observed the lipid and hemolysis indices in specimens with high concentrations of bilirubin. These findings may help laboratories understand more about other interferents' indices in lipemic or icterus specimens.

Conclusion

It has been recommended that clinically significant bias should be expressed as a reference change value (RCV).[9,10] The RCV is considered to be the best tool for assessing clinical significance, incorporating both biological and analytical variations, for most clinical chemistry assays except TDM assays. The biological variations of TDM assays cannot be assessed from healthy patients who do not receive drug treatment. Therefore, evaluating the interferences at the clinical decision cutoffs of each TDM assay may be the best way to assess clinically significant bias. Because of the importance of knowing the degree of interferences at clinical decision-making values, it is crucial for a laboratory to define its own cutoff of the interferents for clinically significant bias for each TDM assay. Proper management such as suppressing results or recollecting blood needs to be defined based on the laboratory's own data.

REFERENCES

1. Weber TH, Käpyaho KI, Tanner P. Endogenous interference in immunoassays in clinical chemistry. A review. *Scand J Clin Lab Invest Suppl.* 1990;201:77–82.
2. Bornhorst JA, Roberts RF, Roberts WL. Assay-specific differences in lipemic interference in native and intralipid-supplemented samples. *Clin Chem.* 2004;50(11):2197–2201.
3. Viljoen A, Cockrill G, Martin SC. The ability of the lipemic index to predict assay interference. *Clin Chem.* 2006;52(S6):A8.
4. Wenk RE. Mechanism of interference by hemolysis in immunoassays and requirements for sample quality. *Clin Chem.* 1998;44(12):2554.
5. Noir BA, Boveris A, Garaza Pereira AM, Stoppani AO. Bilirubin: a multi-site inhibitor of mitochondrial respiration. *FEBS Lett.* 1972;27(2):270–274.
6. Perlstein MT, Thibert RJ, Watkins RJ, Zak B. Spectrophotometric study of bilirubin and hemoglobin interactions in several hydrogen peroxide generating procedures. *Clin Chem.* 1978;23(1):13–27.
7. Mainali S, Davis SR, Krasowski MD. Frequency and causes of lipemia interference of clinical chemistry laboratory tests. *Pract Lab Med.* 2017;8:1–9.
8. Jaben EA, Koch CD, Karon BS. Lipid emulsion solution: a novel cause of hemolysis in serum and plasma blood samples. *Clin Biochem.* 2011;44(2-3):254–256.
9. Lippi G, Cadamuro J, von Meyer A, Simundic A-M; European Federation of Clinical Chemistry and Laboratory Medicine (EFLM) Working Group for Preanalytical Phase (WG-PRE). Practical recommendations for managing hemolyzed samples in clinical chemistry testing. *Clin Chem Lab Med.* 2018;56(5):718–727.
10. Simundic A-M, Baird G, Cadamuro J, Costelloe SJ, Lippi G. Managing hemolyzed samples in clinical laboratories. *Crit Rev Clin Lab Sci.* 2020;57(1):1–21.

Trimethylamine-N-Oxide and Precursors as Novel Potential Biomarkers for Anxiety Disorder

Juan Le, MSc, Rui Peng, PhD, Yan Li, PhD*

Clinical Laboratory, Renmin Hospital, Wuhan University, Wuhan, China; *To whom correspondence should be addressed. lejuan0323@whu.edu.cn

Keywords: gut microbiota, TMAO, anxiety disorder, biomarker, choline, betaine

Abbreviations: AD, anxiety disorder; TMAO, trimethylamine N-oxide; DSM-IV, *Diagnostic and Statistical Manual, Fourth Edition*; sdLD-C, small-density lipoprotein cholesterol; LC-MS/MS, liquid chromatography–tandem mass spectrometry; ESI, electrospray ionization; MRM, multiple reaction monitoring; IQR, interquartile range; ERN, error-related negativity; TMA, trimethylamine; FMO3, flavin monooxygenase 3; CUMS, chronic unpredictable mild stress; … , nonappplicable

Laboratory Medicine 2022;53:177–182; https://doi.org/10.1093/labmed/lmab063

ABSTRACT

Background: Anxiety disorder (AD) is closely related to changes in the composition of the gut microbiota, and changes in gut microbiota abundance affect the synthesis of trimethylamine N-oxide (TMAO).

Objective: To explore whether TMAO is related to and serves as a potential biomarker for the diagnosis of AD.

Methods: The concentrations of TMAO, choline, and betaine were analyzed in 60 patients with AD and 60 control individuals using a liquid chromatography–tandem mass spectrometry (LC-MS/MS) method.

Results: Compared with controls, TMAO was significantly reduced in patients with AD. Logistic regression analysis demonstrated that decreased TMAO concentrations were associated with an increased risk of AD. The multiplication of TMAO and its precursors (choline and betaine) produced the best AUC for the diagnosis of AD (AUC = 0.847; 95% CI, 0.780–0.914; $P < .001$).

Conclusion: The decrease of TMAO concentration is related to the increase of anxiety disorder. TMAO and precursors could be identified as novel potential biomarkers for the diagnosis of AD.

Anxiety disorder (AD), a chronic and disabling condition, is the most common mental disorder, with a worldwide prevalence rate of 7.3%.[1] AD was characterized by fear and distress, impaired quality of life, and impaired ability to function in society, all of which impose a considerable global burden on families and societies.[2] Therefore, earlier diagnosis and intervention may be particularly important before symptoms appear and damage occurs. However, the current diagnosis mainly depends on patient symptoms and is not yet based on objective biomarkers.[3] Therefore, there is an urgent need to identify biomarkers to accurately predict the occurrence of AD and to promptly implement effective strategies.

The human intestines host 100 trillion bacteria; maintaining the normal composition of the intestinal microbiota is vital to the physiological functions of the central nervous system. The concept of the brain-gut-bacteria axis is proposed on the basis of the brain-gut axis, which refers to the complex network between the gut, microbiota, and the brain.[4] In recent years, the role of intestinal flora in central-nervous-system diseases has attracted more and more attention, including depression,[5] schizophrenia,[6] and anxiety.[7,8] Evidence demonstrated that due to changes in colonic mobility, anxiety is often accompanied by alterations in the composition and stability of the gut microbiota, including changes in some bacterial populations, such as *Fusobacterium*[7] and *Clostridium*.[9]

This finding suggests that specific gut microbes could serve as a biomarker for AD.[10] However, microbial analysis is often conducted by pyrosequencing 16S rRNA genes, which is complicated, time-consuming, and expensive. Therefore, biomarkers that can be easily and quickly detected are necessary. Trimethylamine N-oxide (TMAO) is a naturally compound produced by the metabolism of choline and betaine through the gut microbiota,[11] some of which include *Fusobacterium* and *Clostridium*.[12] Therefore, changes in the proportions of *Fusobacterium* to *Clostridium* in patients with AD may affect the synthesis of TMAO, which may result in the changed concentration of TMAO in vivo.

Although it has been known that AD is closely related to changes in gut microbiota composition, and that changes in gut-microbiota abundance affect the synthesis of TMAO, little is known about TMAO levels in patients with AD. Therefore, this study aims to detect the level of TMAO in patients with AD and to evaluate whether TMAO can be used as a novel biomarker for AD.

Methods

Study Participants

We conducted a case-control study with 72 patients with AD recruited and 60 healthy controls at the Renmin Hospital of Wuhan University,

China. The flow diagram of this study is displayed in **FIGURE 1**. We obtained basic clinical information from all participants through consulting the clinical data file. The diagnosis of AD was based on the criteria in the *Diagnostic and Statistical Manual, Fourth Edition* (DSM-IV). The following criteria were used to exclude certain patients: having cardiovascular disease, diabetes, kidney disease, gastrointestinal cancers, and mental diseases other than AD; having a history of drug or alcohol abuse during the past 3 months; currently using antibiotics and probiotics. This study was ethically approved by the Ethics Committee of Renmin Hospital of Wuhan University. All participants provided written informed consent.

Blood Specimen Collection and Routine Laboratory Analyses

Blood specimens were collected from antecubital veins of the participants. After centrifuging at 7500*g* for 5 minutes, the serum specimens were separated and stored at −80°C until further analysis. We tested the levels of ALT, AST, creatinine, urea, uric acid (UA), triglycerides, cholesterol, HDL-C, LDL-C, and small-density lipoprotein cholesterol (sdLD-C) by routine laboratory procedures using the Siemens ADVIA 2400 automatic biochemistry analyzer (Siemens AG).

Measurement of TMAO and Its Precursor-Metabolites Concentrations

The concentrations of TMAO and its precursor metabolites, choline and betaine, were measured using a liquid chromatography–tandem mass spectrometry (LC-MS/MS) method. The LC-MS/MS platform consisted of a LC-20AD (Shimadzu) and an AB SCIEX 4500 QTRAP mass spectrometer (Thermo Fisher Scientific Inc), equipped with an electrospray ionization (ESI) source operating in positive mode. The ESI inlet parameters were curtain gas (25.0), collision gas (medium), ionspray voltage (5500.0), temperature (500.0), ion source gas 1 (30.0) and ion source gas 2 (30.0). The chromatographic separations of analytes were performed on a Polar-Imidazole column (2.2 μm, 2.1 × 100 mm, Sepax Technologies) with a flow rate of 0.50 mL/min at 45°C. Data acquisition and processing were performed using AB SCIEX Analyst 1.6.2 Software (DH Tech. Dev. Pte. Ltd.). The injection volume was 10 μL. Acetonitrile with 0.2% formic acid (v/v, Solution-A) and water with 0.2% formic acid (v/v, Solution-B) were wielded as mobile phases. The following isocratic elution condition was used: 0–4.5 min 80% solvent A. The LC-MS/MS chromatograms of 3 analytes in serum are presented in Supplemental Figure 1.

Multiple reaction monitoring (MRM) was used to monitor the optimized mass transitions of TMAO, choline, and betaine (m/z 76.0 → 58.0 for TMAO and m/z 84.9 → 66.1 for TMAO-d9; m/z 104.1 → 60.1 for choline and m/z 113.1 → 69.2 for choline-d9; m/z 118.2 → 58.0 for betaine and m/z 120.9 → 61.2 for betaine-d3). The MRM parameters are listed in Supplemental Table 1. For specimen preparation, 10 μL serum was precipitated with 200 μL acetonitrile containing internal standard TMAO-d9 (20 ng/mL), choline-d9 (100 ng/mL), and betaine-d3 (500 ng/mL), followed by vortexing (5 minutes) and centrifugation (12,000*g* for 3 minutes). Then, the supernatant was separated and injected into the LC-MS/MS platform. To achieve the quantification of 3 analytes, we conducted the standard curves using 6 known levels of TMAO (10, 20, 50, 100, 250, and 500 ng/mL), choline (50, 100, 250, 500, 1250, and 2500 ng/mL), and betaine (250, 500, 1250, 2500, 6250, and 12500 ng/mL). The intra-assay and interassay coefficient of variation were each <13%, and the absolute recoveries were between 89.6% and 112.5%. The lower limit of quantifications (LLOQs) of TMAO, choline, and betaine were 0.5 ng/mL, 10 ng/mL, and 50 ng/mL, respectively.

Statistical Analysis

Continuous variables were expressed as mean (SD) if normally distributed, and median (interquartile range [IQR]) if not normally distributed. Categorical data were expressed as the number (percentage). Continuous variables were compared by applying the *t* test or the nonparametric Mann-Whitney U test, as appropriate. The correlation between TMAO and precursors was evaluated using nonparametric Spearman rank correlation analysis and the correlation coefficients (*r*) was calculated. To evaluate the diagnostic values of TMAO in AD, ROC curves were generated, and the AUCs were calculated. The combined diagnosis of multiple variables was performed

FIGURE 1. Flow diagram for this study.

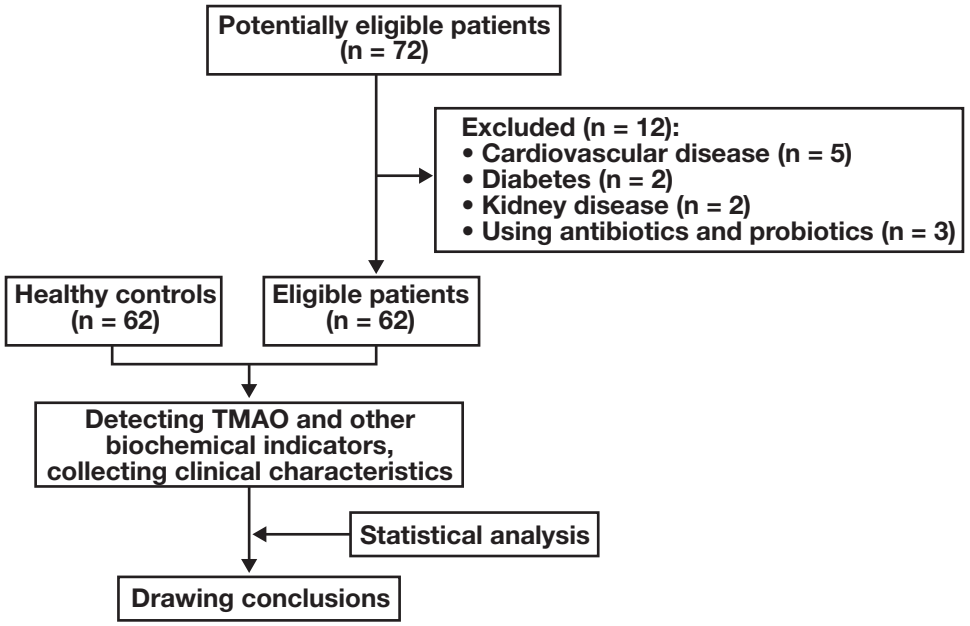

by applying a fitted multiple logistic regression model. Binary logistic regression analysis was applied to estimate the OR and 95% CI of AD across TMAO quartiles. We calculated the *P* value for trend by modeling the median value of each quartile as a continuous variable. A 2-sided value of $P < .05$ was considered statistically significant. All statistical analyses were performed using SPSS software, version 20.0 (IBM Corporation) and GraphPad Prism software, version 8 (GraphPad Software Inc.).

Results

Characteristics of the Participants

Baseline characteristics of the participants were summarized in **TABLE 1**. There were no significantly statistical differences in age, sex, ALT, AST, creatinine, triglyceride, UA, and HDL-C between the 2 groups. Compared with controls, patients with AD had lower levels of urea, cholesterol, LDL-C, and sdLDL-C. We note that the concentrations of TMAO (101.51 [75.50–140.67] ng/mL vs 213.69 [116.93–333.3] ng/mL, $P < .001$], choline (1402.72 [1154.66–1826.25] ng/mL vs 2355.87 [1446.37–3152.13] ng/mL, $P < .001$) and betaine (3437.63 [851.69–4281.93] ng/mL vs 4793.17 [3760.34–5408.63] ng/mL, $P < .001$) were significantly lower in patients with AD than in controls, respectively (**FIGURE 2A**, **2B**, and **2C**). Heatmapping visually represents the concentrations of the 3 compounds, indicating the presence of low concentrations in patients with AD (**FIGURE 2D**).

TABLE 1. Demographic Characteristics and Laboratory Indicators of Participants

Variable	Patients with Anxiety Disorders (*n* = 60)	Control Individuals (*n* = 60)	*P* Value
Age, y, median (IQR)	56 (43–66)	56 (52–62)	.74
Male, no. (%)	18 (30.0%)	20 (33.3%)	.70
ALT, U/L, median (IQR)	15 (12–18)	15 (12–20)	.61
AST, U/L, median (IQR)	21.0 (16.0–22.0)	21.5 (18.0–25.0)	.12
Creatinine, μmol/L, median (IQR)	59.50 (52.25–72.00)	56.0 (52.0–69.0)	.53
Triglyceride, mmol/L, median (IQR)	1.23 (0.77–1.37)	1.15 (0.93–1.39)	.72
Urea, mmol/L, median (IQR)	3.66 (3.06–4.33)	4.71 (4.07–5.46)	<.001
UA, μmol/L, mean (SD)	305.15 (69.66)	310.80 (80.06)	.68
Cholesterol, mmol/L, median (IQR)	4.32 (3.83–4.62)	4.88 (4.52–5.17)	<.001
HDL-C, mmol/L ,mean (SD)	1.36 (0.33)	1.32 (0.30)	.49
LDL-C, mmol/L, median (IQR)	2.21 (2.02–2.60)	2.78 (2.29–3.03)	<.001
sdLDL-C, mmol/L, median (IQR)	0.60 (0.49–0.72)	0.77 (0.64–0.95)	<.001
TMAO, ng/mL, median (IQR)	101.51 (75.50–140.67)	213.69 (116.93–333.3)	<.001
Choline, ng/mL, median (IQR)	1402.72 (1154.66–1826.25)	2355.87 (1446.37–3152.13)	<.001
Betaine, ng/mL, median (IQR)	3437.63 (2851.69–4281.93)	4793.17 (3760.34–5408.63)	<.001

IQR, interquartile range; UA, uric acid; sdLDL-C, small dense low-density-lipoprotein cholesterol; TMAO, trimethylamine-N-oxide.

Correlation Among TMAO, Choline, and Betaine

According to Spearman rank correlation analysis, the concentrations of TMAO were positively and significantly correlated with choline ($r = 0.319$; $P < .001$) and betaine ($r = 0.3978$; $P = .002$). After adjusting for age, sex, ALT, AST, creatinine, urea, UA, triglyceride, cholesterol, HDL-C, LDL-C, and sdLDL-C, the correlation between TMAO and choline was still evident ($P < .001$), whereas significant correlation between TMAO and betaine disappeared ($P = .22$).

Logistic Regression Analysis of TMAO Predicting Anxiety Disorder

To evaluated the ORs of variables for AD, we conducted univariate and multivariate logistic regression analysis. First, the results of univariate logistic regression analysis showed TMAO was associated with AD (OR = 0.991; 95% CI, 0.987–0.995; $P < .001$). Multivariate analysis indicated that TMAO remained independently associated with the risk of AD (OR = 0.993; 95% CI, 0.988–0.998; $P = .01$) after adjusting for sex, age, ALT, AST, creatinine, urea, UA, triglyceride, cholesterol, HDL-C, LDL-C, and sdLDL-C.

Association between TMAO and Risk of AD

To further explore the association of TMAO with AD, we calculated the ORs and 95% CI values of AD across quartiles of TMAO and tested the liner trend via binary logistic regression analysis. TMAO concentrations were categorized in 4 quartiles: quartile 1, <93.89 ng/mL; quartile 2, 93.89–129.75 ng/mL; quartile 3, 129.76–275.53 ng/mL; and quartile 4, >275.53 ng/mL. Quartile 1 was used as the reference category. As shown in **TABLE 2** and **FIGURE 3**, quartile 4 and quartile 3 of TMAO showed significant association with decreased risk of AD without adjustment (crude model) (OR = 0.076, 95% CI: 0.022–0.261, $P < .001$; and OR = 0.152, 95% CI: 0.049–0.474, $P = .001$, respectively); the P_{trend} for the crude model was less than .001.

After adjusting for sex, age, ALT, AST, creatinine, urea, UA, triglyceride, cholesterol, HDL-C, LDL-C, and sdLDL-C (model 1), we found decreased ORs of the quartile 4 and quartile 3 for AD compared with quartile 1 (OR = 0.117, 95% CI: 0.022–0.620, $P = .01$; and OR = 0.201, 95% CI: 0.042–0.963, $P = .05$, respectively), and the P_{trend} for model 1 was 0.004. These results showed that decreased TMAO concentrations were associated with an increased risk of AD.

ROC Curve of TMAO for Diagnosing AD

We performed ROC analysis to evaluated the diagnostic performance of TMAO on AD. As shown in **FIGURE 4** and **TABLE 3**, with the optimal cutoff value of 146.75 ng/mL, TMAO can achieve a diagnostic sensitivity of 70% and a specificity of 80%. The sensitivity at the optimal cutoff point of choline and betaine were 65% and 72%, and the specificity was 85% and 70%, respectively. Compared with individual variables, the multiplication of TMAO, choline, and betaine resulted in the highest

FIGURE 2. Comparisons in trimethylamine N-oxide (TMAO) (A), choline (B), and betaine (C) between patients with anxiety disorder (AD) and control individuals, and a heatmap (D) of the concentrations of 3 compounds in 2 groups. Red indicates high concentration, whereas blue represents low concentrations, showing that red grids were more common in controls than in patients with AD.

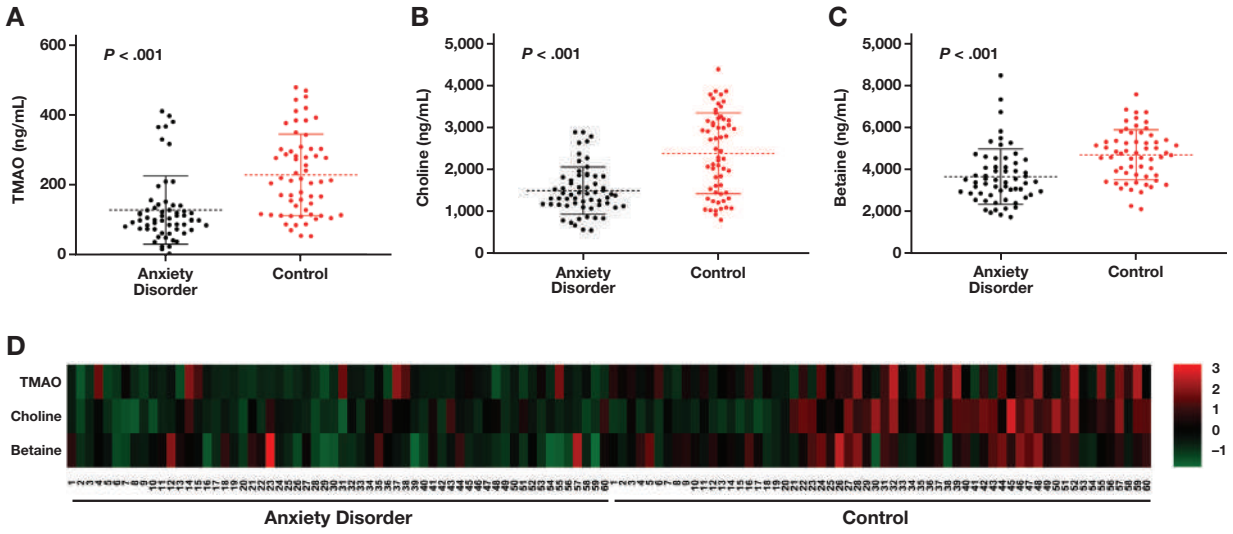

TABLE 2. The Quartiles of Plasma TMAO and ORs with 95% CI of Anxiety Disorder, Compared with Quartile 1

Variable	Quartile of TMAO Concentration (ng/mL)							P Value for Trend
	Quartile 1 (<93.89)	Quartile 2 (93.89–129.75), Median (IQR)	P Value	Quartile 3 (129.76–275.53), Median (IQR)	P Value	Quartile 4 (>275.53), Median (IQR)	P Value	
Crude	1 [reference]	0.710 (0.225–2.246)	.56	0.152 (0.049–0.474)	.001	0.076 (0.022–0.261)	<.001	<.001
Model 1[a]	1 [reference]	0.874 (0.190–4.023)	.86	0.201 (0.042–0.963)	.05	0.117 (0.022–0.620)	.01	.004

TMAO, trimethylamine-N-oxide; IQR, interquartile range; UA, uric acid; sdLDL-Ch, small dense low-density-lipoprotein cholesterol.
[a]Adjusted for age, sex, ALT, AST, creatinine, urea, UA, triglycerides, cholesterol, HDL-C, LDL-C, and sdLDL-C.

FIGURE 3. ORs (95 % CI) of anxiety disorder across quartiles of trimethylamine N-oxide (TMAO) in a crude model (A) and model 1 (B). Model 1: adjusted for age, sex, ALT, AST, creatinine, urea, uric acid (UA), triglyceride, cholesterol, HDL-C, LDL-C, and small dense low-density-lipoprotein cholesterol (sdLDL-C).

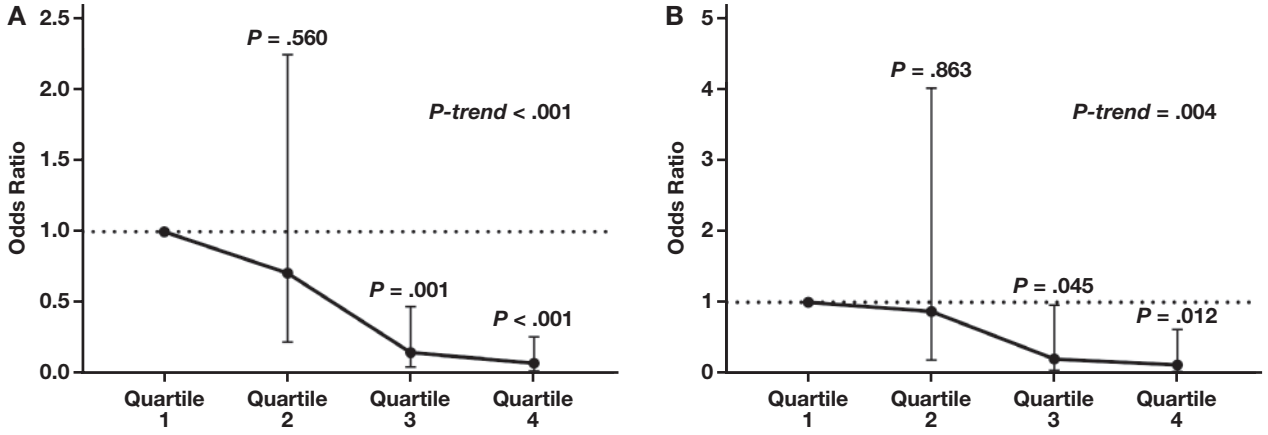

diagnostic value (AUC = 0.847) and simultaneously higher sensitivity (85%) and specificity (70%). These results demonstrated that TMAO, especially in combination with choline and betaine, could be a potential laboratory diagnostic marker for AD.

Discussion

In this study, we discovered, for the first time, that concentrations of TMAO, as well as choline and betaine, were significantly decreased in patients with AD compared with controls, and reduced TMAO

2022;53;177–182 | https://doi.org/10.1093/labmed/lmab063

FIGURE 4. ROC curves of trimethylamine-n-oxide (TMAO), choline, betaine, and other combination models for the diagnosis of anxiety disorder.

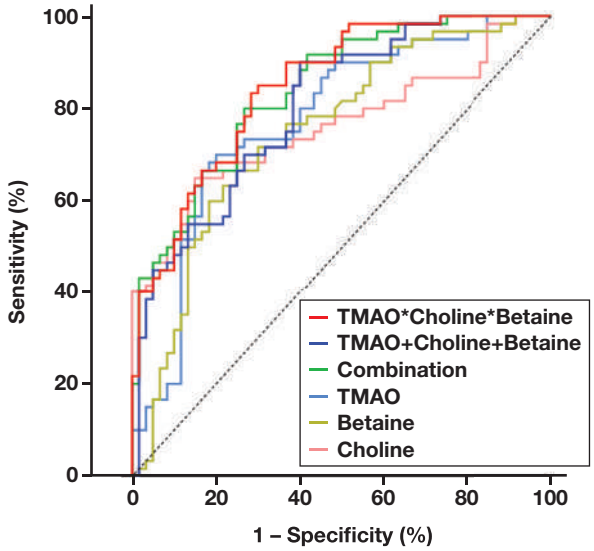

TABLE 3. The Diagnostic Performance of TMAO and its Precursors for Anxiety Disorder[a]

Variable	AUC	95% CI	Cutoff Value (ng/mL)	Sensitivity	Specificity
TMAO	0.773	0.688–0.859	146.75	70%	80%
Choline	0.761	0.674–0.849	1960.78	65%	85%
Betaine	0.747	0.658–0.836	3955.4	72%	70%
Combination[b]	0.839	0.771–0.908	…	80%	74%
TMAO + choline + betaine[c]	0.802	0.725–0.879	…	90%	60%
TMAO * choline * betaine[d]	0.847	0.780–0.914	…	85%	70%

… , nonapplicable; TMAO, trimethylamine-N-oxide.
[a]P<.001 for each.
[b]Using depression or healthy mental state as the dependent variable and 3 indicators (TMAO + betaine + choline) as covariates, the prediction probability of the 3 indicators combined was derived and calculated through binary logistic regression analysis. Doing so predicted probability as a new indicator to obtain the ROC curve. The cutoff values for TMAO, betaine, and choline were 111.17 ng/mL, 2205.7 ng/mL, and 3139.64 ng/mL, respectively.
[c]Added the detected values of the 3 indicators to obtain a new indicator, and performed ROC curve analysis on this new indicator. The cutoff value for TMAO, betaine, and choline were 126.68 ng/mL, 1856.98 ng/mL, and 3386.27 ng/mL, respectively.
[d]Multiply the detected values of the 3 indicators to obtain a new indicator, and perform ROC curve analysis on this new indicator. The cutoff value for TMAO, betaine, and choline were 82.89 ng/mL, 2194.78 ng/mL, and 3953.28 ng/mL, respectively.

concentrations were associated with an increased risk of AD. The association remained consistent after adjusting for the cofounding factors. Also, the results of ROC analysis demonstrated that TMAO could serve as a potential biomarker for the diagnosis of AD.

Previous studies have suggested many potential biomarkers pertaining to neurochemistry or neurophysiology for diagnosing AD, such as plasma oxytocin,[13] error-related negativity (ERN),[14] amygdala functional connectivity,[15] and goal-conflict-specific electroencephalography rhythmicity.[3] At present, despite that accumulating research focusing on biomarkers of AD has improved awareness regarding the neurobiological causes of AD, these biomarkers have failed to specifically and sensitively diagnose AD.[16]

TMAO, a small-molecular-weight metabolite, was synthesized depending on the metabolism of its precursors by gut microbiota. Briefly, trimethylamine (TMA)–containing species including choline and betaine were enzymatically converted to gas TMA by intestinal microbes. Then TMA was efficiently absorbed and rapidly metabolized by the hepatic flavin monooxygenase 3 (FMO3) to form TMAO.[11] At present, several research groups have reported that TMAO could serve as a novel biomarker for plaque rupture in patients with ST-segment–elevation myocardial infarction,[17] metabolic syndrome,[18] and ischemic brain lesions after carotid-artery stenting.[19] However, the concentrations of TMAO were elevated in these diseases, and different cutoff values of TMAO has been established to ensure the diagnostic specificity (1.95 μM for plaque rupture, 8.74 μM for metabolic syndrome, and 4.29 μM for ischemic brain lesions).

In contrast, in our study, the concentration of TMAO was significantly decreased rather than increased. The reason for this occurrence may be that the composition of the gut microbiota of patients with AD was different from the aforementioned diseases.

A metabonomic study in an animal model showed serum TMAO significantly decreased in rats undergoing a chronic unpredictable mild stress (CUMS) procedure, which was often used to create the model of AD or depression.[20,21] This can corroborate the decline in TMAO levels we have observed in patients with AD in this study. Also, reduced appetite and dietary intervention[22,23] (including healthy dietary pattern of fruits, vegetables, fish, olive oil, nuts, and low consumption of red meat) may lead to a reduction of red-meat intake in the diets of patients with AD, thereby causing a decrease in their TMAO level.[24]

This research applied accurate and reliable measurement for the determination of serum TMAO and its precursors, and conducted professional statistical analyses. To our knowledge, our study is the first to confirm the decline of serum TMAO in patients with AD, and further identified TMAO as a novel biomarker for the diagnosis of AD.

However, some limitations should be acknowledged. First, we could not collect data regarding participant food intake, which may affect the distribution of their gut microbiota. Second, we noticed that the *DSM-V* (the most recent edition) has been published. Because there was little difference in the diagnostic criteria for AD between the *DSM-IV* and the *DSM-V*, the use of the *DSM-IV* diagnostic criteria has little effect on the research and conclusions of this study. Third, the sample size of participants was limited. Therefore, our finding in this study should be confirmed in future research containing larger sample sizes and including data regarding the dietary intake of participants.

Conclusion

This study provides the first experimental evidence that the concentration of TMAO was significantly decreased in patients with AD compared with controls. Therefore, TMAO could serve as a novel biomarker for the diagnosis of AD.

REFERENCES

1. Maron E, Nutt D. Biological markers of generalized anxiety disorder. *Dialogues Clin Neurosci.* 2017;19(2):147–158.
2. Baxter AJ, Vos T, Scott KM, Ferrari AJ, Whiteford HA. The global burden of anxiety disorders in 2010. *Psychol Med.* 2014;44(11):2363–2374.
3. Shadli SM, Glue P, McIntosh J, McNaughton N. An improved human anxiety process biomarker: characterization of frequency band, personality and pharmacology. *Transl Psychiatry.* 2015;5:e699.
4. Thursby E, Juge N. Introduction to the human gut microbiota. *Biochem J.* 2017;474(11):1823–1836.
5. Valles-Colomer M, Falony G, Darzi Y, et al. The neuroactive potential of the human gut microbiota in quality of life and depression. *Nat Microbiol.* 2019;4(4):623–632.
6. Dinan TG, Borre YE, Cryan JF. Genomics of schizophrenia: time to consider the gut microbiome? *Mol Psychiatry.* 2014;19(12):1252–1257.
7. Peirce JM, Alviña K. The role of inflammation and the gut microbiome in depression and anxiety. *J Neurosci Res.* 2019;97(10):1223–1241.
8. Jiang H-Y, Zhang X, Yu Z-H, et al. Altered gut microbiota profile in patients with generalized anxiety disorder. *J Psychiatr Res.* 2018;104:130–136.
9. Lach G, Schellekens H, Dinan TG, Cryan JF. Anxiety, depression, and the microbiome: a role for gut peptides. *Neurotherapeutics.* 2018;15(1):36–59.
10. Kang SS, Jeraldo PR, Kurti A, et al. Diet and exercise orthogonally alter the gut microbiome and reveal independent associations with anxiety and cognition. *Mol Neurodegener.* 2014;9:36.
11. Chen Y, Zhou J, Wang L. Role and mechanism of gut microbiota in human disease. *Front Cell Infect Microbiol.* 2021;11:625913.
12. Koeth RA, Wang Z, Levison BS, et al. Intestinal microbiota metabolism of L-carnitine, a nutrient in red meat, promotes atherosclerosis. *Nat Med.* 2013;19(5):576–585.
13. Carson DS, Berquist SW, Trujillo TH, et al. Cerebrospinal fluid and plasma oxytocin concentrations are positively correlated and negatively predict anxiety in children. *Mol Psychiatry.* 2015;20(9):1085–1090.
14. Meyer A, Nelson B, Perlman G, Klein DN, Kotov R. A neural biomarker, the error-related negativity, predicts the first onset of generalized anxiety disorder in a large sample of adolescent females. *J Child Psychol Psychiatry.* 2018;59(11):1162–1170.
15. Makovac E, Watson DR, Meeten F, et al. Amygdala functional connectivity as a longitudinal biomarker of symptom changes in generalized anxiety. *Soc Cogn Affect Neurosci.* 2016;11(11):1719–1728.
16. Bandelow B, Baldwin D, Abelli M, et al. Biological markers for anxiety disorders, OCD and PTSD: a consensus statement. Part II: neurochemistry, neurophysiology and neurocognition. *World J Biol Psychiatry.* 2017;18(3):162–214.
17. Tan Y, Sheng Z, Zhou P, et al. Plasma trimethylamine N-oxide as a novel biomarker for plaque rupture in patients with ST-segment-elevation myocardial infarction. *Circ Cardiovasc Interv.* 2019;12(1):e007281.
18. Barrea L, Annunziata G, Muscogiuri G, et al. Trimethylamine-N-oxide (TMAO) as novel potential biomarker of early predictors of metabolic syndrome. *Nutrients*. 2018;10:1971.
19. Wu C, Li C, Zhao W, et al. Elevated trimethylamine *N*-oxide related to ischemic brain lesions after carotid artery stenting. *Neurology.* 2018;90(15):e1283–e1290.
20. Lomazzo E, Bindila L, Remmers F, et al. Therapeutic potential of inhibitors of endocannabinoid degradation for the treatment of stress-related hyperalgesia in an animal model of chronic pain. *Neuropsychopharmacology.* 2015;40(2):488–501.
21. Du Preez A, Law T, Onorato D, et al. The type of stress matters: repeated injection and permanent social isolation stress in male mice have a differential effect on anxiety- and depressive-like behaviours, and associated biological alterations. *Transl Psychiatry.* 2020;10(1):325.
22. Oddy WH, Allen KL, Trapp GSA, et al. Dietary patterns, body mass index and inflammation: Pathways to depression and mental health problems in adolescents. *Brain Behav Immun.* 2018;69:428–439.
23. Opie RS, O'Neil A, Itsiopoulos C, Jacka FN. The impact of whole-of-diet interventions on depression and anxiety: a systematic review of randomised controlled trials. *Public Health Nutr.* 2015;18(11):2074–2093.
24. Wang Z, Bergeron N, Levison BS, et al. Impact of chronic dietary red meat, white meat, or non-meat protein on trimethylamine N-oxide metabolism and renal excretion in healthy men and women. *Eur Heart J.* 2019;40(7):583–594.

Molecular Monitoring of *BCR-ABL* Fusion Transcripts in Patients with Chronic Myeloid Leukemia During Treatment Using the Endpoint Fluorescence Method

Huma Amin, MBBS, MPhil,[1,*] *Suhaib Ahmed, FCPS, PhD*[2]

[1]Department of Pathology, Rawalpindi Medical University, Rawalpindi, Pakistan; [2]Islamic International Medical College, Rawalpindi, Pakistan, and Riphah International University, Islamabad, Pakistan; *To whom correspondence should be addressed. humaamin2000@hotmail.com

Keywords: *BCR-ABL*, chronic myeloid leukemia, endpoint fluorescence, molecular monitoring, quantitative real-time polymerase chain reaction, tyrosine kinase inhibitors

Abbreviations: EPF, endpoint fluorescence; QPCR, quantitative real-time polymerase chain reaction; CML, chronic myeloid leukemia; TKI, tyrosine kinase inhibitors; CCyR, complete cytogenic response; MRD, minimum residual disease; FL, fluorescence; Ct, cycle threshold; RFU, relative fluorescence units; RT-PCR, reverse transcription polymerase chain reaction.

Laboratory Medicine 2022;53:183–189; https://doi.org/10.1093/labmed/lmab075

ABSTRACT

Objective: The purpose of the study was to compare results and evaluate the agreement between the endpoint fluorescence (EPF) method and quantitative real-time polymerase chain reaction (QPCR) during molecular monitoring of patients with chronic myeloid leukemia (CML) receiving treatment.

Materials and Methods: The study was conducted at Molecular Lab of Riphah International University, Islamabad, Pakistan, from January 2017 to December 2018. A total of 150 blood specimens from 30 patients with CML were analyzed at regular intervals during therapy. The detection/quantification of transcript mRNA was done simultaneously using QPCR and the EPF method.

Results: Out of a total of 150 RNA specimens analyzed, 117 (78%) specimens were positive, whereas 33 (22%) were negative for the transcript using both methods at various stages of treatment. Strong linear negative correlations between the cycle threshold and relative fluorescence unit values were observed with $P < .0001$ at 0, 3, 6, 9, and 12 months of treatment. No significant difference ($P > .05$) between the means of the *BCR-ABL* percentage was observed in either method at all stages of treatment. The bias between the 2 methods was calculated as 0.069 ± 3.50, and 95% limits of agreement were 6.92% to –6.79%.

Conclusion: We found that EPF is s simple method to detect/quantify *BCR-ABL* mRNA expression during treatment with comparable results to QPCR.

Remission in patients with chronic myeloid leukemia (CML) during treatment with tyrosine kinase inhibitors (TKI) is usually assessed by blood counts and by cytogenetic techniques. In patients with complete cytogenetic response (CCyR), there can be as many as 10^7 leukemic cells still present.[1] After a patient achieves CCyR, it is only possible to follow the minimal residual disease (MRD) using molecular methods.[2] Molecular analysis of *BCR-ABL* transcripts shows a detectable level for many years, and gradual decline is seen in most patients.[3] Regular scrutiny of MRD helps identify the effectiveness of therapy and make decisions about alternative interventions in patients without optimum response.[3,4]

Because TKI therapy for CML reduces the disease burden below the threshold of hematologic and cytogenetic detection, molecular monitoring with quantitative real-time polymerase chain reaction (QPCR) is the best method to study therapy response.[3] It quantifies the disease with an increased sensitivity of up to 10^{-8} and has become the gold standard approach in the management of these patients.[4,5] However, QPCR presents some complexity because of its evolving and nonstandardized methodologies.[6] Efforts are being made for a better harmonization of the quantitative molecular monitoring of patients with CML.[7]

Currently, QPCR for drug monitoring is routinely not available in our region of the world. Major barriers to implementing routine QPCR in patients with CML in underresourced regions are its high cost and lack of technical expertise. The initial setup, including the instrumentation of QPCR, is quite expensive compared to the setup for conventional PCR.[8] The negative aspect of the QPCR machine is the expense of the instrument, which combines a thermocycler with an online fluorescence (FL) detector. Unavailability of this diagnostic facility provides a potential to investigate a method of post-PCR endpoint detection.

With the endpoint fluorescence (EPF) method, target fluorescence can be measured after performing PCR in an ordinary thermocycler with a fluorescent labeled probe. Fluorometry is often selected because

of its sensitivity and high specificity.[9] It was first used for qualitative testing, but its quantitative results correlate very well with QPCR results.[10] Other advantages of this analytical technique are its low cost and simplicity of handling. It is used in medical diagnostics, DNA sequencing, forensics, genetic analysis, and biotechnology applications and has proved to be a helpful tool for both quantitative and qualitative analysis.[11]

The implementation of a cost-effective and simple strategy for monitoring therapeutic response in patients with CML is indispensable in underresourced populations. This study evaluated patients' test results obtained using QPCR and EPF to determine the specificity, sensitivity, and mean difference between transcript percentages. The results of QPCR and EPF were correlated, and agreement between the 2 methods was also established using blood specimens from patients with CML at different stages of treatment.

Materials and Methods

A total of 150 peripheral blood specimens from newly diagnosed patients with CML in the chronic phase were studied. Thirty patients were consecutively enrolled from tertiary care hospitals in Rawalpindi, Pakistan from January 2017 to December 2017 and were followed until December 2018. Molecular analysis was carried out in the laboratory of Riphah International University. Informed consent was taken from every patient, and the study was approved by the ethical review committee of Islamic International Medical College, Riphah International University, (reference number Riphah/IIMC/ERC/16/0115).

The diagnosis of CML was made according to clinical presentation and morphologic criteria of peripheral blood film and bone marrow aspirate. Only those patients who started treatment with TKI after their diagnosis were included in the study regardless of age and sex. Patients with atypical fusion transcript (other than e13a2 and e14a2) were not included in the study.

Peripheral blood specimens were obtained before starting therapy for baseline record and then after every 3 months during the first 12 months of treatment. Peripheral blood specimens were rapidly transported at 2° to 8°C to the laboratory for extraction of total RNA using the TRIzol reagent (TRI Reagent L.S.).

The concentration of RNA specimens obtained was determined using the Nanondrop spectrophotometer (Thermo Fisher Scientific) by measuring the absorbance at 260 nm. The presence of protein and contamination in RNA specimens was measured at A260/280 and A260/230. If these ratios were <2, then RNA extraction was repeated. The RNA specimens were normalized to a concentration of approximately 500 ng for cDNA synthesis for real-time amplification and EPF detection (EPF) using a fluorometer.

The reverse transcription and amplification for the fusion transcript at baseline and 3, 6, and 12 months was performed using Taqman probe based on real-time PCR using an already described method in previous studies with little modification[12,13] on the Sa Cycler 96 (Sacace Biotechnologies). The cDNA synthesis and DNA amplification were conducted in a 15 µL reaction mixture containing 8 µL of PCR Mix (Invitrogen PCR Super Mix, with buffer, Mg++, dNTPs, and recombinant *Taq*DNA polymerase), 1 µL of Primer mix (forward, reverse primer and probe) (Primer mix ABL gene for internal control or Primer mix BCR-ABL fusion gene for each specimen), 0.25 µL of enzyme RT (SuperScript III Reverse Transcriptase) (Invitrogen), and 6 µL of RNA template.

Various primer combinations of *ABL-2* with *M-BCR* and *BCR-ABL* and *ABL* probes were used.[14,15] Primer and probe sequences for QPCR are given in the next paragraph. All primers and probes were obtained from Integrated DNA Technologies in lyophilized form and stored at –20°C. The primer sequences were verified using the National Center for Biotechnology Information nucleotide Basic Local Alignment Search Tool (https://blast.ncbi.nlm.nih.gov/). Two forward primers, e-13 and e-14, were used with a common reverse primer, *ABL-2*. A common *BCR-ABL* TaqMan probe complementary to the *ABL* gene was used. A fragment of the *ABL* gene was amplified as an internal control and for normalization using a separate pair of *ABL* primers and probe.

The primer sequences for the *BCR-ABL* fusion gene were as follows:
BCR e13-F GCA TTC CGC TGA CCA TCA ATA A
BCR e14- F CAG CCA CTG GAT TTA AGC AGA GT
ABL-2–R TCC AAC GAG CGG ATT CAC T
BCR-ABL probe:
6-FAM/AAG CCC TTC /ZEN/AGC GGC CAG TAG CAT CT/3 IABkFQ
Primer sequences for *ABL* gene:
ABL-2F GCT GGG TCC CAA GCA ACT AC
ABL-2–R ACA CAG GCC CAT GGT ACC A
ABL probe:
5HEX/TCA CGC CAG/ZEN/TCA ACA GTC TGG AGA AAC A/3IABkFQ
Cycling conditions for QPCR:
Reverse transcription × 1 cycle at 42°C for 15 minutes
Initial denaturation × 1 cycle at 95°C for 10 minutes
PCR cycling × 40 cycles at 95°C for 15 seconds
60°C for 60 seconds

The results were expressed in a cycle threshold (Ct) value in each specimen. The percentage of the *BCR-ABL* transcript was extrapolated from the standard curve made from the dilution of the known positive control (the value of the positive specimen was ascertained using the GeneXpert BCR-ABL; Cepheid) and was expressed as a normalized ratio of the *BCR-ABL* transcript to the control *ABL* gene transcript. In each QPCR batch, the known positive and negative RNA for *BCR-ABL* was included.

At the end of each QPCR, every PCR product in the same 0.2 mL PCR tube was transferred to a fluorometer (GTI PCR Reader, Genetic Technology Instrumentation). Reaction vials of all positive and negative specimens were read in the fluorometer. The amount of green fluorescence (FAM dye) was recorded in the computer software, and the results were expressed in relative fluorescence units (RFU) after subtracting the background fluorescence of a known negative specimen. The same PCR template, primers, probe, and thermocycling conditions were used as described earlier. The estimated expenditures for RNA extraction, reverse transcription PCR (RT-PCR) on conventional thermocycler, and technician time were also calculated as per the local market price and converted into US$ to observe the cost-effectiveness of the method.

Molecular detection and quantification of the *BCR-ABL* fusion gene were performed using QPCR and the EPF method on all specimens. The amount of target DNA was determined by the FL emitted by the FAM green dye. In QPCR, FL measurements were carried out at the end of each thermal cycle, and in EPF, offline FL measurements were carried out using a PCR reader after completion of the PCR.

To approximately calculate the target DNA in unknown specimens using the EPF method, a calibration graph was constructed. The RFU of serial dilutions of known *BCR-ABL* positive RNA were plotted with the value of each dilution.

The sensitivity of the 2 assays for the detection of the fusion transcript were compared by generating a 10-fold serial dilution of known RNA concentration (1/10, 1/100, 1/1000, 1/10,000, 1/100,000). These 5 dilutions and 1 known negative specimen were run using the RT-PCR protocol on both instruments in identical conditions in 5 separate reaction tubes. Repeated measures of specimen dilutions were performed and compared with known negative specimens. Each specimen of a corresponding dilution point was tested in duplicate (n = 10), and the assay response (detected or not detected) was noted.

All statistical calculations were done using SPSS 22 software for descriptive and inferential statistics. Frequency and percentages were calculated for the presence or absence of the transcript. Sensitivity and specificity were calculated using PCR as the gold standard. Results of EPF and QPCR were compared using the Fisher's exact test. Descriptive data were expressed as mean ± standard deviation. Pearson correlations between Ct and RFU values were calculated. The paired *t*-test was used to observe the difference between the mean percentages of the transcript in both methods. A *P* value <.05 was taken as a level of significance. Using the method comparison procedure of Bland and Altman, the bias and 95% limits of agreement between the 2 methods were determined.

Results

One hundred fifty specimens from 30 newly diagnosed patients with CML (18 male and 12 female) in the chronic phase were studied at different stages of treatment (0, 3, 6, 9, and 12 months). The mean age of the patients was 41.2 ± 8.61 years, with an age range of 11 to 70 years.

The qualitative results of QPCR and EPF (transcript status: positive or undetectable) in patients with CML analyzed 5 times at regular treatment intervals are summarized in **TABLE 1**. Analysis of all the specimens taken at the time of diagnosis and after 3 months of treatment showed 100% positivity for the *BCR-ABL* transcript. However, after 6 months of therapy, transcripts disappeared in 3 patients (10%). The *BCR-ABL* transcripts could not be detected in 10 (33%) and 20 (66%) patients after 9 and 12 months of treatment, respectively (**TABLE 1**).

Every specimen with a detectable Ct value using QPCR was considered as positive. For the EPF method, specimens with >20 RFU were considered positive.

TABLE 2 indicates that of the 150 RNA specimens that were analyzed from 30 patients at different treatment intervals, 117 (78%) specimens were found positive, whereas 33 (22%) were found negative for the transcript using both the methods at various stages of treatment.

TABLE 1. QPCR and EPF Results for Detection of *BCR-ABL* Transcript at Different Stages of Treatment

Duration of Treatment	Qualitative			
	QPCR		EPF	
	Positive	Negative	Positive	Negative
Baseline	30 (100%)	0	30 (100%)	0
3 mo	30 (100%)	0	30 (100%)	0
6 mo	27 (90%)	3 (10%)	27 (90%)	3 (10%)
9 mo	20 (67%)	10 (33%)	20 (67%)	10 (33%)
12 mo	10 (33%)	20 (67%)	10 (33%)	20 (67%)

EPF, endpoint fluorescence; QPCR, quantitative real-time polymerase chain reaction.

TABLE 2. QPCR vs EPF in Detecting *BCR-ABL* Transcripts in Patients with CML Undergoing Treatment

EPF	Q PCR		Total
	BCR-ABL (Positive)	BCR-ABL (Negative)	
Positive	117 (TP) a	0 (FP) b	117
Negative	0 (FN) c	33 (TN) d	33
Total	117	33	150

CML, chronic myeloid leukemia; EPF, endpoint fluorescence; FN, false negative; FP, false positive; QPCR, quantitative real-time polymerase chain reaction; TN, true negative; TP, true positive.
Sensitivity = a/a + c × 100% = 117/117 + 0 × 100 = 100%.
Specificity = d/b + d = 33/0 + 33 × 100 = 100%.
P *value = .000.*

A contingency table for the calculation of the sensitivity and specificity of the EPF method, considering QPCR as the gold standard is shown in **TABLE 2**. The sensitivity and specificity for EPF were both 100%. The Fisher's exact test was applied to determine the statistical significance, which was found to be high (*P* value of .000).

In determining the analytical sensitivity, we found that the dilutions that were tested showed that as few as 1 cell in a background of 10^4 normal cells could be detected using both methods repeatedly. The 1/100,000 dilution was consistently negative for the fusion transcript using EPF and QPCR. A dilution of 1/10,000 was consistently positive using both the methods, indicating a limit of detection of 10^{-4} (95% confidence interval).

The quantitative results of QPCR and the EPF method in patients with CML are summarized in **TABLE 3**. The mean Ct value of QPCR varied with the duration of treatment in patients with CML, ranging from 24.56 to 37.2 cycles (see **TABLE 3**). As the duration of treatment increased, the mean Ct increased. The mean Ct was 24.5 at the time of diagnosis and gradually increased to 30.27, 34.25, 36.11, and 37.2 at 3, 6, 9, and 12 months of treatment, respectively (a Ct value is inversely proportional to the amount of target DNA present in a specimen). The QPCR results showed a strong positive correlation between the duration of treatment and the mean Ct values (r = 0.956).

The mean RFU value of EPF also altered with the duration of treatment, ranging from 199.06 at the beginning of treatment to 26.50 at the end of 1 year (**TABLE 3**; the RFU value is directly proportional to the amount of target DNA present in a specimen). The EPF results indicated a strong negative correlation with the duration of treatment and the mean RFU values (r = –0.889).

Using the EPF method, fluorescence was detected by the PCR reader in every specimen. Keeping in mind the mean EPF results in all the negative specimens (mean, 6 RFU; range, 1–16) and in the highest dilution of the positive DNA specimens (weakest positive specimens; mean, 31 RFU; range, 21–37), the cutoff limit for positive specimens was arbitrarily identified at 20 RFU. This finding was also validated in another study using the same instrument.[10] In all QPCR negative specimens, the EPF method had a clear negative result (<20 RFU).The EPF results in the QPCR positive specimens ranged from 21 to 332 RFU (**TABLE 3**).

The mean *BCR-ABL* percentages at regular treatment intervals in patients with CML were also calculated using both methods (**TABLE 3**). A paired *t*-test was applied on the mean percentages of *BCR-ABL*, and no significant difference was observed between 2 readings using QPCR and the EPF method in all stages of treatment (**TABLE 3**).

TABLE 3. QPCR and EPF Results for Quantification of Detectable *BCR-ABL* Transcripts at Regular Treatment Intervals

Treatment Duration	Mean Ct (QPCR)	Mean RFU (EPF)	Correlation Coefficient (*r* Value)	Mean % of *BCR-ABL*		*P* Value
				QPCR	EPF	
Baseline	24.56 ± 2.36 (20–29.16)	199.063 ± 55.38 (87–332)	−0.96 ($P < .0001$)	81.93 ± 15.7 (45%–100%)	81.19 ± 15.25 (40%–100%)	.366
3 months	30.27 ± 2.01 (26.4–34.1)	79.76 ± 28.87 (35–149)	−0.97 ($P < .0001$)	30.53 ± 15.87 (8%–65%)	30.13 ± 15.16 (5%–60%)	.571
6 months	34.25 ± 2.29 (29.5–38.2)	45.5 ± 19.9 (21–97)	−0.96 ($P < .0001$)	9.73 ± 9.4 (1%–35%)	10.19 ± 10.7 (1%–40%)	.356
9 months	36.11 ± 1.73 (32.4–38.2)	32.8 ± 11.55 (21–59)	−0.98 ($P < .0001$)	4.1 ± 3.7 (1%–15%)	4.89 ± 5.2 (1%–20%)	.09
12 months	37.22 ± 0.92 (35.8–38.2)	26.50 ± 5.31 (21–34)	−0.97 ($P < .0001$)	1.9 ± 0.99 (1%–3%)	1.6 ± 1.49 (0%–5%)	.188

Ct, cycle threshold, EPF, endpoint fluorescence; QPCR, quantitative real-time polymerase chain reaction; RFU, relative fluorescence unit.

FIGURE 1. Correlation of Ct and RFU values of QPCR with EPF in patients with CML at different stages of treatment. CML, chronic myeloid leukemia; Ct, cycle threshold; EPF, endpoint fluorescence; QPCR, quantitative real-time polymerase chain reaction; RFU, relative fluorescence units.

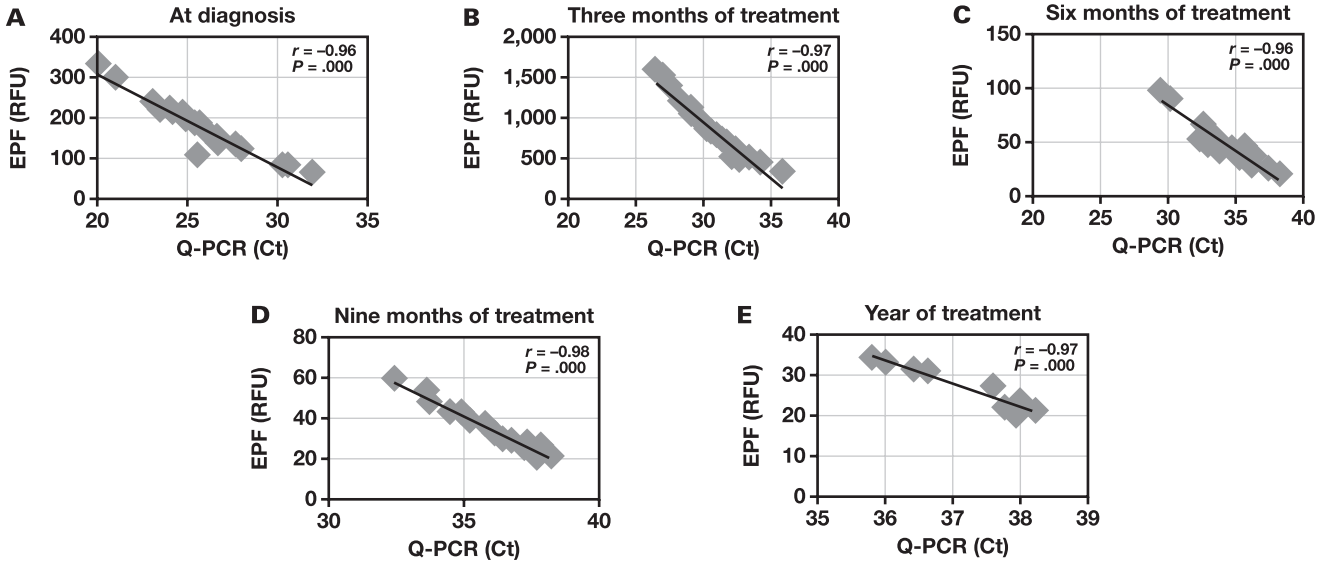

FIGURE 2. Correlation of Ct and RFU values of QPCR with EPF in patients with CML in aggregate. CML, chronic myeloid leukemia; Ct, cycle threshold; EPF, endpoint fluorescence; QPCR, quantitative real-time polymerase chain reaction; RFU, relative fluorescence units.

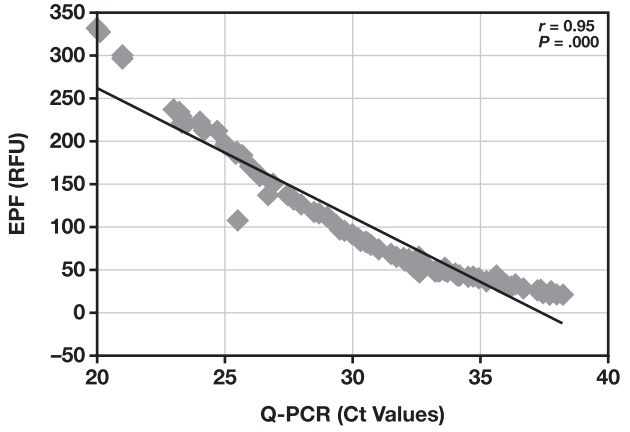

The Ct values of specimens that were detected as *BCR-ABL* positive using QPCR were correlated with their corresponding RFU values. The correlation curve revealed a strong linear negative association with a correlation coefficient (*r*) of −0.96, −0.97, −0.96, −0.98, and −0.97, respectively, at different stages of treatment (**FIGURE 1**). **FIGURE 2** represents the correlation between Ct values and their corresponding RFU in aggregate.

The values of RFU using EPF were compared directly to the Ct values using RT-PCR. The Ct value was less when the quantity of target DNA was more, and vice versa. The direct comparison of the fluorescence units of the PCR reader with the Ct values of RT-PCR showed an inverse association of signal intensities (the lower the Ct values, the higher the fluorescence; **FIGURE 3**). **FIGURE 3** presents the CT value for a similar amount of target DNA in a specimen and its corresponding RFU value using EPF, which provides a clearer idea about the relations of both displayed units.

A scatterplot was obtained by plotting the difference between the test results of the EPF method and QPCR on the *y* axis and the mean of the percentage transcript using both methods on the *x* axis. Graphing test laboratory values on a Bland-Altman plot showed good agreement

FIGURE 3. Direct comparison of fluorescence units with Ct values of QPCR (amount of target DNA). Ct, cycle threshold; QPCR, quantitative real-time polymerase chain reaction.

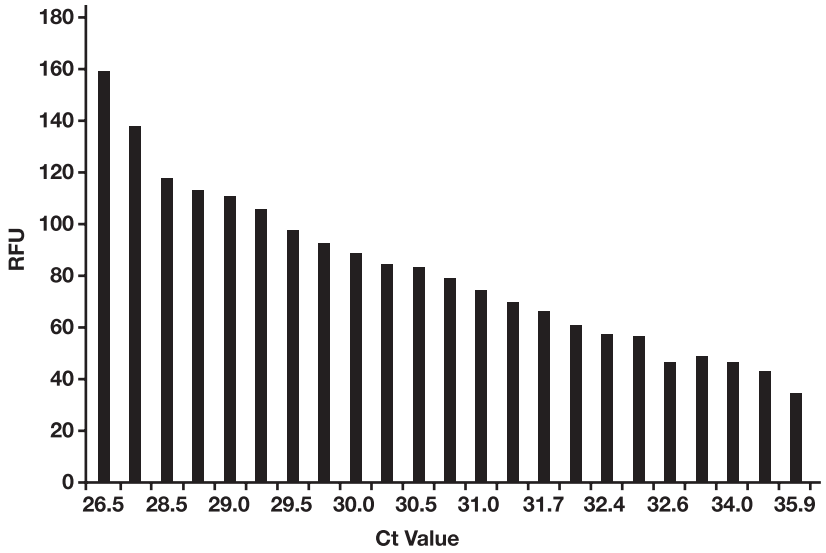

FIGURE 4. Bland-Altman scatterplot of the distribution of the percentage of the *BCR-ABL* transcript in patients with CML measured using QPCR and EPF. The *y* axis shows the mean differences in the percentage of the transcript and the *x* axis shows the average of the percentage of the transcript. The lines represent the mean difference and the upper and lower limits of agreement. CML, chronic myeloid leukemia; EPF, endpoint fluorescence; QPCR, quantitative real-time polymerase chain reaction.

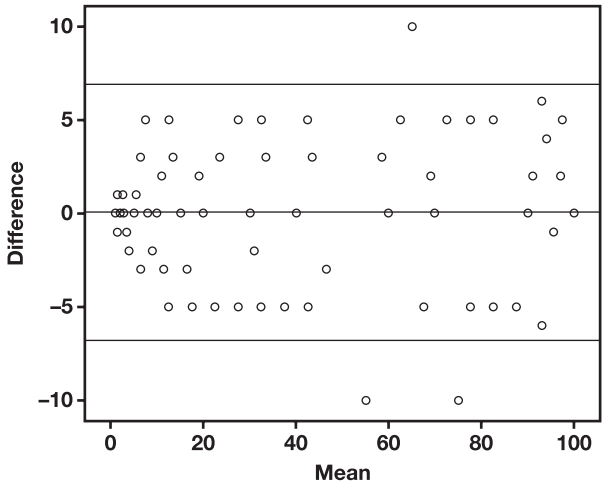

between the methods. The constant bias was 0.069%, the standard deviation was 3.50, and 95% limits of agreement values were found to be from 6.92% to –6.79% (**FIGURE 4**). The cost estimated for RNA extraction, the thermocycler, the RT-PCR, and technician time was estimated to be approximately $10 to $12 per test.

Discussion

The constitutively active oncogenic feature of the *BCR-ABL* gene is targeted by TKI. It is an effective and standard therapeutic option for patients with CML.[16] For the best optimization and outcome of the therapy, it is essential to monitor these patients with treatment.[17]

Therapy progressively decreases the disease burden; therefore, the sensitivity of the technique to measure the residual disease must be increased accordingly.[18] Testing of MRD at the molecular level is performed using QPCR, which is very useful for monitoring different types of hematological neoplasms; however, this method is not easy to use and is confined to specialized laboratories. The PCR technique is much easier to use for qualitative analysis but becomes a complicated procedure when quantification is required.[19] It is also afflicted with interlaboratory variability, resulting in difficulty in the interpretation and comparison of data. To address this problem, international standardization has been proposed but is offered in only few specialized laboratories.[20]

The lack of diagnostic capabilities is an enormous challenge in treating patients with this targeted therapy. The cost of monitoring by QPCR in Pakistan rupee (PKR) is estimated to be Rs 10,000 to Rs 16,000 (approximately $60–$110), depending upon whether a manual or an automated system is used. This high cost becomes more relevant when frequent testing is required with lifelong therapy.[20] The recommended protocol for patients with CML during therapy is quantification of the *BCR-ABL* transcript every 3 months.[21] This schedule becomes quite difficult to follow in our geographic region, owing to the affordability issue for most of our patients. The prices of RT-PCR instruments range from $20,000 to $90,000, depending on the manufacturer, and are therefore not easily affordable for the majority of laboratories. The cost of reagents, supplies, and trained technical staff is also very high. The approximate cost of *BCR-ABL* detection using QPCR, including the cost of the QPCR

instrument, RNA extraction, RT-PCR, and technician time, was found to be $60 in our center.

For EPF, the cost of the PCR reader is approximately $1000. Studies have shown that EPF reading invites no extra expenditure or specialized technical expertise. The cost of the entire procedure, along with the cost of the PCR reader (fluorometer), thermal cycler, RNA extraction, RT-PCR, and technician time, was calculated in US$ as per the local market price and was estimated to be $10 to $12 per test in our center. Meanwhile, *BCR-ABL* monitoring with an automated cartridge-based detection system (GeneXpert; Cepheid) in our country ranges between $100 and $110. The EPF method has a clear edge over QPCR in terms of cost and ease of reporting and can well serve the purpose of molecular monitoring in underresourced countries.

Keeping in mind the above scenario, this study tried to compare the test results of a simple and cost-effective methodology to determine whether it could be a used as an alternative to a QPCR assay for monitoring the MRD of patients with CML. This methodology is based on an approach of performing RT-PCR on any conventional thermocycler (countering the high cost and unavailability issues of real-time instruments) followed by *BCR-ABL* transcript detection and quantification using a fluorometer (PCR reader). Although real-time QPCR provides a direct measurement of the PCR product during the amplification process and also provides an accurate number of targets present,[22] it requires international standardization for the reliable clinical management of patients with CML,[23] which is a logistical and fiscal challenge for many laboratories in our region. The EPF technique uses the same primer/probe combination as in QPCR, but fluorescence is measured at the end of the PCR reaction. We found that EPF was a sensitive and specific method for the detection of the BCR-ABL fusion transcript.

Both methods displayed a strong linear negative correlation ($r = -0.9$) between the Ct and RFU values. The standard curves were later generated to calculate the *BCR-ABL* transcript percentage at different treatment intervals and for direct comparison of the means between the 2 assays. These results established that EPF can reliably quantify the *BCR-ABL* percentage compared with that obtained by QPCR assay. It can quantify *BCR-ABL* concentrations almost as low as 1 copy in 10,000 reference copies, a magnitude much more sensitive than the clinical cutoff values of 1 in 1000 for MRD in patients with CML.

This system may prove beneficial over currently used QPCR or other commercially used *BCR-ABL* fusion detection methods by providing low-cost results, requiring fewer technical skills and offering ease of reporting. Although this assay may not be as ideal and sophisticated as an automated cartridge-based detection system (eg, GeneXpert; Cepheid) and cannot match sensitivity at extremely low copy numbers, it may prove to be accessible and sustainable in the MRD assessment of the majority of patients with CML in low-resource countries.

Conclusion

Molecular methods were used to assess the kinetics of the BCR-ABL transcript in patients with CML undergoing treatment. We found that EPF is a less-complicated and cost-effective method with the same sensitivity and specificity as QPCR in patients with CML. The quantification of the mean transcript percentages at different stages of treatment exhibited no significant difference between QPCR and EPF results. Good agreement was also evident between the 2 methods with a relatively constant mean difference. Therefore, the EPF method may be considered in patients with CML undergoing treatment for the detection and quantification of transcripts.

Acknowledgments

Special thanks to Riphah International University, Islamabad, for partly funding this study, and the Genetic Resource Centre, Rawalpindi, for providing the laboratory facilities for conducting this study.

REFERENCES

1. Foroni L, Wilson G, Gerrard G, et al. Guidelines for the measurement of BCR-ABL1 transcripts in chronic myeloid leukaemia. *Br J Haematol.* 2011;153(2):179–190.
2. Soverini S, De Benedittis C, Mancini M, Martinelli G. Best practices in chronic myeloid leukemia monitoring and management. *Oncologist.* 2016;21(5):626–633.
3. Branford S. Monitoring after successful therapy for chronic myeloid leukemia. *Hematology Am Soc Hematol Educ Program.* 2012;2012:105–110.
4. Kantarjian H, Schiffer C, Jones D, Cortes J. Monitoring the response and course of chronic myeloid leukemia in the modern era of BCR-ABL tyrosine kinase inhibitors: practical advice on the use and interpretation of monitoring methods. *Blood.* 2008;111(4):1774–1780.
5. Baccarani M, Saglio G, Goldman J, et al; European LeukemiaNet. Evolving concepts in the management of chronic myeloid leukemia: recommendations from an expert panel on behalf of the European LeukemiaNet. *Blood.* 2006;108(6):1809–1820.
6. Bagg A. Chronic myeloid leukemia: a minimalistic view of post-therapeutic monitoring. *J Mol Diagn.* 2002;4(1):1–10.
7. Singh Z, Medlin S, Usmani SZ. Molecular monitoring and treatment of chronic myeloid leukemia (CML). *J Clin Exp Pathol.* 2012;2(4):113.
8. Sultana TA, Abdul Mottalib M, Islam S, Khan MA, Choudhury S. Rt-PCR method for diagnosis and follow-up of hematological malignancies: first approach in Bangladesh. *Bangladesh Med Res Counc Bull.* 2008;34(1):1–11.
9. Khetan D, Gupta N, Chaudhary R, Shukla JS. Comparison of UV spectrometry and fluorometry-based methods for quantification of cell-free DNA in red cell components. *Asian J Transfus Sci.* 2019;13(2):95–99.
10. Naeem MA, Ahmed S, Khan SA. Detection of asymptomatic carriers of malaria in Kohat district of Pakistan. *Malar J.* 2018;17(1):44.
11. Naresh K. Applications of fluorescence spectroscopy. *J Chem Pharm Sci.* 2014; special issue (5):18–21.
12. Tashfeen S, Ahmed S, Bhatti FA, Ali N. Real time polymerase chain reaction in diagnosis of chronic myeloid leukemia. *J Coll Physicians Surg Pak.* 2014;24(3):190–193.
13. Ting CY, Shamsuddin AF, Chang KM, Makmor-Bakry M, Azmi N. Quantification of BCR-ABL transcripts in peripheral blood cells and plasma of chronic myeloid leukemia patients at different stages of tyrosine kinase inhibitor treatment response. *Trop J Pharm Res.* 2017;16(3):657–663.
14. Nandagopalan SR, Kuila N, Biswas S, Pattnayak NC, Biswas G, Chakraborty S. Dual transcripts of BCR-ABL and different polymorphisms in chronic myeloid leukaemia patients. *Indian J Med Res.* 2016;143(Supplement):136–141.
15. Preudhomme C, Révillion F, Merlat A, et al. Detection of BCR-ABL transcripts in chronic myeloid leukemia (CML) using a "real time" quantitative RT-PCR assay. *Leukemia.* 1999;13(6):957–964.
16. Giles FJ. Molecular monitoring of BCR-ABL transcripts standardization needed to properly use, and further investigate the value of, a critical surrogate marker for success in therapy of chronic myeloid leukemia. *US Oncol Hematol.* 2011;7:138–142.

17. Ashariati A, Ugroseno S. Profile of BCR-ABL transcript levels based on Sokal prognostic score in chronic myeloid leukemia patients treated with imatinib. *Acta Med Indones.* 2013;45(2):107–113.
18. Radich JP. How I monitor residual disease in chronic myeloid leukemia. *Blood.* 2009;114(16):3376–3381.
19. Martinelli G, Testoni N, Montefusco V, et al. Detection of BCR-ABL transcript in chronic myelogenous leukemia patients by reverse-transcription-polymerase chain reaction and capillary electrophoresis. *Haematologica.* 1998;83(7):593–601.
20. Ganesan P, Kumar L. Chronic myeloid leukemia in India. *J Glob Oncol.* 2017;3(1):64–71.
21. Hochhaus A, Saussele S, Rosti G, et al. Chronic myeloid leukaemia: ESMO clinical practice guidelines for diagnosis, treatment and follow-up. *Ann Oncol.* 2017;28(Supplement 4):41–51.
22. Amabile M, Giannini B, Testoni N, et al. Real-time quantification of different types of BCR-ABL transcript in chronic myeloid leukemia. *Haematologica.* 2001;86(3):252–259.
23. Azad NA, Shah ZA, Pandith AA, et al. Real-time quantitative PCR: a reliable molecular diagnostic and follow-up tool for "minimal residual disease" assessment in chronic myeloid leukemia. *Biosci Rep.* 2018;38(5):BSR20180974.

Red Blood Cell Transfusion Volumes According to AIMS65 Scores in Patients with Peptic Ulcer Bleeding

Moon Won Lee, MD,[1] Hyun-Ji Lee, MD, PhD,[2,] Kyung-Hwa Shin, MD, PhD,[3] Gwang Ha Kim, MD, PhD,[1] Hyung-Hoi Kim, MD, PhD[3]*

[1]Department of Internal Medicine, Pusan National University School of Medicine, and Biomedical Research Institute, Pusan National University Hospital, Busan, Korea; [2]Department of Laboratory Medicine, Pusan National University School of Medicine, and Research Institute for Convergence of Biomedical Science and Technology, Pusan National University Yangsan Hospital, Busan, Korea; [3]Department of Laboratory Medicine, Pusan National University School of Medicine, and Biomedical Research Institute, Pusan National University Hospital, Busan, Korea; *To whom correspondence should be addressed. hilhj1120@pusan.ac.kr

Keywords: hemostasis, endoscopic hemostasis, peptic ulcer hemorrhage, blood transfusion, peptic ulcer, AIMS65 score

Abbreviations: RBC, red blood cell; UGIB, upper gastrointestinal bleeding; Hb, hemoglobin; INR, international normalized ratio.

Laboratory Medicine 2022;53:190–193; https://doi.org/10.1093/labmed/lmab080

ABSTRACT

Objective: Fluid supplementation and red blood cell (RBC) transfusions form first-line management strategies to maintain circulating blood volumes in patients with upper gastrointestinal bleeding (UGIB). In this study, we aimed to analyze the utility of the AIMS65 score in predicting the volume of RBC transfusion required in patients with bleeding peptic ulcers.

Methods: In this single-center, retrospective study, the data of patients admitted between January 2019 and December 2019 with suspected UGIB were retrospectively reviewed. The RBC volume transfused during pre- and postendoscopic hemostasis was measured in relation to various patient factors including the AIMS65 scores.

Results: Transfusion rates, the mean number of transfused RBC units, and the duration of hospital stay differed significantly between patients with low AIMS65 scores and those with high AIMS65 scores. Patients with an AIMS65 score of 3 were transfused with more RBC units in the postendoscopic hemostasis period, compared with those with an AIMS65 score of 0, 1, or 2 (with a mean of 4.33 ± 2.07 and 2.67 ± 4.1 units transfused during the pre-endoscopic and postendoscopic hemostasis periods, respectively).

Conclusion: Patients with UGIB and with an AIMS65 score of 3 were more likely to require transfusions of RBCs.

Upper gastrointestinal bleeding (UGIB) is common worldwide and occurs in 40 to 150 per 100,000 people.[1] It is associated with high morbidity and mortality, especially in older adults. Patients with peptic ulcers (duodenal and gastric) reportedly account for approximately 28% to 59% of all patients with UGIB.[1] Fluid supplementation and packed red blood cell (RBC) transfusion are indicated in patients presenting with UGIB, according to clinical severity, to maintain circulating blood volumes.[2,3]

Appropriate blood transfusion is necessary not only to improve patient outcomes and ensure good prognosis but also to cope with unstable blood supply and demand.[4] Current guidelines use the hemoglobin (Hb) level as the primary decisive criterion for transfusion.[5] In patients presenting with acute bleeding, the volume of blood loss is calculated and the transfusion volume is determined based on the tissue oxygenation index.[5] Transfusions are difficult to carry out in patients whose blood loss cannot be accurately estimated or in those requiring urgent intervention. An easily calculable index to assist in the prediction of RBC volume required for transfusion among affected patients is needed, making it easier to manage the donor blood supply in instances when blood transfusion is required but availability is limited. The AIMS65 score is useful for risk stratification in UGIB and is calculated using the albumin level, mental status assessment, prothrombin time, age, and systolic blood pressure level. The AIMS65 scoring system is simpler to assess than either the Glasgow-Blatchford Bleeding Score (GBS) or the Rockall score.[6]

In this study, we aimed to analyze the utility of the AIMS65 score in predicting the required volume of RBC transfusion among patients with bleeding peptic ulcers.

Methods

All patients admitted to our hospital between January 2019 and December 2019 with suspected UGIB were retrospectively evaluated. Patients diagnosed with class Ia, IIb, or IIa gastric/duodenal ulcers as per the Forrest classification (**TABLE 1**)[7] were included in the study. Patients with Forrest class Ib ulcers were also included if they required endoscopic treatment based on the reclassification of the ulcer after removal of the adherent clot. Exclusion criteria were ulcers that did not require

endoscopic treatment, bleeding from causes other than peptic ulcer, age <18 years, or pregnancy.

A blood transfusion was performed if the Hb level at the time of bleeding was <7 g/dL. In affected patients with Hb levels ranging between 7 and 10 g/dL, a blood transfusion was performed based on the clinician's judgment, according to the patient's underlying medical history, or if additional bleeding was anticipated. We measured the volume of RBCs transfused before an endoscopic hemostasis procedure (pre-endoscopic volume, transfused during the period between hospitalization or upon the decision for endoscopic hemostasis until the procedure was performed and hemostasis was achieved) and the volume administered after the procedure (postendoscopic, transfused within 7 days from achieving endoscopic hemostasis). Data including age, sex, underlying medical history, ulcer pattern, and AIMS65 scores were collected by dividing patients into 2 groups of those who did and those who did not receive blood transfusions. Data of patients' hospital stay, complications from the procedure, and 30-day in-hospital mortality rates were analyzed.

The AIMS65 score is calculated by assigning scores to criteria including albumin level (threshold <3 g/dL), prothrombin time (international normalized ratio [INR]) (threshold INR >1.5), presence/absence of altered mental status, systolic blood pressure (≤90 mm Hg), and age (≥65 years).[8] Rebleeding was defined as the recurrence of hematemesis or melena, associated with either shock or with a >2 g/dL decrease in the patient's Hb concentration within a 24-hour period after initial stabilization of the pulse rate, blood pressure, and Hb level.

Medical and Endoscopic Treatment

Management of patients was initiated with fluid resuscitation and proton pump inhibitor infusion (pantoprazole: 80 mg intravenous bolus followed by continuous infusion at 8 mg/hour). Endoscopic procedures were performed by the gastroenterologists who had performed therapeutic endoscopy within 24 hours of admission. Endoscopic hemostasis was achieved solely with the application of hemoclips or thermal therapy, or in combination with localized epinephrine injection. We used an HQ290 endoscopy system (Olympus Corporation, Shinjuku, Tokyo, Japan). Endoscopic hemoclip treatment was performed using hemoclips with an arm length of 7.5 mm and a jaw angle of 135° (EZClip HX-610-135, Olympus Corporation, Shinjuku, Tokyo, Japan). The hemoclips were applied with a rotatable clip fixing device (HX-110LR, Olympus Corporation, Shinjuku, Tokyo, Japan) until the bleeding or visible vessel was effectively grasped to achieve hemostasis. Thermal therapy was performed using monopolar hemostatic forceps (FD-410LR Coagrasper, Olympus Corporation, Shinjuku, Tokyo, Japan). An electrosurgical unit (VIO 300S, Erbe, Tübingen, Germany) was used with the following configuration: 60 W, effect 4, and soft coagulation mode.

TABLE 1. Forrest Classification of Peptic Ulcers

Forrest Class	Endoscopic Appearance
Ia	Active spurting
Ib	Active oozing
IIa	Nonbleeding visible vessel
IIb	Adherent clot
IIc	Flat pigmented hematin on ulcer base
III	Clean base

Statistical Analysis

Statistical significance of the results was calculated using nonparametric tests. The Mann-Whitney *U* test was used for continuous variables, and the Fisher's exact test and paired *t*-test were applied for categorical variables. Statistical tests were conducted using the SPSS version 22.0 software (SPSS, Chicago, IL). Results were considered statistically significant at $P < .05$.

Results

Of the 61 patients with peptic ulcer bleeding who underwent endoscopic hemostasis, 10 (16.3%) were inpatients who were initially admitted for other reasons before experiencing UGIB. Baseline characteristics of all patients are presented in **TABLE 2**. In all, 43/61

TABLE 2. Baseline Characteristics of Patients

	Nontransfusion (n = 18)	Transfusion (n = 43)	*P* Value
Age, y, mean ± SD	59.61 ± 17.03	69.95 ± 12.42	.028
Sex, male (%)			
Alcohol	6 (33.3%)	11 (25.6%)	.538
Smoking	9 (50.0%)	7 (16.3%)	.006
Comorbidity			
Hypertension	12 (66.7%)	21 (48.8%)	.202
Diabetes mellitus	5 (27.8%)	20 (46.5%)	.175
Cardiovascular disease	0 (0 %)	5 (11.6%)	.131
Cerebrovascular accident	4 (22.2%)	7 (16.3%)	.582
Chronic renal failure stage 2–4	4 (22.2%)	7 (16.3%)	.582
Hemodialysis	2 (11.1%)	1 (2.3%)	.148
Liver disease	2 (11.1%)	5 (11.6%)	.954
Bleeding developed in hospital	4 (22.2%)	6 (14.0%)	.611
Ulcer location, gastric/duodenum	12 (66.7%)/ 6 (33.3%)	28 (65.1%)/ 15 (64.9%)	.907
Forrest class			.053
Ia	3 (16.7%)	3 (7.0%)	
Ib	4 (22.2%)	6 (14.0%)	
IIa	8 (44.4%)	33 (76.7%)	
IIb	3 (16.7%)	1 (2.3%)	
Symptom			.049
No symptom	5 (27.8%)	5 (11.6%)	
Melena	5 (27.8%)	23 (53.5%)	
Hematemesis	0 (0%)	5 (11.6%)	
Both	8 (44.4%)	10 (23.3%)	
AIMS65*			.008
0–1	15 (83.3%)	20 (46.5%)	
2–3	3 (16.7%)	23 (53.5%)	
Hb (g/dL) mean ± SD			
Initial at admission	10.19 ± 1.11	7.26 ± 2.11	.000
24 hours after endoscopic hemostasis	9.41 ± 0.83	9.00 ± 1.16	.134

Hb, hemoglobin; INR, international normalized ratio; SD, standard deviation.
**AIMS65, albumin <3 g/dL, INR >1.5, alteration in mental status, systolic blood pressure ≤90 mm Hg, age ≥65 years.*

(70.5%) patients received RBC transfusions. Many patients in the nontransfusion group were asymptomatic, whereas many of those in the transfusion group exhibited symptoms such as melena and hematemesis. The initial Hb level in the transfusion group (7.26 ± 2.11 g/dL) was lower than that in the nontransfusion group (10.19 ± 1.11 g/dL; P <.001). The Hb level measured 24 hours after achieving endoscopic hemostasis was not significantly different between the 2 groups (mean 9.00 ± 1.16 g/dL, transfusion group; 9.41 ± 0.83 g/dL, nontransfusion group; P = .134).

Analysis as per the Forrest classification showed that patients with class 2a ulcers were more likely to require blood transfusions than those with ulcers of other classes (P = .014). The transfusion rate was higher in patients with an AIMS65 score of 2 than in patients with a score of ≤1 (25/35, 57.1%; P = .008). There was no difference in the success rate of hemostasis and in the occurrence of rebleeding after hemostasis between the 2 groups. Although the average length of hospital stay was higher in the transfusion group than in the nontransfusion group, this difference was not statistically significant (**TABLE 3**). Overall, 3/61 (4.9%) patients died because of exacerbations of hepatocellular carcinoma with portal vein thrombosis, Klatskin tumor, and a carcinoma with an unknown primary, respectively.

Transfused patients received a median of 3 (interquartile range 2.0–4.75) RBC units. On average, 2.96 and 1.11 units of RBC were transfused during the pre-endoscopic and the postendoscopic hemostasis periods, respectively. Patients with low AIMS65 scores differed significantly from those with high scores with respect to factors including transfusion rates, mean RBC units transfused, and duration of hospital stay (**TABLE 4**). The analysis for the number of transfused RBC units also included patients who did not receive transfusions. The volume of blood transfused differed significantly according to the AIMS65 score (**FIGURE 1**). Patients with an AIMS65 score of 3 were transfused with a higher number of RBC units during the postendoscopy period as compared with that administered to patients in the remaining 3 groups (patients with an AIMS65 score of 0, 1, or 2) with a mean 4.33 ± 2.07 and 2.67 ± 4.1 units transfused during the pre- and postendoscopic hemostasis periods, respectively.

TABLE 3. Comparison of Treatment Outcomes between Transfusion and Nontransfusion Groups

	Nontransfusion (n = 18)	Transfusion (n = 43)	*P* Value
Initial hemostasis success	17 (94.4%)	39 (90.7%)	.781
Recurrent bleeding	0 (0%)	4 (9.3%)	.181
Additional treatment			.888
Embolization	1 (5.6%)	4 (9.3%)	
Endoscopy	3 (16.7%)	7 (16.3%)	
Mortality in 30 days	1 (5.6%)	2 (4.7%)	.882
Hospital stay, d, mean ± SD	9.5 ± 10.18	12.74 ± 15.60	.342
Total procedure time, min, mean ± SD	7.83 ± 4.96	8.5 ± 7.12	.673

SD, standard deviation.

Discussion

Patients with UGIB may experience shock or clinically significant anemia because of decreased circulating blood volume. Although basic treatment of acute blood loss involves addressing the cause of hemorrhage, the correlation between the volume of blood loss and Hb levels is not clear. To determine the volume of blood required for transfusion, it is necessary to consider the estimated volume of blood loss and clinical symptoms, along with objective indicators of systemic/main organ oxygen supply adequacy including blood pressure, heart rate, oxygen saturation, electrocardiography findings, echocardiography findings, urine volume, local brain oxygen saturation, and arterial blood gas levels.[5] In a meta-analysis, hemodynamic shock was associated with an odds ratio of 3.3 for rebleeding.[9] Therefore, RBC transfusion is one of the most common interventions for gastrointestinal hemorrhage, with 43% of patients being transfused during acute admission with UGIB.[1] Patients with UGIB requiring a transfusion should be carefully chosen, and the number of RBC units to be administered should be based on specific indicators. In our study, the AIMS65 score showed a direct, positive correlation with the volume of RBCs transfused in patients who underwent endoscopic hemostasis for UGIB.

The Rockall, AIMS65, and Glasgow-Blatchford scores are known useful indicators for assessing the condition of patients presenting with UGIB and for predicting prognosis. The Rockall score is a factor related to rebleeding and transfusion rates; the higher the score, the higher the likelihood of transfusion.[1] The score is calculated as a tally of points assigned to factors including age, shock, comorbidity, endoscopic findings, and stigmata of recent bleeding.[3] The Glasgow-Blatchford score is calculated using points allocated to blood urea nitrogen level, Hb level, systolic blood pressure level, and other markers (such as heart rate, melena, syncope, hepatic disease, and cardiac failure).[8] Of these 3 scoring methods, the AIMS65 score is a more accurate predictor of mortality.[3,10]

TABLE 4. Mortality, Rebleeding, and RBC Transfusion by AIMS65 Score

	AIMS65 Score (n = 61)				
	0 (n = 10)	1 (n = 25)	2 (n = 20)	3 (n = 6)	*P* Value
RBC transfusion n (%)	4 (40.0%)	16 (64.0%)	17 (85.0%)	6 (100.0%)	.023
Transfused RBC units, mean ± SD	1.8 ± 1.75	2.16 ± 2.06	3.85 ± 4.52	7.00 ± 4.20	.007
Rebleeding, n (%)	1 (10.0%)	3 (12.0%)	4 (10.0%)	2 (33.3%)	.553
Mortality, n (%)	0 (0.0%)	1 (4.0%)	2 (10.0%)	0 (0.0%)	.577
Hospital stay, d, mean ± SD	6.4 ± 5.02	8.24 ± 7.89	11.65 ± 10.96	28.28 ± 11.55	.000
Melena, n (%)	10 (100.0%)	17 (68.0%)	15 (75.0%)	4 (66.7%)	.236
Hematemesis, n (%)	6 (60.0%)	9 (36.0%)	6 (30.0%)	2 (33.3%)	.44

RBC, red blood cell; SD, standard deviation.

FIGURE 1. Relationship between the AIMS65 score and the number of RBC units transfused. Pre-endoscopic RBC volume, transfused between admission or upon the decision to perform endoscopic hemostasis until the procedure was performed and hemostasis was achieved; postendoscopic RBC volume, transfused within 7 days after endoscopic hemostasis. RBC, red blood cell.

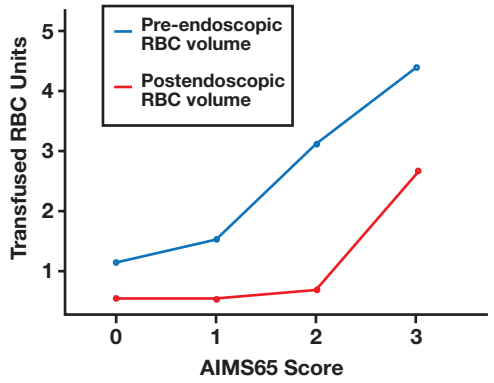

According to a study on the correlation between AIMS65 scores and blood transfusion volume, the R value of the area under the curve analysis was 0.6 to 0.7, and it differed according to the analyzed patient group.[6,11] In 2 other studies, the volume of blood transfusion according to the AIMS65 score was not analyzed.[6,11] In our study, patients with an AIMS65 score of ≥2 had a transfusion rate of 88.5%. Patients with an AIMS65 score of 3 were transfused with more units of RBCs in the postendoscopic hemostasis period. A simple calculation of the AIMS65 score may be of great benefit to healthcare professionals when planning blood transfusions for patients with UGIB.

It is known that a restrictive transfusion policy governed by a transfusion threshold of <7.0 g/dL is associated with a lower mortality than a liberal transfusion policy.[5] Further, in patients with peptic ulcer bleeding, the former is more beneficial than the latter.[5,8,11,12] In this study, each mortality (n = 3, 4.92%) was a result of exacerbation of an underlying malignancy. The overall low mortality rate in this study may be related to stringent implementation of a restrictive transfusion policy.

Our study has some limitations. It was a single-center study of a limited population. Because our transfusion policy was restrictive, the volume of blood transfused did not indicate an association with rebleeding and mortality. Therefore, further comprehensive studies involving a larger sample size are warranted to confirm our conclusions.

Conclusion

Patients with an AIMS65 score of 3 had a higher RBC transfusion requirement during hospitalization after endoscopic hemostasis was achieved. Patients with an AIMS65 score of 3 were transfused with a mean 4.33 ± 2.07 and 2.67 ± 4.1 units of RBCs in the pre-endoscopic and postendoscopic hemostasis periods, respectively. These findings may help treating clinicians predict and accordingly prepare for blood transfusions in patients with bleeding peptic ulcers.

Acknowledgments

This work was supported by a clinical research grant from Pusan National University Hospital in 2020. MWL and HJL designed the research, analyzed the data, and wrote the manuscript. SKH and KGH edited the manuscript. All authors reviewed and approved the manuscript.

REFERENCES

1. Hearnshaw SA, Logan RF, Lowe D, Travis SP, Murphy MF, Palmer KR. Acute upper gastrointestinal bleeding in the UK: patient characteristics, diagnoses and outcomes in the 2007 UK audit. *Gut.* 2011;60(10):1327–1335.
2. Villanueva C, Colomo A, Bosch A, et al. Transfusion strategies for acute upper gastrointestinal bleeding. *N Engl J Med.* 2013;368(1):11–21.
3. Gu L, Xu F, Yuan J. Comparison of AIMS65, Glasgow-Blatchford and Rockall scoring approaches in predicting the risk of in-hospital death among emergency hospitalized patients with upper gastrointestinal bleeding: a retrospective observational study in Nanjing, China. *BMC Gastroenterol.* 2018;18(1):98.
4. Huh J, Lim YA, Hong YJ, et al. The experience of applying an Australian red blood cell safety stock calculation to Korean hospitals. *Korean J Blood Transfus.* 2018;29:140–150.
5. Carson JL, Guyatt G, Heddle NM, et al. Clinical practice guidelines from the AABB: red blood cell transfusion thresholds and storage. *JAMA.* 2016;316(19):2025–2035.
6. Robertson M, Majumdar A, Boyapati R, et al. Risk stratification in acute upper GI bleeding: comparison of the AIMS65 score with the Glasgow-Blatchford and Rockall scoring systems. *Gastrointest Endosc.* 2016;83(6):1151–1160.
7. Sung J. Current management of peptic ulcer bleeding. *Nat Clin Pract Gastroenterol Hepatol.* 2006;3(1):24–32.
8. Alzoubaidi D, Lovat LB, Haidry R. Management of non-variceal upper gastrointestinal bleeding: where are we in 2018? *Frontline Gastroenterol.* 2019;10(1):35–42.
9. García-Iglesias P, Villoria A, Suarez D, et al. Meta-analysis: predictors of rebleeding after endoscopic treatment for bleeding peptic ulcer. *Aliment Pharmacol Ther.* 2011;34(8):888–900.
10. Al-Jaghbeer M, Yende S. Blood transfusion for upper gastrointestinal bleeding: is less more again? *Crit Care.* 2013;17(5):325.
11. Park SM, Yeum SC, Kim BW, et al. Comparison of AIMS65 score and other scoring systems for predicting clinical outcomes in Koreans with nonvariceal upper gastrointestinal bleeding. *Gut Liver.* 2016;10(4):526–531.
12. Odutayo A, Desborough MJ, Trivella M, et al. Restrictive versus liberal blood transfusion for gastrointestinal bleeding: a systematic review and meta-analysis of randomised controlled trials. *Lancet Gastroenterol Hepatol.* 2017;2(5):354–360.

Red Blood Cell Alloimmunization Rates and Related Factors of Patients with Thalassemia in Shiraz, Iran

Leila Kasraian, MD,[1] Elahe Khodadi, MSc,[2] Abolfazl Talei, BSc,[1] Mohamad Reza Morvarid, GP,[3] Davood Haddadi, GP,[3] Hossein Foruozandeh, PhD[4,]*

[1]Blood Transfusion Research Center, High Institute for Research and Education in Transfusion Medicine—Microbiology Department, Shiraz, Iran; [2]Thalassemia and Hemoglobinopathy Research Center, Health Research Institute, Ahvaz Jundishapur University of Medical Sciences, Ahvaz, Iran; [3]Medical Department, Shiraz University of Medical Science, Shiraz, Iran; [4]Cellular and Molecular Biology Research Center, Larestan University of Medical Sciences, Larestan, Iran; *To whom correspondence should be addressed. hosainforuozandeh62@gmail.com

Keywords: thalassemia major, alloimmunization, red blood cell, blood transfusion, leukoreduced blood, antibody screening

Abbreviations: RBC, red blood cell; DAT, direct antibody test; IAT, indirect antibody test.

Laboratory Medicine 2022;53:194–198; https://doi.org/10.1093/labmed/lmab079

ABSTRACT

Objective: The development of antibodies against red blood cell (RBC) antigens is one of the most significant adverse effects of chronic blood transfusions. This study aimed to estimate the frequency and causes of RBC immunization in patients with major thalassemia.

Methods: The findings could help determine the limitation of current practices and help future developments in the selection of suitable blood units for the transfusion support of patients with thalassemia.

Results: The alloimmunization rate was detected in 52 of 650 patients with major thalassemia (8%). The most frequent antibodies were against K (50%), D (26%), and E (15.4%). Sex, age, and splenectomy did not have any impact on the immunization rate. Immunization was lower in patients who had received only leuko-reduced blood units.

Conclusion: It is recommended that antibody screening before the first transfusion and extended RBC matching particularly for the most frequent antigens (ABO/Rh/Kell) should be performed for patients with thalassemia.

Thalassemia is the most common genetic disorder in Iran, defined as congenital hemolytic anemia caused by anomalies in the synthesis of the globulin chain.[1] More than 2 million thalassemia carriers live in Iran, of whom >20,000 patients have major thalassemia.[2] Although blood transfusion is a lifesaver for patients with thalassemia, it may be associated with some complications such as iron overload and platelet and red blood cell (RBC) alloimmunization.[3] According to the Iranian transfusion policy for patients with thalassemia, it is necessary to maintain a hemoglobin level of approximately 9 to 10.5 g/dL. Therefore, patients with major thalassemia must receive blood transfusions every 2 to 5 weeks.[4]

The development of antibodies (alloantibodies and autoantibodies) against (RBC) antigens is one of the most significant adverse effects of chronic blood transfusions. The recipient's immune status, the RBC antigen potency, the differences in RBC phenotypes between donors and recipients, and the duration and amount of the blood transfusion may influence alloimmunization rates.[5] The risk of developing RBC alloimmunization after the transfusion of a single unit of blood has been reported to be <1%, although this rate may increase to 60% in patients with regular blood transfusions.[6] The rate of alloimmunization ranged from 5.2% to 23.5% in patients with major thalassemia in previous studies.[7] Furthermore, the frequency of alloimmunization in patients with thalassemia has been reported to be 2.87% to 18.7% in different parts of Iran.[3,8-10]

A number of complications are related to alloimmunization and autoimmunization, including clinical or laboratory signs of hemolysis, lower survival, the need for more transfusion, iron overload, and difficulty and delay in providing compatible blood.[11] Preparing fully matched blood by identifying the types of antigens before the blood transfusion may prevent antibody formation against RBC antigens.[1] This study aimed to evaluate the frequency, type, and factors that may be associated with the development of antibodies in patients with major thalassemia in Shiraz, Iran. This finding can help clinicians determine the limitations of current practices and plan specific measures to decrease these limitations.

Materials and Methods

This cross-sectional study was conducted from November 2017 to November 2018 in Dastgheib Hospital in Shiraz, Iran, which is the only medical center where blood is transfused to patients with thalassemia. Informed consent was obtained from patients or their parents. Six hundred fifty patients with major thalassemia were evaluated during the study period. The demographic characteristics (age, sex, and age at the start of transfusion; duration of the intervals between transfusion; blood type; frequency of acute transfusion reactions; laboratory data; and history of splenectomy) of the patients were recorded. Next, the background

information of immunized and nonimmunized patients was compared. According to the Iranian transfusion policy, patients with thalassemia received blood to maintain a target hemoglobin level of 9 to 11.5 g/dL. Patients with thalassemia must also receive fresh blood (<7 days). Every patient received only ABO and Rh (D) matched packed RBCs after compatibility testing using a serological (RBC cross-match) technique in the anti-human globulin phase (type and cross-match policy).

Antibody Screening Test

In the present study, before the transfusion, a specimen was collected for a direct antiglobulin test (DAT) and antibody screening tests. A polyspecific antiglobulin reagent (IBTO, Homemadekit, Iran) was used to perform DAT using a 3% to 5% suspension of the patients' RBCs and appropriate controls. The results were read macroscopically and microscopically, and all negative results were confirmed by adding Coombs control cells.

A commercial 3-cell panel (IBTO, Homemadekit, Iran) was used for antibody screening by standard serological blood bank methods (Tube technique; saline, 37°C with albumin, and Coombs phases). Tubes were observed after centrifugation for agglutination and/or hemolysis. Antibody screen–positive specimens were subjected to antibody identification. Sensitized cells were added to all negative tubes. All positive samples for the alloantibody screening were evaluated to identify the antibody specificity using a commercial 11-cell identification panel (D, C, E, e, c, K, k, M, N, S, s, Fya, Fyb, Jka, Jkb, Lea, Leb, and P; IBTO, Homemadekit, Iran). Patients who were positive for alloantibodies received ABO and Rh (D) matched blood transfusion that was particular for the negative antigen (against which they had alloantibody). If patients had autoantibodies, we compared the grading of the reaction with autocontrols. Units showing a lower degree of reaction compared to autocontrols were selected. Afterward, the least-incompatible or best-matched blood units were prepared for the patients.

Ethics Statement

This study was approved by the Dastgheib Hospital ethics committee, Shiraz, Iran, with reference number 1322 (12 .03.2014).

Statistical Analysis

The data were analyzed using a statistical analysis software package (SPSS, version 22; Chicago, IL). An independent-sample *t*-test, χ^2 tests, and logistic regression were used for statistical analysis. *P* values <.05 were considered statistically significant.

Results

In this study, 650 patients with major thalassemia were evaluated. Their mean age was 21.28 + 10.66 years (range, 1–58 years). There were 322 (49.6%) males and 328 (50.4%) females. The mean transfusion interval was 17.7 ± 14.2 days. The background information of the patients is shown in **TABLE 1**. We found RBC immunization (alloantibody and autoantibody) in 76 (11.7%) patients. Among the immunized patients, the indirect antigiobulin test (IAT) was positive in 46 (60.5%) patients and the DAT was positive in 24 (31.6%) participants. In addition, 6 (7.9%) patients showed positive results of both the DAT and the IAT. Therefore, the alloimmunization rate was 8% (52 out of 650 patients). Autocontrol tests for all of the patients with a positive DAT were positive. Positive results of the DAT were more frequent among patients with blood groups O and B (*P* <.001), whereas IAT positive results were more frequent in patients with blood groups O and A (*P* <.001).

Patients' medical history and information regarding age at first transfusion, transfusion intervals, mean number of blood units in 6 months, transfusion reaction, and laboratory data of both groups are shown in **TABLE 2**. The immunization was lower in patients who had only received leuko-reduced blood units. The level of hemoglobin before transfusion was lower in immunized patients (8.02 vs 9.58 g/dL; *P* = .04). Our result indicated that the age at first transfusion did not have any impact on immunization rates (10.22 vs 15.43 months; *P* = .98). In addition, the immunization rates were not related to splenectomy (*P* = .17). Moreover, acute transfusion reactions were more frequent among immunized patients compared to nonimmunized patients (*P* < .001). Furthermore, the most frequent symptoms of acute transfusion reactions were urticaria (40.9%), chills (39.9%), and rash (36.4%); there was no record of hematuria in the patients' history.

The logistic regression results showed that alloimmunization was greater in patients over 18 years old (*P* = .04). The types of antibodies in the alloimmunized patients are summarized in **TABLE 3**. The most common alloantibodies detected were against K (50%), D (26%), and E (15.4%).

Discussion

Blood transfusion is one of the main treatments for patients with thalassemia because it decreases the complications of severe anemia, improves the quality of life, and prolongs survival. However, it has some disadvantages, which include bacterial or chronic viral infections, hemosiderosis, and antibody formation against RBCs. Research has shown that RBC alloimmunization is one of the most serious complications of blood transfusions in multitransfused patients. The development of alloantibodies may create acute or delayed hemolytic transfusion reactions and problems in finding compatible blood for transfusion.[12] In this study, the alloimmunization rate was 8%. The prevalence rate of alloimmunization ranged from 2.9% to 18.7%

TABLE 1. Background Information of Immunized and Nonimmunized Patients

Variables	Immunized Patients n (%)	Nonimmunized Patients n (%)	*P* Value	95% Confidence Interval
Sex				
Female	41 (12.5)	287 (87.5)	.60	–3.34 to 6.54
Male	35 (10.9)	287 (89.1)		
Age, y				
<12	12 (10)	108 (90)	.04	
12–18	12 (8.2)	133 (91.8)		
>18	52 (13.5)	333 (86.5)		
Transfusion reaction				
Yes	10 (22.7)	34 (77.3)	.03	–0.82 to 24.42
No	66 (10.9)	540 (89.1)		
Splenectomy				
Yes	51 (10.5)	433 (89.5)	.15	–1.58 to 10.58
No	25 (15)	141 (85)		
Receiving only leuko-reduced blood units				
No	26 (46.4)	30 (53.6)	<.001	24.75 to 51.25
Yes	50 (8.4)	544 (91.6)		

in previous studies in Iran.[3,8,9,13-15] In comparison, the rate of alloimmunization in Asia varied from 3.7% in Pakistan to 30% in Kuwait[16-20]; in Africa, it varied from 7.7% in Tunisia to 19% in Sudan[21-24]; and in Europe, it varied from 3.7% in Greece to 11.8% in Albania.[25-27] Alloimmunization rates may be related to the differences between RBC phenotypes in both donors and recipients. Thus, the alloimmunization rates have been higher in areas with heterogeneous populations and bulky ethnic/genetic admixtures.[28,29]

In this study, the most frequent antibodies were against K (52.2%), D (26.0%), and E (17.4%). Similarly, previous studies also showed antibodies against the Rh and Kell blood groups to be the most common alloantibodies.[13,16,29-32] However, other studies have reported antibodies against E as the most common antibodies.[16,18,33,34] Alloimmunization rates may be related to the immunity of RBC antigens.[15] The immunogenicity of the Rh and Kell blood group antigens was higher than that of the other antigens, which may explain higher antibody formation against these antigens.[15]

The prevalence of anti-D among the patients with thalassemia in this study was 26%. A previous study estimated that approximately 1% of D-positive blood donors were typed as weak D. Thus, some Rh-negative thalassemia patients may have received weak D units, which may explain the higher prevalence of anti-D in these patients. However, we could not find the exact prevalence of patients with weak D types in Iran.[3,35] A previous report showed the prevalence rate of Rh negative in the north of Iran to be approximately 10.2%.[36]

The level of D antigen has decreased in weak D red blood cells so that it may not be detected in an IAT. Hence, such RBCs may be grouped as Rh-negative units.[33,34] In addition, differences in methods and reagents used in D antigen typing may also cause false results. Furthermore, some individuals with partial D variants may create anti-D antibodies,[37] so standard guidelines must be implemented for performing weak D tests to detect potentially immunogenic weak D RBCs for Rh-negative donors.

The result of DATs may be positive not only in the presence of autoantibodies but also in other situations such as patients with neonatal hemolytic disease, intravenous administration of IgG, bone marrow transplantation, administration of some drugs, infections, and acute and chronic leukemia. These conditions occur rarely in patients with major thalassemia.[38,39] However, definitive identification of an autoantibody requires confirmation of all DAT-positive specimens using elution or adsorption tests. Because of the limitations of our laboratory, we did not perform elution and adsorption tests. We assumed the presence of autoantibodies in patients with positive DAT results, because the prevalence of the above-mentioned conditions was quite rare in our study population.

In this study, there were no significant differences in the rate of alloimmunization in patients with splenectomy. Similar results were also obtained in other studies.[15,35] However, other studies reported higher immunization rates in these patients.[12,27,34,40] In patients with splenectomy, the damaged RBCs are not removed by the spleen, which may increase immunization.[12,41]

In addition, the mean number of RBC units transfused in 6 months was higher in immunized patients, and transfusion intervals decreased in immunized patients (16.89 vs 19.67 days). These findings indicate that alloimmunization increases not only the transfusion need but also the rate of adverse transfusion reactions resulting from patients receiving more blood units. Similar findings were also reported in another study.[42] The results of this study indicated that the age at first transfusion did not have any impact on immunization rates (P = .98). Similar results have been reported in other studies.[8,13,34,37,43] However, other studies revealed that patients who had received a transfusion at an early age were less prone to antibody formation because of the immaturity of the immunological system.[18,25,44]

In the present study, the immunization rate was higher in older patients. Previous studies have also reported a higher immunization rate in older age groups.[11,45,46] The reasons for these higher immunization rates in older adults may include patients receiving more blood transfusions over time and having more exposure to different RBC antigens. In addition, younger patients may have received only leuko-reduced RBCs, which may prevent immunization.[27,43,47–49,51]

We found that RBC immunization was not related to sex. Similar results have been reported in other studies.[10,31,34,40] In contrast, other studies have reported a correlation between immunization rate and sex.[18,29]

In the present study, 30 (4.61%) patients had positive DAT results. The rate of positive DATs was 45% and 25% in 2 previous studies.[22,26] However, the role of a positive DAT in patients developing significant clinical problems has not been identified.[16,50] In our study,

TABLE 2. Clinical and Laboratory Data of Immunized and Nonimmunized Patients

Clinical and Laboratory Variables	Immunized Patients	Nonimmunized Patients	*P* Value	95% Confidence Interval
Age of starting transfusion (mo)	10.22 ± 4.21	15.43 ± 6.63	.98	–16.12 to 5.67
Blood transfusion interval (d)	16.89 ± 7.59	19.67 ± 15.61	.01	–3.32 to –1.21
Ferritin level (ng/mL)	3037.63 ± 2686.46	2309.61 ± 2070.45	.004	14.59 to 77.44
Hemoglobin (g/dL)	8.02 ± 0.86	9.58 ± 1.03	.04	–0.31 to –1.19
SGPT (IU/L)	37.18 ± 39.99	34.59 ± 31.27	.55	–8.39 to 9.42
SGOT (IU/L)	32.40 ± 28.77	32.08 ± 22.62	.9	–4.73 to 5.36
Bilirubin direct (mg/dL)	0.83 ± 0.56	1.03 ± 3.10	.48	–1.04 to 0.72
Bilirubin total (mg/dL)	2.78 ± 2.10	2.59 ± 1.97	.141	–0.14 to 0.88
Mean number of RBC unit transfusion in 6 mo (units)	8.12 ± 0.56	5.07 ± 0.37	.04	0.03 to 0.1
Frequency of transfusion reactions	0.2 ± 0.52	0.07 ± 0.32	.003	0.05 to 0.19

RBC, red blood cell; SGOT, serum glutamic oxaloacetic transaminase; SGPT, serum glutamic pyruvic transaminase.

TABLE 3. Type of Alloantibodies Detected in Immunized Patients (n = 52)

Number (%)	Type of Antibodies
26 (50)	K
13 (26.0)	D
8 (15.4)	E
2 (3.8)	C
1 (1.6)	Cw
1 (1.6)	Fyb
1 (1.6)	C
52 (100)	Total

patients transfused with non-leuko-reduced RBCs had a higher rate of alloimmunization compared with patients who had leuko-reduced RBC transfusion. Similar results have also been reported in other studies showing the importance of using leuko-reduced RBCs for patients with thalassemia.[15,39,40]

Our study had some limitations. We did not perform elution and adsorption tests because of limitations in our laboratory. The result of DATs may be positive not only in the presence of autoantibodies but also in other situations such as patients with neonatal hemolytic disease, intravenous administration of IgG, bone marrow transplantation, administration of some drugs, infections, and acute and chronic leukemia. These conditions occur rarely in patients with major thalassemia.[38,39] We assumed the presence of autoantibodies in patients with DAT-positive results, because the prevalence of the above-mentioned conditions was quite rare in our study population. We could not estimate the transfusion need by kg/year because the exact weight of patients was not included in their medical records. In addition, delayed transfusion reactions and hemolysis markers such as lactate dehydrogenase and haptoglobin were also not included in patients' records. Furthermore, the results of this study may not be generalized or compared with other studies because the transfusion policies of other studies do not include Rh and Kell phenotype–matched RBCs.

Conclusion

The alloimmunization rate of patients with thalassemia was 8% with respect to the ethnic diversity of the donor populations. We determined that extended phenotype–matched RBCs must be established for blood preparation before the first transfusion, particularly for the Rh and Kell system. Then, the impact of transfusion on the alloimmunization rate should be evaluated. In addition, it is suggested that all patients with major thalassemia should receive only leuko-reduced RBCs beginning with the first transfusion.

AQ19

Acknowledgments

The authors are grateful to the thalassemia center of Dastgheyb Hospital affiliated with Shiraz University of Medical Sciences in Iran. We thank the following people for their support and cooperation: Sanaz Safai, Azadeh Mossalai for her help in collecting the data, and Sahar Dehbidi, Zhale Farrokhizade, and Alison Imani for preparing the manuscript draft.

REFERENCES

1. Azarkeivan A, Ahmadi MH, Zolfaghari S, et al. RBC alloimmunization and double alloantibodies in thalassemic patients. *Hematology.* 2015;20(4):223–227.
2. Kiani A, Shirkhani Y, Kashi M, Abdi J. Prevalence of alloimmunization against RBC antigens in thalassemia major patients of Lorestan province in 1383. *Persian Sci J Iran Blood Transfus Organ.* 2006;3(3):265–271.
3. Prati D. Benefits, and complications of regular blood transfusion in patients with beta-thalassaemia major. *Vox Sang.* 2000;79:129–137.
4. Khanjari S, Talebi R, Haghdoost Oskouie SF. Development of clinical guideline of blood transfusion process in children with thalassemia. *J Hayat.* 2015;21(1):37–55.
5. Natukunda B, Brand A, Schonewille H. Red blood cell alloimmunization from an African perspective. *Curr Opin Hematol.* 2010;17(6):565–570.
6. Alves VM, Martins PR, Soares S, et al. Alloimmunization screening after transfusion of red blood cells in a prospective study. *Rev Bras Hematol Hemoter.* 2012;34(3):206–211.
7. Cheng CK, Lee CK, Lin CK. Clinically significant red blood cell antibodies in chronically transfused patients: a survey of Chinese thalassemia major patients and literature review. *Transfusion.* 2012;52(10):2220–2224.
8. Shamsian BS, Arzanian MT, Shamshiri AR, Alavi S, Khojasteh O. Frequency of red cell alloimmunization in patients with β-major thalassemia in an Iranian referral hospital. *Iran J Pediatr.* 2008;18:149–153.
9. Karimi M, Nikrooz P, Kashef S, Jamalian N, Davatolhagh Z. RBC alloimmunization in blood transfusion-dependent beta-thalassemia patients in southern Iran. *Int J Lab Hematol.* 2007;29(5):321–326.
10. Kasraian L, Shaiegan M. A survey on causes of red blood cell alloimmunization in thalassemia patients in Shiraz, Iran. *Sci J Iran Blood Transfus Organ.* 2018;15(4):265–271.
11. Datta SS, Mukherjee S, Talukder B, Bhattacharya P, Mukherjee K. Frequency of red cell alloimmunization and autoimmunization in thalassemia patients: a report from Eastern India. *Adv Hematol.* 2015;2015:610931.
12. Obaid JM, Abo El-Nazar SY, Ghanem AM, El-Hadidi AS, Mersal BH. Red blood cells alloimmunization and autoimmunization among transfusion-dependent beta-thalassemia patients in Alexandria province, Egypt. *Transfus Apher Sci.* 2015;53(1):52–57.
13. Keikhaei B, Hirad Far A, Abolghasemi H, et al. Red blood cell alloimmunization in patients with thalassemia major and intermediate in Southwest Iran. *Iran J Blood Cancer*. 2013;6(1):41–46.
14. Amin M, Gholamhossein T, Majid N, Marziyeh H, Narges S, Akbar D. Prevalence of alloimmunization against RBC antigens in thalassemia major patients in South East of Iran. *J Blood Disorders Transf.* 2013;4(147):2.
15. Davari K, Soltanpour MS. Study of alloimmunization and autoimmunization in Iranian β-thalassemia major patients. *Asian J Transfus Sci.* 2016;10(1):88–92.
16. Ameen R, Al-Shemmari S, Al-Humood S, Chowdhury RI, Al-Eyaadi O, Al-Bashir A. RBC alloimmunization and autoimmunization among transfusion-dependent Arab thalassemia patients. *Transfusion.* 2003;43(11):1604–1610.
17. Usman M, Saira M, Moinuddun M, Ahmad S, Perveen R, Usman S. Frequency of red cell alloimmunization among patients with transfusion dependent beta thalassemia in Pakistan. *Int J Hematol Oncol.* 2011;26(4):166–169.
18. Singer ST, Wu V, Mignacca R, Kuypers FA, Morel P, Vichinsky EP. Alloimmunization and erythrocyte autoimmunization in transfusion-dependent thalassemia patients of predominantly Asian descent. *Blood.* 2000;96(10):3369–3373.
19. Bashawri LA, Ahmed MS, El Fawaz N, Al Qatary AA, Ahmed MA. Red cell alloimmunization in thalassaemia patients. *Bahrain Med Bull.* 2005;27(2):62–64.

20. Gader AGMA, Al Ghumlas AK, Al-Momen AKM. Transfusion medicine in a developing country—alloantibodies to red blood cells in multi-transfused patients in Saudi Arabia. *Transfus Apher Sci.* 2008;39(3):199–204.
21. Guirat-Dhouib N, Mezri M, Hmida H, et al. High frequency of autoimmunization among transfusion-dependent Tunisian thalassaemia patients. *Transfus Apher Sci.* 2011;45(2):199–202.
22. Osman NY, Bashir AI, Abdalla SE. Determination of allo-antibodies in multiple transfused thalassemia, sickle cell anemia and Hb C disease among Sudanese patients. *NMJ.* 2013;3(11):14–23.
23. Abdelrazik AM, Elshafie SM, El Said MN, et al. Study of red blood cell alloimmunization risk factors in multiply transfused thalassemia patients: role in improving thalassemia transfusion practice in Fayoum, Egypt. *Transfusion.* 2016;56(9):2303–2307.
24. Ahmed AM, Hasan NS, Ragab SH, Habib SA, Emara NA, Aly AA. Red cell alloimmunization and autoantibodies in Egyptian transfusion-dependent thalassaemia patients. *Arch Med Sci.* 2010;6(4):592–598.
25. Spanos T, Karageorga M, Ladis V, Peristeri J, Hatziliami A, Kattamis C. Red cell alloantibodies in patients with thalassemia. *Vox Sang.* 1990;58(1):50–55.
26. Economidou J, Constantoulakis M, Augoustaki O, Adinolfi M. Frequency of antibodies to various antigenic determinants in polytransfused patients with homozygous thalassaemia in Greece. *Vox Sang.* 1971;20(3):252–258.
27. Seferi I, Xhetani M, Face M, Burazeri G, Nastas E, Vyshka G. Frequency and specificity of red cell antibodies in thalassemia patients in Albania. *Int J Lab Hematol.* 2015;37(4):569–574.
28. Dhawan HK, Kumawat V, Marwaha N, et al. Alloimmunization and autoimmunization in transfusion dependent thalassemia major patients: study on 319 patients. *Asian J Transfus Sci.* 2014;8(2):84–88.
29. Habibzadeh F, Yadollahie M, Merat A, Haghshenas M. Thalassemia in Iran: an overview. *Arch Iran Med.* 1998;1(1):27–33.
30. el-Danasoury AS, Eissa DG, Abdo RM, Elalfy MS. Red blood cell alloimmunization in transfusion-dependent Egyptian patients with thalassemia in a limited donor exposure program. *Transfusion.* 2012;52(1):43–47.
31. Saied DA, Kaddah AM, Badr Eldin RM, Mohaseb SS. Alloimmunization and erythrocyte autoimmunization in transfusion-dependent Egyptian thalassemic patients. *J Pediatr Hematol Oncol.* 2011;33(6):409–414.
32. Iqbal I, Ahmed N. Frequency of red cell alloantibodies and auto antibodies in thalassemia major children. *Biomedica.* 2014;30(1):25–28.
33. Noor Haslina MN, Ariffin N, Illuni Hayati I, Rosline H. Red cell immunization in multiply transfused Malay thalassemic patients. *Southeast Asian J Trop Med Public Health.* 2006;37(5):1015–1020.
34. Ho HK, Ha SY, Lam CK, et al. Alloimmunization in Hong Kong southern Chinese transfusion-dependent thalassemia patients. *Blood.* 2001;97(12):3999–4000.
35. Oodi A, Daneshvar Z, Goudarzi S, Amirizadeh N. RHD genotyping of serological weak D phenotypes in the Iranian blood donors and patients. *Transfus Apher Sci.* 2020;59(5):102870.
36. Ayatollahi H, Rafatpanah H, Khayyami ME, et al. Association between ABO and Rhesus blood group systems among confirmed human T lymphotropic virus type 1-infected patients in Northeast Iran. *AIDS Res Hum Retroviruses.* 2008;24(9):1155–1158.
37. Dogra A, Sidhu M, Kapoor R, Kumar D. Study of red blood cell alloimmunization in multitransfused thalassemic children of Jammu region. *Asian J Transfus Sci.* 2015;9(1):78–81.
38. Anstee DJ. The relationship between blood groups and disease. *Blood.* 2010;115(23):4635–4643.
39. Bıçakçı Z, Öztürkmen S, Akyay A, Olcay L. False positive result of the direct antiglobulin test (DAT): the role of the elevated level of immunoglobulin G. *Pediatr Hematol Oncol.* 2012;29(7):611–619.
40. Jansuwan S, Tangvarasittichai O, Tangvarasittichai S. Alloimmunization to red cells and the association of alloantibodies formation with splenectomy among transfusion-dependent β-thalassemia major/HbE patients. *Indian J Clin Biochem.* 2015;30(2):198–203.
41. Hodge G, Lloyd JV, Hodge S, Story C, Han P. Functional lymphocyte immunophenotypes observed in thalassaemia and haemophilia patients receiving current blood product preparations. *Br J Haematol.* 1999;105(3):817–825.
42. Zaidi U, Borhany M, Ansari S, et al. Red cell alloimmunisation in regularly transfused beta thalassemia patients in Pakistan. *Transfus Med.* 2015;25(2):106–110.
43. Hussein E, Ahmed Eldesoukey N, Rihan A, Kamal A. Predictors of red cell alloimmunization in multitransfused Egyptian patients with β-thalassemia. *Arch Pathol Lab Med.* 2014;138(5):684–688.
44. El Sewefy DA, Al Feky MA, Fatah MFA, El Sakhawy YN, Ragab IA, El Sayed HTN. Clinically significant red blood cell antibodies in multitransfused Egyptian thalassemic patients. *Egypt J Haematol.* 2014;39(3):171.
45. Reid M, Lomas-Francis C. *The Blood Group Antigen Facts Book. 2nd ed*. Amsterdam, the Netherlands: Elsevier Academic Press; 2004.
46. Cserti CM, Dzik WH. The ABO blood group system and *Plasmodium falciparum* malaria. *Blood.* 2007;110(7):2250–2258.
47. Tormey CA, Fisk J, Stack G. Red blood cell alloantibody frequency, specificity, and properties in a population of male military veterans. *Transfusion.* 2008;48(10):2069–2076.
48. Tournamille C, Meunier-Costes N, Costes B, et al. Partial C antigen in sickle cell disease patients: clinical relevance and prevention of alloimmunization. *Transfusion.* 2010;50(1):13–19.
49. Lannan KL, Sahler J, Spinelli SL, Phipps RP, Blumberg N. Transfusion immunomodulation—the case for leukoreduced and (perhaps) washed transfusions. *Blood Cells Mol Dis.* 2013;50(1):61–68.
50. Castellino SM, Combs MR, Zimmerman SA, Issitt PD, Ware RE. Erythrocyte autoantibodies in paediatric patients with sickle cell disease receiving transfusion therapy: frequency, characteristics and significance. *Br J Haematol.* 1999;104(1):189–194.
51. Rizzo C, Castiglia L, Arena E, Gangi S, Mazzola G, Caruso C, et al. Weak D and partial D: our experience in daily acticity. *Blood Transfus.* 2012;10(2):235–236.

AQ14 AQ16 AQ21

The Direct Spectrophotometric Method Is Reliable for Initial Assessment of Total Bilirubin in Neonatal Venous Plasma

Paspimon Makkong, BSc,[1] Pensiri Choosongsang, BSc,[1] Phattanapong Choosongsang, BSc,[1] Sasipong Trongnit, MD,[2] Wilaiwan Sriwimol, PhD[1,]*

[1]Clinical Chemistry Laboratory and [2]Division of Human Genetics, Department of Pathology, Faculty of Medicine, Prince of Songkla University, Songkhla, Thailand; *To whom correspondence should be addressed. wilaiwan.sr@psu.ac.th

Keywords: bilirubin, venous plasma, direct spectrophotometric method, colorimetric diazo method, neonate, method comparison

Abbreviations: CLSI, Clinical and Laboratory Standards Institute; $\%CV_{WL}$, within-laboratory coefficients of variation; PCCC, PreciControl Clin Chem; RBCs, red blood cells; TEa, total allowable error; CLIA, Clinical Laboratory Improvement Amendments; PPV, positive predictive value; NPV, negative predictive value

Laboratory Medicine 2022;53:199–205; https://doi.org/10.1093/labmed/lmab086

ABSTRACT

Objective: To determine the consistency of bilirubin values between the direct spectrophotometric (DS) and colorimetric diazo (diazo) methods in neonatal venous plasma specimens.

Methods: We measured the total bilirubin via the DS and diazo methods in 255 neonatal venous plasma specimens and compared the overall and subgroup results.

Results: Slight underestimation of total bilirubin values in most specimens using the DS method was observed, with higher mean biases found in higher concentrations. Significantly high positive correlations were found in all groups in which most of the different values were within the limits of agreement. DS cutoff of > 12 mg/dL showed 100% for all predictive indices in comparison with the diazo cutoff > 15 mg/dL.

Conclusions: Measurement of total bilirubin in neonatal venous plasma using the DS method had favorable agreement and high correlation with the diazo method. Therefore, the direct spectrophotometric method can be used as a reliable screening method.

Neonatal jaundice, one of the most common pediatric problems, is caused by hyperbilirubinemia.[1,2] This jaundice is generally physiological in most healthy term neonates affected during the first week of life.[2] However, some infants develop severe jaundice, usually due to the presence of risk factors such as prematurity, low birth weight, lactation failure, and/or a birth mother with diabetes. The American Academy of Pediatrics guideline recommends that all cases of neonatal jaundice during the first 24 hours should have a bilirubin measurement.[3] When the total bilirubin exceeds a certain level, phototherapy is started. The appropriate management requires timely detection and accuracy of the bilirubin measurement.

Neonatal bilirubin levels can be measured through primary specimen types, mainly transcutaneous, capillary blood, or venous blood.[4] The difference in bilirubin levels between these different specimen types is one of the problems in decision-making in clinical practice. It was previously reported[4–6] that the bilirubin level measured through a capillary specimen was significantly lower than when measured through a venous specimen, especially when the total bilirubin level was higher than 10 mg/dL. The measurement of total bilirubin in the venous specimen reflects the true bilirubin level in neonatal blood circulation. If the bilirubin value is discovered to be high in the capillary specimen, the bilirubin level is remeasured using a venous specimen before beginning the treatment for neonatal jaundice in many hospitals. Thus, an initial examination of bilirubin using a venous specimen will reduce the resampling process and minimize neonatal pain.

Different methods for measuring the neonatal bilirubin level are presently used.[7] The colorimetric diazo (diazo) biochemical method is widely used in clinical medical laboratories to measure the total bilirubin in venous specimens using an automated chemistry analyzer.[7] This method is accepted to provide high accuracy for bilirubin measurements; however, this measurement has a limitation in the high volume of the venous specimen required.[7] The direct spectrophotometric method is commonly used to measure bilirubin in a capillary blood specimen from a finger stick or a heel stick.[7] This method is simple and rapid, and it requires only a small specimen for analysis. Comparison studies of the bilirubin values between these 2 methods have been performed.[6,8–11] However, 2 of these studies examined only the correlations between bilirubin values obtained by different methods and sampling types.[6,8]

Other studies[9–11] compared bilirubin values between these 2 methods using capillary blood specimens. However, to our knowledge, there are currently no comparisons in the literature of bilirubin levels between these 2 methods in venous specimens.

Therefore, this study aimed to compare the consistency of total bilirubin level measurements in neonatal venous plasma, as measured by the direct spectrophotometric method and the diazo method. We believed that if we discovered high comparability and strong correlation of the total bilirubin values, using the direct spectrophotometric method to measure neonatal bilirubin in venous specimens would be a practical alternative in clinical practice.

Materials and Methods

Specimen Collection

The research protocol was approved by the Ethics Committee, Faculty of Medicine, Prince of Songkla University, Songkhla, Thailand (REC. 63-422-5-7). The 255 blood specimens used in the study were leftover specimens originally obtained during routine neonate bilirubin testing at the Clinical Chemistry Laboratory, Songklanagarind Hospital, Thailand between November 2020 and February 2021. The whole-blood specimens were collected by venipuncture at the back of the hand into 4 heparinized capillary tubes for each neonate and transported to the laboratory in approximately 20 minutes, with protection from light. Clinical data regarding sex, gestational age at delivery, birth weight, postnatal age, ethnicity, delivery method, maternal age, and clinical jaundice status were extracted from chart reviews.

Precision Study

Following the Clinical and Laboratory Standards Institute (CLSI) EP15-A3 guideline,[12] the total precision of the 2 methods was evaluated by running 5 replicates of the commercial control materials during a 5-day period (5 × 5 precision), followed by the calculation of within-laboratory coefficients of variation ($\%CV_{WL}$). The 2-level commercial control materials used were PreciControl Clin Chem (PCCC) Multi level-1 (0.962 mg/dL) lot 160407 and level-2 (3.769 mg/dL) lot 160393 for the diazo method and APEL Bilirubin Control (15.5 mg/dL) lot CP19G001 for the direct spectrophotometric method.

Measurements of Total Bilirubin

The total bilirubin in the venous specimens was measured by the 2 different methods as soon as possible within 2 hours after specimen collection, which is an acceptable time delay for bilirubin measurement.[13] All analyzers were operated according to manufacturer instructions.

The cobas 8000: c702 module (F. Hoffman- La Roche) is used for total bilirubin measurement via the principle of the colorimetric diazo method.[14] To measure the total bilirubin in a neonate, 3 heparinized capillary tubes containing approximately 50 μL of whole blood per tube are required, which are centrifuged at 21,000*g* for 5 minutes to separate the plasma from the red blood cells (RBCs). The plasma portions are collected and pooled in a specimen cup. The plasma specimen is mixed with the reagents, and the total bilirubin is then bound with 3, 5-dichlorophenyl diazonium to produce the red azo product. After that, the color intensity of the product is photometrically measured with bichromatic light of wavelengths of 546 and 600 nm, giving a value which is directly proportional to the total bilirubin in the specimen. The reaction time is 10 minutes per specimen.

The Bilirubin Meter APEL: BR-5200 (APEL) is a small analyzer. The direct spectrophotometric method is used to measure the bilirubin value in a heparinized capillary tube containing approximately 50 μL of whole blood.[15] The whole blood specimen in the heparinized capillary tube is centrifuged at 21,000*g* for 5 minutes to separate the plasma from the RBCs, and then this capillary tube is inserted into the holder of an analyzer. Dual wavelengths at 461 and 577 nm are used to measure the bilirubin. The bilirubin value appears very quickly on a results meter—within approximately 1 second. A blank specimen is run daily using distilled water to zero out the machine before measuring the control and patient specimens.

Statistical Analysis

The statistical analyses were performed using the MEDCALC statistical program, version 19.1. All results are presented as mean (SD) or median and mean difference (1.96 SD), as appropriate. Coefficients of variation ($\%CV_{WL}$) were calculated to determine the within-laboratory precision. The normality of the total bilirubin results was tested via the Shapiro-Wilk test. The total group was evaluated as normal distribution, whereas the 4 subgroups were evaluated as non-normal distributions. The differences of mean and median were compared via paired *t*-testing and Wilcoxon signed-rank testing, respectively. Bias estimation, method agreement, and concordance between the pairwise methods comparisons were evaluated by Bland-Altman plots[16] and linear regression analysis or Passing-Bablok regression testing.[17] Correlations were determined by Pearson or Spearman rank correlation. $P < .05$ was considered statistically significant. If more than 5% of all percentage differences were outside the total allowable error (TEa) limit (±20%) according to the Clinical Laboratory Improvement Amendments (CLIA) criteria,[18] the results were considered to be clinically significant. The ability of the direct spectrophotometric method with various cutoff values (>12–>15 mg/dL) to predict total bilirubin value obtained by the diazo method (cutoff > 15 mg/dL) was analyzed using 2 × 2 analysis; sensitivity, specificity, positive predictive value (PPV), negative predictive value (NPV), and accuracy were calculated.

Results

A total of 255 venous specimens from 197 neonates (52% male and 48% female) were used in this study, 56 from preterm (28%) and 141 from term (72%) neonates, with a mean gestational age at delivery of 38 weeks (range: 21^{+1}–41^{+0} weeks). The means (ranges) of birth weight, postnatal age at the time of blood specimen collection, and maternal age were 2862 g (690–4676 g), 4.5 days (1–20 days), and 32 years (19–43 years), respectively. In total, 44% of the neonates were delivered by cesarean section, whereas 34% and 22%, respectively, were delivered via normal labor and vacuum extraction. A total of 38% of all neonates were diagnosed as having clinical jaundice.

The total precisions of the diazo and direct spectrophotometric methods were evaluated by using commercial control specimens. The study found that the total precisions of both methods were within the acceptable criteria of less than 1/3 of TEa (6.67%) (**TABLE 1**).

Overall, the total bilirubin values ranged from 2.57–23.13 mg/dL and 2.60–21.90 mg/dL for the diazo and direct spectrophotometric methods, respectively. The mean total bilirubin of the direct spectrophotometric method was significantly lower than that of the diazo method in which the means (SD) (95% CI) were 10.96 (3.12) mg/dL (10.57–11.34)

and 11.92 (3.77) mg/dL (11.45–12.38), respectively (**FIGURE 1**). The Pearson correlation coefficient (*r*) was 0.9756 (95% CI, 0.9689–0.9809), indicating a high, statistically significant positive correlation (P <.001). Linear regression analysis revealed that the 2 methods had a very strong linear association; the regression equation was $y = 0.808x + 1.326$ with R^2 of 0.9518 (**FIGURE 2A**).

A Bland-Altman plot was used to assess the agreement between total bilirubin values in the total group from the 2 methods in which the average value was shown on the *x*-axis with the difference value on the *y*-axis (**FIGURE 2B**). The mean difference and limits of agreement (LoA, defined as mean difference [1.96 SD]) were –1.0 mg/dL and –2.9 to 1.0 mg/dL, respectively. This plot revealed that only 15 of the 255 specimens (5.9%) were not within the LoA (**FIGURE 2B**). When the percentages of total bilirubin differences between the 2 methods were evaluated, only 9 of the 255 specimens (3.5%) were not within the TEa limits (**FIGURE 2C**); this value was less than 5%, indicating no clinically significant difference.

We then determined the agreement and correlation between the 2 methods in the 4 subgroups (≤9.0, 9.1–12.0, 12.1–15.0, and ≥15.1 mg/dL) classified according to the values of the direct spectrophotometric method (**TABLE 2** and **FIGURE 3**). The median total bilirubin of the direct spectrophotometric method was lower than that of the diazo method in all subgroups (**TABLE 2**). In the Bland-Altman analysis, the mean differences were –0.23, –0.9, –1.4, and –1.9 mg/dL for subgroups 1 to 4, respectively; the mean differences were higher when the total bilirubin values were increased. Good agreements between the total bilirubin values from the 2 methods were observed in all subgroups in which more than 95% of the different values for each subgroup were within the LoA (**FIGURE 3**). The Spearman rank correlation coefficients of all subgroups showed high to very high positive correlations with statistical significance (P <.001), with the highest correlation coefficient found in subgroup 1.

We determined the highest cutoff value of the direct spectrophotometric method that resulted in 100% sensitivity for detecting significant hyperbilirubinemia compared with the diazo method. Predictive indices for the total bilirubin with the diazo method of interest (>15 mg/dL) using various cutoff values (>12 – >15 mg/dL) with the direct spectrophotometric method are shown in **TABLE 3**. Using the direct spectrophotometric cutoff value of >12 mg/dL to predict the diazo total bilirubin >15 mg/dL resulted in sensitivity, specificity, and accuracy of 100%, indicating that if total bilirubin obtained by the direct spectrophotometric method was ≤12 mg/dL, then no neonate had total bilirubin more than 15 mg/dL measured by the diazo method.

Discussion

To identify, treat, and monitor neonatal jaundice, it is necessary to acquire laboratory measurements of total bilirubin, for which immediate and accurate results are important in clinical decision making. The most commonly used methods for measuring total bilirubin in neonates are the biochemical and direct spectrophotometric methods, which quantify the bilirubin values by chemical assessment and native spectral properties, respectively.[7] However, to our knowledge, no studies reported on in the literature have attempted to standardize these 2 methods. The accuracy and precision of any laboratory methods and instruments are important for providing reliable results. In general, several factors such as light intensity and temperature may affect measurement accuracy in the device. The APEL device uses an LED light source, providing a stable light intensity and a long lifetime.[15] Also, the measurement of bilirubin is performed at room temperature, which is within the operating temperature range (10°C–40°C) of the device according to manufacturer suggestions.[15] Our study did not directly examine the effects of these parameters on the bilirubin level. However, we first did a precision study to elucidate the methods and instruments met the required performance levels according to the acceptance criterion of less than 1/3 of TEa (6.67%).[17,18] The total precision of diazo and direct spectrophotometric methods was within this acceptance criterion, providing reliable results (**TABLE 1**).

Our study found that total bilirubin values in neonatal venous plasma were underestimated by approximately 1 mg/dL using the direct spectrophotometric method (**FIGURES 1** and **2B**). This agrees with the study findings of Chen et al.[10] which included a systemic underestimation of the bilirubin concentration in capillary blood by a nonchemical photometric device compared with the biochemical method, but in contrast to the findings of Kuzniewicz et al[19] and Greene et al,[20] which included a positive bias of the bilirubin levels using the reflectance-spectrophotometric method (Vitros) compared with the diazo method (AU680).

The different findings between the present study and these latter studies may have resulted from different principle assays, calibration, and manufacturers. Also, we found that the mean bias was small in low concentrations but tended to be higher in higher concentrations (**FIGURE 3**). This agrees with the findings of another comparative study between different methods that also reported higher bias in higher concentrations.[4] However, the mean bias in our findings was higher than that reported in another previous work.[9] In our total of 255 specimens, 8 specimens showed a high discrepancy (>3 mg/dL) in total bilirubin values between the 2 methods. The measurements of these specimens were not repeated because the specimens had been discarded. Clinically, 4 of the patients whose specimens we studied were diagnosed with neonatal jaundice and treated with phototherapy. Therefore, recalibration of the direct spectrophotometric device is essential to reduce the potential bias.

Our correlation studies revealed high positive correlations in subgroups 2 to 4 and very high positive correlations in subgroup 1 and the total group in which all correlations showed statistical significance

TABLE 1. Total Precision Study of the Direct Spectrophotometric and Colorimetric Diazo Methods for Total Bilirubin Measurement in Venous Plasma

Variable	Diazo Method		Direct Spectrophotometric Method
	PCCC Level 1	PCCC Level 2	APEL Bilirubin Control
Total precision (%CV_{WL})	1.47%	0.80%	0.35%

Abbreviations: *%CV_{WL}, within-laboratory coefficient of variation; PCCC, PreciControl Clin Chem.*

FIGURE 1. Total concentrated bilirubin in venous plasma, as determined via direct spectrophotometric and diazo testing methods.

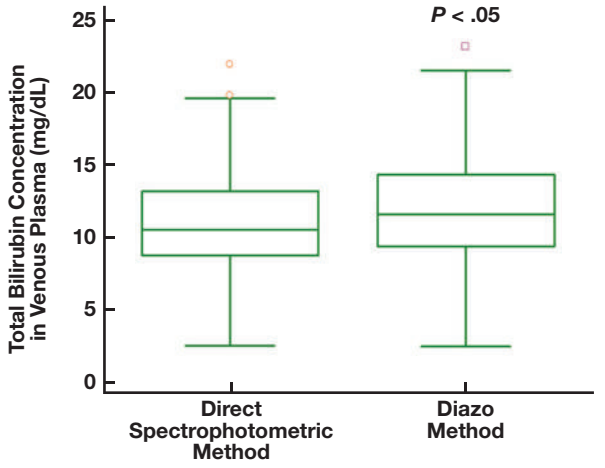

(**TABLE 2** and **FIGURE 2A**). Our Bland-Altman plots demonstrated that approximately 94% of the different values in the total group were within the LoA (**FIGURE 2B**); also, more than 95% of the different values were within the LoA in all subgroups (**FIGURE 3**), indicating that the agreement was maintained over a wide range of total bilirubin values. Moreover, more than 95% of percentage difference values were also within the TEa limit, overall showing no clinically significant differences of total bilirubin between these 2 methods (**FIGURE 2C**). Considering our results, we believe the direct spectrophotometric method is suitable for laboratory use. In a previous study report, good agreement and high correlation were discovered between the direct spectrophotometric method using the Unistat POC device and the diazo method using the Olympus AU64E analyzer (Olympus Corporation), although this was a comparative study using only capillary blood specimens.[9]

The American Academic of Pediatrics recommends the Bhutani nomogram for risk assessment of hyperbilirubinemia.[3] The Bhutani nomogram is generated by plotting the hours of age of

FIGURE 2. Bilirubin values. A, Concentration via the direct spectrophotometric and diazo methods. B, Mean (SD) values determined via the direct spectrophotometric and diazo testing methods. C, Percentage of difference between the values derived via the direct spectrophotometric and diazo testing methods.

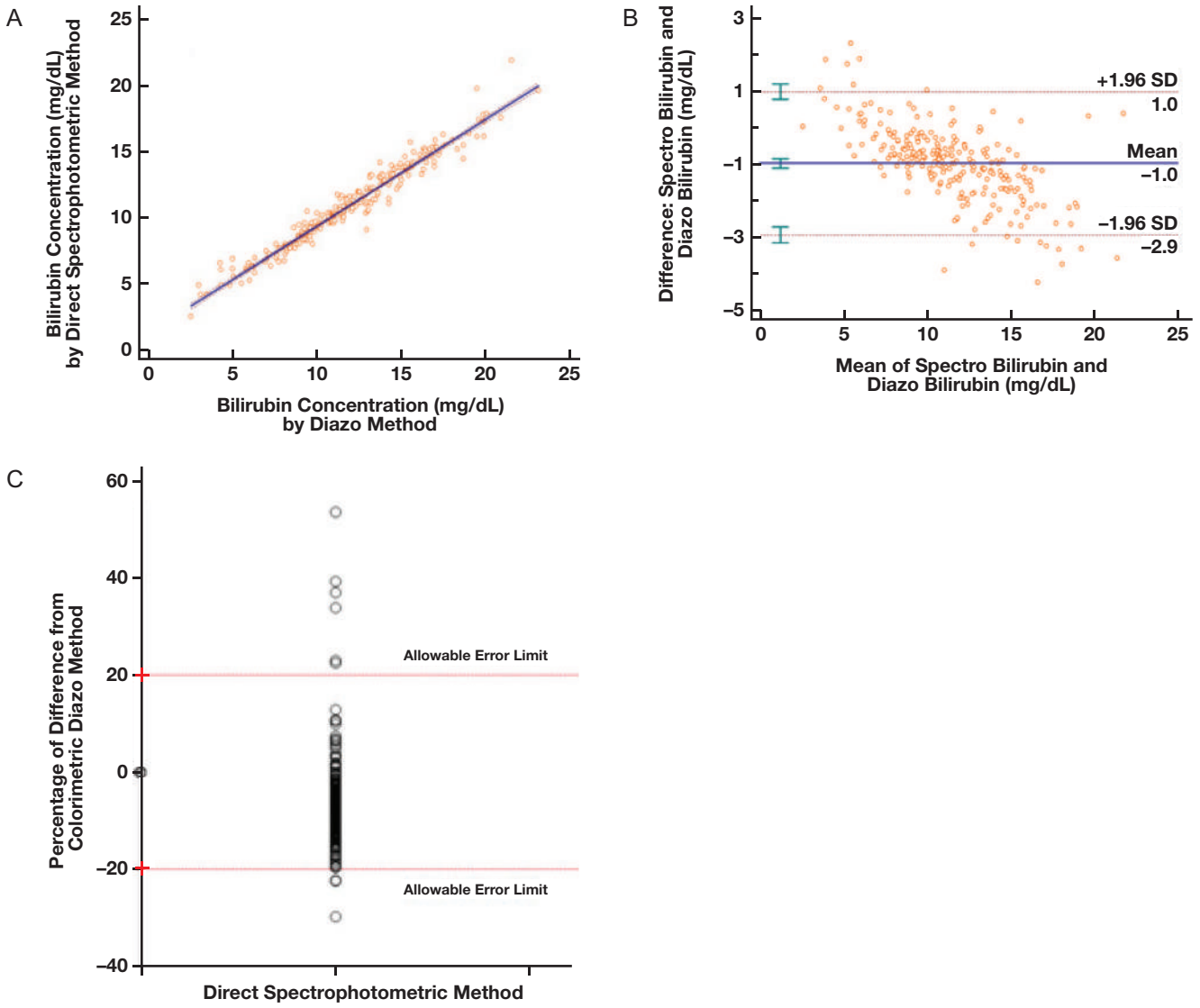

2022;53;199–205 | https://doi.org/10.1093/labmed/lmab086

TABLE 2. Comparison of Median Total Bilirubin Values and Spearman Rank Correlation Study in Subgroup Analysis Obtained by the Direct Spectrophotometric and Colorimetric Diazo Methods

Subgroup[a]	No.	Total Bilirubin in Venous Plasma (mg/dL)		*P* Value	Spearman Rank Correlation Coefficient
		Direct Spectrophotometric Method, Median (95% CI)	Diazo Method, Median (95% CI)		(95% CI)
Subgroup 1 (≤9.0 mg/dL)	70	7.70 (7.00–8.00)	8.14 (7.41–8.64)	<.05	0.934[b] (0.895–0.958)
Subgroup 2 (9.1–12.0 mg/dL)	97	10.40 (10.30–10.66)	11.39 (11.08–11.65)		0.787[b] (0.697–0.853)
Subgroup 3 (12.1–15.0 mg/dL)	62	13.30 (13.18–13.80)	14.82 (14.35–15.22)		0.782[b] (0.661–0.863)
Subgroup 4 (≥15.1 mg/dL)	26	15.90 (15.40–16.81)	18.17 (17.07–19.54)		0.815[b] (0.624–0.914)

[a]*Subgroups are classified based on the total bilirubin values obtained by the direct spectrophotometric method.*
[b]P *value <.001.*

FIGURE 3. Mean and difference bilirubin values. A, Subgroup 1. B, Subgroup 2. C, Subgroup 3. D, Subgroup 4.

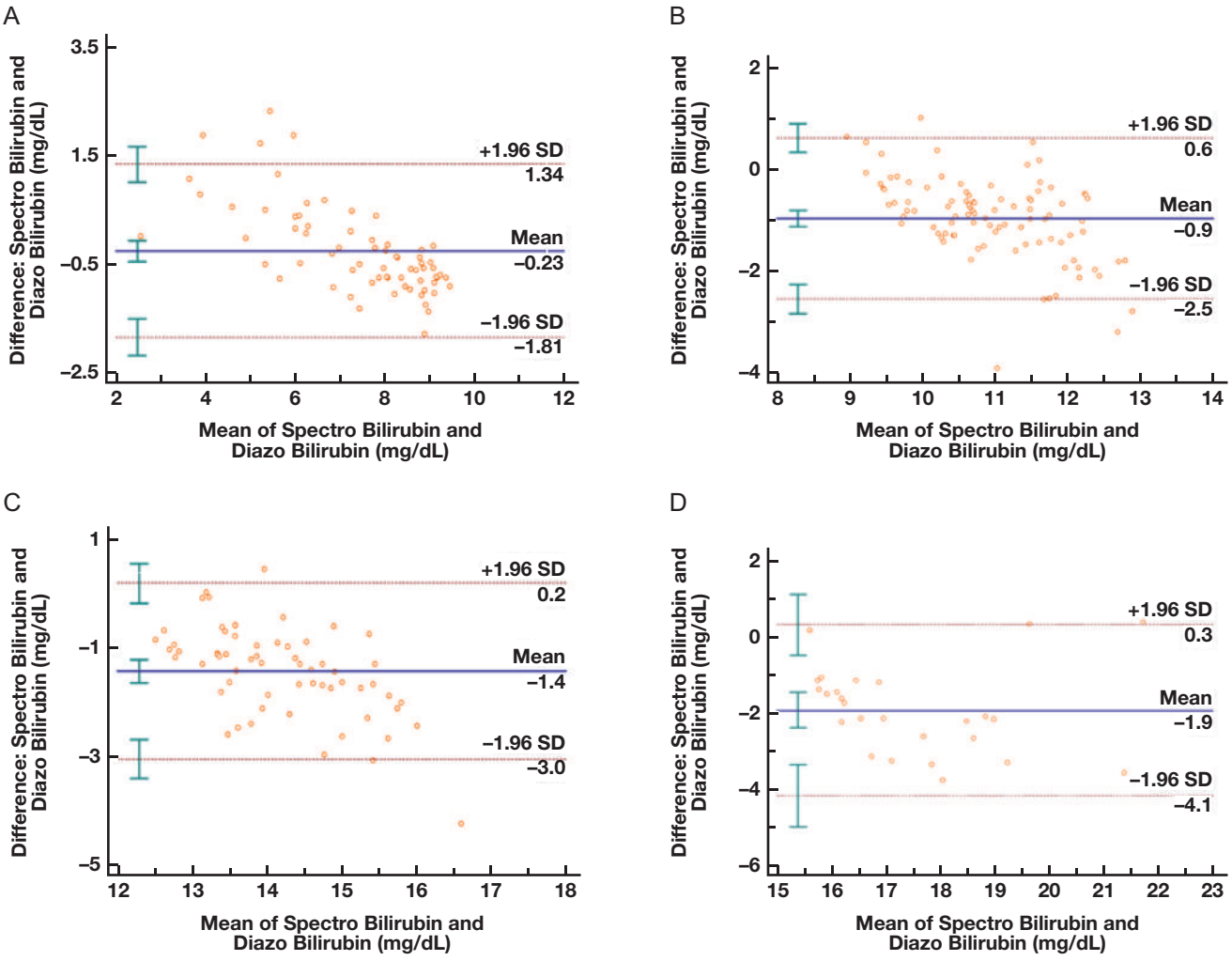

the infant against the total bilirubin values measured by the diazo method using the Hitachi 747 analyzer an instrument no longer manufactured.[21] The total bilirubin values are currently measured by modern instruments or different methods from the previous study.[21] Therefore, the interpretation of risk levels for hyperbilirubinemia using the Bhutani nomogram is questionable and concerning.

In our study, a negative bias of the direct spectrophotometric bilirubin values was found, compared with the diazo method. Therefore, it is essential to define a cutoff value of the direct spectrophotometric

TABLE 3. Predictive Indices for Total Bilirubin Outcome of Interest via the Colorimetric Diazo Method and Various Cutoff Values of the Direct Spectrophotometric Method

Total Bilirubin via Diazo Method (mg/dL)	Total Bilirubin by Direct Spectrophotometric Method (mg/dL)	Predictive Indices for Direct Spectrophotometric Method				
		Sensitivity (%) (95% CI)	Specificity (%)	PPV (%)	NPV (%) (95% CI)	Accuracy (%) (95% CI)
Cutoff >15.0	Cutoff >12.0	100.00 (93.15–100.00)	100.00	100.00	100.00	100.00 (98.56–100.00)
	>13.0	98.08 (89.74–99.95)	100.00	100.00	99.51 (96.68–99.93)	99.61 (97.83–99.99)
	>14.0	80.77 (67.47–90.37)	100.00	100.00	95.31 (92.08–97.26)	96.08 (92.91–98.10)
	>15.0	50.00 (35.81–64.19)	100.00	100.00	88.65 (85.61–91.11)	89.80 (85.42–93.23)

Abbreviations: *CI, confidence interval; NPV, negative predictive value; PPV, positive predictive value.*

method without missing a neonate in need of therapeutic intervention. Total bilirubin levels higher than 15 mg/dL have been reported as critical for neonates,[22,23] so we selected this point as the cutoff value. We discovered that when both methods used the same cutoff value (>15 mg/dL) of total bilirubin, the sensitivity of the direct spectrophotometric method was only 50%, with an 88.65% NPV and 89.80% accuracy (**TABLE 3**). When the cutoff value of the direct spectrophotometric method was decreased to >12 mg/dL, the sensitivity, NPV, and accuracy all improved to 100%. We therefore suggest that if the total bilirubin value using the direct spectrophotometric method is higher than 12 mg/dL, it should be interpreted with care and should be remeasured with a standard laboratory method such as diazo before making any decisions concerning therapeutic intervention.

Conclusion

In conclusion, we found that the measurement of total bilirubin using the direct spectrophotometric method in the neonatal venous plasma provided high correlation, good agreement, high sensitivity, and accuracy with the diazo method, as long as the total bilirubin was below 12 mg/dL, but neonates with a value higher than this should have confirmatory testing using the standard diazo method. There are several advantages to being able to confidently use a direct spectrophotometric method, notably, the small instrument size, small specimen volume required, rapid turnaround time, and high measurement performance. Our study findings confirm that this direct spectrophotometric method can be regarded as a reliable alternative screening method for hyperbilirubinemia in neonates.

Acknowledgments

We thank Dave Patterson, BSc, of the International Affairs Office, Faculty of Medicine, Prince of Songkla University, Songkhla, Thailand, for proofreading and editing the manuscript. This study and coauthor P.M. were funded by the Faculty of Medicine, Prince of Songkla University, Songkhla, Thailand (contract No. REC. 63-422-5-7). The funding sponsor did not have any additional role in the study design, data collection and analysis, manuscript writing, and decision to submit the article for publication.

Personal and Professional Conflicts of Interest

None declared.

REFERENCES

1. Hanson TW. Bilirubin oxidation in brain. *Mol Genet Metab.* 2000;71(1-2):411–417.
2. Porter ML, Dennis BL. Hyperbilirubinemia in the term newborn. *Am Fam Physician.* 2002;65(4):599–606.
3. American Academy of Pediatrics, Subcommittee on Hyperbilirubinemia. Management of hyperbilirubinemia in the newborn infant 35 or more weeks of gestation. *Pediatrics.* 2004;114(1):297–316.
4. Aranda CC, Torrubia DB, Álvarez LC, et al. Determining the correlation and accuracy of three methods of measuring neonatal bilirubin concentration: serum, capillary and transcutaneous bilirubin. *Biomed J Sci & Tech Res.* 2017;1(3):722–726.
5. Leslie GI, Philips JB 3rd, Cassady G. Capillary and venous bilirubin values: are they really different? *Am J Dis Child.* 1987;141(11):1199–1200.
6. Mussavi M, Niknafs P, Bijari B. Determining the correlation and accuracy of three methods of measuring neonatal bilirubin concentration. *Iran J Pediatr.* 2013;23(3):333–339.
7. Puppalwar PV, Goswami K, Dhok A. Review on "Evolution of methods of bilirubin estimation." *J Appl Dent Med Sci.* 2012;1(3):17–28.
8. Grohmann K, Roser M, Rolinski B, et al. Bilirubin measurement for neonates: comparison of 9 frequently used methods. *Pediatrics.* 2006;117(4):1174–1183.
9. Barko HA, Jackson GL, Engle WD. Evaluation of a point-of-care direct spectrophotometric method for measurement of total serum bilirubin in term and near-term neonates. *J Perinatol.* 2006;26(2):100–105.
10. Chen S-D, Wang C-M, Lee W-L, Wang W-C, Chen C-J. Two different tests for total bilirubin in neonates and infants. *Pediatr Neonatol.* 2009;50(6):291–293.
11. Kazmierczak SC, Robertson AF, Catrou PG, Briley KP, Kreamer BL, Gourley GR. Direct spectrophotometric method for measurement of bilirubin in newborns: comparison with HPLC and an automated diazo method. *Clin Chem.* 2002;48(7):1096–1097.
12. Clinical and Laboratory Standards Institute (CLSI). *User Verification of Precision and Estimation of Bias-Third Edition. EP15-A3.* CLSI: Wayne, PA; 2014.
13. Hussien FA, Fadl-Elmula TM, Hussien AM, et al. Evaluation of bilirubin degradation in plasma specimen exposed to room light at room temperature. *Asian J Biomed Pharm Sci*. 2013:3(22): 79–83.
14. *Colorimetric Diazo Method® Bilirubin Total Gen. 3. Leaflet for Cobas c701/702 Module Analyzers.* Roche Diagnostics; CH-6343 Rotkreuz, Switzerland; 2016.
15. *Bilirubin Meter BR-5200 Analyzer Operation Manual.* Kawaguchi, Saitama, 333-0834 Japan: APEL; 2016.

16. Giavarina D. Understanding Bland Altman analysis. *Biochem Med (Zagreb).* 2015;25(2):141–151.

17. Bilić-Zulle L. Comparison of methods: passing and Bablok regression. *Biochem Med (Zagreb).* 2011;21(1):49–52.

18. Sun Diagnostics. Recommended total allowable error limits. https://mes-global.com/wp-content/uploads/2019/06/TotalAllowableErrorLimitsTableExample_rev20120725.pdf. Accessed September 15, 2021.

19. Kuzniewicz MW, Greene DN, Walsh EM, McCulloch CE, Newman TB. Association between laboratory calibration of a serum bilirubin assay, neonatal bilirubin levels, and phototherapy use. *JAMA Pediatr.* 2016;170(6):557–561.

20. Greene DN, Liang J, Holmes DT, Resch A, Lorey TS. Neonatal total bilirubin measurements: still room for harmonization. *Clin Biochem.* 2014;47(12):1112–1115.

21 Bhutani VK, Johnson L, Sivieri EM. Predictive ability of a predischarge hour-specific serum bilirubin for subsequent significant hyperbilirubinemia in healthy term and near-term newborns. *Pediatrics.* 1999;103(1):6–14.

22. Department of Pathology and Laboratory Medicine, University of California. Critical values for infants (<12 months). http://www.pathology.uci.edu/services/infants.asp. Accessed September 15, 2021.

23. Don-Wauchope AC, Wang L, Grey V. Pediatric critical values: laboratory-pediatrician discourse. *Clin Biochem.* 2009;42(16-17):1658–1661.

AQ28

CASE STUDY

EDTA-Induced Pseudothrombocytopenia up to 9 Months after Initial COVID-19 Infection Associated with Persistent Anti-SARS-CoV-2 IgM/IgG Seropositivity

Dániel Bereczki, MD, PhD, DSc, FRCP Edin, FESO,[1,2,3,] Béla Nagy Jr, MD, PhD,[4] Adrienne Kerényi, MD, PhD,[4,5] Gábor Nagy, MD,[4] Krisztina Szarka, MSc, PhD,[6] Katalin Kristóf, MD, PhD,[7] Balázs Szalay, MD, PhD,[7] Barna Vásárhelyi, MD, PhD, DSc,[7] Harjit P. Bhattoa, MD, PhD,[4] János Kappelmayer, MD, PhD, DSc[4]*

[1]Department of Neurology, Semmelweis University, Budapest, Hungary; [2]MTA-SE Neuroepidemiological Research Group ELKH, Budapest, Hungary; [3]EANcore COVID-19 Task Force, European Academy of Neurology, Vienna, Austria; [4]Department of Laboratory Medicine, Faculty of Medicine, University of Debrecen, Debrecen, Hungary; [5]Faculty of Pharmacy, University of Debrecen, Debrecen, Hungary; [6]Department of Medical Microbiology, Faculty of Medicine, University of Debrecen, Debrecen, Hungary; [7]Department of Laboratory Medicine, Semmelweis University, Budapest, Hungary; *To whom correspondence should be addressed. bereczki.daniel@med.semmelweis-univ.hu

Keywords: EDTA-induced pseudothrombocytopenia, SARS-CoV-2 virus infection, COVID-19, persisting anti-SARS-CoV-2 IgM/IgG seropositivity, antinucleocapsid antibody, anti-Spike 1 receptor binding domain (anti-S1-RBD), anti-Spike 1 and Spike 2 (anti-S1/S2) IgG test

Abbreviations: GPIIb/IIIa, glycoprotein IIb/IIIa; PCR, polymerase chain reaction

Laboratory Medicine 2022;53:206–209; https://doi.org/10.1093/labmed/lmab050

ABSTRACT

Platelets have a role in vascular complications of COVID-19-related viral coagulopathy. Although immune-induced thrombocytopenia has been described mostly in moderate-to-severe COVID-19, the prognostic role of platelet count in COVID-19 is still controversial. Pseudothrombocytopenia has been reported to represent COVID-19-associated coagulopathy in critical illness, and transient EDTA-dependent pseudothrombocytopenia lasting less than 3 weeks was described in a patient with severe acute COVID-19 pneumonia. In our case study, EDTA-induced pseudothrombocytopenia was still present at 9 months after an initial SARS-CoV-2 virus infection in an apparently recovered 60 year old man. The persistence of antinucleocapside and antispike antibodies 9 months after the initial infection suggests that EDTA-induced pseudothrombocytopenia may be related to anti-SARS-CoV-2 IgG or IgM antibodies. We should acknowledge the possibility that pseudothrombocytopenia may also appear in some patients after seroconversion after the launch of large-scale vaccination programs.

The COVID-19 disease caused by the SARS-CoV-2 virus is an ongoing pandemic that began in December 2019, resulting in >142 million identified patients and >3 million fatalities through April 20, 2021.[1] Endothelial cell activation[2] and viral coagulopathy have an important role in COVID-19-related complications.[3] Thrombocytopenia at hospital admission is often reported in patients with more severe cases of illness, suggesting increased platelet consumption.[4] Immune-induced thrombocytopenia has been described as a complication of COVID-19, appearing mostly in moderate-to-severe illness.[5] In routine clinical care, platelet count is usually determined by hematologic analyzers using EDTA-anticoagulated blood specimens. In rare instances, EDTA induces time- and temperature-dependent in vitro platelet aggregation, resulting in a misleading underestimation of platelet counts termed as EDTA-induced pseudothrombocytopenia.[6] This phenomenon often occurs because of a conformational change of platelet surface glycoprotein IIb/IIIa (GPIIb/IIIa) induced by EDTA, which allows natural IgM or IgG autoantibodies to bind to the GPIIb/IIIa receptor, leading to platelet agglutination.[7-9] EDTA-induced pseudothrombocytopenia is only present in vitro and has no known associated clinical significance.[10] It can be persistent or transient, sometimes showing alternating periods without the generation of aggregates.[11]

The development of EDTA-induced pseudothrombocytopenia can be complicated by COVID-19 disease. Others have reported transient EDTA-dependent pseudothrombocytopenia in a 59 year old woman with severe COVID-19 pneumonia, lasting from the second to the 17th day of hospital treatment.[12] The plausible reason is that the SARS-CoV-2–specific antibody has the epitope to bind to the cryptic platelet antigen that causes a cross-reaction.[12] We here report on an apparently recovered patient in whom pseudothrombocytopenia was still present at 9 months after initial SARS-CoV-2 virus infection.

Case Report

The patient in this case report was a 60 year old man with a past medical history of rapid eye movement sleep–related obstructive sleep apnea syndrome and hypertension. The patient reported compliance with continuous positive airway pressure equipment for his sleep apnea. He developed fever (up to 38.9°C), generalized weakness, ageusia, and anosmia. A polymerase chain reaction (PCR) analysis of the nasal and throat swab identified SARS-CoV-2 infection (Azureseq 200, Omixon Ltd, Budapest, Hungary). Fever lasted for 7 days; fatigue and insomnia diminished over this time period but persisted for several weeks. Arterial blood oxygen saturation assessed by fingertip pulse oximetry was normal initially but dropped to 85% to 87% between day 5 and day 10 of the infection with a respiration frequency of 30 to 34/min. There was no cough, dyspnea, or chest pain. During the 14-day home quarantine there was no need for hospitalization, and only multivitamins and antipyretics were administered in addition to the regular antihypertensive medication. No corticosteroids or agents with potential antiviral effect were used. At the end of the quarantine, the repeated nasal and throat swab PCR tests on 2 consecutive days for SARS-CoV-2 did not identify the presence of the virus, and several further PCR tests up until the end of December 2020 consistently remained negative.

A laboratory checkup was performed at 2 months after the acute phase, and thrombocytopenia (82 G/L) was detected in the EDTA-anticoagulated whole blood sample on a hematology analyzer (Sysmex 2000 hematology analyzer, Sysmex, Japan). Since 2002, the patient had 14 normal platelet counts evaluated (range, 182–277 G/L); the most recent had been determined 11 months before COVID-19 symptoms (**FIGURE 1**). At 9 months after the acute SARS-CoV-2 infection, platelet counts were consistently low in EDTA-anticoagulated blood specimens but were practically normal in specimens in which sodium citrate was used for anticoagulation (**FIGURE 1**). In addition, platelet aggregates were observed in the EDTA-anticoagulated blood smear (**FIGURE 2**). This phenomenon was established when the repeatedly assessed platelet count increased in citrate-anticoagulated blood (**FIGURE 1**). From the citrate-anticoagulated blood, the platelet count was calculated by multiplying the platelet result by a factor of 1.1. Pseudothrombocytopenia may not be exclusively an in vitro phenomenon in this patient, because the platelet distribution width increased (69.2 fL; reference range: 25.0–65.0 fL) and the mean platelet volume was in the high-normal range (mean platelet volume = 11.0 fL; reference range: 7.2–11.1 fL).

Using the Abbott antinucleocapsid SARS-CoV-2 IgG and IgM tests (Abbott Diagnostics, Wiesbaden, Germany), high SARS-CoV-2 IgG titer was detected after 4 months of infection. We then found decreasing levels of anti-SARS-CoV-2 IgG antibody over time (**FIGURE 3**), but both IgG and IgM antibodies were over the cutoff value even at 9 months after the acute infection. To confirm these results, two different Roche Cobas SARS-CoV-2 serology tests (Elecsys Anti-SARS-CoV-2 and Anti-SARS-CoV-2 S, Roche, Switzerland) were performed in a sample obtained at December 21, 2020 with the following results: anti-nucleocapsid total Ig cut-off index (COI) value: 107.3 at the cutoff value of 1.0, and anti-Spike 1 receptor binding domain (anti-S1-RBD) total Ig titer >250 U/mL at the cutoff value of 0.8 U/mL. In parallel, Diasorin anti-Spike 1 and Spike 2 (anti-S1/S2) IgG test was also used (IgG titer: 91.8 AU/mL, cut-off value: 15 AU/mL) (DiaSorin S.p.A., Saluggia, Italy). All these analyses confirmed the persistence of anti-SARS-CoV-2 antibodies at 9 months after the initial infection.

By 9 months after the acute phase, fatigue and sleep disturbance gradually decreased, and although physical load capacity had not returned to the pre-COVID-19 level, there were no clinical signs of reinfection, and SARS-CoV-2 PCR from whole blood using different methods (automatically using the MagNA Pure 96 DNA and Viral NA Small Volume Kit and manually using the Perkin Elmer SARS-CoV-2 real-time PCR assay, N and ORFlab SARS-CoV-2 targets; and using the Azureseq 200, Omixon Ltd, Budapest, Hungary) in 2 independent laboratories excluded virus persistence in the blood.

Discussion

The prevalence of EDTA-induced pseudothrombocytopenia is estimated to be 0.03% to 0.27% of the general outpatient population and does

FIGURE 1. Platelet counts in EDTA- and citrate-anticoagulated specimens in the history of the patient. Arrow marks the time of SARS-CoV-2 infection.

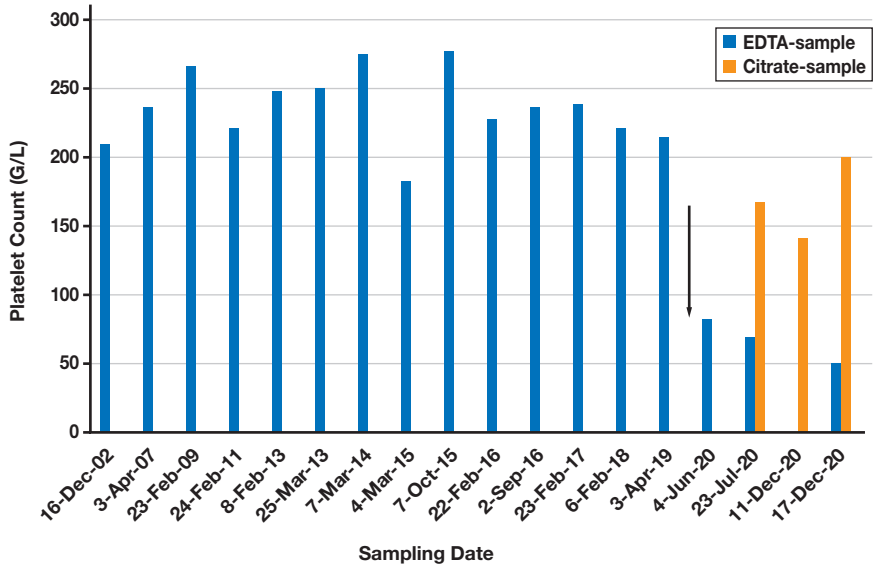

not appear to be related to age and sex.[11] Pseudothrombocytopenia may also be induced by viral infection. As such, hepatitis A virus infection has been the most common culprit, followed by cytomegalovirus and influenza A H1N1 infections.[13] Transient EDTA-induced pseudothrombocytopenia has also been associated with infectious mononucleosis; the pseudothrombocytopenia phenomenon resolved after 2 months, when the patient recovered from the infection.[14] Furthermore, pseudothrombocytopenia may be linked to dengue virus infection[15] or after an acute viral gastroenteritis.[16] Kuhlman et al[17] reported a patient with pan-pseudothrombocytopenia and suggested that it may represent COVID-19-associated coagulopathy in COVID-19-caused critical illness. COVID-19 may result in thrombocytopenia via the enhanced activation of platelets, because SARS-CoV-2 infection is associated with an increased surface expression of the GPIIb/IIIa complex of nonstimulated platelets of patients with COVID-19 and the GPIIb/IIIa complex remains upregulated after stimulation.[18] Consequently, platelet agglutination and clump formation indicate abnormal in vivo platelet activity that increases the risk of microthrombotic disorder.[17] In contrast, in COVID-19 disease, a SARS-CoV-2-specific antibody can bind to the cryptic platelet antigen, which causes a cross-reaction of the antigen-antibody, leading to EDTA-induced pseudothrombocytopenia.[12] It has also been speculated that inflammation may be essential to the generation of this phenomenon. Notably, platelet clumping may resolve with the use of citrate and patient recovery.[12]

Although no other viral testing was performed in our patient, he had no clinical signs or symptoms of any other viral illness that may have caused this pseudothrombocytopenia. In another patient with COVID-19, transient pseudothrombocytopenia was detected along with the appearance of anti-SARS-CoV-2 antibodies and disappeared by day 17, when there were no detectable antibodies in the patient anymore.[12] In the current patient, pseudothrombocytopenia was observed at 9 months after the initial SARS-CoV-2 infection, and anti-SARS-CoV-2 antibodies were still present. Further, although there has already been 1 previous report on the association between COVID-19 and EDTA-induced pseudothrombocytopenia,[12] this phenomenon may be a coincidence and should not be considered as an evidence of a causal relationship.

Note that these results in the citrated specimens were still lower than pre-COVID-19 values, which could be a late consequence of former SARS-CoV-2 infection. It remains unclear whether in this patient pseudothrombocytopenia was related to antinucleocapsid or antispike antibodies against the SARS-CoV-2 virus because both types of antibodies were present 9 months after the acute infection.

To date, we know of only 1 reported patient with COVID-19-associated EDTA-induced pseudothrombocytopenia.[12] In addition to the current case report, we have no information regarding further reports on COVID-19-associated, EDTA-induced pseudothrombocytopenia in either hospitalized or unhospitalized patients. As reported in Li et al,[12] if low platelet counts are found in a patient with COVID-19 by the routine automatic analyzers in EDTA-anticoagulated blood specimens, then repeating the determination of platelet count in a citrate-anticoagulated blood specimen before a therapeutic decision is made to correct thrombocytopenia is suggested. Furthermore, because thrombocytopenia has been reported after SARS-CoV-2 vaccination,[19-21] health care professionals should consider that pseudothrombocytopenia—al-

FIGURE 2. Platelets in the smear of the EDTA-anticoagulated specimen at 9 months after the acute infection. Arrows point to the platelet aggregates. May-Grünwald-Giemsa staining, original magnification.

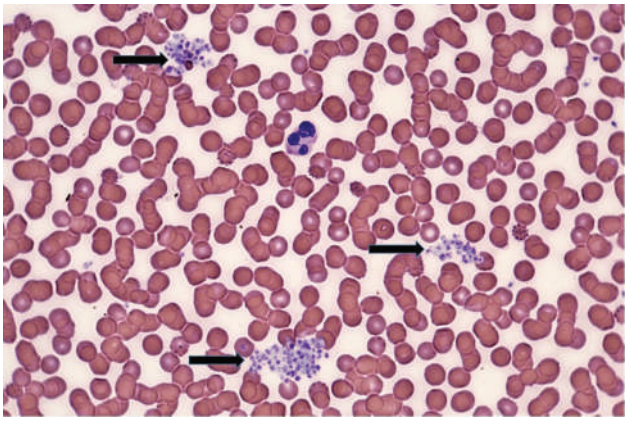

FIGURE 3. COVID-19 status of the patient with PCR of the nasal-throat swab and serum IgG/IgM status using the Abbott test. PCR, polymerase chain reaction.

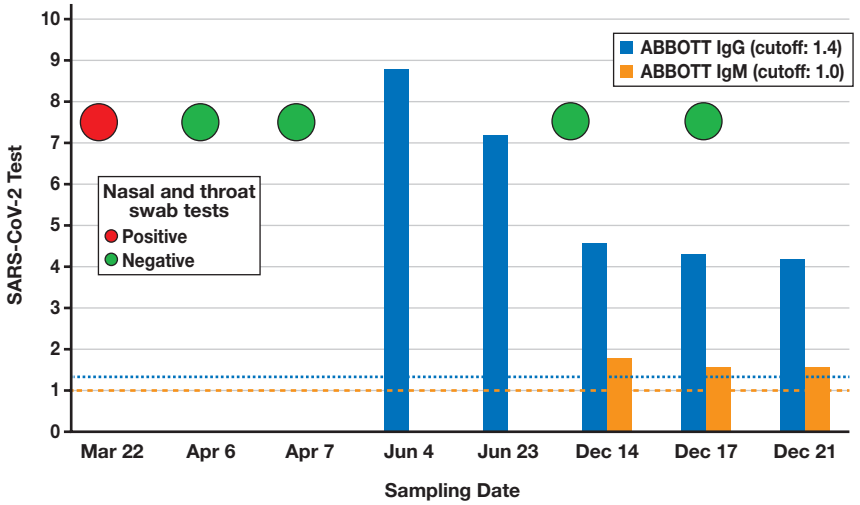

2022;53:206–209 | https://doi.org/10.1093/labmed/lmab050

though not observed to date—may also appear in some patients after seroconversion after the start of large-scale vaccination programs.

The study was approved by the Scientific and Research Ethics Committee of the University of Debrecen and the Ministry of Human Capacities under registration number 32568-3/2020/EÜIG. The patient gave written consent to publish his case report.

This study was funded by the GINOP-2.3.2-15-2016-00043 project. The project is cofinanced by the European Union and the European Regional Development Fund. BN is a recipient of the Lajos Szodoray Grant and an OTKA Bridging Fund (Faculty of Medicine, University of Debrecen).

Acknowledgments

DB designed the study, provided specimens, and wrote consecutive versions of the manuscript. BN, AK, GN, KS, KK, BS, BV, HPB, and JK performed laboratory investigations, selected methods for the study, prepared the methodology, commented on all versions of the manuscript, and approved the final manuscript for submission. The first author of this report is grateful to Dr. T. Magyar (General Practice No. 4 of the Town of Diósd, Hungary) for the care provided during the acute phase of the disease.

REFERENCES

1. Worldometer. Reported cases and deaths by country or territory. https://www.worldometers.info/coronavirus/#countries. Accessed July 26, 2021.
2. Nagy B Jr, Fejes Z, Szentkereszty Z, et al. A dramatic rise in serum ACE2 activity in a critically ill COVID-19 patient. *Int J Infect Dis.* 2021;103:412–414.
3. Kipshidze N, Dangas G, White CJ, et al. Viral coagulopathy in patients with COVID-19: treatment and care. *Clin Appl Thromb Hemost.* 2020;26:1076029620936776.
4. Lippi G, Plebani M, Henry BM. Thrombocytopenia is associated with severe coronavirus disease 2019 (COVID-19) infections: a meta-analysis. *Clin Chim Acta.* 2020;506:145–148.
5. Bhattacharjee S, Banerjee M. Immune thrombocytopenia secondary to COVID-19: a systematic review. *SN Compr Clin Med.* Published ahead of print September 19, 2020. doi: 10.1007/s42399-020-00521-8.
6. Schuff-Werner P, Mansour J, Gropp A. Pseudo-thrombocytopenia (PTCP). A challenge in the daily laboratory routine? *Lab Med.* 2020;44:295–304.
7. van Vliet HH, Kappers-Klunne MC, Abels J. Pseudothrombocytopenia: a cold autoantibody against platelet glycoprotein GP IIb. *Br J Haematol.* 1986;62(3):501–511.
8. De Caterina M, Fratellanza G, Grimaldi E, et al. Evidence of a cold immunoglobulin M autoantibody against 78-kD platelet glycoprotein in a case of EDTA-dependent pseudothrombocytopenia. *Am J Clin Pathol.* 1993;99(2):163–167.
9. Fiorin F, Steffan A, Pradella P, Bizzaro N, Potenza R, De Angelis V. IgG platelet antibodies in EDTA-dependent pseudothrombocytopenia bind to platelet membrane glycoprotein IIb. *Am J Clin Pathol.* 1998;110(2):178–183.
10. Bizzaro N, Brandalise M. EDTA-dependent pseudothrombocytopenia. Association with antiplatelet and antiphospholipid antibodies. *Am J Clin Pathol.* 1995;103(1):103–107.
11. Lardinois B, Favresse J, Chatelain B, Lippi G, Mullier F. Pseudothrombocytopenia—a review on causes, occurrence and clinical implications. *J Clin Med.* 2021;10(4):594.
12. Li H, Wang B, Ning L, Luo Y, Xiang S. Transient appearance of EDTA dependent pseudothrombocytopenia in a patient with 2019 novel coronavirus pneumonia. *Platelets*. 2020;31:825–826.
13. Choe WH, Cho YU, Chae JD, Kim SH. Pseudothrombocytopenia or platelet clumping as a possible cause of low platelet count in patients with viral infection: a case series from single institution focusing on hepatitis A virus infection. *Int J Lab Hematol.* 2013;35(1):70–76.
14. Hsieh AT, Chao TY, Chen YC. Pseudothrombocytopenia associated with infectious mononucleosis. *Arch Pathol Lab Med.* 2003;127(1):e17–e18.
15. Vaidya P, Venkataraman R. Pseudothrombocytopenia in a child with dengue. *Indian J Pediatr.* 2014;81(12):1395–1396.
16. Zhong L, Chadha J, Ameri A. A curious case of pseudothrombocytopenia due to in vitro agglutination. *Case Rep Hematol.* 2020;2020:6236350.
17. Kuhlman P, Nasim J, Goodman M. Pan-pseudothrombocytopenia in COVID-19: a harbinger for lethal arterial thrombosis? *Fed Pract.* 2020;37(8):354–358.
18. Bongiovanni D, Klug M, Lazareva O, et al. SARS-CoV-2 infection is associated with a pro-thrombotic platelet phenotype. *Cell Death Dis.* 2021;12(1):50.
19. Lee EJ, Cines DB, Gernsheimer T, et al. Thrombocytopenia following Pfizer and Moderna SARS-CoV-2 vaccination. *Am J Hematol.* 2021;96(5):534–537.
20. Schultz NH, Sørvoll IH, Michelsen AE, et al. Thrombosis and thrombocytopenia after ChAdOx1 nCoV-19 vaccination. *N Engl J Med.* 2021;384:2124–2130.
21. Greinacher A, Thiele T, Warkentin TE, Weisser K, Kyrle PA, Eichinger S. Thrombotic thrombocytopenia after ChAdOx1 nCov-19 vaccination. *N Engl J Med*. 2021:384(22):2092–2101.

A Novel Mutation of the Membrane Metallo-Endopeptidase Gene Related to Late-Onset Hereditary Polyneuropathy: Case Report and Review of the Literature

Konstantinos I. Tsamis, MD, PhD,[1,] Georgia Xiromerisiou, MD, PhD,[2] Ilias P. Nikas, MD, PhD,[3] Alexandros Giannakis, MD,[1] Spiridon Konitsiotis, MD, PhD,[1] Ioannis Sarmas, MD[1]*

[1]Department of Neurology, University Hospital of Ioannina, Ioannina, Greece; [2]Department of Neurology, University Hospital of Larissa, Larissa, Greece; [3]School of Medicine, European University Cyprus, Nicosia, Cyprus; *To whom correspondence should be addressed. ktsamis@uoi.gr and ktsamis1981@yahoo.gr

Keywords: neprilysin, membrane metallo-endopeptidase, MME, late-onset CMT, HMSN, CD10

Abbreviations: MME, membrane metallo-endopeptidase; CMT2, Charcot-Marie-Tooth disease type 2; CPK, creatine phosphokinase; CMAP, compound muscle action potential; SNAP, sensory nerve action potential; gnomAD, Genome Aggregation Database.

Laboratory Medicine 2022;53:210–214; https://doi.org/10.1093/labmed/lmab060

ABSTRACT

The advent of next generation sequencing has revolutionized diagnostic approaches to hereditary polyneuropathies. Recently, mutations on the membrane metallo-endopeptidase (MME) gene, encoding neprilysin, have been related to the development of late-onset Charcot-Marie-Tooth disease type 2 (CMT2). Here, we report the first Greek patient presenting with a slowly progressive late-onset axonal polyneuropathy and a novel, likely pathogenic, heterozygous variant in the MME gene. In addition, we have performed a systematic review of all published case reports of patients with MME mutations. The results of the studies show that MME variants can be inherited as both fully penetrant autosomal-recessive and incompletely penetrant autosomal-dominant traits. A number of heterozygous variants characterized as incompletely penetrant impose an increased risk of developing a CMT2-like phenotype late in life, identical to the case study described here. Greater mutation numbers in different populations and mutation-specific functional studies will be essential to identify the pathogenicity and inheritance of more MME variants.

Hereditary motor sensory neuropathy, or Charcot-Marie-Tooth disease (CMT), consists of a heterogenous group of inherited disorders affecting either the axons or the myelin sheaths of the peripheral nerves.[1] Clinical characteristics, neurophysiological findings, pathology, and genetics are used for the classification of CMT neuropathies, but the rapidly expanding field of molecular diagnosis challenges physicians and researchers, changing their approach to the pathogenesis and categorization of these disorders.[2]

Typically, the onset of symptoms in CMT is observed in childhood, adolescence, or young adulthood. However, there is a subset of hereditary neuropathies with late onset of symptoms, after the fourth decade of life, and it so far has an unknown genetic substrate.[3] The late onset and the slowly progressive course of these neuropathies make differentiating them from acquired subacute and chronic polyneuropathies difficult. Next-generation sequencing has expanded and simplified the diagnostic yield of genes associated with all types of CMT,[4] but for the late-onset hereditary neuropathies, a relatively small number of genes have been implicated in the pathogenicity of the disorder.[5] Among these genes, mutations on the membrane metallo-endopeptidase (MME) gene have also been recently associated with late-onset CMT disease type 2 (CMT2), inherited either as fully penetrant autosomal-recessive or as incompletely penetrant autosomal-dominant traits.[6-11]

Case Report

Clinical Description

In this report, we describe a patient with adult-onset hereditary polyneuropathy. We received an informed consent from our patient and approval for the study from the hospital's ethics committee. A 48 year old male patient was admitted to our department because of slowly progressive weakness of the lower extremities (mainly of the right leg), beginning 2 years ago, resulting in difficulty in walking. The patient reported no previous history of any neurologic or systematic disease, apart from elevated creatine phosphokinase (CPK) serum levels (2500 IU/L; reference value 25–160 IU/L) after administration of hypolipidemic medication, which persisted at lower levels (660 IU/L) after discontinuation of the medication. Furthermore, after a thorough investigation, no family history of polyneuropathy or any other neurologic disorder was reported.

The neurologic examination revealed moderate muscular atrophy, weakness of the lower extremities at the peripheral parts and loss of tendon reflexes in the upper and lower extremities (**FIGURE 1**). Sen-

sory system examination seemed normal, for both somatosensation and proprioception. Laboratory testing confirmed the elevated levels of serum CPK. We then proceeded to an electroneurographic and electromyographic testing. Nerve conduction studies revealed a sensorimotor polyneuropathy affecting mainly the lower extremities. The upper extremities had normal values of compound muscle action potentials (CMAPs) whereas the lower extremities were affected in an asymmetric way. The CMAP of the right peroneus nerve had a latency of 6.0 milliseconds, an amplitude of 1.6 mV, a conduction velocity of 39.4 meters per second, and an absent F wave. For the left peroneus nerve, the respective values were as follows: a latency of 3.7 milliseconds, an amplitude of 7.5 mV, a conduction velocity of 45.5 meters per second, and a minimal F wave latency of 41.7 milliseconds. The examination of the sensory nerves revealed a symmetrical reduction in the amplitude of the compound sensory nerve action potentials (SNAPs) mainly involving the superficial peroneus nerve of the lower extremities (absent SNAP) and in the upper extremities the radial and ulnar nerves (4.0 μV). Electromyography showed fibrillations and positive waves in both the peripheral and proximal muscles of the lower extremities, predominantly in the right side distally. The diagram of the voluntary muscle activation and the morphology of motor units' potentials had chronic neuropathic characteristics.

Based on the aforementioned findings that showed a slowly progressive late-onset axonal polyneuropathy, we suspected a chronic acquired polyneuropathy with multiple polyneuritis characteristics. However, intensive laboratory testing of the cerebrospinal fluid and the peripheral blood revealed normal values. Furthermore, to evaluate the muscles, because of the patient's elevated CPK values, we proceeded with a muscular biopsy to a severely affected muscle, the gastrocnemius. The biopsy did not reveal any muscular pathology apart from widespread denervated muscle fibers.

Genetic Analysis

The polyneuropathy was classified as one of undetermined etiology, and we then proceeded to genetic testing with whole-exome sequencing according to the following described protocol. A DNA library construction using the Ion AmpliSeq Whole Exome RDY (Thermo Fisher Scientific, Waltham, MA) was performed. Briefly, 100 ng of gDNA was amplified and indexed with a unique adapter using the Ion Xpress barcode adapters kit (Thermo Fisher Scientific). Bar-coded libraries were purified using the Agencourt AMPure XP Beads (Beckman Coulter, Brea, CA), quantified using the Qubit 2.0 fluorometer (Thermo Fisher Scientific) and diluted to 100 pM. Template preparation was carried out on an Ion Chef instrument using the Ion 540 Kit—Chef (Thermo Fisher Scientific). Sequencing was performed on an Ion S5XL Semiconductor Sequencer, on 540 chip (Thermo Fisher Scientific). All procedures were performed according to the manufacturer's instructions. Sequencing raw data were analyzed for base calling, demultiplexing, alignment to the hg19 reference genome (GRCh37), coverage analysis, and variant calling on Torrent Suite 5.10 software (https://assets.thermofisher.com/TFS-Assets/LSG/manuals/MAN0017599_TorrentSuiteSoftware_5_10_RN.pdf), using a default parameter. The resulting variants (.vcf file) were imported for filtering, prioritization, and evaluation into the ClinGenics Exome Management Application-EM pipeline software, version 1.0.0.1 (ClinGenics Ltd., London, UK). Selected clinically significant variants were confirmed by standard DNA Sanger sequencing.

We detected a heterozygous mutation on MME gene c.617G > A (p.Gly206Asp). According to the American College of Medical Genetics and Genomics and the Association for Molecular Pathology (ACMG-AMP) 2015 guidelines, the variant was likely pathogenic based on the following criteria: (i) the absence of the c.617G > A (p.Gly206Asp) variant from control patients in the Exome Sequencing Project, the 1000 Genomes Project, or the Genome Aggregation Database (gnomAD) (moderate evidence of pathogenicity [PM2]); (ii) *in silico* bioinformatics tools (PolyPhen2, SIFT, and MutationTaster) that predicted that the variant causes a deleterious effect on the gene (supporting evidence of pathogenicity [PP3]); and (iii) the patient's phenotype was specific for the disease because mutations in MME have been associated with polyneuropathy. Variant novelty was assessed based on its absence from public databases and an in-house database housing >200 exomes belonging to Greek individuals (**FIGURE 2**).

Discussion

The MME gene encodes the enzyme neprilysin, which was first identified in 1973 in the kidneys and then in 1978 in the brain.[12,13] A few years later, in 1988, neprilysin was described as being identical to the common acute lymphocytic leukemia antigen.[14] Since then, the terms *neprilysin, membrane metallo-endopeptidase, neutral endopeptidase, cluster of differentiation 10,* and *common acute lymphoblas-*

FIGURE 1. Distal muscle atrophy in the lower extremities of the patient.

FIGURE 2. Chromatogram from Sanger Sequencing showing (A) the novel mutation in MME gene p.Gly206Asp and (B) a negative control. MME, membrane metallo-endopeptidase.

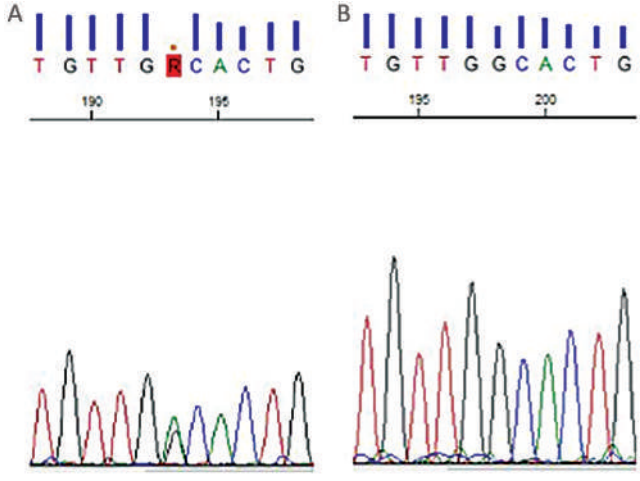

AQ7

TABLE 1. **Mutations on MME Gene Related to Late-Onset Polyneuropathies**

MME Mutation	Study	Number of Families	Mean Age of Onset	Origin	Inheritance	Clinical Diagnosis
c.654+1G > A (p.Gly179fs)	Higuchi et al, 2016[8]	3	47	Japan	AR	CMT2
c.1861T > C (p.Cys621Arg)	Higuchi et al, 2016[8]	1	56	Japan	AR	CMT2
c.661C > T (p.Gln221X)	Higuchi et al, 2016[8]	1	48	Japan	AR	CMT2
c.1231_1233delTGT (p.Cys411del)	Higuchi et al, 2016[8]	1	54	Japan	AR	CMT2
c.43912T > A (p.exon5del)	Higuchi et al, 2016[8]	1	50	Japan	AR	CMT2
c.1817G > A (p.Trp606X)	Higuchi et al, 2016[8]	1	40	Japan	AR	CMT2
c.65522A > G (p.exon8del)	Higuchi et al, 2016[8]	1	37	Japan	AR	CMT2
c.43912T > A (p.exon5del); c.65522A > G (p.exon8del)	Higuchi et al, 2016[8]	1	47	Japan	AR/sporadic; biallelic	CMT2
c.1579CNT (p.R527X)	Hsiao et al, 2017[9]	3	49	Taiwan	AR	CMT2
c.2075ANC (p.Q692R)	Hsiao et al, 2017[9]	2	56	Taiwan	AD	CMT2
c.466delC (p.Pro156Leufs*14)	Auer-Grumbach et al, 2016[6]; Lupo et al, 2018[7]	7	57	Sweden, United Kingdom, United States, Austria, Spain	AD; AR; sporadic	CMT1/CMT2; HMN; ALS
c.71G > A (p.Trp24*)	Auer-Grumbach et al, 2016[6]; Senderek et al, 2020[10]	1	60	Austria	AD/sporadic	CMT2
c.35A > C (p.Asp12Ala)	Auer-Grumbach et al, 2016[6]; Senderek et al, 2020[10]	1	69	Austria	AD/sporadic	CMT2
c.1040A > G (p.Tyr347Cys)	Auer-Grumbach et al, 2016[6]; Senderek et al, 2020[10]	2	50	Austria	AD/sporadic	CMT2
c.1042G > C (p.Ala348Pro)	Auer-Grumbach et al, 2016[6]; Senderek et al, 2020[10]	2	55	Austria	AD/sporadic	CMT2
c.1265C > A (p.Ala422Asp)	Auer-Grumbach et al, 2016[6]; Senderek et al, 2020[10]	2	39	Austria	AD/sporadic	CMT2/PNP
c.440_2A > C	Auer-Grumbach et al, 2016[6]; Senderek et al, 2020[10]	1	>35	Austria	AD/sporadic	CMT2
c.298_298delA (p.Thr100Profs*11)	Auer-Grumbach et al, 2016[6]; Senderek et al, 2020[10]	1	33	Germany	AD/sporadic	ALS
c.957delG (p.Lys319Asnfs*6)	Auer-Grumbach et al, 2016[6]	1	40	United States	AD/sporadic	CMT2
c.202C > T (p.Arg68*)	Auer-Grumbach et al, 2016[6]	2	42	United States	AD/sporadic	CMT2
c.1342 C > T (p.Arg448*)	Auer-Grumbach et al, 2016[6]; Lupo et al, 2018[7]; Senderek et al, 2020[10]	6	35	United States, Spain, Austria, Germany, Czech Republic, Poland	AD/AR; sporadic	CMT2; CMT2 + deafness
c.674G > C (p.Gly225Ala)	Lupo et al, 2018[7]	3	35	Spain	Sporadic	CMT1/dHMN
c.1229G > A (p.Arg410His)	Lupo et al, 2018[7]	1	51	Spain	Sporadic	CMT (possible)
c.773A > G (p.Gln258Arg)	Lupo et al, 2018[7]	1	30	Spain	AD	ALS
c.2248delT (p.Trp750Glyfs*24)	Lupo et al, 2018[7]	1	54	Spain	AD	ALS
c.1495G > A (p.Glu499Lys)	Lupo et al, 2018[7]	1	53	Spain	Sporadic	CMT2
c.1883A > G (p.Asn628Ser)	Lupo et al, 2018[7]	1	54	Spain	Sporadic	CMT1
c.1810G > A (p.Val604Ile)	Lupo et al, 2018[7]	1	55	Spain	AR	CMT2
c.1666C > T (p.Pro556Ser); c.1972G > A (p.A658T)	Lupo et al, 2018[7]	1	42	Spain	Sporadic; biallelic	CMT2
c.227delC (p.Thr77Leufs*16); c.1342C > T (p.Arg448*)	Lupo et al, 2018[7]	3	46	Spain	AR; biallelic	CMT2
c.1342C > T (p.Arg448*); c.2248delT (p.Trp750Glyfs*24)	Lupo et al, 2018[7]	1	35	Spain	Sporadic; biallelic	CMT2

TABLE 1. Continued

MME Mutation	Study	Number of Families	Mean Age of Onset	Origin	Inheritance	Clinical Diagnosis
c.196+1G > A; c.1342C > T (p.Arg448*)	Lupo et al, 2018[7]	1	44	Spain	AR; biallelic	CMT2
c.2134C > T (p.His712Tyr); c.71G > A (p.Trp24*)	Lupo et al, 2018[7]	2	63	Spain	AR; biallelic	CMT2
c.2067C > A (p.Asn689Lys); c.2242C > T (p.Arg748Trp)	Lupo et al, 2018[7]	1	40	Spain	AR; biallelic	CMT2
c.358G > A (p.Asp120Asn)	Senderek et al, 2020[10]	1	>35	Austria, Germany, Czech Republic, Poland	AR	CMT2
c.467delC (p.Pro156Leufs*14)	Senderek et al, 2020[10]	1	>35	Austria, Germany, Czech Republic, Poland	AD AR	CMT2
c.958-4_958-3delinsG	Senderek et al, 2020[10]	1	>35	Austria, Germany, Czech Republic, Poland	AR	CMT2
c.1345G > T (p.Glu449*)	Senderek et al, 2020[10]	1	>35	Austria, Germany, Czech Republic, Poland	AD; sporadic	CMT2
c.1505A > C (p.Tyr502Ser)	Senderek et al, 2020[10]	1	>35	Austria, Germany, Czech Republic	AD; sporadic	CMT2
c.1564C > T (p.Gln522*)	Senderek et al, 2020[10]	1	>35	Austria, Germany, Czech Republic, Poland	AR	CMT2
c.1706A > C (p.Gln569Pro)	Senderek et al, 2020[10]	1	>35	Austria, Germany, Czech Republic, Poland	AD; sporadic	CMT2
c.1946T > G (p.Ile649Ser)	Senderek et al, 2020[10]	1	>35	Austria, Germany, Czech Republic, Poland	AR; sporadic	CMT2
c.156317031G > A (p.Cys143Tyr)	Depondt et al, 2016[11]	7	56	Belgium	AD	CMT2/SCA43
c.617G > A (p.Gly206Asp)	Present study	1	46	Greece	Sporadic	CMT2

AD, autosomal dominant; AR, autosomal recessive; ALS, amyotrophic lateral sclerosis; CMT1, Charcot-Marie-Tooth type 1 (demyelinating); CMT2, Charcot-Marie-Tooth type 2 (axonal), dHMN, distal hereditary motor neuropathy; HMN, hereditary motor neuropathy; MME, membrane metallo-endopeptidase; PNP, peripheral neuropathy; SCA43, spinocerebellar ataxia 43.

tic leukemia antigen have been used indistinguishably to describe the enzyme that is encoded by the MME gene (BRENDA:EC3.4.24.11). Neprilysin belongs to a family of zinc metalloproteinases, highly conserved during the course of evolution, that plays an important role in turning off peptide signaling events at the cell surface and is involved in the metabolism of a number of regulatory peptides of the mammalian nervous, cardiovascular, inflammatory, and immune systems.[15] The wide distribution of neprilysin in different organs and its involvement in diverse functions justifies its implication in the pathogenesis of different disorders, like heart failure, tumors, and Alzheimer disease, making it an attractive target for diagnosis and therapeutic interventions.[16]

In 2016, mutations in the MME gene were identified as the cause of late-onset axonal-type CMT in 10 Japanese families with autosomal recessive inheritance.[8] In their study, Higuchi et al[8] were the first to document the causative relation of homozygous or compound heterozygous mutations on MME genes with axonal-type CMT. These mutations resulted in the reduction of neprilysin protein expression in the peripheral nervous system and were characterized as loss-of-function mutations. Likewise, in 2016, an MME mutation was found in a family with dominant spinocerebellar ataxia and neuropathy.[11] Furthermore, the same year, 51 patients of European and North American descent with late-onset CMT were also linked to MME variants.[6] Contrary to the previous study of Higuchi et al, the type of inheritance in this cohort was autosomal dominant with incomplete penetrance, probably leading to haploinsufficiency for neprilysin, interacting with other genetic and environmental factors for the development of the disorder.

In 2017, the genetic analysis of a similar cohort study on hereditary neuropathies of unknown etiology in Taiwan revealed 2 families with mutations in the MME gene and a late-onset axonal-type CMT, 1 with autosomal-recessive inheritance and the other with dominant inheritance.[9] Another study on MME mutations identified 20 Spanish families with 17 different variants of the MME gene with autosomal-recessive inheritance.[7] Almost half of the patients in this cohort seemed to have biallelic mutations in the MME gene, and these patients had a homogeneous phenotype that consisted of late-onset axonal CMT. Interestingly, patients of this study with heterozygous variants presented a more varied spectrum of phenotypes including CMT2, but it is possible that some of the mildest or alternative phenotypes were associated with harmless MME variants and coincidental findings. A recent study on unexplained axonal neuropathies in older adults carried out by Senderek et al[10] reported that MME was the most frequently involved gene identified in the genetically solved case studies. Both incompletely penetrant autosomal-dominant and autosomal-recessive types of inheritance were observed, with the first type being more frequent.[10]

AQ8

The mutations in the MME gene that have been so far associated with late-onset axonal CMT are summarized in **TABLE 1**. Identified MME mutations were either loss-of-function alleles (nonsense, frameshift, splice site) or missense variants and, compared to public databases and control patients, indicated a significant association with late-onset neuropathies.[6-8] The most common MME mutations described in these studies were c.466delC (p.Pro156Leufs*14) and c.1342 C > T (p.Arg448*), appearing in different studies and in families of different origin.

The clinical features and electrophysiological findings of most of the patients harboring MME gene mutations in all 5 studies evaluated were typical for late-onset axonal type CMT. The age at onset for most of them was in the fourth decade of life or later. The patients developed slowly progressive weakness and atrophy, which initiated from the distal lower limbs and spread to the distal upper limb muscles over a period of several years.[6-10] Our patient's clinical phenotype and the course of the disease fit well with the phenotype described in these studies. In addition, the mutation found in our patient's MME gene represented a strong missense change that is not registered in the Genome Aggregation Database (gnomAD; https://gnomad.broadinstitute.org/) and was classified as likely pathogenic according to the American College of Medical Genetics. However, the lack of a segregation study, further functional data, and any replication among other patients from previous studies kept us from attributing a certain pathogenetic role to the identified variant, which was therefore classified as likely pathogenic for late-onset CMT2.

The role of neprilysin in the peripheral nervous system is not yet well understood. It has been isolated from both the developing and the adult mammalian peripheral nervous system.[17,18] Furthermore, overexpression has been observed after axonal damage in adult rat Schwann cells in the sciatic nerve.[19] These findings suggest that neprilysin could play a role in peripheral nerve development and axonal regeneration. But because it is mainly localized on Schwann cells and the patients with mutations in the MME gene typically present with axonal neuropathy, the hypothesis that neprilysin degenerates peripheral nerve axons by impairing Schwann cell–axonal interactions seems reasonable.[8] However, greater mutation numbers in different populations, along with mutation-specific functional studies, will be important for the characterization of the pathogenicity and inheritance of more MME variants.

REFERENCES

1. Hattori N, Yamamoto M, Yoshihara T, et al. Demyelinating and axonal features of Charcot-Marie-Tooth disease with mutations of myelin-related proteins (PMP22, MPZ and Cx32): a clinicopathological study of 205 Japanese patients. *Brain*. 2003;126(Pt 1):134–151.
2. Pipis M, Rossor AM, Laura M, Reilly MM. Next-generation sequencing in Charcot-Marie-Tooth disease: opportunities and challenges. *Nat Rev Neurol.* 2019;15(11):644–656.
3. Bennett CL, Lawson VH, Brickell KL, et al. Late-onset hereditary axonal neuropathies. *Neurology.* 2008;71(1):14–20.
4. Morena J, Gupta A, Hoyle JC. Charcot-Marie-Tooth: from molecules to therapy. *Int J Mol Sci.* 2019;20(14):3419.
5. Callegari I, Gemelli C, Geroldi A, et al. Mutation update for myelin protein zero-related neuropathies and the increasing role of variants causing a late-onset phenotype. *J Neurol.* 2019;266(11):2629–2645.
6. Auer-Grumbach M, Toegel S, Schabhüttl M, et al. Rare variants in MME, encoding metalloprotease neprilysin, are linked to late-onset autosomal-dominant axonal polyneuropathies. *Am J Hum Genet.* 2016;99(3):607–623.
7. Lupo V, Frasquet M, Sánchez-Monteagudo A, et al. Characterising the phenotype and mode of inheritance of patients with inherited peripheral neuropathies carrying MME mutations. *J Med Genet.* 2018;55(12):814–823.
8. Higuchi Y, Hashiguchi A, Yuan J, et al. Mutations in MME cause an autosomal-recessive Charcot-Marie-Tooth disease type 2. *Ann Neurol.* 2016;79(4):659–672.
9. Hsiao CT, Liao YC, Soong BW, Lee YC. Mutations in MME cause axonal CMT in a Taiwanese cohort with inherited polyneuropathy. *J Neurol Sci.* 2017;381:463.
10. Senderek J, Lassuthova P, Kabzińska D, et al. The genetic landscape of axonal neuropathies in the middle-aged and elderly: focus on MME. *Neurology.* 2020;95(24):e3163–e3179.
11. Depondt C, Donatello S, Rai M, et al. MME mutation in dominant spinocerebellar ataxia with neuropathy (SCA43). *Neurol Genet.* 2016;2(5):e94.
12. George SG, Kenny J. Studies on the enzymology of purified preparations of brush border from rabbit kidney. *Biochem J.* 1973;134(1):43–57.
13. Malfroy B, Swerts JP, Guyon A, Roques BP, Schwartz JC. High-affinity enkephalin-degrading peptidase in brain is increased after morphine. *Nature.* 1978;276(5687):523–526.
14. Letarte M, Vera S, Tran R, et al. Common acute lymphocytic leukemia antigen is identical to neutral endopeptidase. *J Exp Med.* 1988;168(4):1247–1253.
15. Turner AJ, Isaac RE, Coates D. The neprilysin (NEP) family of zinc metalloendopeptidases: genomics and function. *Bioessays.* 2001;23(3):261–269.
16. Feygina EE, Katrukha AG, Semenov AG. Neutral endopeptidase (Neprilysin) in therapy and diagnostics: yin and yang. *Biochemistry (Mosc).* 2019;84(11):1346–1358.
17. Kioussi C, Crine P, Matsas R. Endopeptidase-24.11 is suppressed in myelin-forming but not in non-myelin-forming Schwann cells during development of the rat sciatic nerve. *Neuroscience.* 1992;50(1):69–83.
18. Kioussi C, Matsas R. Endopeptidase-24.11, a cell-surface peptidase of central nervous system neurons, is expressed by Schwann cells in the pig peripheral nervous system. *J Neurochem.* 1991;57(2):431–440.
19. Kioussi C, Mamalaki A, Jessen K, Mirsky R, Hersh LB, Matsas R. Expression of endopeptidase-24.11 (common acute lymphoblastic leukaemia antigen CD10) in the sciatic nerve of the adult rat after lesion and during regeneration. *Eur J Neurosci.* 1995;7(5):951–961.

An African American Male Patient with Rare Type B Insulin Resistance Syndrome

Ishwarlal Jialal, MD, PhD, FRCPATH, DABCC,[1,*] *Sridevi Devaraj, PhD, DABCC, FRSC*[2]

[1]VA Medical Center, Mather, California, US; [2]Baylor College of Medicine, Houston, Texas, US; *To whom correspondence should be addressed. kjialal@gmail.com

Keywords: insulin resistance, diabetes, autoantibodies, insulin receptors, insulin, immunosuppressants

Abbreviations: SLE, systemic lupus erythematosus; T2DM, type 2 diabetes mellitus; AA, African American; CHF, congestive heart failure; IVIG, intravenous immunoglobulin; NIH, National Institutes of Health.

Laboratory Medicine 2022;53:215–217; https://doi.org/10.1093/labmed/lmab076

ABSTRACT

Syndromes of severe insulin resistance can result from mutations in the insulin receptor gene or autoantibodies to the insulin receptor. The type B syndrome of insulin resistance results from autoantibodies to the insulin receptor and occurs predominantly in women under age 50 years. Here we report on a 64 year old African American man with systemic lupus erythematosus (SLE) and acanthosis nigricans who had severe insulin resistance requiring up to 5000 units of insulin per day. He was diagnosed with type B insulin resistance syndrome based on his clinical presentation and demonstration of autoantibodies to the insulin receptor in his serum. This case study underscores the importance of assaying for autoantibodies to the insulin receptors especially in African American patients with severe insulin resistance and diabetes requiring excessive doses of insulin, in the setting of an autoimmune disease like SLE. It also behooves reference laboratories to develop and offer this assay because these patients have a very high mortality.

The majority of patients with type 2 diabetes mellitus (T2DM) have some degree of insulin resistance that coupled with insulin deficiency contributes to the genesis of T2DM.[1] Rare syndromes of severe insulin resistance can result from mutations in the insulin receptor gene (type A), resulting in a decrease in receptor numbers, or autoantibodies to the insulin receptor (type B syndrome of insulin resistance).[2] In this case study we report on an African American (AA) male patient with systemic lupus erythematosus (SLE) who had a type B syndrome of severe insulin resistance that responded to high-dose steroid therapy.

Case Study

A 64 year old male patient of AA origin was admitted with complaints of shortness of breath, weakness, and poor appetite with a duration of almost a month. He had 2 previous admissions in another local hospital in the month before his admission to our Veterans Affairs hospital with similar complaints along with chest pain for which he had undergone cardiac catheterization at another hospital, revealing diffuse coronary artery disease. He also had a history of T2DM, hypertension, hyperlipidemia, SLE, chronic kidney disease, peripheral arterial disease, congestive heart failure (CHF), gout, and depression. Almost 2 months before admission he had stopped taking his medications for diabetes and had stopped all other medications almost a month before admission. Family history for chronic disease was positive; his mother had T2DM, hypertension, and a stroke. He was married, consumed alcohol occasionally, was not a smoker, and had no history of any recreational drug use. Medications before admission included metformin 850 mg twice a day, glyburide 10 mg daily, plaquenil 200 mg twice a day, prednisone 5 mg daily, furosemide 40 mg daily, aspirin 81 mg daily, losartan 25 mg daily, atenolol 50 mg daily, and allopurinol 300 mg daily.

Physical examination revealed an older man lying in bed who was slow to answer questions but was alert, awake, and oriented. Examination of his neck showed an elevated jugular venous pressure. His body mass index was 26.5 kg/m^2. The cardiovascular exam revealed a regular heart rate, no murmurs, and bibasilar crackles. His abdominal exam did not reveal any visceromegaly. He had bilateral pedal edema with feeble peripheral pulses bilaterally (1+). Central nervous system exam revealed good muscular power, intact cranial nerves, and normal reflexes and sensation. He had evidence of acanthosis nigricans and skin tags on the back of the neck (both occurring together are clinical signs of insulin resistance).

Routine laboratory tests (reference ranges in parentheses) revealed the following: glucose 372 mg/dL (70–99 mg/dL), sodium 127 mmol/L (136–144 mmol/L), potassium 5.1 mmol/L (3.4–4.8 mmol/L), blood urea nitrogen 38 mg/dL (8–26 mg/dL), creatinine 4.37 mg/dL (0.5–1.1 mg/dL), estimated glomerular filtration rate 16.7 mL/min/m^2 (≥60 mL/min/m^2), albumin 2.4 g/dL (3.3–4.8 g/dL), white blood cell count 4.0 K/mm^3 (4.5–11 K/mm^3), hemoglobin 9.7 g/dL (12–16 g/dL), B-type natruretic peptide 331 pg/mL (0.0–100 pg/mL), and hemoglobin A1c 8.7% (<7%). The patient's laboratory tests supported his diagnoses of chronic kidney disease, diabetes, anemia, and CHF. Chest X-ray revealed bilateral

increased vascular marking consistent with fluid overload and CHF. He was admitted with a diagnosis of decompensated CHF and acute on chronic renal failure in a patient with SLE and uncontrolled T2DM.

For better glycemic control the patient was started on glargine, a long-acting insulin, and aspart insulin, a short-acting insulin. Initially his blood glucose levels remained in the range of 200 to 300 mg/dL and gradually increased to 400 to 500 mg/dL over the next few days, leading to an increase in both long- and short-acting insulin doses and then to an intravenous insulin infusion of up to 60 units/hour. Endocrinology was consulted for management of diabetes. On day 12 of the inpatient stay, the patient was noted to be more somnolent, stopped accepting oral intake, and needed no insulin for a few days because his blood glucose stayed at approximately 100 mg/dL. This development was followed by hypoglycemia with blood glucose levels dropping up to 30 mg/dL, requiring 10% dextrose infusions. A corticotropin stimulation test done at this time was normal, with a peak cortisol of >18 μg/dL (reference range: peak level >18 μg/dL).

The patient was also found to have an elevated sedimentation rate, with antinuclear antibodies (speckled pattern) titres of 1/5120 (<1/40), anti-double-stranded DNA of positive 1:40 (<1/10), and low complement C3 levels of 23 mg/dL (82–167 mg/dL). He was started on plaquenil 200 mg twice a day and intravenous methylprednisone 1000 mg for 3 days, then prednisone 75 mg/day. He again developed hyperglycemia after the burst of high-dose methylprednisone, with blood glucose levels increasing to 710 mg/dL with a normal anion gap and an osmolality of 328 requiring intravenous insulin infusion initially at 20 units/hour, gradually increasing to 250 units/hour. At this stage, the patient's total insulin requirements were 5000 units of insulin per day with blood glucose levels staying in the 300 range. He was also started on pioglitazone 45 mg daily, he continued on prednisone 75 mg daily, and his insulin resistance seemed to be improving as manifested by lower glucose levels, and he was taken off the insulin infusion. This development was again followed by fasting hypoglycemia when he had to go for any procedures requiring 10% dextrose infusions. The patient's serum tested negative for anti-insulin antibodies.

Method of Detecting Autoantibodies to the Insulin Receptor

To determine whether this patient had type B insulin resistance syndrome (characterized by autoantibodies to insulin receptors), insulin receptor autoantibodies were assayed. Because there was no commercial assay for insulin receptor autoantibodies, specimens before and after treatment were tested for insulin receptor autoantibodies following the immunoprecipitation method described by Arioglu et al.[3] For the insulin receptor autoantibodies assay, recombinant human insulin receptors (Santa Cruz, CA) were transfected into Cos7 cells using lipofectamine (all purchased from Thermo Fisher Scientific, Waltham, MA). Solubilized Cos7 cells were incubated with either normal serum (negative control specimen) or the patient's serum or an anti-insulin receptor antibody (positive control specimen; Santa Cruz, CA). The antibody bound receptors were then precipitated with a peroxidase-affinity goat anti-rabbit IgG-Fc fragment-specific antibody (Jackson Laboratories) followed by Western blot using anti-insulin receptor beta-subunit rabbit polyclonal antibody C19 (Santa Cruz, CA).

FIGURE 1 shows the Western blot after immunoprecipitation and indicates that the patient had autoantibodies (lanes 1–4) while on steroid therapy compared to normal serum (lane 5), but they were less

FIGURE 1. Immunoprecipitation assay for detecting insulin receptor autoantibodies. Cos7 cells were transfected with recombinant human insulin receptors. Next, the cellular extract was incubated with the patient's serum on steroid treatment, normal serum (negative control), and a positive control. The antibody bound receptors were then precipitated with a peroxidase-affinity goat anti-rabbit IgG-Fc fragment-specific antibody followed by Western blot using an anti-insulin receptor Beta-subunit rabbit polyclonal antibody. The beta subunit band shown on the gel has a molecular mass of 85 kD.

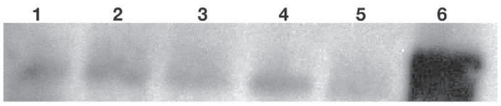

1 Patient, day 1
2 Patient, day 2
3 Patient, day 3
4 Patient, day 4
5 Normal serum
6 Positive control

abundant than in the positive control specimen (lane 6), which seemed to be overloaded.

The patient was then given intravenous immunoglobulin (IVIG) at 30 g × 5 days and then started on mycophenolate mofetil 500 mg twice a day. He finally stabilized on a combined glargine and aspart insulin regimen and was discharged to an extended-care skilled nursing facility on immunosuppressant therapy. During his stay in the skilled nursing facility, his insulin resistance improved and he required lower doses of insulin. He unfortunately died 3 months later while at the nursing facility. The cause of death was not determined.

Discussion

In 1976, Kahn et al described 2 distinct syndromes of insulin resistance: type A and type B.[2] In type A insulin resistance, the number of insulin receptors is decreased because of mutations in the insulin receptor.[2] Autoantibodies to insulin receptors are a rare and difficult-to-treat cause of type B insulin resistance. To date, its prevalence has not been determined. The majority of patients with this condition have been reported at the National Institutes of Health (NIH), which has the largest series of such patients (n = 34).[3,4] In the NIH series, the majority of their patients have been female (85%) and AA (85%), with acanthosis nigricans in 92% along with hyperandrogenism (common in females). These patients can present with hyper- or hypoglycemia. Insulin receptor autoantibodies causing type B insulin resistance occur in patients with autoimmune diseases, mainly SLE and mixed connective tissue disorder.[2,3] The circulating antibodies are polyclonal and of the IgG class.[2–4] The presentation can vary from severe insulin resistance with hyperglycemia refractory to high-dose insulin therapy or hypoglycemia.[2-4]

Our patient had acanthosis nigricans (a clinical marker of insulin resistance), which is present in 92% of patients with type B insulin resistance[2-4]; severe insulin resistance requires very large doses of insulin. He also had SLE, which is the most common autoimmune disease in patients with type B insulin resistance syndrome. In the NIH series, SLE was present in 41% of patients with another 24% having 3 of the 4 criteria for SLE. These patients usually have normal or low triglyceride

2022;53;215–217 | https://doi.org/10.1093/labmed/lmab076

levels (<160 mg/dL).[2-4] We could not confirm this information because we could not have access to the original patient records.

Using an immunoprecipitation assay, we confirmed our clinical diagnoses by showing the presence of antibodies to the insulin receptor in the patient's serum (**FIGURE 1**). Thus, we add to the small number of male patients reported to have type B syndrome. The NIH, which is also a referral center, followed up patients for ≥30 years and have only recorded 5 male patients, underscoring the rarity of type B syndrome in male patients. Interestingly, type B insulin resistance has been shown to manifest after the onset of systemic autoimmune disease, especially SLE.

The type B syndrome of insulin resistance results from an autoantibody acting against the insulin receptor. The autoantibody acts as a partial agonist, stimulating the insulin receptor at low titers causing hypoglycemia. At higher titers it is antagonistic to the insulin receptor, causing the downregulation of cellular responses to insulin, leading to severe insulin resistance and attendant hyperglycemia.[2-4]

Therapy for type B insulin resistance is aimed at correcting hyper- or hypoglycemia and using immunosuppression to decrease the antibody titers. Various steroid preparations, IVIG, plasmapheresis, and immune suppressants including azathioprine, mycophenolate mofetil, and rituximab have been used.[3–6] High-dose steroids were shown to be an effective initial therapy in our patient.

The presence of autoantibodies to the insulin receptor should be considered in any patient with diabetes with severe insulin resistance requiring excessive doses of insulin in the setting of an autoimmune disease like SLE, especially in patients of AA descent. Presently there does not seem to be any commercially available assay for this rare but important and treatable disorder. Hopefully in the future an assay will be developed by reference laboratories to allow clinicians to confirm their clinical diagnosis and manage patients appropriately because immunosuppressant therapy seems to be efficacious. Undiagnosed and untreated, these patients have a very high mortality, approximating 50%.[2-4]

Acknowledgments

We thank the family for allowing us to publish this report, respecting confidentiality. We also thank Dr Jaspreet Kaur for her excellent clinical care of this patient while she was an Endocrine Fellow in our program.

Conflict of Interest

None of the authors have any conflict of interest to declare.

REFERENCES

1. American Diabetes Association. 2. Classification and diagnosis of diabetes: *Standards of Medical Care in Diabetes-2021. Diabetes Care.* 2021;44(Suppl 1):S15–S33.
2. Kahn CR, Flier JS, Bar RS, et al. The syndromes of insulin resistance and acanthosis nigricans. Insulin-receptor disorders in man. *N Engl J Med.* 1976;294(14):739–745.
3. Arioglu E, Andewelt A, Diabo C, Bell M, Taylor SI, Gorden P. Clinical course of the syndrome of autoantibodies to the insulin receptor (type B insulin resistance): a 28-year perspective. *Medicine (Baltimore).* 2002;81(2):87–100.
4. Lupsa BC, Chong AY, Cochran EK, Soos MA, Semple RK, Gorden P. Autoimmune forms of hypoglycemia. *Medicine (Baltimore).* 2009;88(3):141–153.
5. Censi S, Mian C, Betterle C. Insulin autoimmune syndrome: from diagnosis to clinical management. *Ann Transl Med.* 2018;6(17):335.
6. Malek R, Chong AY, Lupsa BC, et al. Treatment of type B insulin resistance: a novel approach to reduce insulin receptor autoantibodies. *J Clin Endocrinol Metab.* 2010;95(8):3641–3647.

IN MEMORIAM

Frieda Carson

Christa Hladik Cappellano and Joshua Weikersheimer

Laboratory Medicine 2022;53:218; https://doi.org/10.1093/labmed/lmac007

Freida L. Carson, PhD, HT(ASCP), an admired teacher, mentor, and friend of students, histology professionals, pathologists, and histology organizations, passed on January 11, 2022, at the age of 95. The advancement and promotion of the histology profession was a life-long commitment for Dr Carson, who shared her knowledge with numerous students and histology professionals for over 65 years. She was a gracious and humble teacher who instilled in her students a passion for the patient while stressing the importance of understanding histologic theory and technique.

In 1947, Dr Carson graduated from Texas State College for Women (now Texas Woman's University) with a Bachelor of Science in Chemistry. In January of 1956, Dr Carson began her employment at Baylor University Medical Center Dallas Texas in the Histology laboratory to assist with troubleshooting staining issues. Six months later, she was promoted to Histology Laboratory Supervisor. During her tenure at Baylor, she developed a histology training program which later become one of the first accredited programs. Over the years histology students have had the honor of being in her training program or attending lectures at state or national meetings. Students observed her passion for sharing technical applications and challenging them to expand their knowledge. The teacher was also a student, completing a master's degree in 1976 and PhD in 1980, both from Baylor University. It was during a graduate school research project she decided to evaluate formalin tissue fixatives in the pursuit of a dual fixative that would work for both electron and light microscopy. From this project the Carson Modified Millonig Formalin was developed and continues to be used today. Dr Carson retired after 40 years from Baylor University Medical Center in 1990.

Early in her career, Dr Carson was encouraged to get involved in affiliated national organizations. Engagement in these organizations set her on a journey of a lifetime promoting the growth, advancement, and evolution of the histology profession through lectures, presentations, and creation of educational materials. She remained active for many years beyond retirement in both state and national organization programs that included the National Society of Histotechnology, College of American Pathologists, and American Society for Clinical Pathology (ASCP), Board of Certification. It would be impossible to calculate the number of hours Dr Carson volunteered over the past 65 years.

The ASCP Dr Carson in as a consultant to the Board of Registry, Histology Examination Committee in 1973 during the time of committee development. Her key contribution was in the development of training materials used for slide grader orientation. She became a committee member in 1980 continuing through 1992, served as Chair from 1982 to 1983, and Board Liaison 1984-1992. Dr Carson served as the National Society for Histotechnology (NSH) representative to the Board of Registry (BOR) Board of Governors from 1983 to 1992, and for six years held the position of Secretary of the Board. Dr Carson's contributions in the development of educational materials used to prepared students to take the ASCP registry certification examination gained her significant recognition. She was awarded the ASCP Technologist of the year in 1992 and the BOG Distinguished Service Award in 1993. In 2010 she was awarded ASCP Mastership.

The other side of Dr Carson's work brought her mastery of histotechnology and her skill as a teacher to a series of books. Her original idea of a correspondence course evolved into a full-fledged textbook specifically designed for both self-instruction and classroom use. The first edition of *Histotechnology: A Self Instructional Text* published in 1990 and became an immediate hit. The book was praised for its comprehensive coverage, clarity of expression, insider tricks of the trade, and exemplary images and illustrations. She continued publication by heading up the *BOR Practice Questions for the Histotechnology Examinations*, which emerged in 2 editions in the 1990s. Her self-instructional text became a standard in the field, and she developed a companion workbook, *Histotechnology: A Self Instructional Workbook* in 1997 to join the second edition of her textbook. She then oversaw development of the practice questions idea into the base for a richer *BOC Study Guide for Histotechnology* in 2013, even while bringing her textbook/workbook--now with her coauthor Christa Cappellano--through 2 more editions. As if that were not enough, she concurrently developed *HistoDeck*, a set of flashcards to bring yet one more study option to bear. In late 2020, her fifth and final editions of *Histotechnology* and its companion workbook premiered, having been developed in defiance of the cancer that began to set in. She was an indefatigable writer who enjoyed working with colleagues as her books expanded in scope to cover new techniques in immunohistochemistry, enzyme histochemistry, and cytopreparatory techniques.

In December 2021, Baylor Scott & White (BS&W) pathology division held a dedication ceremony to honor Dr Carson with the opening of the "Dr Freida Carson Histology Laboratory". Dr Carson was present and celebrated with the BS&W Health administration, pathology leadership and laboratory, representatives from TSH and NSH, ASCP publisher, friends, and professional colleagues. The dedication highlighted Dr Carson's 40 years of service and her contributions to the betterment of the BS&W patients. Dr Carson's work will live on through the BS&W Histology Laboratory, her students, and the future generations of histologists. The reach of her teachings spans across the globe through textbooks, workbooks, and recorded webinars. Dr Carson dedicated her life's work to the field of histology and set the bar high for those who followed. The histology community lost a great icon. She was a trailblazer paving the way for the histology profession. We are forever grateful for her years of tireless dedication.

Reviewers List

The *Laboratory Medicine* staff would like to extend a warm thank you to our 2021 *ad hoc* reviewers. We appreciate your time and dedication to the journal.

Jude Abadie
Omneya Abdel Karem
Emad S. Abood
Florence Abravanel
Wendy Adams
Kehinde Adekola
Gouri Adel
Rajiv Agarwal
Shweta Agarwal
Yash Pal Agarwal
Himansu Aggarwal
Pascale Akl
Ralph Akyea
Kalichamy Alagarasu
Mohammad Alam
Subhi Al'Aref
Emine Tugba Alatas
Hadeel Alboaklah
Maicon Rodrigues Albuquerque
Kevin Alby
Fatima Aldarweesh
Evan Alexander
Khaled ALGhareeb
Mohamed H. Al-Hamed
Mahesheema Ali
Mustafa Ali
Gunay Aliyeva
Ahmed Aljudi
John Alsobrook
Mohammad Al-Tamimi
Mehmet Akif Altay
Carlos Alvarado
Khalid Alyodawi
Olga Amengual
Konstantinos Anagnostopoulos
Simon Anders
Maria Andersson
K Andreasson
Laura Andreoli
Brooke Andrews
Marianna Antonelou
Vidya Arankalle
Sophie Arbefeville
David Armbruster
Emiliano Aroasio
Manuel Arroyo
A. E. Arzuhal
Diler Aslan
Joanna Asprer
Brad C.Astor
Michel Attal
A. Avogaro
Agnes Aysola
Vahid Azimi
Yoshifumi Baba
Esther Babady
Dimitrios Babalis
Ghufran Babar
Zsuzsa Bagoly
Jianfa Bai
David Bailey
Tamam Bakchoul
Steven Baker
Kayode Balogun
Burhan Balta
Niaz Banaei
Thomas Bane
Dithi Banerjee
Vilte Barakauskas
Mustafa Barbhuiya
Alan N. Barkun
Else Marie Bartels
Luisa Barzon
Davood Bashash
Umberto Basile
Nikola Baumann
Rebecca Bearden
Danelle Beaudoin
Charles Beavers
Charlotte Becker
Andjelo Beletic
Andrew Bellizzi
Ghita Benjelloun Touimi
Isabela Judith Martins Bensenor
Laiz Bento
Mary Berg
Daniel Beriault
Jess Francisco Bermejo-Martn
Vipin Bhayana
Bianca Bianco
Beata Biesaga
Giulia Bivona
Einar S. Bjornsson
C-Thomas Bock
Geza Bodor
Francesco Bonfante
Kevin Booth
Roger Bouillon
Brendan Boyce
Tiffany Bratton
Massimo Breccia
John Breneman
Frank Bridoux
Ashton Brock
Laura Brown
Richard N. Brown
Janetta Bryksin
Dustin Bunch
Eileen Burd
Thierry Burnouf
Joshua Buse
Francesco Bussu
Andrew Cameron
Sean Campbell
Ali Canbay
Zheng Cao
Dean Carlow
Analia Carmo
Mark Cervinski
Vimal Chadha
Jasper Fuk-Woo Chan
Pak Cheung Chan
Thomas Chan
Wah Kheong Chan
Wayne Chandler
Kaushik Chatterjee
Shweta Chaudhary
Dong Chen
Qi Chen
Sindhu Cherian
L. Chiovato
Seetharamaiah Chittiprol
Monica Chavez Vivas
Jacky Chow
Candace Chow
Chih-Sheng Chu
Ki Wha Chung
Jorie Colbert-Getz
Jessica Colon-Franco
Laura Cooling
Josef Coresh
Victor M. Corman
C. Corpechot
Claudiu Cotta
Steven Cotten
Barbora de Courten
Benjamin J. Cowling
Genevieve Crane
Michael H. Criqui
Brian R Curtis
Zhi-Jun Dai
Elisa Danese
J. Lucian Davis
Alexandre de Lencastre
M. Dedicoat
George Deeb
Sofie Degerman
Pierre Delanaye
Meghan Delaney
Wael Demian
Diana Desai
Sridevi Devaraj
Yvan Devaux
Katrien Devreese
S. L. Diamond
Jane Dickerson
Johannes Wolfgang Dietrich
Jo-Anne R. Dillon
Angela Dispenzieri
Sabine Dittrich
Wolfram Doehner
Julia Drees
Alexander Duncan
Muhammed Emin Düz
Walter Dzik
R. Eastell
Rebecca Edwards
John Eikelboom
Adetoun Ejilemele
Daniel Eklund
Siba El Hussein
Rehab Abd El-Baky
Walaa El-Gazzar
Joe El-Khoury
Perry Elliott
Tze-Kiong Er
Lise Estcourt
Reza Fadaei
Al Muhaisen Fadi
Ramces Falfan-Valencia
Chunhai Fan
Corinne Fantz
Boris Fehse
Matthew Feldhammer
Yu-Qi Feng
Angela Ferguson

Donna Ferguson
Fernando Fervenza
Theodosios D. Filippatos
William Finn
Judith Fischer
Ryan Fischer
Maria Fleseriu
David Fox
Elizabeth Frank
Simon D Fraser
John Frater
Antonia Garrido Frenich
Marvin Jacob Fritzler
Jonathan Fromm
Shinji Fukata
Andrea Gaedigk
Jonathan Galeotti
Michael Gannett
Shou-Jiang Gao
Jörn-Markus Gass
Mathias Gautel
Michael Gautreaux
Charlotte A. Gaydos
Eric Gehrie
Michael Gelinsky
Carlo Genova
Gareth Gerrard
Antonino Giambona
Richard Gibbs
Pauline Gilson
Alan S. Go
Jeffrey Goldsmith
Brenda PFA Gomes
Alvaro Gonzalez
Cassandra Goulet
Francesca Romana Grati
Dina Greene
Martha Grogan
Bartosz Grzywacz
Ming Guan
Jeannette Guarner
Bayram Gulpamuk
Ming Guo
Gordon Guyatt
Peter Hackman
Jens Andre Hammerl
Timm Harder
Amanda Harrington
Susan Harrington
Cornelis Harteveld
Marwa Hassan
Sanchita Hati
Shannon Haymond
Pei He
Jennifer L. J. Heaney
Robert A. Hegele
Ray Hershberger
Angie S. Hinrichs
Rudolf Hoermann
Paul Hofman
Michael F Holick
Ivana Hollan
Brett Holmquist
Paul Holvoet
Daojun Hong
Pedro Horna
Peter Horvatovich
Mike Horwath
Jonathan Hoyne
Ralph Hruban
Frank Hu
Ying Huang
L. Hui
Romney Humphries
Mina Hur
Ayman Ibrahim
Peter Igaz
Minehiko Inomata
Giovanni Insuasti-Beltran
Tina Ipe
David Isenberg
Vanya Jaitly
Bryksin Janetta
Petr Jezek
Nan Jiang
Kim JiYeon
Ulrika Johansson
Newell W. Johnson
Niels Jonker
Annemiek M. C. P. Joosen
Steven E. Kahn
Hassen Kamoun
F. Karateke
Amy Karger
Prabhjot Kaur
Sukhbir Kaur
Makoto Kawai
Sue Kehl
Tanika N. Kelly
David Keren
Hemamalini Ketha
Boitumelo Kgarebe
Kay-Tee Khaw
Chang-Seok Ki
Fadime Kilinc
Byung-Soo Kim
Won Kim
Bob Kirkcaldy
Ulrich J. Knappe
Joel Kniep
Vijaya Knight
Won-Jung Koh
Zenon J.Kokot
Daryl J. Kor
Nichole Korpi-Steiner
Anne Kruchen
Attila Kumanovics
Pradeep Kumar
Kristine Kuus
Patrick Kyle
Robert Kyle
Helen Lachmann
Ajit Lalvani
Christopher Lam
Michelle Lamendola-Essel
David E. Leaf
Chen Lechuang
Hian Kee Lee
Young Lee
C. Rene Leemans
Guang Lei
Jerome A. Leis
Will Lester
Edward Leung
AS Levey
Stanley Levinson
Sebastien Lhomme
Chi Kong Li
Hui Li
Renhao Li
Songtao Li
Xia Li
Guanfeng Lin
Yulia Lin
Adrian Linacre
Rafael Linden
Giuseppe Lippi
Paul Lips
Petra Liskova
Ton Lisman
Randie Little
Christine Litwin
Stan Lo
Michael Loffelholz
R. Russell Lonser
Stephan Lotitz
Yongning Lu
Zhe Luo
Yitong Ma
Zhongliang Ma
Mark J. MacLachlan
Anu Maharjan
Etienne Mahe
Cheryl Maier
Susan Mallett
Thomas Mandl
Roberto Mandrioli
Jinyuan Mao
Marisa Marques
Julio Gonzalez Martinez
Alan Maschek
Christopher McCudden
Mary Frances McMullin
Rupal Mehta
Asuncion Mejias
Qing Meng
Begona Merinero
Giampaolo Merlini
Pierluigi Meroni
Luisa Mestroni
Ryan Metcalf
Ozgur Mete
Kotb Abbass Metwalley
Klaus H. Metzeler
Antonios G. Mikos
Malgorzata Milkiewicz
Piotr Milkiewicz
Gerald Miller
John D. Minna
Stephanie Mitchell
Atsushi Miyawaki
Koichi Mizuta
Martina Montagnana
Nathan Montgomery
Emily W. Moody
Ichiro Morioka
Gerald Morris
Lorena Mosso
Vaishali Moulton
Pawel Mroz
Alagarraju Muthukumar
Peder Myhre
Megan Nakashima
Sara Nandiwada
Samih H. Nasr
Christopher Naugler
David Navarro
Kenrad Nelson
Peter Nemes
Paul Ness
Karin Neufeld
David Ng
Heyu Ni
Sarah M. Nielsen
Eijun Nishihara
Hitoshi Okada
Olajumoke Oladipo
Horatiu Olteanu
Torbjorn Omland
Sarah Ondrejka
Onya Opota
Raffaella Origa
Tadeusz Osadnik
Yusra Othman

Xueling Ou
Seyda Efsun Ozgunay
Vrajesh Pandya
John Papp
Samantha E. Parker
D. Pastuszak-Lewandoska
Elizabeth Pearce
Michela Pelloso
Morgan Pence
Lisa Peterson
Salvatore Petta
Raffaele Pezzilli
Maria Picken
Massimo Pieri
Marie-Liesse Piketty
Christian Pilarsky
Janne Pitkaniemi
Martha B. Pitman
Fred Plapp
Krizia Pocino
Kris Poppe
Hans Pottel
Olga Pozdnyakova
Oscar J. Pozo
Salvatore Ppicuglia
Michele Protti
Iva Pruner
Angelica Putnam
Amy Pyle-Eilola
Wei-Jun Qian
Julianne Qualtieri
Daniel J. Rader
Philipp Raess
Alex Rai
Vasan S. Ramachandran
Balmiki Ramsaran
Rema Rao
Deepti Reddi
P. Hemachandra Reddy
Heiko Reutter
Raul Ribeiro
Ana C. Ricardo
Vincent Ricchiuti
Paul M. Ridker
Oliviero Riggio
Eric B. Rimm
Karina Rodriguez-Capote
Pierre Ronco
Lars Ronnblom
Stephen Roper
Carolina Rosadas
Flavia Rosado
Helge Rosjo
Julie Rosser
Nareg H. Roubinian
Marie-Claire Rowlinson
Matthew Rubinstein
Kristen Ruby
Maurizio Sanguinetti
Raimon Sanmarti
Stefan Schaub
Howard I. Scher
Amy Schmidt
Robert Schmidt
Inez Schoenmakers
Audrey Schuetz
Erin Schuler
Adam Seegmiller
Claudine Seeliger
Jansen Seheult
Rajeevan Selvaratnam
Jan Senderek
Sertac Sener
Ladislav Senolt
Lisa Senzel
Sanjeev Sethi
Mauli T. Shah
Zahra Shajani-Yi
Valentina Shakhnovich
Ratti Ram Sharma
Lo Sheng-Ying
Min Shi
Michael G. Shlipak
Pranav S. Shrivastav
Gabriel Sica
Alexa Siddon
Bob Siegerink
James Sikora
Christopher Silliman
Tatjana Simic
Patricia Simner
Ashwani Singal
Gurmukh Singh
Nirupama Singh
Sherrill J. Slichter
Geoffrey Smith
James Smith
Kristi Smock
Christine Snozek
Toshiyuki Someya
Linda Sommese
Rajesh Soni
Antionio Buno Soto
A. W. S. de Souza
Bryan R. Spencer
Jerry Squires
Chrysovalantis Stafylis
Tanja Stahl
Adrian Stanley
Ewout W. Steyerberg
Douglas Stickle
Elizabeth Stokes
Gregory A. Storch
Christophe Stove
Sean Stowell
Amit Sud
Brenda Suh-Lailam
Harold Sullivan
Cheng-Cao Sun
Simon Sung
Catur Suci Sutrisnani
Danyel Tacker
Beisha Tang
Zhenya Tang
Giovanni Tarantino
Giovanni Targher
Safaa Tayel
Ethan Taylor
Anne E. Tebo
Ladan Teimoori-Toolabi
Thomas Thum
Nicole Tolan
Sojit Tomo
Tatiana N. Toporcov
Christopher Tormey
Christian Toso
Pamela Tozzo
Ming-Sound Tsao
Thomas Tschoellitsch
Tatiana Tvrdik
Manoj Tyagi
Anetta Undas
Reza Vahidi
Luca Valenti
Miranda Van Eck
Richard Vanbreemen
Judith VanSickle
Maria Vergara-Lluri
Fatma Ferda Verit
Mrigender Virk
Libor Vitek
Joaquim Vives
Charles E. Wade
Caroline Walker
Lars Wallentin
Dorothy Waller
Keith Walley
Johan K. Wallman
Jann-Yuan Wang
Lanlan Wang
Sa Wang
Toby N. Weingarten
Susan T. Weintraub
Elizabeth L. Whitlock
Eli Williams
Maria Alice Willrich
David Winlaw
William Winter
Jedd D. Wolchok
Myles Wolf
Adam Wood
Geoffrey Wool
David Wu
YingSong Wu
Hua Xiao
Xinjie Xu
Zekaun Xu
Cao Yang
Wen-Chi Yang
Yi-Qing Yang
M.H. Yazer
Eric Yee
Marianne Yee
Ai Yoshihara
Constance Yuan
Quan Yuan
Martina Zaninotto
Faiez Zannad
Nicole Zantek
Zhenzhen Zhan
Linsheng Zhang
Victoria Zhang
Wei Zheng
Ting Zhou
Yi Zhou
Polona Zigon
Michael B. Zimmermann

CASE STUDY

Unexpectedly Abnormal Electrolytes in a 60 Year Old Man with Dementia

Ryan M. Mullins, BS, MLT(ASCP),[1] Nasrin Mohamed, MHI, BS, MLS(ASCP)[CM],[1] Ashton T. Brock, PhD, NRCC,[2] Kelly W. Wilhelms, PhD, DABCC, MLS(ASCP)[CM],[2,]*

[1]Department of Laboratory Services, Banner Estrella Medical Center, Phoenix, Arizona, US; [2]General Laboratory, Sonora Quest Laboratories/Laboratory Sciences of Arizona, Phoenix, Arizona, US; *To whom correspondence should be addressed. kelly.wilhelms@bannerhealth.com

Keywords: electrolytes, dehydration, hypernatremia, hyperchloremia, specimen contamination, intravenous fluid

Abbreviations: ED, emergency department; IV, intravenous; AKI, acute kidney injury.

Laboratory Medicine 2022;53:e14–e18; DOI: 10.1093/labmed/lmab058

Patient History

A 60 year old man with pre-existing dementia presented to the emergency department (ED) with mental confusion and signs of dehydration. He had been found awake on the floor in his home and had not been eating or drinking well for several days. His vital signs and physical exam were generally normal (temperature: 36.5°C; blood pressure: 115/81 mmHg; pulse: 69/min; respiratory rate: 18/min; oxygen saturation: 99% on room air) apart from apparent delirium, dry mucous membranes/mouth, and an involuntary jerking of the upper extremities. The ED personnel sent blood specimens to the laboratory for STAT chemistry and hematology tests.

Initial laboratory results revealed markedly elevated sodium and chloride, with both analyte concentrations above their respective reportable range. The medical laboratory scientist reviewing the results considered the specimen potentially contaminated with saline or another intravenous (IV) fluid. She rejected the specimen and requested a re-collection; however, upon receipt of a second and ultimately a third specimen, each set of results was found consistent with the original. The attending physician then requested whole blood sodium measured using a point-of-care device. This result was consistent with those of the main laboratory, with a value >180 mmol/L. Based on this comparison and in consultation with the laboratory medical director, the attending physician deemed the results of all collections to be relevant to the patient's condition. The elevated sodium on the final specimen was identified as a critical value and was appropriately annotated in the hospital information system. Select laboratory values associated with the encounter, including the repeat collections, are presented in **TABLE 1**. The patient was diagnosed with severe hypernatremia resulting from dehydration, leading to hypernatremic encephalopathy and acute kidney injury (AKI). He was admitted to the hospital and underwent extensive fluid replacement (Ringer's lactate, 5% dextrose) with gradual resolution of electrolyte balance, neurological function, and AKI over the next 7 days, after which he was discharged.

Dehydration

Dehydration is generally defined as the excessive loss of body water.[1,2] It is the most common cause of fluid and electrolyte imbalance in older adults and contributes a heavy burden to the medical system in the United States, with more than $5.5 billion spent on related hospital admissions annually.[2,3] Dehydration is categorized into groups based on the final extracellular osmolality within the affected patient (**TABLE 2**). Distinguishing the etiology and category of dehydration present is critical because these aspects define clinical management of the condition.[2]

Older adults are at increased risk for dehydration because of numerous changes in physiology associated with the aging process. For example, as patients age, they may experience decreases in thirst sensation (hypodipsia), a general decline in renal function, decreased activity of the renin-angiotensin system, and changes in renal sensitivity to vasopressin.[2,4] Moreover, aging may affect normal physiological adaptations to volume depletion, including neurohumoral control of blood pressure and cardiovascular responses to changes in blood volume. Enhancing this risk are various pathologic and pharmacologic etiologies that are more common in these age groups, including changes in functional and mental status, reduced mobility, and comorbidities that require pharmacological intervention such as the use of diuretics or laxatives.[2]

Electrolyte Abnormalities

The patient described in this case study presented with hypertonic dehydration that resulted in electrolyte abnormalities most notable for hypernatremia and hyperchloremia. In most patients with hypertonic dehydration, clinical presentation is influenced most prominently by the concentration of extracellular sodium; the effects of other constituents are less pronounced or overshadowed by the severity of the sodium disturbance.[2,5] Signs and symptoms observed in hypernatremia are outlined in **TABLE 3**.

Hypernatremia is defined as a serum sodium concentration that exceeds ~145 to 150 mmol/L.[6,7] It is most commonly caused by a net water loss from the body as described above; however, pathologic changes may occur as a result of any number of conditions that involve the loss of fluid and/or the gain of sodium (**TABLE 4**). Those at the highest risk of net water-

TABLE 1. Select Laboratory Results

Analyte	Specimen 1	Specimen 2	Specimen 3	Units	Reference Interval
Sodium	>180	>180	>180	mmol/L	135–147
Potassium	4.0	4.0	4.1	mmol/L	3.6–5.3
Chloride	>140	>140	>140	mmol/L	96–108
Total CO_2	27	24	24	mmol/L	19–31
Calcium	8.7	8.8	8.8	mg/dL	8.8–10.4
Urea nitrogen	117	118	115	mg/dL	8–25
Creatinine	3.26	3.09	3.05	mg/dL	0.6–1.5
Albumin	3.7	3.5	3.6	g/dL	3.4–4.9
Total protein	7.5	7.3	7.5	g/dL	6.0–8.0
ALT	25	25	25	U/L	5–60
AST	28	30	29	U/L	10–50
Glucose (random)	106	100	101	mg/dL	70–115
cTnT (hs)	32	32	32	ng/L	<12

ALT, alanine aminotransferase; AST, aspartate aminotransferase; cTnT (hs), Cardiac Troponin T (high sensitivity).

TABLE 2. Types of Dehydration

Extracellular Osmolality	Water:Salt* Loss		Causes
Isotonic	Proportionate ratio		Vomiting, secretory diarrhea
Hypertonic	⇧ Water	⇩ Salt	Hypodipsia/low intake, insensible losses, diuretics, DI, RA system abnormalities
Hypotonic	⇩ Water	⇧ Salt	Salt-wasting diuretics

DI, diabetes insipidus; RA, renin-angiotensin.
*For the types of dehydration, see Lacey et al,[1] Weinberg and Minaker,[2] and Rifai et al.[4] *Primarily sodium.*

TABLE 3. Symptoms of Hypernatremia in Adults

Intense thirst, transitioning to hypodipsia
Anorexia
Muscle weakness
Nausea/ vomiting
Altered mental status
Encephalopathy

For the symptoms of hypernatremia, see Adrogué and Madias[6] and Braun et al.[7]

TABLE 4. Causes of Hypernatremia in Older Adults

Net Water Loss	Sodium Gain
Pure water loss	Hypertonic sodium containing infusions
Dehydration/insensible loss	Ingestion of salt water (eg, sea water)
Hypodipsia	Primary hyperaldosteronism
Diabetes insipidus	Cushing's syndrome
Neurogenic, congenital, acquired	…
Hypotonic fluid loss	…
Renal disease, diuretics, osmotic diuresis	…
Gastrointestinal loss (vomiting, diarrhea)	…
Cutaneous loss (burns, sweating)	…

For the causes of hypernatremia, see Adrogué and Madias[6] and Braun et al.[7]

loss hypernatremia include infants, older adults, and patients with mental impairment.[6] In adults, symptoms are relatively mild until values exceed 160 mmol/L. In patients with the most severe cases, hypernatremia results in significant fluid redistribution within the central nervous system, leading to encephalopathy and altered mental status as observed in this patient.[7,8]

In contrast, hyperchloremia is considered a serum chloride that exceeds ~108 mmol/L.[5] Because chloride is the primary anion in the body, conditions that cause hypernatremia often lead to concurrent hyperchloremia. However, independent increases in chloride, when encountered, are associated with various physiological effects, including hyperchloremic metabolic acidosis, gastrointestinal symptoms, and impairment of renal function.[9] Chloremic excess may be observed in patients receiving aggressive treatment with normal saline (0.9% NaCl) because of its relatively high chloride content in contrast to normal physiological levels (serum: ~100 mmol/L; 0.9% saline: 154 mmol/L). In addition, chloride may be elevated in some patients with respiratory alkalosis, in whom the renal retention of chloride offsets the loss of bicarbonate.[5]

Laboratory Assessment

In this case study, severe hypernatremia and hyperchloremia presented an interpretive challenge to the laboratory scientist on duty. Many laboratory professionals can certainly attest that in isolation, it is difficult at times to recognize that exceptionally abnormal laboratory values can reflect both clinical reality and error. In this instance, although the electrolyte values may have been surprising, they were accompanied with other results that were not consistent with dilutional contamination by saline or other IV fluids (eg, the elevated urea nitrogen and creatinine).

Clinicians routinely use IV fluids for the repletion, maintenance, or selective movement of ions, metabolites, and water throughout the body. They may be isotonic, hypertonic, or hypotonic in nature and are generally classified as crystalloid or colloid.[10-12] Isotonic solutions are employed to maintain hydration or replete lost intravascular fluid (eg, because of blood loss or routine dehydration, or during surgery). In contrast, hypotonic solutions replete lost intracellular fluids in tissue

(eg, in hyperosmolar states) and hypertonic solutions replace deficient ions and draw interstitial fluids back into the vascular space (eg, with edema).[12] Crystalloid fluids consist of small molecules and ions that easily diffuse across capillary membranes, moving from the vascular space into the tissues. Common constituents of these fluids include sodium, chloride, potassium, calcium, lactate, and glucose. Examples of crystalloid fluids and their uses are outlined in **TABLE 5**. Colloid fluids contain larger molecules that do not easily pass through the capillary membrane, contributing direct vascular volume and drawing fluid from the interstitium into the intravascular space. Common constituents of colloid fluids include albumin, hydroxyethyl starch, and various forms of gelatin. Because of recent evidence suggesting that colloid solutions may contribute to patient harm, crystalloid IV fluid usage is more common.[11]

In our experience, specimen contamination is most often observed (or recognized) when there is contamination with crystalloid fluids, where marked changes in electrolytes, glucose, or other small molecules are easily noted. The complexities involved are considerable because the baseline values of the patient, fluid constituents, and sheer displacement volume in a collected specimen combine to have a significant effect on laboratory results.[13,14] For example, contamination with isotonic (0.9%) saline (NaCl) or Ringer's lactate solution has a relatively mild effect on patient sodium and chloride until the displacement volume is extensive; however, notable decreases in other analytes (eg, calcium, total protein) may be observed earlier (see **FIGURE 1A and 1B**).[15] In contrast, contamination with small amounts of highly concentrated solutions (eg, 5% dextrose, hypertonic (3%) saline) can lead to marked deviations in analyte concentration with little dilutional effect on other analytes. Using this type of information, some authors have proposed methods to detect potentially contaminated specimens using direct cut points (eg, Na^+: >180 mmol/L paired with K^+ <2.5 mmol/L) and statistically guided algorithms.[16-18]

Case Resolution

The events that occurred in the laboratory were investigated, and in-services were provided to instruct laboratory staff on the evaluation of chemistry results in the context of potential contamination. In this case, the patient presented with markedly abnormal sodium and chloride; however, the remainder of the analytes were normal, near normal, or even elevated, reflecting a true pathologic condition. In particular, the patient's urea nitrogen and creatinine were elevated, suggesting that the results were accurate. As part of the educational process, involved staff performed dilution studies and estimated the calculated effects of commonly administered fluids on laboratory values in heparinized whole blood. These studies provided a reference point that staff could employ in deciphering dilutional patterns that might be observed in true contamination (see **FIGURE 1A and 1B**). Moreover, we proposed the following general guidelines for the staff:

1. Evaluate the entire picture of laboratory results; do not focus on 1 or 2 greatly abnormal values.
2. Review for markedly or inappropriately decreased results, considering that although the intent of infusions is to correct/normalize certain blood constituents, solutions free of an analyte will artificially decrease other values quickly.
3. Use automated flagging algorithms such as delta checks or contamination sentinel rules (eg, those of Hernandez[16]) to assist in identifying abnormalities.
4. If possible, correlate results with other departments. For example, a marked shift in a patient's mean corpuscular volume without recent transfusion may support an abnormally hyper- or hypotonic condition.[19,20]
5. Use available resources, such as a review of patient charts or contacting the patient's clinician or nurse directly.
6. When all else fails, ask for help. Contact a supervisor or the laboratory medical director for assistance. Unilateral decisions to reject potentially contaminated specimens can lead to complaints, delays to patient care, and even patient harm.[21]

The assessment of potentially contaminated specimens can be complex; however, following the above suggestions is likely to assist most

TABLE 5. Select Crystalloid Solutions

Fluid	Constituent (mmol/L)		Use/Considerations
Isotonic saline (0.9%)	Sodium:	154	Most common for volume repletion and resuscitation; high chloride content
	Chloride:	154	
Hypotonic saline (0.45%)	Sodium:	77	Fluid repletion; risk of hyponatremia
	Chloride:	77	
Hypertonic saline (3%)	Sodium:	513	Treatment of hyponatremia; "small-volume" resuscitation protocols; risk of hypernatremia
	Chloride:	513	
Hartmann's solution	Sodium:	131	Volume and ion repletion, fluid maintenance; reduced chance of hyperchloremic effects
	Chloride:	111	
	Potassium:	5.4	
	Calcium:	2.0	
	Lactate:	29	
Ringer's lactate solution	Sodium:	130	Volume and ion repletion, fluid maintenance; reduced chance of hyperchloremic effects; potential to cause metabolic alkalosis in high rate infusions
	Chloride:	109	
	Potassium:	4.0	
	Calcium:	2.7	
	Lactate:	28	

For the select crystalloid solutions, see Myburgh and Mythen[10] and Finfer et al.[12]

FIGURE 1. 1A/1B. Dilutional effects of IV contamination from isotonic saline (A) and Ringer's lactate solution (B) on select analytes. Cl–, chloride; IV, intravenous; K+, potassium; Na+, sodium; tCa, total calcium; TProt, total protein.

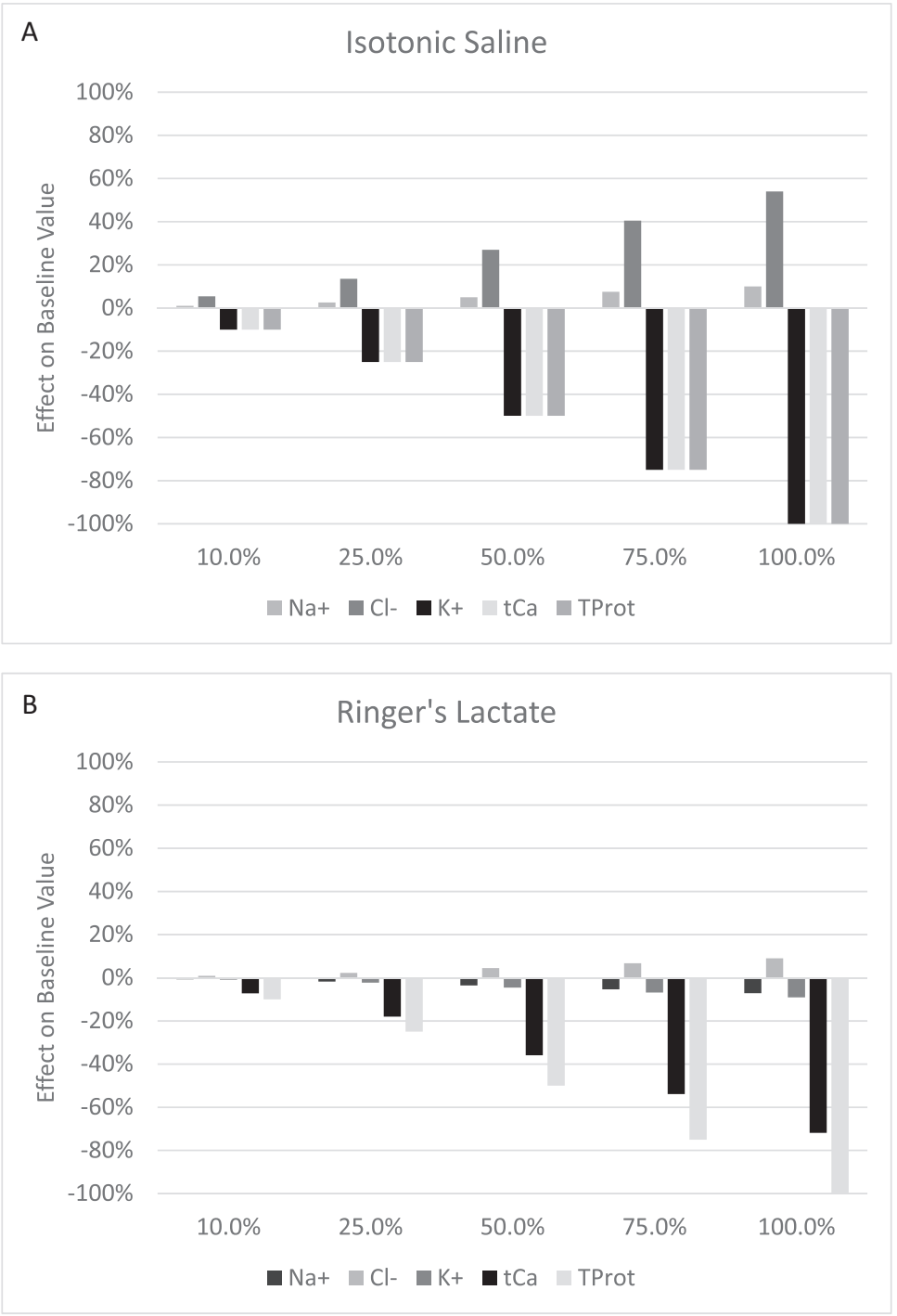

laboratory staff in dealing with situations such as that described in this case study in their day-to-day work.

REFERENCES

1. Lacey J, Corbett J, Forni L, et al. A multidisciplinary consensus on dehydration: definitions, diagnostic methods and clinical implications. *Ann Med.* 2019;51(3–4):232–251.
2. Weinberg AD, Minaker KL. Dehydration. Evaluation and management in older adults. Council on Scientific Affairs, American Medical Association. *JAMA.* 1995;274(19):1552–1556.
3. Miller HJ. Dehydration in the older adult. *J Gerontol Nurs.* 2015;41(9):8–13.
4. Sands JM. Urine concentrating and diluting ability during aging. *J Gerontol A Biol Sci Med Sci.* 2012;67(12):1352–1357.
5. Cheng S, Schindler EI, Scott MG. Disorders of water, electrolytes, and acid-base metabolism. In: Rifai N, Horvath AR, Wittwer CT, eds. *Tietz Textbook of Clinical Chemistry and Molecular Diagnostics*. St. Louis, MO: Elsevier; 2018: 1324–1347.

6. Adrogué HJ, Madias NE. Hypernatremia. *N Engl J Med.* 2000;342(20):1493–1499.
7. Braun MM, Barstow CH, Pyzocha NJ. Diagnosis and management of sodium disorders: hyponatremia and hypernatremia. *Am Fam Physician.* 2015;91(5):299–307.
8. Sterns RH. Disorders of plasma sodium—causes, consequences, and correction. *N Engl J Med*. 2015;372(1):55–65.
9. Handy JM, Soni N. Physiological effects of hyperchloraemia and acidosis. *Br J Anaesth.* 2008;101(2):141–150.
10. Myburgh JA, Mythen MG. Resuscitation fluids. *N Engl J Med.* 2013;369(13):1243–1251.
11. Hoorn EJ. Intravenous fluids: balancing solutions. *J Nephrol.* 2017;30(4):485–492.
12. Finfer S, Myburgh J, Bellomo R. Intravenous fluid therapy in critically ill adults. *Nat Rev Nephrol.* 2018;14(9):541–557.
13. Watson KR, O'Kell RT, Joyce JT. Data regarding blood drawing sites in patients receiving intravenous fluids. *Am J Clin Pathol.* 1983;79(1):119–121.
14. Hengeveld RCC, Gerards MC, Olofsen BE, et al. Flushing of an intravenous catheter: a cause for unreliable laboratory results. *Biochem Med (Zagreb).* 2019;29(3):031001.
15. Allen TL, Wolfson AB. Spurious values of serum electrolytes due to admixture of intravenous infusion fluids. *J Emerg Med.* 2003;24(3):309–313.
16. ClinLabNavigator [Internet]. Contamination of blood samples with IV fluids gives inaccurate results. Washington, DC: Guidelines for detecting IV contamination in blood samples. Accessed June 24, 2021. http://www.clinlabnavigator.com/guidelines-for-detecting-iv-contamination-of-blood-samples.html
17. Baron JM, Mermel CH, Lewandrowski KB, Dighe AS. Detection of preanalytic laboratory testing errors using a statistically guided protocol. *Am J Clin Pathol.* 2012;138(3):406–413.
18. Patel DK, Naik RD, Boyer RB, Wikswo J, Vasilevskis EE. Methods to identify saline-contaminated electrolyte profiles. *Clin Chem Lab Med.* 2015;53(10):1585–1591.
19. Philipsen JP, Madsen KV. Hypo- and hypernatremia results in inaccurate erythrocyte mean corpuscular volume measurement in vitro, when using Sysmex XE 2100. *Scand J Clin Lab Invest.* 2015;75(7):588–594.
20. Decaux G, Efira A, Dhaene M, Unger J. Interference of serum tonicity with the measurement of red cell mean corpuscular volume. *Acta Haematol.* 1982;67(1):62–66.
21. Noguez J. Enhancing communication of potentially compromised test results. American Association of Clinical Chemistry, Clinical Laboratory News. Published July 1, 2018. Accessed January 19, 2021. https://www.aacc.org/cln/articles/2018/july/enhancing-communication-of-potentially-compromised-test-results.

SPECIAL REPORT

SARS-CoV-2 Antibody Testing: Where Are We Now?

Elizabeth Smerczak, (MLS)ASCP[CM]*, MA**

Detroit Medical Center University Laboratories, Sinai-Grace Hospital, Detroit, Michigan, USA; *To whom correspondence should be addressed. esmerczak@gmail.com

Keywords: SARS-CoV-2 antibody testing, SARS-CoV-2 serology, COVID-19 testing, SARS-CoV-2 review, COVID-19 review, serology testing, antibody testing

Abbreviations: CDC, Centers for Disease Control & Prevention; WHO, World Health Organization; RT-PCR, real-time polymerase chain reaction; FDA-EUA, U.S. Food & Drug Administration-Emergency Use Authorization; NAAT, nucleic acid amplification test; NIH, National Institutes of Health; NCI, National Cancer Institute; BARDA, Biomedical Advanced Research and Development Authority; RBD, receptor binding domain; ACE2, angiotensin-converting enzyme-2; HCovs, human coronaviruses; nAbs, neutralizing antibodies; PSO, postsymptom onset; LFIA, lateral flow immunoassay; ELISA, enzyme-linked immunoassay; CLIA, chemiluminescent immunoassay; TAT, turnaround time; POC, point-of-care; CI, confidence interval; BSL, biosafety level; DBS, dried blood spot; PPV, positive predictive value; NPV, negative predictive value.

Laboratory Medicine 2022;53:e19–e29; https://doi.org/10.1093/labmed/lmab061

Background

On January 10th, 2020, the sequence to a novel coronavirus, SARS-CoV-2, was uploaded to Genbank.[1] At the time, it was associated with what was reported as a small outbreak of an atypical pneumonia in the Wuhan province of China.[2] The first confirmed case of this mysterious virus in the United States was reported by the Centers for Disease Control & Prevention (CDC) on January, 21, 2020.[3] On January 30, the World Health Organization (WHO) declared a public health emergency, and one day later, so did the United States.[4,5] By February 11, the WHO introduced the name of this disease: COVID-19, caused by the SARS-CoV-2 virus. Just over 1 month after the first cases had been reported, there were more than 42,000 cases in China and hundreds of suspected cases in 24 other countries.[6] On March 11, the WHO declared COVID-19 a pandemic,[4] and it was becoming increasingly clear that the world was on the brink of a public health crisis the likes of which has not been seen in any of our lifetimes.

The scope of human life lost, and devastation on many levels, is impossible to understate. At the time of this writing there have been more than 2.5 million COVID-19 deaths worldwide and more than 500,000 in the United States.[7] The economic and societal repercussions are still unfolding, and the pandemic is not over. The sacrifices and accommodations to daily life surely did have—and continue to have—an impact on slowing the spread of the SARS-CoV-2 virus and the COVID-19 disease it causes. But as the pandemic unfurled in unprecedented ways, so did the response by the medical and scientific community. Governments, private companies, educational institutions, and philanthropists joined forces in massive collaborative efforts to meet the challenges of the pandemic, all with common goals of understanding the SARS-CoV-2 virus, finding effective treatments, and developing accurate diagnostic strategies in the face of this fast-moving foe.[8,9] We need only look at the remarkable vaccine development to understand the fruits of such labor.[10,11]

We can also look to the development and distribution of diagnostic tests as a mark of achievement. Assays for SARS-CoV-2 became available to laboratories for this emerging analyte with astonishing speed and variety. The first report of a reverse transcriptase real-time polymerase chain reaction (RT-PCR) test developed with the intent of mass production was published on January 23, 2020.[12] By February 2, the WHO had 250,000 test kits delivered.[13] The CDC was granted a U.S. Food & Drug Administration Emergency Use Authorization (FDA-EUA) for an RT-PCR test on February 4 and had shipments to all 50 states the next day.[14,15] By the end of that month, there were more than 14 nucleic acid amplification tests (NAATs) commercially available.[13] This number soon skyrocketed, and NAATs quickly became the gold standard for COVID-19 diagnosis.[16] However, NAATs do have some performance issues, particularly false negative results, mostly because of difficulty in nasopharyngeal specimen collection and viral load. In addition, supply has not always been able to keep up with demand for NAATs. Antigen tests have emerged as well, but their lack of sensitivity relegates them to screening tools. Although detecting acute infection is of paramount importance, both the molecular and antigen methods have a limited detection window and cannot detect past infection.[17,18] And there are some questions they cannot answer. Early in the pandemic, little was known about the rate of transmission, asymptomatic infection, or the immunologic response to the novel virus.[19] The need to broaden testing strategies to include antibody testing (also known as serology testing) was clear, and commercially available tests followed before long.

The first SARS-CoV-2 antibody test was granted EUA on April 1, 2020.[20] Unlike NAATs, used as a primary diagnostic tool, antibody tests detect the humoral response to SARS-CoV-2 and are not to be used as a sole mode of diagnosis. They confirm past infection. As such, the FDA initially only suggested but did not require EUA for SARS-CoV-2 antibody tests.[21] Within the first week of April, there were at least 70 SARS-CoV-2 antibody tests on the market without such authorization. With them came false claims of diagnostic capabilities and false claims of FDA approval.[22] On May 5, amidst a slew of performance concerns and inappropriate marketing claims, the FDA tightened the reins on antibody tests and required EUA approval for their use.[23] But reports of underperformance persisted, and public trust was breached. In response, in-

dependent evaluations began in a collaborative effort with the FDA, the CDC, the National Institutes of Health (NIH), the National Cancer Institute (NCI), and the Biomedical Advanced Research and Development Authority (BARDA).[24] On June 19, the FDA created a "Do Not Use" list for SARS-CoV-2 antibody tests.[25] To date, more than 100 antibody tests have been removed from the market.

With better regulation and more rigorous evaluations, the list of FDA-EUA tests grew. Clinicians and laboratories still had to navigate the implementation of testing from a rapidly developed and densely populated market. Confusion and concern around performance, what the results mean, what tests can be used for, and what they say about immune status have persisted. It is now just past 1 year since the start of the COVID-19 pandemic, and much has been learned, but SARS-CoV-2 diagnostics is still a complex topic. This article focuses on 1 facet of SARS-CoV-2 testing: antibody testing. It is written from the perspective of clinical laboratory science and for the enrichment of knowledge thereof. With so many tests available, and so much research produced at breakneck speed, it is important to look back at what we have learned and to understand the SARS-CoV-2 antibody tests available, how they should and should not be used, what their limitations are, what questions they answer, and what questions remain.

Form and Function of SARS-CoV-2

Before discussing the humoral response, it is helpful to have a basic understanding of the SARS-CoV-2 virus. Coronaviruses are a large family that infect a range of mammalian and avian hosts. In humans, disease is typically mild, but some, like SARS-CoV-1 and MERS-COV, have more severe pathology. The SARS-CoV-2 virus is uniquely devastating, not just in the severity of the COVID-19 disease but in how infectious it is and the novel challenge it is to our immune system. The SARS-CoV-2 virus is a betacoronavirus. Members of this family are known to jump from zoonotic to human hosts. The closest relative of SARS-CoV-2 is BatCoV RaTG13, found in horseshoe bats.[26] This relationship sparked the theory that the virus made a zoonotic leap in street markets where horseshoe bats are sold. However, at 96% homology with SARS-CoV-2, this bat source theory remains a possibility but not a certainty.[27] In fact, SARS-CoV-2 shares considerable homology with many other coronaviruses as well.[28] However, small changes in this virus's RNA have given rise to striking changes in transmission and pathogenesis.

The SARS-CoV-2 genome is 29,881 bp, encoding 4 structural proteins—spike (S), envelope (E), membrane (M), and nucleocapsid (N)—and several nonstructural proteins (open reading frames, proteases, accessory proteins).[1] The genome forms a single strand of positive-sense RNA contained within a nucleocapsid, enveloped by a membrane from which abundant spike proteins protrude. As in other coronaviruses, the SARS-CoV-2 S protein is composed of a short intravirion domain, an anchoring transmembrane domain, and an n-terminus stalk with 2 subunits, S1 and S2.[29] It assembles into trimers that give the "corona"-like motif seen by electron microscopy. Heavy glycosylation of the S protein may initially shield the SARS-CoV-2 virus from immune surveillance; however, this camouflage is not sufficient because the S protein is highly immunogenic.[30,31] The S2 subunit is a conserved region, facilitating fusion. The most distal S1 subunit contains the receptor binding domain (RBD), which is where the virus directly binds to host cells—angiotensin-converting enzyme 2 (ACE2) receptors in the case of SARS-CoV-2—triggering conformational changes that facilitate entry into the cell. The key to what makes SARS-CoV-2 both novel and pathogenic lies in this region of the S protein. The S1 subunit of SARS-CoV-2 is unique, particularly at the RBD, in that it has more binding residues and a higher affinity for the ACE2 receptor than previously seen, making the SARS-CoV-2 virus both novel and distinctly pathogenic.[32]

Antibody Targets in SARS-CoV-2 Testing

To develop antibody tests, the question of which SARS-CoV-2 antigens elicit an immune response had to be answered. Phage display libraries, epitope maps, and peptide arrays were quickly assembled. Across multiple platforms, antibodies against the RBD, S, and N proteins emerged as the most potently immunogenic, selective, and widely produced by those patients infected with COVID-19.[33-36] Although exact epitopes may differ, virtually all commercially available tests—and all EUA assays—rely on detecting antibodies to these proteins, either separately or in combination.[37]

Many test platforms focus on the RBD of the S1 subunit. Some target the S1 subunit or the S protein as a whole. Antibodies against these antigens correlate with viral neutralization and indicate the sensitivity and specificity needed for clinical utility.[38-40] Some serologic assays include antibodies directed against the S2 subunit in their detection schema (eg, Liaison, DiaSorin).[37] Although the S2 subunit is immunogenic, it does not make a good target by itself. The S2 subunit is highly conserved among human coronaviruses (HCovs), and IgG against the S2 subunit is common in those unexposed to SARS-CoV-2.[41] This potential for cross-reactivity excludes the S2 subunit as a stand-alone target.[42,43]

The N protein that forms the RNA-housing nucleocapsid also elicits potent activation of the immune system.[44] Like the S2 subunit, the N protein is highly conserved across HCovs.[45] However, it does make an attractive target for serologic testing because the immune response during and directly after COVID-19 infection is so pronounced.[46] Clearly established cutoff values for detection and minimal cross-reactivity have been shown across multiple platforms (eg, Abbott, Bio-Rad).[37] Some studies have suggested that the detection of N antibodies is more sensitive than for those that target the S protein.[47-49]

When considering which test platform is suitable, it is essential to understand the goal of serologic testing. For example, both the Pfizer and Moderna vaccines elicit an immune response against the S protein. If evaluating vaccine response is a goal, then a test that targets S protein antibodies must be used. If, on the other hand, a population is being studied for infection rates, especially a population that may include persons who have been vaccinated, then a test that targets N protein antibodies would be more informative.

Antibody Dynamics

Analysis of plasma from those with COVID-19 confirmed an early consensus around targeting antibodies against the S, RBD, and N proteins of SARS-CoV-2 for assay development. However, an understanding of antibody dynamics was not immediately clear. Early studies often consisted of small specimen sizes and lacked the kind of longitudinal data that only time could provide. Heterogeneity in the intensity and duration of antibody production—a feature that continues to be observed—

contributed to conflicting and unclear information regarding antibody dynamics.[50,51] At the time of this writing, 1 year out from the beginning of the COVID-19 pandemic and many studies later, some uncertainty remains, but much has been revealed.

Antibody response in those with moderate to severe symptoms is the most studied and the most clearly characterized. The IgA, IgM, and IgG binding antibodies against the S, RBD, and N antigens, along with neutralizing antibodies (nAbs), are produced by the vast majority of those with symptomatic COVID-19.[52-55] Some studies have reported IgA and IgM as early detection markers,[46,50,56] whereas many others have reported that IgG appears almost simultaneously.[51,52,54,57,58] Explanations for this distinctive feature include a lengthy asymptomatic period or a slow buildup to detectable levels of IgA and IgM, but a definitive answer has yet to be found. It has also been reported that IgG production is delayed in some severely ill patients, whereas other studies have found that some severely ill patients have a delayed IgM response.[51,59] More study is needed to investigate these discrepant findings, but perhaps heterogeneity in early antibody response is itself the underlying feature.

Regardless of which isotype is detected first, antibody levels of IgA, IgM, and IgG are low in the first week of infection. Median seroconversion appears by days 7 to 12 postsymptom onset (PSO), with virtually 100% seroconversion by days 14 to 15 (**FIGURE 1**). The IgA and IgM levels gradually rise until approximately week 3 PSO, then decline.[52,53,57] Furthermore, IgG rises sharply in early infection at levels much higher than IgA and IgM, peaks at approximately week 5, and stays elevated for at least 7 weeks PSO.[50-52] Neutralizing antibodies correlate strongly with levels of binding IgG against the S and RBD antigens and moderately with anti-N IgG.[52,60,61] This development is encouraging, although not established, proof of durable immunity. Disease severity does correlate with the robustness of antibody response in the vast majority of patients; however, a correlation with clinical outcome has not been established.[50,57,60]

FIGURE 1. SARS-CoV-2 RNA levels peak approximately 1 week from exposure, then decline, becoming undetectable in most by approximately day 14. Median seroconversion occurs just after the first week PSO and reaches nearly 100% by day 14. IgM may or may not appear before IgG and IgA, but its half-life is the shortest, becoming undetectable by approximately 4 weeks PSO for many. IgG levels rise the highest and stay elevated for an extended period of time. PSO, postsymptom onset.

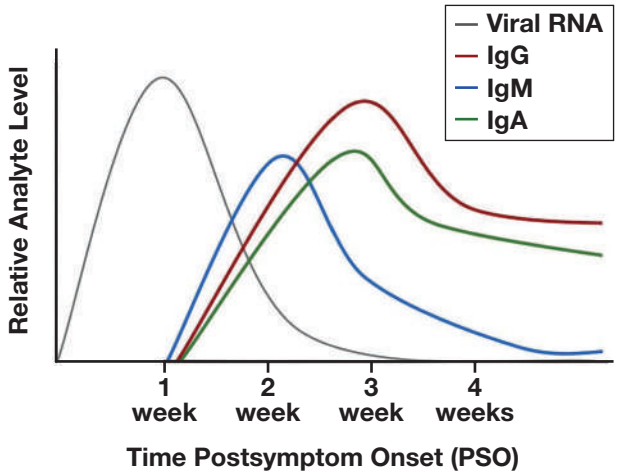

FIGURE 2. Moderate to severe infections elicit a markedly more robust immune response than mild to asymptomatic infections. Less is known about the duration of circulating antibodies in mild and asymptomatic infection, and whether or not an immune response correlates with lasting immunity is unknown at this time. PSO, postsymptom onset.

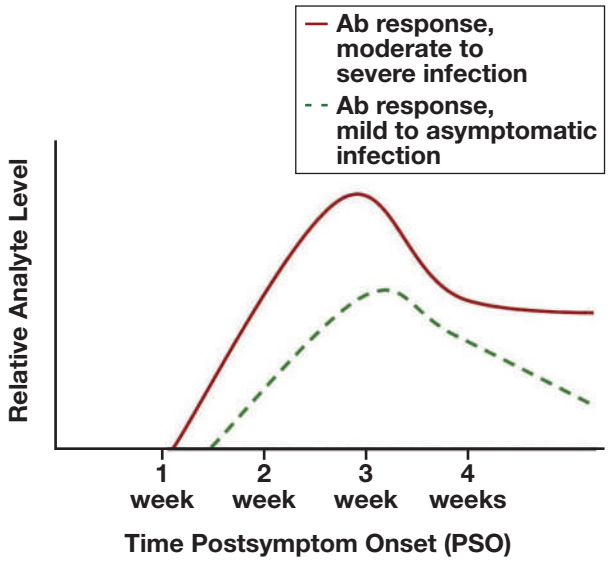

Antibody dynamics of mild to asymptomatic infection are less understood. Even the most recent studies include small specimen sizes and substantial heterogeneity. That said, 1 reproducible finding is that mild to asymptomatic SARS-CoV-2 infections do produce an antibody response, albeit less pronounced than moderate or severe infections (**FIGURE 2**).[50,62-64] The level of IgM seems to be short-lived or undetectable in a mild to asymptomatic infection, but IgG and total antibody levels are often detectable for weeks after exposure.[54,65] Seronegativity in moderate to severe illness is rare, but rates are unknown in mild to asymptomatic infection. This detail is something to consider when using antibody tests for epidemiological study. Neutralizing antibody production has been reported with mild infection, and some evidence supports nAb production in asymptomatic infection.[62] However, little is known about the prevalence and duration of nAb production in people with mild and asymptomatic infection at this time, and it is not known if or how the immune response relates to durable immunity.[66]

The groundwork for developing and implementing commercially available antibody tests would not have been possible without first characterizing SARS-CoV-2 antibody dynamics. All applications, from seroprevalence studies to convalescent plasma collection, rely on this basic understanding. A substantial body of research to this end emerged rapidly, and the work continues. Longitudinal studies that extend further and further from the time of symptom onset are underway, and a clearer picture of their duration will soon be realized. Measuring antibody titers may not help predict disease outcome, but they can help gauge severity and monitor disease progression. The relationship to antibody production, particularly nAbs, points to durable immunity, although this question remains a topic of intense interest. The immune response to SARS-CoV-2 varies substantially depending on disease severity, and heterogeneity, even within severity stratifications, seems to be a hallmark of the disease. Larger studies, with more participants, especially those with mild to asymptomatic infection, will deepen our understanding of antibody dynamics.

Types of Testing

There are currently more immunoassays on the market for SARS-CoV-2 testing than for any other pathogen.[67] The rapid development of hundreds of tests is both impressive and cause for scrutiny. Performance concerns and fraudulent claims undermined the credibility of SARS-CoV-2 antibody testing as a whole, but after underregulated and oversaturated beginnings, a clear menu of test methodologies with strong performance characteristics has emerged. That said, the menu is still large and diverse. At the time of this writing there are 65 SARS-CoV-2 antibody tests with EUA,[37] and many more are available on the global market. There is no gold standard for antibody tests, and different methodologies fulfill different testing needs. With such a broad range of tests available, the focus in this report is on tests that are available in the United States with FDA-EUA. The major types of SARS-CoV-2 antibody tests commercially available are lateral flow immunoassays (LFIAs), enzyme-linked immunosorbent assays (ELISAs), and chemiluminescent immunoassays (CLIAs). Although they are not routinely used in clinical laboratories, neutralization assays are discussed here as well. For each test, the principle, characteristics, usage, advantages, and limitations are addressed.

LFIAs

The LFIAs are a simple, qualitative method for detecting antibodies against the SARS-CoV-2 virus. Whole blood, serum, or plasma is applied to a membrane, and the specimen moves by capillary action laterally along a test strip. When the specimen reaches a conjugate pad, antibodies of interest bind to reporter-tagged antigens. The conjugate complexes move down the strip until they are captured by a test region. Tagged control antibodies get carried along as well. If the specimen has the antibodies of interest, then capture antibodies embedded in the test region will bind with the complex and a colorimetric or fluorescent signal will be produced. If the test is valid, then a control line will be present.[68] Studies have shown that SARS-CoV-2 LFIAs target antibodies against epitopes of the S or N protein, or both. Most LFIAs detect a combination of IgM and IgG. Some detect total antibodies or IgG alone.[37]

The LFIAs are rapid tests, with turnaround times (TATs) of less than 30 minutes. They are simple to perform, require a small amount of specimen, are relatively inexpensive, and can be scalable for mass testing. The demand for LFIAs for point-of-care (POC) testing has been strong, but of the 19 LFIAs granted EUA, only 2 are Clinical Laboratory Improvement Amendments (CLIA) waived and approved for POC testing. Both CLIA waived assays are validated for finger-stick specimens; the rest require phlebotomy and are considered to be of moderate to high complexity.[37]

Specificity of the SARS-CoV-2 antibody LFIA >95% has been widely reported, but independent evaluations of sensitivity vary considerably. Meta-analysis of commercially available LFIA has found pooled sensitivity to be between 66% and 76%.[69,70] Difficulty in reading and interpreting faintly positive tests and inconsistent reproducibility have also been reported.[71] Cross-reactivity remains a concern because large-scale studies evaluating cross-reactivity with other viruses, particularly other betacoronaviruses, are lacking.

In general, LFIAs underperform in comparison to manufacturer evaluations, but their ease of use and economical production mean that demand for SARS-CoV-2 LFIA testing is high. Great caution must be applied to this demand.[72] The LFIAs simply determine prior exposure to SARS-CoV-2, and the accuracy of this determination should be viewed with scrutiny. Contact tracing, knowledge of serostatus, and aid in diagnostics are all potential uses for LFIAs, but it is important to recognize potential shortcomings and not to overestimate what individual results mean. Where SARS-CoV-2 LFIA testing can have an important role is in serosurveillance and epidemiological study.[73] According to the CDC, the prevalence of SARS-CoV-2 remains largely unknown.[74] The LFIAs offer a simple, economical option that can be applied to large-scale testing and by minimally trained personnel. It is likely that they will be instrumental in population serosurveillance, especially in underserved areas. The CDC, FDA, and independent organizations are continuing evaluations, which will be important moving forward.

ELISAs

Although many variations exist, the basic principle for SARS-CoV-2 ELISA testing begins with coating microtiter wells with a SARS-CoV-2 antigen of interest, allowing antibodies in serially diluted patient specimens to bind with the antigens, followed by the addition of an enzyme-conjugated reporter antibody that produces a signal when substrate is added. The signal can be colorimetric or fluorescent (the latter are described as enzyme-linked fluorometric assays). These sensitive assays can be used for qualitative or semi-quantitative analysis. Researchers and clinical laboratories use ELISAs widely for SARS-CoV-2 antibody testing.

Currently there are 19 SARS-CoV-2 ELISA tests with EUA. Detection includes IgM, IgG, a combination, or total antibody. Most ELISAs detect antibodies directed at epitopes on the S protein. Two detect antibodies against the N protein, and 2 detect both. Specificity is widely found to be >95%. Pooled meta-analysis has described sensitivity for IgM or IgG at approximately 85% and combination IgM/IgG sensitivity at >90%.[69,70]

The ELISAs are moderate- to high-complexity tests. They require skilled personnel in a certified laboratory for clinical use. They are much more costly and labor-intensive than LFIAs, and TATs are on the order of 1 to 4 hours. A standard microtiter plate can run batches of 96 specimens, and high-throughput platforms are available. Much of what we know about SARS-CoV-2 antibody dynamics and the determination of which antigen and antibody isotypes yield the best sensitivity and specificity comes from ELISA testing.[46,49,57,75-77] Quantitative tests may be used to monitor disease progression, and the sensitivity of qualitative tests outperforms LFIAs when serostatus is being established. Their moderate to high throughput makes ELISA tests a good candidate for high-volume testing, including serosurveillance, and epidemiological studies. They may also play a role in monitoring vaccine response.[78]

CLIAs

The newest antibody detection technology on the market, CLIAs are similar in principle to ELISAs in many respects (eg, direct, indirect, and sandwich formats), but they rely on light emission to detect analytes. The general principle of SARS-CoV-2 CLIA testing begins with an antigen-coated solid phase, such as a polystyrene well, or more commonly paramagnetic beads. The patient specimen is added and allowed to bind to the antigen, and then an enzyme-conjugated antihuman antibody is added that binds to that complex. A substrate containing a luminescent, like luminol, initializes an oxidation reaction. As the luminescent

goes from an excited to a ground state, a photon is emitted. The photons are measured by a luminometer. The amount of antibody present in the specimen correlates to the amount of light produced by the reaction.[79]

Currently there are 25 CLIAs with EUA. Eighteen detect antibodies against epitopes on the S protein, 3 detect antibodies against the N protein, and 4 detect both S and N antibodies. Most detect IgM or IgG, 3 detect a combination of IgM and IgG, and fo4ur are pan-Ig assays.[37] Like ELISAs, CLIAs can be qualitative or quantitative and are useful for fulfilling many of the same testing needs. However, CLIAs are the most sensitive platform available. Pooled meta-analysis indicates >95% specificity and >96% sensitivity.[69,70] Another advantage is that many CLIA platforms are high-throughput and several are fully automated, offering excellent scalability for mass testing.

The CLIAs are not rapid tests. The TATs are approximately 1 hour, but automation makes testing less labor-intensive than most ELISAs. They are moderate- to high-complexity tests, requiring skilled personnel and a certified laboratory. A major disadvantage is cost. Platforms for CLIAs are the most expensive of any immunoassay platforms, although an argument can be made that the greater productivity allowed by these platforms offsets the cost of operation for high-volume settings.[79] For laboratories that have the means, CLIAs make an excellent platform for monitoring disease progression, serosurveillance, epidemiologic study, and monitoring vaccine response.[80] Another important use of CLIAs is convalescent plasma production, used by the American Red Cross to screen all donations and to select candidates for convalescent plasma donation.[81] Whatever the application, CLIAs' superior sensitivity offers richer information about the length of antibody response and better detection of antibodies at low levels.

Neutralization Assays

The aforementioned tests detect binding antibodies, but their detection does not necessarily indicate a humoral response capable of overcoming a virus. A better measure of this response is through the detection of nAbs. Neutralization assays use live virus or a pseudovirus to assess protective immunity. Patient serum is incubated with the live virus, and the mixture is inoculated onto a cell culture. Neutralization is measured by how much viral growth is inhibited, as compared to controls to which no patient serum is added.[82] Live SARS-CoV-2 viral neutralization assays require a biosafety level (BSL) 3 laboratory; pseudovirus tests require a BSL2. Tests are labor-intensive and take 3 to 4 days for results. They are expensive and high-complexity tests, not feasible for large-scale testing or for most clinical laboratories. However, antibody tests like ELISAs and CLIAs may be able to act as a surrogate. Many studies have reported that binding IgG levels, particularly to the RBD domain of the S protein, strongly correlate with nAbs.[54,83-85] Research continues to investigate this correlation, and it is likely that ELISA and CLIA testing can be an alternative to the costly and time-consuming neutralization assays. The FDA has given EUA clearance to 1 ELISA described as a neutralization assay because it measures the blocking of RBD binding to the ACE2 receptor protein by antibodies present in patient serum.[86] Although it is not a traditional neutralization assay, it is a good example of the ongoing evolution of antibody testing and of the roles that antibody testing can fulfill.

Role of Antibody Testing

Antibody tests are indirect; they measure the immune response to SARS-CoV-2 rather than directly detecting the virus. As such, they are not a primary diagnostic tool. However, antibody tests can complement diagnosis, especially in patients in whom there has been a delay between symptom onset and testing or when clinical presentation indicates COVID-19 but NAAT tests are negative.[87] As the virus is cleared, it drops below the limits of NAAT detection. After 14 days PSO, the ability of NAATs to detect SARS-CoV-2 infection drops to approximately 50% (**FIGURE 3**). By day 30, most who have contracted COVID-19 will be NAAT-negative.[88,89] Conversely, seroconversion—and reliable antibody testing—occurs by day 14 PSO. Thus, antibody testing can be a useful adjunct to diagnosis when NAAT is negative but clinical presentation indicates COVID-19. Some suggest combining NAAT and antibody testing for optimal diagnostic accuracy, especially as variants emerge.[89] After diagnosis, clinicians may use antibody testing to monitor the duration and magnitude of patients' antibody response as part of disease course management and to predict when the virus has been cleared.

Arguably, antibody tests are the most important tool for surveillance and epidemiologic studies.[90-92] They indicate past infection long after the infection has cleared, and specimen collection is more reliable than nasopharyngeal swabs. There is a great need for accurate and sensitive testing on a large scale for monitoring outbreaks and establishing actual population prevalence. Because of the limitations of NAAT, seroprevalence provides a more accurate measure of true infection rates. The CDC, NIH, and WHO have massive seroprevalence study efforts underway, and smaller-scale efforts by academic and clinical institutions continue to build our body of knowledge. For population studies, especially where prevalence is expected to be low, choosing a test with high specificity is key to minimizing false positives. The CDC recommends using tests with specificities of 99.5% or above.[93] And at this stage in test development, we do have the means to execute studies with this performance goal.

Antibody testing for SARS-CoV-2 is used in blood donor screening and in convalescent plasma preparation.[94] Antibody testing is also used to evaluate vaccine effectiveness.[95] Both applications require sensitive methodologies. The American Red Cross, for example, is interested in quantitative data for convalescent plasma preparation and has a high test volume with routine screening. The organization relies on CLIA methodology to address these needs.[94] Monitoring vaccine response requires sensitive test methodologies, because immune response is typi-

FIGURE 3. As the SARS-CoV-2 virus is cleared, the sensitivity of RT-PCR tests diminishes. However, antibody test sensitivity is highest 2 to 3 weeks PSO. Sensitivity typically remains high for weeks after this peak and long after the window of RT-PCR clinical utility. PSO, postsymptom onset; RT-PCR, real-time polymerase chain reaction.

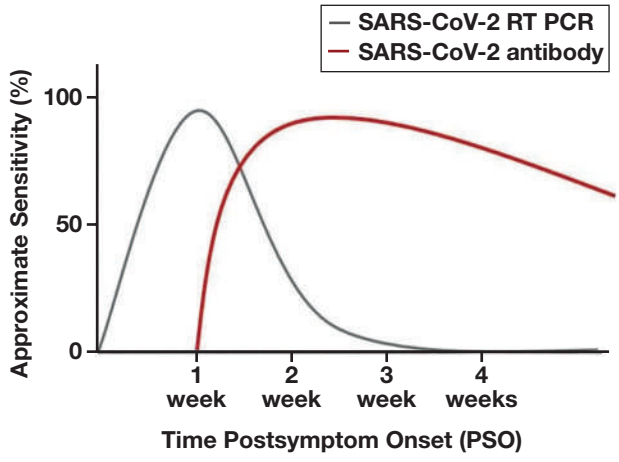

cally less pronounced than natural infection. Both CLIA and ELISA tests can be appropriate. But it is important to be mindful of which antibodies are expected from vaccine inoculation. For example, both FDA-approved mRNA vaccines utilize the S protein. Choosing a test that detects antibodies against the S protein would be necessary for evaluating vaccine efficacy. Tests that detect antibodies against the N protein would be useful in differentiating those infected by the virus vs those who gained immunity through vaccination.

Antibody testing can also play a role in contact tracing.[96,97] With the window of time that NAATs are reliably positive, it is unreasonable to use them as a sole method of contact tracing. Most commonly, LFIAs are used for this application, but any methodology could be used. There has been an interest in using antibody testing as "return-to-work passports."[98] But reinfection rates and durable immunity remain in question. At this time, the CDC advises against using antibody testing as a determinant for returning to the workplace.[93] The recommended appropriate uses of LFIAs, ELISAs, and CLIAs for patient antibody production to SARS-CoV-2 are summarized in **FIGURE 4**.

Specimen Types

Most LFIAs are validated for plasma, serum, and whole blood. Currently, 2 LFIAs with EUA are approved for finger-stick, POC testing. This number may change, because the demand for quick and accessible POC antibody testing is high. There is also a great demand for at-home specimen collection because it reduces the chances of exposure, and the ease of collection may lead to a higher number of people participating in testing. To this end, assays that rely on IgA detection in saliva and assays that can be performed from dried blood spot (DBS) specimens are being explored, but none have reached the level of performance required by the FDA, and at-home specimen collection poses its own set of issues.[99,100] One CLIA assay has EUA to perform testing from DBS, but the overwhelming specimen types acceptable for these tests are serum and plasma. Manufacturer instructions vary, but in general, specimens may be refrigerated at 4°C for 2 to 3 days before testing and frozen at −20°C for 1 month.[37]

Predictive Value

Sensitivity is the ability of a test to detect a true positive. Specificity is the ability of a test to detect a true negative. Accuracy is the ability of a test to differentiate between true positive and negative specimens.[101] These terms are commonly understood by anyone working in a clinical laboratory. But SARS-CoV-2 antibody test performance is often further characterized by looking at an assay's positive predictive value (PPV) and negative predictive value (NPV). See **TABLE 1** for a definition and comparison of these diagnostic terms. These terms may be less familiar, but they are important to understand. PPV is the probability an individual positive test result represents true antibody positivity, and NPV is the probability an individual negative test result represents a true antibody negativity.[37] These values are based not only on the sensitivity and specificity of an assay but also on the prevalence of the disease in a population. Research has shown that PPVs increase with disease prevalence and that NPVs increase the lower the disease prevalence. The key to using antibody testing for large-scale prevalence studies is using tests with high PPVs. The FDA calculates NPVs and PPVs for SARS-CoV-2 antibody assays based on the assumption of 5% disease prevalence. All FDA-EUA assays have NPV >98%, but PPV varies considerably. Several LFIAs have PPV <60%; the lowest is 49.6%. The ELISA and CLIA platforms have PPVs that range from >80% to 100%. Online calculators are available, including one provided by the FDA and the *British Medical Journal* (**TABLE 1**).[37,102]

Following is an example of a calculation of PPV and NPV: For a test has 90% sensitivity, 98% specificity, and 5% disease prevalence, and 1000 people are tested, one can expect 19 false-positive results and 5 false-negative results. There is a 70.3% chance that a positive test reflects an antibody-positive person (PPV) and a 99.5% chance that a negative test reflects an antibody-negative person (NPV).[103]

FIGURE 4. Uses of SARS-CoV-2 antibody testing according to test methodology. CLIA, chemiluminescent immunoassay; ELISA, enzyme-linked immunosorbent assay; LFIA, lateral flow immunoassay.

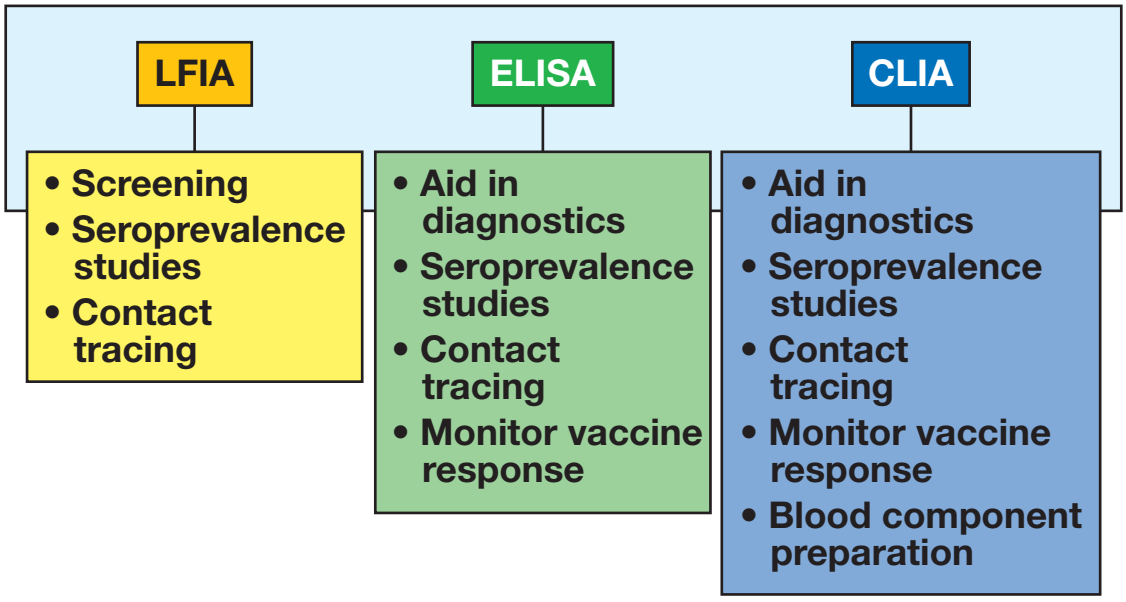

TABLE 1. Definition and Comparison of Diagnostic Terms

	Has SARS-CoV-2 Antibodies	Does Not Have SARS-CoV-2 Antibodies
Positive results	True positive (a)	False positive (b)
Negative results	False negative (c)	True negative (d)

Algorithms that use more than 1 test with differing antigenic targets are a strategy for increasing PPV for laboratories that have the resources to do so. Ideally, only tests with the highest sensitivity and specificity would be used. But for many laboratories and testing facilities, this level of testing is not feasible. For each application of SARS-CoV-2 testing, the pros and cons, including predictive value, must be balanced against the reality of the skill level of the labor force and the resources of the testing facility.

Limitations

As with any humoral response, antibodies to SARS-CoV-2 take time to build to detectable levels. Sensitivity does not reach EUA acceptable limits on any platform until 8 to 14 days PSO. Thus, SARS-CoV-2 antibody tests do not detect acute infection. Most manufacturers include sensitivity and specificity data based on days from symptom onset. However, the majority of COVID-19 infections are mild to asymptomatic. Establishing this crucial timing of collection is often not possible, especially in serosurveillance and epidemiologic studies. In addition, studies suggest that patients with mild to asymptomatic infections produce a less-robust immune response that wanes faster than that in more severely affected individuals.[62] There are a small portion of those who have been infected by SARS-CoV-2 that do not produce antibodies to the virus, and few studies have characterized the SARS-CoV-2 antibody response of immunosuppressed patients.[104,105] False negatives resulting from assay sensitivity, an inability to optimally time specimen collection, and individual immune responses are a limiting factor with SARS-CoV-2 antibody testing.

The true prevalence of COVID-19 in the U.S. population is not known at this time.[37] Prevalence can vary substantially across different populations, but overall, estimates remain low in the general population.[106,107] Antibody testing is a tool at the forefront of gathering the data necessary to make better estimates, but even assays that meet the FDA standards for sensitivity and specificity can have poor PPV in low-prevalence populations.[37] This possibility means that false positives are a limitation of SARS-CoV-2 antibody testing, particularly in low-prevalence populations. Choosing tests with high specificity mitigates this limitation, as does using 2 test algorithms.

Interfering substances can be an issue with any immunoassay. Potential interfering substances for SARS-CoV-2 immunoassays include endogenous factors like hemoglobin, triglycerides, and elevated protein and exogenous factors like acetaminophen, ascorbic acid, biotin, and hydroxychloroquine.[37] Manufacturers of EUA assays provide evaluations of known potential interfering substances. Performance above these thresholds can affect results. Patient medication history and visual evaluation of specimens help discern spurious results from such substances, but the risk cannot be eliminated.

Cross-reactivity from other antibodies must be considered when using SARS-CoV-2 antibody tests on any platform. Because of the expedited validation process and the limited availability of reference material, cross-reactivity studies for EUA SARS-CoV-2 antibody tests are scant. Although manufacturer specimen sizes are small across all FDA-EUA assays, cross-reactivity with noncoronavirus antibodies (eg, antibodies against HIV, cytomegalovirus, hepatitis B virus, and influenza; antionuclear antibodies, and rheumatoid factor) seem to pose little threat to commercially available SARS-CoV-2 antibody testing.[37] Of more concern is the potential for cross-reactivity by antibodies to viruses that share significant homology with SARS-CoV-2. Here, the data are sorely lacking. Some manufacturers have not evaluated the cross-reactivity of antibodies against other coronaviruses at all. This includes MERS, SARS-CoV-1, alpha-COV 229E, beta-COV OC43, and beta-COV HKU1. Of those that have, specimen sizes were small—often 5 or fewer. Two ELISA manufacturers have noted cross-reactivity with SARS-CoV-1,[37] but these are hardly enough data to make any broad statements about cross-reactivity. Cross-reactivity is an issue that urgently requires further evaluation.

Considering the circumstances of this novel virus, some accommodations to study design have been taken to accomplish important work. However, not all studies were conducted with the kind of rigor that avoids bias. Two large meta-analysis studies evaluated bias in SARS-CoV-2 antibody testing, and both arrived at similar findings.[69,70] Some studies from the meta-analyses showed bias in how the index test was used and some with application of the reference standard test, but these bias risks were minimal. A major risk of bias was found in the timing of the specimen collection. Cochrane et al identified this bias in 54% of studies[70] and Lisboa-Bastos et al[69] in 67% of studies. Participants were either not stratified according to time PSO, or the timing was unclear. The overwhelming and more concerning bias was found in participant selection. Cochrane et al. identified participant selection bias in 89% of the studies,[70] and Lisboa-Bastos et al[69] identified this bias in 98% of the studies. The main reason for this finding was the tendency to select hospitalized patients with COVID-19 for inclusion in the study, with little to no inclusion of patients with mild and asymptomatic infection. Bias in how assays are evaluated means that accuracy in clinical settings may be lower than expected; however, it is not always possible, especially in the midst of a pandemic, to mitigate the risks. As performance evaluation studies continue, we can expect improvement in the areas that need attention.

Conclusion

It is just past 1 year since COVID-19 was declared a pandemic in the United States. The medical and scientific community's response to meet testing needs is nothing short of astonishing. However, the urgency for the testing and rapid development of assays has not been without its problems. The flurry of antibody tests with dubious claims and subpar performance showcases the importance of oversight by the FDA and the benefit of entities like the CDC, NIH, and NCI. With their guidance, numerous independent performance evaluations of SARS-CoV-2 antibody tests have been published, and efforts on this front continue.[37,107-110] For example, the NIH developed the Rapid Acceleration of Diagnostics program, which helps with validating SARS-CoV-2 tests.[111] In addition, panels have been developed by the collaborative efforts of the FDA, CDC, NIH, NCI, and BARDA to aid the validation

process. Shortcomings like study design bias and limited cross-reactivity studies are perhaps unavoidable with such a novel and devastating virus, and developing a validation strategy takes time. But it is clear that we are moving along the trajectory of filling in the gaps that need to be filled.

Today we have a diverse test menu to choose from, many have sensitivities and specificities that exceed the FDA's requirements, and we know how to use them. The SARS-CoV-2 antibody tests may not be used as primary diagnostic tools, but they are a helpful component of diagnostics when used in conjunction with NAATs, and particularly with patients who are past 14 days PSO. They are used in convalescent plasma donor selection and contact tracing, and to monitor vaccine response. Antibody tests are invaluable to surveillance studies. In fact, the NIH just released a massive seroprevalence study (still in preprint), and more are underway.[112] A better grasp on true population prevalence will be realized with continued efforts like these. As we move into the second year of the pandemic, we can now have the testing capability and the time postpandemic outbreak to conduct the studies to answer the questions surrounding antibody dynamics at all severity stratifications, particularly mild to asymptomatic infection.

Early public confusion about antibody testing has been met with clear, transparent, and meaningful education by entities like the CDC and FDA. This guidance includes the messaging that a positive antibody test result does not confirm immunity. Preliminary studies, and the studies of related HCovs, do suggest durable immunity for some period of time; however, we still do not know the extent of immunity after infection with the SARS-CoV-2 virus. This is a question that accurate and reliable antibody tests will play a role in answering. But for now, we must not conflate a detectable antibody response with durable immunity.

Emerging variants and rising infection rates remind us that this pandemic is not over. There is concern that new strains may evade detection by molecular methods, which require precise sequence agreement for primers to bind and viral RNA to be detected. The CDC is closely monitoring variants in the United States.[113] Current molecular testing seems to be effective at detecting SARS-CoV-2 variants.[114] But should this change, antibody testing may prove instrumental in detecting outbreaks.

Regardless of the direction the virus takes us, it is clear that antibody testing has been invaluable to developing and understanding the SARS-CoV-2 virus and the COVID-19 pandemic. The questions that remain are answerable through reliable testing and diligent work. Although this is the first time in our lifetimes that a pandemic like COVID-19 has been seen, it brings to our collective attention that it may not be the last. How academic institutions, private companies, and governmental agencies have interfaced provides a kind of blueprint for challenges we may face in the future. The development and implementation of SARS-CoV-2 antibody testing has not been without its challenges, but it has been a remarkable process, one that is still in motion, and one that will continue being beneficial in moving us forward to a postpandemic world.

Acknowledgments

The author acknowledges Michigan State University's School of Natural Science Biomedical Laboratory Science Program, with special thanks to Rachel Morris, PhD, and Kathleen Hoag, PhD, for their encouragement and guidance. The author has no conflicting affiliations or interests (financial or professional) related to this work.

REFERENCES

1. National Center for Biotechnology Information. Severe acute respiratory syndrome coronavirus 2 isolate Wuhan-Hu-1, complete genome. https://www.ncbi.nlm.nih.gov/nuccore/MN908947. Published March 18, 2020. Accessed June 18, 2021.
2. European Centre for Disease Prevention and Control. Threat assessment brief: Pneumonia cases possibly associated with a novel coronavirus in Wuhan, China. https://www.ecdc.europa.eu/en/publications-data/pneumonia-cases-possibly-associated-novel-coronavirus-wuhan-china. Published January 9, 2020. Accessed April 28, 2021.
3. Centers for Disease Control & Prevention. First travel-related case of 2019 novel coronavirus detected in United States. https://www.cdc.gov/media/releases/2020/p0121-novel-coronavirus-travel-case.html. Published January 21, 2020. Accessed June 18, 2021.
4. World Health Organization. Timeline: WHO's COVID-19 response. https://www.who.int/emergencies/diseases/novel-coronavirus-2019/interactive-timeline. Accessed April 28, 2021.
5. U.S. Department of Health & Human Services. Secretary Azar declares public health emergency for United States for 2019 novel coronavirus. https://www.hhs.gov/about/news/2020/01/31/secretary-azar-declares-public-health-emergency-us-2019-novel-coronavirus.html. Published January 31, 2020. Accessed April 28, 2021.
6. World Health Organization. WHO Director-General's remarks at the media briefing on 2019-nCoV on 11 February 2020. https://www.who.int/director-general/speeches/detail/who-director-general-s-remarks-at-the-media-briefing-on-2019-ncov-on-11-february-2020. Accessed April 28, 2021.
7. Johns Hopkins University & Medicine. COVID-19 dashboard. https://coronavirus.jhu.edu/map.html. Accessed June 18, 2021.
8. World Health Organization. Global partnership to make available 120 million affordable, quality COVID-19 rapid tests for low- and middle-income countries. https://www.who.int/news/item/28-09-2020-global-partnership-to-make-available-120-million-affordable-quality-covid-19-rapid-tests-for-low--and-middle-income-countries. Published September 28, 2020. Accessed June 18, 2021.
9. FIND Diagnosis for All. ACT-accelerator: access to COVID-19 tools. https://www.finddx.org/covid-19/act-accelerator/. Published July 20, 2020. Accessed June 18, 2021.
10. U.S. Department of Defense. Coronavirus: Operation Warp Speed. https://www.defense.gov/Explore/Spotlight/Coronavirus/Operation-Warp-Speed. Accessed June 18, 2021.
11. World Health Organization. COVAX: working for global equitable access to COVID-19 vaccines. https://www.who.int/initiatives/act-accelerator/covax. Accessed June 18, 2021.
12. Corman VM, Landt O, Kaiser M, et al. Detection of 2019 novel coronavirus (2019-nCoV) by real-time RT-PCR. *Euro Surveill*. 2020;25(3):2000045.
13. Sheridan C. Coronavirus and the race to distribute reliable diagnostics. *Nat Biotechnol.* 2020;38(4):382–384.
14. U.S. Food & Drug Administration. FDA takes significant step in coronavirus response efforts, issues emergency use authorization for the first 2019 novel coronavirus diagnostic. https://www.fda.gov/news-events/press-announcements/fda-takes-significant-step-coronavirus-response-efforts-issues-emergency-use-authorization-first. Published April 2, 2020. Accessed June 18, 2021.
15. Centers for Disease Control & Prevention. Shipping of CDC 2019 novel coronavirus diagnostic test kits begins. https://www.cdc.gov/media/releases/2020/p0206-coronavirus-diagnostic-test-kits.html. Published February 6, 2020. Accessed June 18, 2021.
16. Goudouris ES. Laboratory diagnosis of COVID-19. *J Pediatr (Rio J).* 2021;97(1):7–12.
17. Arevalo-Rodriguez I, Buitrago-Garcia D, Simancas-Racines D, et al. False-negative results of initial RT-PCR assays for COVID-19: a systematic review. *PLoS One.* 2020;15(12):e0242958.

18. American Society for Microbiology. Supply shortages impacting COVID-19 and non-COVID testing. https://asm.org/Articles/2020/September/Clinical-Microbiology-Supply-Shortage-Collecti-1. Accessed June 18, 2021.
19. Bai Y, Yao L, Wei T, et al. Presumed asymptomatic carrier transmission of COVID-19. *JAMA.* 2020;323(14):1406–1407.
20. U.S. Food & Drug Administration. Coronavirus (COVID-19) update: daily roundup April 2, 2020. https://www.fda.gov/news-events/press-announcements/coronavirus-covid-19-update-daily-roundup-april-2-2020. Published February 4, 2020. Accessed April 29, 2021.
21. U.S. Food & Drug Administration. Coronavirus (COVID-19) update: FDA provides more regulatory relief during outbreak, continues to help expedite availability of diagnostics. https://www.fda.gov/news-events/press-announcements/coronavirus-covid-19-update-fda-provides-more-regulatory-relief-during-outbreak-continues-help. Published March 16, 2020. Accessed June 18, 2021.
22. U.S. Food & Drug Administration. Coronavirus disease 2019 (COVID-19). https://www.fda.gov/emergency-preparedness-and-response/counterterrorism-and-emerging-threats/coronavirus-disease-2019-covid-19. Published 2021. Accessed April 29, 2021.
23. Shah A. Insight into FDA's revised policy on antibody tests: prioritizing access and accuracy. U.S. Food & Drug Administration. https://www.fda.gov/news-events/fda-voices/insight-fdas-revised-policy-antibody-tests-prioritizing-access-and-accuracy. Published May 4, 2020. Accessed June 18, 2021.
24. U.S. Food & Drug Administration. Coronavirus (COVID-19) update: FDA publicly shares antibody test performance data from kits as part of validation study. https://www.fda.gov/news-events/press-announcements/coronavirus-covid-19-update-fda-publicly-shares-antibody-test-performance-data-kits-part-validation. Published June 4, 2020. Accessed April 29, 2021.
25. U.S. Food & Drug Administration. Removal of COVID-19 tests that should no longer be used and/or distributed for COVID-19: FAQs on testing for SARS-CoV-2. https://www.fda.gov/medical-devices/coronavirus-covid-19-and-medical-devices/removal-lists-tests-should-no-longer-be-used-andor-distributed-covid-19-faqs-testing-sars-cov-2. Published June 11, 2021. Accessed June 18, 2021.
26. Zhou P, Yang XL, Wang XG, et al. A pneumonia outbreak associated with a new coronavirus of probable bat origin. *Nature.* 2020;579(7798):270–273.
27. van Dorp L, Acman M, Richard D, et al. Emergence of genomic diversity and recurrent mutations in SARS-CoV-2. *Infect Genet Evol.* 2020;83:104351.
28. Jaimes JA, André NM, Chappie JS, Millet JK, Whittaker GR. Phylogenetic analysis and structural modeling of SARS-CoV-2 spike protein reveals an evolutionary distinct and proteolytically sensitive activation loop. *J Mol Biol.* 2020;432(10):3309–3325.
29. Bosch BJ, van der Zee R, de Haan CA, Rottier PJ. The coronavirus spike protein is a class I virus fusion protein: structural and functional characterization of the fusion core complex. *J Virol.* 2003;77(16):8801–8811.
30. Watanabe Y, Allen JD, Wrapp D, McLellan JS, Crispin M. Site-specific glycan analysis of the SARS-CoV-2 spike. *Science.* 2020;369(6501):330–333.
31. de Assis RR, Jain A, Nakajima R, et al. Analysis of SARS-CoV-2 antibodies in COVID-19 convalescent blood using a coronavirus antigen microarray. *Nat Commun.* 2021;12(1):6.
32. Wang Q, Zhang Y, Wu L, et al. Structural and functional basis of SARS-CoV-2 entry by using human ACE2. *Cell*. 2020;181(4):894–904.e9.
33. Zamecnik CR, Rajan JV, Yamauchi KA, et al. ReScan, a multiplex diagnostic pipeline, pans human sera for SARS-CoV-2 antigens. *Cell Rep Med.* 2020;1(7):100123.
34. Rosado J, Pelleau S, Cockram C, et al. Multiplex assays for the identification of serological signatures of SARS-CoV-2 infection: an antibody-based diagnostic and machine learning study. *Lancet Microbe.* 2021;2(2):e60–e69.
35. Stoddard CI, Galloway J, Chu HY, et al. Epitope profiling reveals binding signatures of SARS-CoV-2 immune response and cross-reactivity with endemic HCoVs. *Cell Rep.* 2021;35(8):109164.
36. Poh CM, Carissimo G, Wang B, et al. Two linear epitopes on the SARS-CoV-2 spike protein that elicit neutralising antibodies in COVID-19 patients. *Nat Commun.* 2020;11(1):2806.
37. U.S. Food & Drug Administration. EUA authorized serology test performance. https://www.fda.gov/medical-devices/coronavirus-disease-2019-covid-19-emergency-use-authorizations-medical-devices/eua-authorized-serology-test-performance. Published May 25, 2021. Accessed June 18, 2021.
38. Manthei DM, Whalen JF, Schroeder LF, et al. Differences in performance characteristics among four high-throughput assays for the detection of antibodies against SARS-CoV-2 using a common set of patient samples. *Am J Clin Pathol.* 2021;155(2):267–279.
39. Dan JM, Mateus J, Kato Y, et al. Immunological memory to SARS-CoV-2 assessed for up to eight months after infection. *Science.* 2021;371(6529):eabf4063.
40. Premkumar L, Segovia-Chumbez B, Jadi R, et al. The receptor binding domain of the viral spike protein is an immunodominant and highly specific target of antibodies in SARS-CoV-2 patients. *Sci Immunol*. 2020;5(48):eabc8413.
41. Nguyen-Contant P, Embong AK, Kanagaiah P, et al. S protein-reactive IgG and memory B cell production after human SARS-CoV-2 infection includes broad reactivity to the S2 subunit. *mBio*. 2020;11(5):e01991-20.
42. Khan S, Nakajima R, Jain A, et al. Analysis of serologic cross-reactivity between common human coronaviruses and SARS-CoV-2 using coronavirus antigen microarray. Preprint. Posted online March 25, 2020. bioRxiv 006544. doi:10.1101/2020.03.24.006544
43. Zheng Z, Monteil VM, Maurer-Stroh S, et al. Monoclonal antibodies for the S2 subunit of spike of SARS-CoV-1 cross-react with the newly-emerged SARS-CoV-2. *Euro Surveill*. 2020;25(28):2000291.
44. Liu SJ, Leng CH, Lien SP, et al. Immunological characterizations of the nucleocapsid protein based SARS vaccine candidates. *Vaccine.* 2006;24(16):3100–3108.
45. Tilocca B, Soggiu A, Sanguinetti M, et al. Comparative computational analysis of SARS-CoV-2 nucleocapsid protein epitopes in taxonomically related coronaviruses. *Microbes Infect.* 2020;22(4-5):188–194.
46. Guo L, Ren L, Yang S, et al. Profiling early humoral response to diagnose novel coronavirus disease (COVID-19). *Clin Infect Dis.* 2020;71(15):778–785.
47. Burbelo PD, Riedo FX, Morishima C, et al. Sensitivity in detection of antibodies to nucleocapsid and spike proteins of severe acute respiratory syndrome coronavirus 2 in patients with coronavirus disease 2019. *J Infect Dis.* 2020;222(2):206–213.
48. Tehrani ZR, Saadat S, Saleh E, et al. Specificity and performance of nucleocapsid and spike-based SARS-CoV-2 serologic assays. *PLoS One*. 2020;15(11):e0237828.
49. Liu W, Liu L, Kou G, et al. Evaluation of nucleocapsid and spike protein-based enzyme-linked immunosorbent assays for detecting antibodies against SARS-CoV-2. *J Clin Microbiol*. 2020;58(6):e00461-20.
50. Lynch KL, Whitman JD, Lacanienta NP, et al. Magnitude and kinetics of anti-severe acute respiratory syndrome coronavirus 2 antibody responses and their relationship to disease severity. *Clin Infect Dis.* 2021;72(2):301–308.
51. Li K, Huang B, Wu M, et al. Dynamic changes in anti-SARS-CoV-2 antibodies during SARS-CoV-2 infection and recovery from COVID-19. *Nat Commun.* 2020;11(1):6044.
52. Hueston L, Kok J, Guibone A, et al. The antibody response to SARS-CoV-2 infection. *Open Forum Infect Dis.* 2020;7(9):ofaa387.
53. Hsueh PR, Huang LM, Chen PJ, Kao CL, Yang PC. Chronological evolution of IgM, IgA, IgG and neutralisation antibodies after infection with SARS-associated coronavirus. *Clin Microbiol Infect.* 2004;10(12):1062–1066.
54. Iyer AS, Jones FK, Nodoushani A, et al. Dynamics and significance of the antibody response to SARS-CoV-2 infection. Preprint. Posted online July 20, 2020. medRxiv 20155374. doi:10.1101/2020.07.18.20155374

55. Wang Y, Zhang L, Sang L, et al. Kinetics of viral load and antibody response in relation to COVID-19 severity. *J Clin Invest.* 2020;130(10):5235–5244.
56. Yu H-Q, Sun B-Q, Fang Z-F, et al. Distinct features of SARS-CoV-2-specific IgA response in COVID-19 patients. *Eur Respir J*. 2020;56(2):2001526.
57. Iyer AS, Jones FK, Nodoushani A, et al. Persistence and decay of human antibody responses to the receptor binding domain of SARS-CoV-2 spike protein in COVID-19 patients. *Sci Immunol*. 2020;5(52):eabe0367.
58. Long QX, Liu BZ, Deng HJ, et al. Antibody responses to SARS-CoV-2 in patients with COVID-19. *Nat Med.* 2020;26(6):845–848.
59. Shen L, Wang C, Zhao J, et al. Delayed specific IgM antibody responses observed among COVID-19 patients with severe progression. *Emerg Microbes Infect.* 2020;9(1):1096–1101.
60. Wang P, Liu L, Nair MS, et al. SARS-CoV-2 neutralizing antibody responses are more robust in patients with severe disease. *Emerg Microbes Infect.* 2020;9(1):2091–2093.
61. Brochot E, Demey B, Touzé A, et al. Anti-spike, anti-nucleocapsid and neutralizing antibodies in SARS-CoV-2 inpatients and asymptomatic individuals. *Front Microbiol.* 2020;11:584251.
62. Long QX, Tang XJ, Shi QL, et al. Clinical and immunological assessment of asymptomatic SARS-CoV-2 infections. *Nat Med.* 2020;26(8):1200–1204.
63. Wellinghausen N, Plonné D, Voss M, Ivanova R, Frodl R, Deininger S. SARS-CoV-2-IgG response is different in COVID-19 outpatients and asymptomatic contact persons. *J Clin Virol.* 2020;130:104542.
64. Hansen CB, Jarlhelt I, Pérez-Alós L, et al. SARS-CoV-2 antibody responses are correlated to disease severity in COVID-19 convalescent individuals. *J Immunol.* 2021;206(1):109–117.
65. Liu ZL, Liu Y, Wan LG, et al. Antibody profiles in mild and severe cases of COVID-19. *Clin Chem.* 2020;66(8):1102–1104.
66. van der Heide V. Neutralizing antibody response in mild COVID-19. *Nat Rev Immunol.* 2020;20(6):352.
67. Johns Hopkins Bloomberg School of Public Health. Serology tests for COVID-19. https://www.centerforhealthsecurity.org/covid-19TestingToolkit/serology/Serology-based-tests-for-COVID-19.html. Published April 27, 2021. Accessed June 18, 2021.
68. O'Farrell B. Evolution in lateral flow–based immunoassay systems. In: Wong R, Tse H, eds. *Lateral Flow Immunoassay*. Totowa, NJ: Humana Press; 2009:1–33.
69. Lisboa Bastos M, Tavaziva G, Abidi SK, et al. Diagnostic accuracy of serological tests for covid-19: systematic review and meta-analysis. *BMJ.* 2020;370:m2516.
70. Deeks JJ, Dinnes J, Takwoingi Y, et al.; Cochrane COVID-19 Diagnostic Test Accuracy Group. Antibody tests for identification of current and past infection with SARS-CoV-2. *Cochrane Database Syst Rev.* 2020;6:CD013652.
71. Ragnesola B, Jin D, Lamb CC, Shaz BH, Hillyer CD, Luchsinger LL. COVID19 antibody detection using lateral flow assay tests in a cohort of convalescent plasma donors. *BMC Res Notes.* 2020;13(1):372.
72. House Committee on Oversight and Reform. Subcommittee briefing examined state of coronavirus antibody testing. https://oversight.house.gov/news/press-releases/subcommittee-briefing-examined-state-of-coronavirus-antibody-testing. Published June 9, 2020. Accessed April 29, 2021.
73. Augustine R, Das S, Hasan A, et al. Rapid antibody-based COVID-19 mass surveillance: relevance, challenges, and prospects in a pandemic and post-pandemic world. *J Clin Med*. 2020;9(10):3372.
74. Centers for Disease Control & Prevention. Estimated disease burden of COVID-19. https://www.cdc.gov/coronavirus/2019-ncov/cases-updates/burden.html. Updated May 19, 2021. Accessed June 18, 2021.
75. Lassaunière R, Frische A, Harboe ZB, et al. Evaluation of nine commercial SARS-CoV-2 immunoassays. Preprint. Posted online April 10, 2020. bioRxiv 20056325. doi:10.1101/2020.04.09.20056325
76. Traugott M, Aberle SW, Aberle JH, et al. Performance of severe acute respiratory syndrome coronavirus 2 antibody assays in different stages of infection: comparison of commercial enzyme-linked immunosorbent assays and rapid tests. *J Infect Dis.* 2020;222(3):362–366.
77. Amanat F, Stadlbauer D, Strohmeier S, et al. A serological assay to detect SARS-CoV-2 seroconversion in humans. *Nat Med.* 2020;26(7):1033–1036.
78. Poland GA, Ovsyannikova IG, Kennedy RB. SARS-CoV-2 immunity: review and applications to phase 3 vaccine candidates. *Lancet.* 2020;396(10262):1595–1606.
79. Cinquanta L, Fontana DE, Bizzaro N. Chemiluminescent immunoassay technology: what does it change in autoantibody detection? *Auto Immun Highlights.* 2017;8(1):9.
80. Abbott. Abbott receives CE Mark for its COVID-19 IgG quantitative antibody blood test. https://abbott.mediaroom.com/2020-12-15-Abbott-Receives-CE-Mark-for-its-COVID-19-IgG-Quantitative-Antibody-Blood-Test. Published December 15, 2020. Accessed June 18, 2021.
81. Dodd RY, Xu M, Stramer SL. Change in donor characteristics and antibodies to SARS-CoV-2 in donated blood in the US, June-August 2020. *JAMA.* 2020;324(16):1677–1679.
82. Peaper DR, Landry ML. Laboratory diagnosis of viral infection. *Handb Clin Neurol.* 2014;123:123–147.
83. Wang K, Long Q-X, Deng H-J, et al. Longitudinal dynamics of the neutralizing antibody response to SARS-CoV-2 infection. *Clin Infect Dis*. Published online ahead of print August 3, 2020. doi:10.1093/cid/ciaa1143.
84. Salazar E, Kuchipudi SV, Christensen PA, et al. Convalescent plasma anti-SARS-CoV-2 spike protein ectodomain and receptor-binding domain IgG correlate with virus neutralization. *J Clin Invest.* 2020;130(12):6728–6738.
85. Lau EHY, Tsang OTY, Hui DSC, et al. Neutralizing antibody titres in SARS-CoV-2 infections. *Nat Commun.* 2021;12(1):63.
86. U.S. Food & Drug Administration. Coronavirus (COVID-19) update: FDA authorizes first test that detects neutralizing antibodies from recent or prior SARS-CoV-2 infection. https://www.fda.gov/news-events/press-announcements/coronavirus-covid-19-update-fda-authorizes-first-test-detects-neutralizing-antibodies-recent-or. Published November 6, 2020. Accessed June 18, 2021.
87. Centers for Disease Control & Prevention. Using antibody tests for COVID-19. https://www.cdc.gov/coronavirus/2019-ncov/lab/resources/antibody-tests.html. Published November 3, 2020. Accessed June 18, 2021.
88. Mallett S, Allen AJ, Graziadio S, et al. At what times during infection is SARS-CoV-2 detectable and no longer detectable using RT-PCR-based tests? A systematic review of individual participant data. *BMC Med.* 2020;18(1):346.
89. Sethuraman N, Jeremiah SS, Ryo A. Interpreting diagnostic tests for SARS-CoV-2. *JAMA.* 2020;323(22):2249–2251.
90. Centers for Disease Control & Prevention. COVID-19 serology surveillance strategy. https://www.cdc.gov/coronavirus/2019-ncov/covid-data/serology-surveillance/index.html. Published February 12, 2021. Accessed April 29, 2021.
91. Centers for Disease Control & Prevention. Large-scale geographic seroprevalence surveys. https://www.cdc.gov/coronavirus/2019-ncov/cases-updates/geographic-seroprevalence-surveys.html. Updated October 2, 2020. Accessed June 18, 2021.
92. Angulo FJ, Finelli L, Swerdlow DL. Estimation of US SARS-CoV-2 infections, symptomatic infections, hospitalizations, and deaths using seroprevalence surveys. *JAMA Netw Open.* 2021;4(1):e2033706.
93. Centers for Disease Control & Prevention. Interim guidelines for COVID-19 antibody testing. https://www.cdc.gov/coronavirus/2019-ncov/lab/resources/antibody-tests-guidelines.html. Published March 17, 2021. Accessed April 29, 2021.
94. American Red Cross. How convalescent plasma may help fight COVID-19. https://www.redcrossblood.org/local-homepage/news/article/how-convalescent-plasma-may-help-fight-covid-19.html. Published November 19, 2020. Accessed June 18, 2021.

95. Peterhoff D, Glück V, Vogel M, et al. A highly specific and sensitive serological assay detects SARS-CoV-2 antibody levels in COVID-19 patients that correlate with neutralization. *Infection.* 2021;49(1):75–82.

96. Quilty BJ, Clifford S, Hellewell J, et al.; Centre for the Mathematical Modelling of Infectious Diseases COVID-19 working group. Quarantine and testing strategies in contact tracing for SARS-CoV-2: a modelling study. *Lancet Public Health.* 2021;6(3):e175–e183.

97. Winter AK, Hegde ST. The important role of serology for COVID-19 control. *Lancet Infect Dis.* 2020;20(7):758–759.

98. Abbasi J. The promise and peril of antibody testing for COVID-19. *JAMA.* 2020;323(19):1881–1883.

99. Isho B, Abe KT, Zuo M, et al. Persistence of serum and saliva antibody responses to SARS-CoV-2 spike antigens in COVID-19 patients. *Sci Immunol*. 2020;5(52):abe5511.

100. Karp DG, Danh K, Espinoza NF, Seftel D, Robinson PV, Tsai CT. A serological assay to detect SARS-CoV-2 antibodies in at-home collected finger-prick dried blood spots. *Sci Rep.* 2020;10(1):20188.

101. Baratloo A, Hosseini M, Negida A, El Ashal G. Part 1: simple definition and calculation of accuracy, sensitivity and specificity. *Emerg (Tehran).* 2015;3(2):48–49.

102. Watson J, Richter A, Deeks J. Testing for SARS-CoV-2 antibodies. *BMJ.* 2020;370:m3325.

103. Penn State Eberly College of Science. STAT 507: epidemiological research methods: 10.3—sensitivity, specificity, positive predictive value, and negative predictive value. https://online.stat.psu.edu/stat507/lesson/10/10.3. Accessed June 18, 2021.

104. Baron RC, Risch L, Weber M, et al. Frequency of serological nonresponders and false-negative RT-PCR results in SARS-CoV-2 testing: a population-based study. *Clin Chem Lab Med.* 2020;58(12):2131–2140.

105. Freeman MC, Rapsinski GJ, Zilla ML, Wheeler SE. Immunocompromised seroprevalence and course of illness of SARS-CoV-2 in one pediatric quaternary care center. *J Pediatric Infect Dis Soc*. 2021;10(4):426–431.

106. Bajema KL, Wiegand RE, Cuffe K, et al. Estimated SARS-CoV-2 Seroprevalence in the US as of September 2020. *JAMA Int. Med.* 2021;181(4):450–460.

107. Sutton M, Cieslak P, Linder M. Notes from the field: seroprevalence estimates of SARS-CoV-2 infection in convenience sample—Oregon, May 11–June 15. *Morb. Mortal. Weekly Rep.* 2020;69(32):1100.

108. Pickering S, Betancor G, Galão RP, et al. Comparative assessment of multiple COVID-19 serological technologies supports continued evaluation of point-of-care lateral flow assays in hospital and community healthcare settings. *PLoS Pathog.* 2020;16(9):e1008817.

109. Findeisen P, Stiegler H, Lopez-Calle E, et al. Clinical performance evaluation of a SARS-CoV-2 rapid antibody test for determining past exposure to SARS-CoV-2. *Int J Infect Dis.* 2021;103:636–641.

110. Whitman JD, Hiatt J, Mowery CT, et al. Test performance evaluation of SARS-CoV-2 serological assays. Preprint. Posted online May 17, 2020. medRxiv 20074856. doi:10.1101/2020.04.25.20074856.

111. National Institutes of Health. Rapid acceleration of diagnostics (RADx). https://www.nih.gov/research-training/medical-research-initiatives/radx. Accessed June 18, 2021.

112. Kalish H, Klumpp-Thomas C, Hunsberger S, et al. Mapping a pandemic: SARS-CoV-2 seropositivity in the United States. *Preprint posted* online January 31, 2021. *medRxiv 21250570*. doi:10.1101/2021.01.27.21250570.

113. Centers for Disease Control & Prevention. Science brief: emerging SARS-CoV-2 variants. https://www.cdc.gov/coronavirus/2019-ncov/science/science-briefs/scientific-brief-emerging-variants.html?CDC_AA_refVal=www.cdc.gov/coronavirus/2019-ncov/more/science-and-research/scientific-brief-emerging-variants.html. Published January 28, 2021. Accessed June 18, 2021.

114. West R, Gronvall GK, Kobokovich A. Variants, vaccines and what they mean for COVID-19 testing. https://www.jhsph.edu/covid-19/articles/variants-vaccines-and-what-they-mean-for-covid19-testing.html. Published February 2, 2021. Accessed June 18, 2021.

CASE STUDY

Massive Transfusion Protocol in a 69 Year Old Woman with Alloantibodies

Jesse Qiao, MD,[1] *Jude M. Abadie, PhD, DABCC, FAACC, DABMGG, FACMG*[1,*]

[1]Department of Pathology, Paul L. Foster School of Medicine, Texas Tech University Health Sciences Center, El Paso, Texas, United States; *To whom correspondence should be addressed. jude.abadie@ttuhsc.edu

Keywords: transfusion, incompatible, uncrossmatched, RBC antibodies, transfusion, blood banking

Abbreviations: RBC, red blood cell; MHP, massive hemorrhage protocol; TXA, tranexamic acid; DAT, direct antiglobulin test; LDH, lactate dehydrogenase.

Laboratory Medicine 2022;53:e30–e32; https://doi.org/10.1093/labmed/lmab066

ABSTRACT

Unlike routine blood transfusions that are managed by attending providers and rely on compatibility testing, massive transfusions are managed by the trauma team members, who usually do not have immediate access to compatibility testing. Incompatible C or E antigens, when present in uncrossmatched O positive blood, require transfusion support so that health care professionals can manage potential causes for extravascular hemolysis. Herein, we describe a massive transfusion situation in which immediate patient management was required to mitigate potentially fatal clinical consequences of transfused red blood cell antibodies. In addition, this case study shows how the utility of chemistry and hematology laboratory results can illustrate the complexities of massive transfusion management in the context of incompatible C or E antigens.

The characterization of massive transfusion has been historically described as the transfusion replacement of 10 red blood cell (RBC) units within 24 hours in response to massive and uncontrolled bleeding.[1] Through the development of more rapid and effective therapy, updated criteria have been proposed to identify patients requiring rapid products for serious injuries related to uncontrolled bleeding.[1] Newer criteria include administering 3 units of RBCs during 1 hour or any 4 blood components within 30 minutes, and universal ABO products are used for resuscitation. This usually includes group O packed RBCs, with group AB or low-titer group A plasma, or, less commonly, low-titer group O whole blood. Because the compatibility of non-ABO is not immediately prioritized in acute hemorrhage, the aforementioned is considered standard-of-care until the ABO group is confirmed using 2 separate specimens.

Case Report

A 69 year old female patient with a past medical history of obesity, uncontrolled diabetes mellitus type II, hypertension, and hypothyroidism presented to the emergency department with multiple episodes of nausea and acute-onset hematemesis. On arrival, she had a hemoglobin level of 8.1 g/dL, an international normalized ratio within normal limits, and platelets of 87,000/μL. Additional laboratory values and corresponding reference ranges are summarized in **TABLE 1**. Her blood type was assessed as group O, Rh positive. Subsequently, 3 units of emergency-release, uncrossmatched O positive RBCs were administered. The patient was rapidly decompensating because of hemorrhagic shock secondary to severe bleeding in her upper gastrointestinal tract. During that time, the attending physician activated a massive hemorrhage protocol (MHP), the rapid administration of large amounts of blood products (at least 6 units of packed RBCs) in fixed 1:1:1 ratios (plasma:platelets:RBCs) for the management of hemorrhagic shock. This procedure is significant, considering that up to 20% of deaths are potentially preventable with better control of bleeding.[2]

TABLE 1. Laboratory Results After Transfusion of the 3 O Positive, Uncrossmatched Blood Units

Analyte	Result		
White blood count	9.13 × 10^3/mm^3	(4.50–11.00)	
Hemoglobin	8.1 g/dL	(12.0–15.0)	L
Hematocrit	25.2%	(36.0–47.0)	L
Platelets	87 × 10^3/mm^3	(150–450)	L
Potassium	4.2 mmol/L	(3.5–5.1)	
Creatinine	0.6 mg/dL	(0.52–1.04)	
Bilirubin total	0.90 mg/dL	(0.2–1.3)	
INR	1.4	(0.9 – 1.1)	H
Partial thromboplastin time	30.8 sec	(23.3–33.6)	
Fibrinogen level	118 mg/dL	(234–500)	L
DAT	Weakly positive, polyspecific		

DAT, direct antiglobulin test; H, high; INR, international normalized ratio; L, low.
Reference ranges included in parentheses.

The blood bank initiated a plasma thaw in anticipation of an emergent need for massive transfusion. During this time, blood bank testing revealed that the patient had a positive antibody screen indicating the presence of an anti-C and anti-E antibody. This testing was performed using solid-phase (Immucor Echo) antibody panel detection, with strong (3+ to 4+) reactivity against panel cells with C and E antigen positivity. Based on these results and the patient's presentation, the clinical team decided to forego the use of additional uncrossmatched O positive blood and wait for the arrival of antigen-compatible O positive blood. There was an approximately 1-hour average time for this product to arrive via delivery from the local blood supplier. However, during that time, the patient's hypotension worsened, which, combined in the setting of hemorrhagic shock, led to her death approximately 90 minutes after the initial transfusion.

Just before the patient's death, a final hematocrit result was 9.0 g/dL and did not show evidence of gross hemolysis. Additional specimens, including urine, were not available for evaluation before the time of death and posttransfusion. Phenotyping of the 3 emergently transfused blood showed 2 units positive for the C and E antigens (crossmatch-incompatible). Because a transfusion reaction workup was not ordered, there was concern that transfusion of the incompatible units may have led to the death of the patient.

Questions for Consideration

1. How are massive transfusions different from routine blood transfusions?
2. What should have been done differently in the immediate clinical course of this patient, to better meet transfusion requirements?
3. How are anti-C and anti-E RBC antibodies addressed in the context of massive transfusion?
4. What additional laboratory workup could include or exclude hemolysis?
5. Should there be concern for a hemolytic transfusion reaction as the *cause* of death?

Discussion

When managing transfusions, it is critical to understand how massive transfusions differ from routine transfusions. Both are regulated through hospital transfusion services that are governed by the US Food & Drug Administration and either the College of American Pathologists, as in this case study, the American Association of Blood Banks (AABB), or both organizations. During routine, nonemergent circumstances, laboratory testing is performed on all patients before they receive blood products. This practice ensures compatibility and supports proper identification of the patient's ABO blood type. At a minimum, approximately 1 to 1.5 hours are usually required for a patient to receive crossmatch-compatible blood, including time to receive and perform the ABO/Rh type, antibody screen, and an immediate spin or electronic crossmatch (assuming a negative antibody screen result). Any blood products emergently required before the completion of testing would be uncrossmatched, universal donor products (O positive RBCs and AB plasma).

However, during a massive transfusion, compatibility testing is not routinely performed, mainly because of time constraints in the blood bank in the preparation of blood products to be used for emergency transfusion and resuscitation of patients with acute and active mass hemorrhage. Much of the preparation time includes the thawing of fresh frozen plasma (up to 20 minutes) and the continued preparation and thawing of products that are directed by the clinical team managing the massive hemorrhage protocol.

In retrospect, the immediate clinical management of our patient could have been approached differently to meet transfusion requirements. Instead of waiting for C and E antigen negative units from the blood supplier, uncrossmatched universal donor products (O positive RBCs and AB fresh frozen plasma) could have been accepted. Given the patient's low fibrinogen levels, units of cryoprecipitate that are routinely administered during our massive transfusion protocol could have been an appropriate course. Tranexamic acid (TXA) was not considered by the clinical team as a course of treatment units. Accepting universal donor products initially could save lives, and waiting for crossmatch-compatible units during massive transfusions could lead to poor outcomes. Based on the CRASH-2 and WOMAN trials,[3] early administration of TXA in this patient with hemorrhage could have resulted in a more favorable outcome.

Research has shown that 15% to 20% of the White donor population and 50% to 60% of Black populations are negative for both the C and E antigens.[4] Given this prevalence, it can be difficult to address the presence of anti-C and anti-E RBC antibodies in the context of massive transfusions. It follows that if any given patient receives several rounds of O positive universal donor RBCs, then it would be likely that more than half of those units would be incompatible because they would contain either the C or the E antigens.

Anti-C and anti-E are present usually from exposure to C and E antigen positive RBCs, respectively, and they are typically acquired from prior transfusion(s) or pregnancies.[5] Hemolysis caused by anti-C and anti-E is usually of delayed onset, meaning that these antigens are IgG in nature and do not usually cause immediate clinical consequences. Furthermore, during a mass hemorrhage event, a patient's blood volume will undergo rapid turnover because of exsanguination and replacement. Therefore, during such rapid turnover and transfusion, delayed hemolysis is not an immediate clinical concern. Hemolysis secondary to anti-C and anti-E may arise after acute resuscitation, in which routine transfusions of C and E antigen negative units would then be appropriate to boost endogenous RBC production. This factor becomes critical in the management of a patient's subsequent anemia.

After a massive transfusion in the setting of known anti-C and anti-E, the blood bank usually requests C and E antigen negative units from the supplier and ensures crossmatch compatibility with the patient. During the next few days, the clinical team monitors serial hemoglobin and hematocrit, along with other signs of extravascular hemolysis. Transfusion support is subsequently provided on a routine and as-needed basis with the C and E antigen negative units received from the blood supplier.

Because the prevalence of C and E antigen negative units in the O-positive donor population is low, an additional consideration would be to administer O negative RBC units as an alternative to antigen negative RBC units, when there is insufficient time to perform antigen typing. Furthermore, D-negative donors are likely to be C and E negative because of the r haplotype (dce) being the most common D negative haplotype. However, in the case of our patient, we had only 4 units of O negative blood at the time, and those units are reserved for women aged ≤45 years (childbearing age) with unknown blood type. In addition, the timing of this patient's case coincidentally occurred during peak COVID-19 events that drastically reduced blood donations.

TABLE 2 lists different types of RBC antibodies that can cause hemolysis and that clinicians can use to help identify additional labora-

TABLE 2. Different Types of RBC Antibodies That Can Cause Hemolysis[5]

Antibody Type	IgM (mainly ABO)	IgG (most other blood groups)
Hemolysis type	Intravascular	Extravascular (reticuloendothelial system of the spleen)
Clinical severity	Severe to fatal	Mild to moderate
Onset of symptoms	Immediate	Delayed[a]
Patient complaints or presentation	Fever, back pain, chills, shortness of breath, an "impending sense of doom," confusion, jaundice.	Mild to no symptoms, jaundice/itching within several days of transfusion
Hyperkalemia	Usually present	Not present
Renal failure	May be present	Not present
Evidence of shock/DIC	May be present	Absent
Blood in urine	Usually present	May be present
Hemoglobin	Decreased	Decreased
Haptoglobin	Decreased	May be decreased
LDH	Increased	May be increased
Serum bilirubin	Increased	Increased
DAT	Positive, specific for C3 (may also show IgG positivity)	Sometimes positive, specific for IgG only

DAT, direct antiglobulin test; DIC, disseminated intravascular coagulopathy; LDH, lactate dehydrogenase
[a]Usually 3–14 days.

tory tests that could rule in or rule out hemolysis. In our case study, as listed in **TABLE 1**, a comprehensive metabolic panel was ordered that included potassium, bilirubin, and creatinine. All were within normal limits. A direct antiglobulin test (DAT) performed by the blood bank was weakly positive with immunoglobulin polyspecificity. Additional tests that could have been ordered to better assess hemolysis include serial hemoglobin and hematocrits, lactate dehydrogenase (LDH), haptoglobin, urine hemoglobin, and RBC elution studies. A posttransfusion type and screen and compatibility testing on returned units may have provided a better assessment of the clinical picture.

Based on the information presented in this case study, it is unlikely that a hemolytic transfusion reaction was the cause of death. Hemolysis was not identified in the posttransfusion specimen assayed for hemolysis and hemoglobin, and other related test values were within normal limits. However, a complete assessment to exclude hemolysis was not definitive because additional testing was not performed for haptoglobin or LDH or on posttransfusion urine specimens. Furthermore, although a positive DAT alone does not equate to hemolysis, it indicates that a patient has bound antibodies to RBCs.[6] A positive DAT is not specific for hemolysis and often presents secondary to drug effects.[7] In the absence of clinical or laboratory evidence of hemolysis after several days, most patients with anti-C, anti-E, and a positive DAT should raise suspicion for a delayed serologic (not hemolytic) transfusion reaction. An additional specimen was not available to confirm the presence or absence of an eluate in this patient. To confirm a delayed serologic/hemolytic reaction, the presence of the offending antibody must be detected by RBC elution studies after the DAT.

In summary, the anti-C and anti-E RBC antibodies are IgG in nature and therefore do not cause intravascular hemolysis that is usually associated with IgM antibodies. Furthermore, IgM antibodies (mostly ABO) often lead to devastating clinical consequences and metabolic derangements.[8] Because the patient in this case study decompensated during a few hours, the timing for extravascular hemolysis because of anti-C and anti-E would have been too soon for symptoms to develop. Furthermore, in patients in whom symptoms do develop, those symptoms should be mild to moderate and not consistent with the life-threatening symptoms observed in acute intravascular hemolysis. A central factor when assessing patients with similar challenging transfusion cases is to distinguish between acute and delayed hemolysis in roles for posttransfusion outcomes and assess whether the transfusion itself may have been a contributing factor.

Acknowledgments

We thank Ms. Jennifer Davila, supervisor of blood bank and transfusion services.

Conflict of Interest

The authors have no disclosures or conflicts of interest.

REFERENCES

1. Jennings LK, Watson S. Massive transfusion. In: Jennings LK, Watson S. *StatPearls*. Treasure Island, FL: StatPearls Publishing; 2020.
2. Miller TE. New evidence in trauma resuscitation—is 1:1:1 the answer? *Perioper Med.* 2013;2(1):13.
3. Holcomb JB, Fox EE, Zhang X, et al.; PROMMTT Study Group. Cryoprecipitate use in the PROMMTT study. *J Trauma Acute Care Surg.* 2013;75(1 Suppl 1):S31–S39.
4. Daniels G. *Rh and RHAG blood group systems*. In: Daniels G. *Human Blood Groups. 3rd ed. Hoboken, NJ: Wiley; 2013:* 184–187.
5. Harmening D. *Adverse effects of transfusion*. In: Harmening D. *Modern Blood Banking and Transfusion Practices. 6th ed.* Philadelphia, PA: F.A. Davis Company; 2012: 367–390.
6. Mejia Buritica L, Zapata Alvarez J, Vergara Quintero L, Villegas Molina JP, Torres Hernandez JD. Autoimmune hemolytic anemia after cyanocobalamin replacement in a patient with a previous diagnosis of pernicious anemia: a case report. *Cureus.* 2020;12(10):e10797.
7. de Araújo CDSR, Machado BA, Fior T, et al. Association of positive direct antiglobulin test (DAT) with nonreactive eluate and drug-induced immune hemolytic anemia (DIHA). *Transfus Apher Sci.* 2021;60(1):103015.
8. Galvez C, Abutaleb A, Iams WT, Lindholm PF, Kwaan HC. Fatal massive hemolysis caused by immunoglobulin M anti-c antibody in a patient with newly diagnosed B-cell acute lymphoblastic leukemia: a case report. *Clin Case Rep.* 2018;6(6):1090–1093.

CASE STUDY

From A to AB: A Caucasian Mother with High Anti-B Titer Causing Hemolytic Disease of the Newborn

Nathanael Schooley, ARNP[1] *Shilpi Chabra, MD,*[1,2] *Moritz Stolla, MD*[3,4]✉

[1]Seattle Children's Hospital, Seattle, Washington, US; [2]Department of Neonatology, University of Washington School of Medicine, Seattle, Washington, US; [3]Bloodworks Northwest Research Institute, Seattle, Washington, US; [4]Department of Medicine, Division of Hematology, University of Washington School of Medicine, Seattle, Washington, US; *To whom correspondence should be addressed. mstolla@bloodworksnw.org

Keywords: ABO, HDFN, phototherapy, hemolysis, isosensitization, IVIG.

Abbreviations: RBC, red blood cell; HRZ, high-risk zone; PT, phototherapy; DAT, direct antiglobulin test; HDFN, hemolytic disease of the fetus and newborn; IVIG, intravenous immunoglobulin.

Laboratory Medicine 2022;53:e33–e35; https://doi.org/10.1093/labmed/lmab067

ABSTRACT

We report on a term infant with clinically significant hemolysis and hyperbilirubinemia. Testing revealed ABO incompatibility between maternal type A and infant type AB. The maternal alloantibody screen was negative. The infant's direct antiglobulin test was positive, and anti-B IgG was eluted off the infant's red blood cells (RBCs). Testing of the mother's plasma revealed a high anti-B titer. The infant was successfully treated with phototherapy and intravenous immunoglobulin. The bilirubin and hematocrit stabilized, and the infant was discharged home. This case was unusual because of its severity and unusual ABO constellation. Furthermore, this report is an exemplary educational case study on how effective collaboration between the clinical team and the blood bank laboratory is critical in reaching the correct diagnosis. In summary, the differential diagnosis of more unusual and atypical ABO-incompatible constellations must be considered when an infant presents with unexplained hemolysis.

Clinical History

A 39-week gestational age infant was born via vaginal delivery to a 30 year old White multigravida mother. At age 20 hours, the infant developed clinically significant hyperbilirubinemia and anemia because of hemolysis. The infant was transferred to the neonatology service for evaluation and management of hyperbilirubinemia. The admission laboratory tests had shown a total bilirubin of 13.3 mg/dL at age 17 hours, which was in the high-risk zone (HRZ), and intensive phototherapy (PT) was started (**TABLE 1**). The hematocrit had initially decreased from 39% at age 3 hours to 29% at age 17 hours. The initial reticulocyte count was elevated to 12%, suggesting hemolysis and a high RBC turnover. The blood bank reported the mother's ABO type as A with a negative alloantibody test. The infant's ABO type was AB with a 1+ positive direct antiglobulin test (DAT). Both mother and child were RhD-positive. Because the vast majority of ABO-mediated hemolytic disease of the fetus and newborn (HDFN) in the literature describes mothers with type O giving birth to infants with type A or B, the care team considered this diagnosis less likely. Abdominal and cranial ultrasounds within 24 hours of birth revealed no evidence of active hemorrhage. The Kleihauer-Betke test was negative within 24 hours of birth, essentially ruling out significant fetomaternal hemorrhage.

At age 24 hours, the bilirubin had risen to 14.9 mg/dL (exchange transfusion threshold 16.5 mg/dL)[1,2] despite intensive phototherapy. Intravenous immunoglobulin (IVIG) was administered because of laboratory evidence of hemolysis. Based on the hyperbilirubinemia severity, one of the differential diagnoses suspected by the team was minor blood group incompatibility (not covered by the maternal alloantibody screen). The PT was briefly discontinued at approximately age 62 hours because of reduced bilirubin levels to the low intermediate risk zone. However, PT was restarted at 80 hours because bilirubin increased again to the HRZ (above the PT treatment threshold). Repeat testing for alloantibodies against RBCs with less common "low frequency" antigens was negative, ruling out this differential diagnosis. A smear to examine RBC morphology showed moderate anisopoikilocytosis and ruled out spherocytosis. However, an eluate from the infant's RBCs revealed anti-B IgG antibodies, and the mother's plasma revealed a high titer of 512. By age 105 hours, the infant's bilirubin levels decreased, the hematocrit stabilized at 27%, and the reticulocyte count decreased to 9% (**TABLE 1**). Therefore, PT was discontinued. On day 6, the infant was discharged home and we advised his mother to follow up with the pediatrician. In summary, our clinical

TABLE 1. Total Serum Bilirubin by Hours of Age

Hours of Age	Total Serum Bilirubin	Intervention
16	13.3 (HRZ)	Started PT
24	14.9 (HRZ)	Given IVIG
30	11.6 (HRZ)	Stopped PT
80	15.2 (HIR)	Restarted PT
105	12.2 (LRZ)	Stopped PT

HIR, high-intermediate risk; HRZ, high-risk zone; LRZ, low-risk zone; PT, phototherapy.

AQ13 and laboratory evaluation established a diagnosis of HDFN resulting from isoimmunization based on ABO incompatibility between mother and infant.

Discussion

The case we describe here is unusual for 3 reasons; (i) HDFN occurring with a rare ABO configuration between mother and infant (A vs AB, respectively), (ii) high anti-B titers are unusual in White patients without an isohemagglutinin-stimulating event, and (iii) the disease severity. Mothers of infants with HDFN resulting from ABO incompatibility are almost exclusively typed O. There are numerous case reports describing patients with severe HDFN with mothers typed as O with Anti-B, or mothers typed as B with anti-A-causing HDFN.[3-8] Generally, mothers typed as O are far more likely to have anti-A, anti-B, or anti-A,B IgG antibodies, which allow for transplacental passage.[9,10] Although mothers with type A and anti-B-induced HDFN have been described, they are exceedingly rare, involve patients of other races/ethnicities, or are not available in English-language publications.[11-13]

Research has shown that ABO-associated HDFN is usually mild because of low expression levels of the A and B antigen on neonatal erythrocytes and the wide distribution of A- and B-expressing tissues in the body, allowing for relative neutralization of the antibodies.[1] When severe ABO is observed, one or all alleviating factors are altered, eg, higher expression levels on RBCs based on race or ethnicity, or higher maternal antibody titers.[1] For White patients, anti-A titers are usually higher than anti-B titers. This is true when comparing titers in mothers with group A with those in mothers with group B and both antibodies in mothers with group O. In addition, anti-A titers are usually higher in patients with group O than in those with group B, and similarly, anti-B titers are higher in patients with group O than in those with group A.[14] Therefore, in White patients with type A, anti-B titers should be the lowest isohemagglutinin titers reported across all ABO groups.

Notably, all ABO isohemagglutinins have the capacity to cause clinical sequelae,[15] and IgG isohemagglutinins can fix complement and cause intravascular and extravascular hemolysis.[16] Anti-A,B has been reported to be the most clinically significant antibody in ABO HDFN: Infants' RBCs that are coated by anti-A,B are more likely to require treatment compared to those coated by anti-A or anti-B.[16]

In newborns, early B1 B lymphocytes start producing mostly IgM anti-ABO isohemagglutinins without previous exposure to antigens. Later in life, B2 B lymphocytes make predominantly IgG ABO isohemagglutinins. The B2 B lymphocyte pathway requires the contribution of T lymphocytes and adaptive immunity and is triggered by external antigens.[15,17-22] The mother we describe in this case report had 3 previous pregnancies with the same partner. The naturally occurring antibody was anti-B IgM, which usually predominates in group A individuals. The infant's father is AB, RhD-positive, and they had previous children, theoretically allowing for previous HDFN
AQ12 or fetomaternal hemorrhages. Therefore, previous pregnancies could theoretically have contributed by exposing the mother to B antigen–expressing RBCs of the neonate, thereby facilitating the production of high-titer anti-B IgG antibodies by her immune system. Increased isohemagglutinin titers after incompatible ABO transfusions have been described in the literature. The high density of A or B antigens on erythrocytes allows for the adsorption of large amounts of the antibody after ABO-incompatible transfusions, leading to titer decrease via the clearance of the antibody-coated incompatible RBCs. After a nadir, the levels increase, eventually exceeding the baseline.[23-26] This phenomenon has been described after the transfusion of as little as 4 mL of ABO-incompatible RBCs.[27] However, it remains speculative whether there was fetomaternal hemorrhage in any previous pregnancies in this mother. Other possible explanations for increased ABO titers include the use of probiotics or previous vaccinations.[28-31] The patient did not report any probiotic use or recent vaccinations. Finally, living on the African continent for a prolonged period of time has been discussed as a potential reason for higher anti-B titers, but it is unknown whether this is due to environmental or genetic factors.[32-34] Still, the mother in this report is White and did not live outside of the United States, leaving the etiology of the high anti-B titer cryptic.

The use of IVIG in ABO incompatibility occurs less often than in RhD incompatibility. There are conflicting reports in the literature regarding the efficacy of IVIG in preventing hemolysis in ABO HDFN.[35] Although postnatal IVIG administration is linked to shorter hospitalizations and PT use, it has risks to consider, including hemolysis from anti-B antibodies.[36] Research has shown that IVIG reduces hemolysis of neonatal erythrocytes, presumably by obstructing Fc receptor sites on reticuloendothelial cells. Thus, it prevents significant ongoing lysis of neonatal erythrocytes. In this patient's case, there was a decrease in the reticulocyte count from 12% to 9% in 88 hours, but whether this occurred because of the disease's natural progression or because of successful treatment with IVIG is unclear.

Laboratory Role in Diagnosis

The blood bank laboratory was critical in our staff reaching a diagnosis by providing the ABO type and antibody screen (including screening for low-frequency antibodies). Furthermore, we performed the DAT, the eluate, and a titer of anti-B.

We found the maternal anti-B IgG titer to be 512 by tube testing. A meta-analysis from 2015 showed that the level of maternal IgG anti-A or anti-B antibodies correlates with the risk of ABO HDFN.[37] In general, a titer of 512 or higher was found to be very suggestive of HDFN. One review found that titers of 512 had a sensitivity of 90% and a specificity of 72% for predicting immunoglobulin treatment and severe hyperbilirubinemia.[38] Previous research also established a significant link between maternal anti-B IgG titers, as seen in this case study, and hemolysis-induced hyperbilirubinemia, requiring treatment. Anti-B antibodies have also been reported to cause more severe hemolysis than anti-A antibodies.[39] The laboratory workup showed a 1+ positive DAT. Contrary to RhD HDFN, patients with ABO HDFN can show very weak DATs with severe disease.[40]

There are very few case studies in the literature with a similar presentation, but one study found an incidence of severe anti-B ABO incompatibility resulting in severe fetal anemia, necessitating intrapartum transfusion and early delivery because of recurrent anemia.[3]

Other reasons for the presentation can include erythrocyte membrane defects such as spherocytosis, erythrocyte enzyme defects such as G6PD, and Gilbert syndrome. We ruled out spherocytosis through an RBC morphology smear. Research has shown that ABO antibodies occur naturally, and there was no trauma history, so the value of testing for fetomaternal hemorrhage was limited.[41] Nevertheless, a Kleihauer-Betke test was sent and reported as negative, essentially out significant fetomaternal hemorrhage. Gilbert syndrome was considered unlikely because of the presence of anemia and reticulocytosis.

Acknowledgments

The authors thank Sue Groshong, the librarian at Seattle Children's Hospital. She was integral in completing a literature search for this case report. In addition, the authors thank Greg Valentine, MD, who provided great feedback of the initial draft and perspective on the process of publication.

Conflicts of Interest

M.S. received research funding from Cerus Corp.

REFERENCES

1. Murray NA, Roberts IA. Haemolytic disease of the newborn. *Arch Dis Child Fetal Neonatal Ed.* 2007;92(2):F83–F88.
2. Padmanabhan A, Connelly-Smith L, Aqui N, et al. Guidelines on the use of therapeutic apheresis in clinical practice—evidence-based approach from the writing committee of the American Society for Apheresis: the eighth special issue. *J Clin Apher.* 2019;34(3):171–354.
3. Ziprin JH, Payne E, Hamidi L, Roberts I, Regan F. ABO incompatibility due to immunoglobulin G anti-B antibodies presenting with severe fetal anaemia. *Transfus Med.* 2005;15(1):57–60.
4. McDonnell M, Hannam S, Devane SP. Hydrops fetalis due to ABO incompatibility. *Arch Dis Child Fetal Neonatal Ed.* 1998;78(3):F220–F221.
5. Sherer DM, Abramowicz JS, Ryan RM, Sheils LA, Blumberg N, Woods JR Jr. Severe fetal hydrops resulting from ABO incompatibility. *Obstet Gynecol.* 1991;78(5 Pt 2):897–899.
6. Suria AA, Nurasyikin Y, Adibah AG, Cheah FC, Leong CF. ABO incompatibility and glucose-6-phosphate dehydrogenase deficiency presenting as Hydrops Foetalis. *Clin Ter.* 2014;165(3):151–154.
7. Metcalf RA, Khan J, Andrews J, Mayock D, Billimoria Z, Pagano MB. Severe ABO hemolytic disease of the newborn requiring exchange transfusion. *J Pediatr Hematol Oncol.* 2019;41(8):632–634.
8. Wang R, Li Y, Tong Y, Su N. Hemolytic disease of the fetus and newborn caused by anti-group A IgG from a group B mother. *J Pediatr Hematol Oncol.* Published online ahead of print September 29, 2020. doi: 10.1097/mph.0000000000001948.
9. Kochwa S, Rosenfield RE, Tallal L, Wasserman LR. Isoagglutinins associated with ABO erythroblastosis. *J Clin Invest.* 1961;40:874–883.
10. Rawson AJ, Abelson NM. Studies of blood groups antibodies. III. Observations on the physicochemical properties of isohemagglutinins and isohemolysins. *J Immunol.* 1960;85:636–639.
11. Munk-Andersen G. Excess of group O-mothers in ABO-haemolytic disease. *Acta Pathol Microbiol Scand.* 1958;42(1):43–80.
12. Kumlien G, Sarman I, Shanwell A. A case of neonatal ABO immunization which was difficult to diagnose. The mother with blood group A2 and the infant with negative direct antiglobulin test. Article published in Swedish. *Lakartidningen.* 2000;97(38):4138–4140.
13. Haque KM, Rahman M. An unusual case of ABO-haemolytic disease of the newborn. *Bangladesh Med Res Counc Bull.* 2000;26(2):61–64.
14. Ichikawa Y. A study of the iso-agglutinin titres in the sera of Australian subjects (white). *Jpn J Med Sci Biol.* 1959;12:1–7.
15. Branch DR. Anti-A and anti-B: what are they and where do they come from? *Transfusion.* 2015;55(Suppl 2):S74–S79.
16. Mollison PL. *Blood Transfusion in Clinical Medicine*. Oxford, UK: Blackwell Scientific Publications; 1983: 290–291.
17. Yamamoto S. The occurrence of materials cross-reacting with anti-A and -B agglutinins in fruit or seed extracts of higher plants. *J Immunogenet.* 1977;4(5):325–330.
18. Chattoraj A, Gilbert R Jr, Josephson AM. Serological demonstration of fetal production of blood group isoantibodies. *Vox Sang.* 1968;14(4):289–291.
19. Thomaidis T, Fouskaris G, Matsaniotis N. Isohemagglutinin activity in the first day of life. *Am J Dis Child.* 1967;113(6):654–657.
20. De Biasi B. Studies on iso-agglutinins in the blood of the new-born. *JAMA*. 1923;81(21):1776–1778.
21. Wuttke NJ, Macardle PJ, Zola H. Blood group antibodies are made by CD5+ and by CD5- B cells. *Immunol Cell Biol.* 1997;75(5):478–483.
22. Springer GF, Williamson P, Brandes WC. Blood group activity of gram-negative bacteria. *J Exp Med.* 1961;113(6):1077–1093.
23. Wiener AS, Samwick AA, Morrison H, Cohen L. Studies on immunization in man. I. The blood group substances A and B. *Exp Med Surg.* 1953;11(4):267–275.
24. Boorman KE, Dodd BE, Mollison PL. Iso-immunisation to the blood group factors A, B and Rh. *J Path Bacteriol.* 1945;57(2):157–169.
25. Thalheimer W. Hemoglobinuria after a second transfusion with the same donor. *JAMA*. 1921;76(20):1345–1347.
26. Wiener AS. Subdivisions of group A and group AB. *J Immunol.* 1941;41(2):181–199.
27. Chaplin H Jr. Studies on the survival of incompatible cells in patients with hypogammaglobulinemia. *Blood.* 1959;14(1):24–36.
28. Daniel-Johnson J, Leitman S, Klein H, et al. Probiotic-associated high-titer anti-B in a group A platelet donor as a cause of severe hemolytic transfusion reactions. *Transfusion.* 2009;49(9):1845–1849.
29. Gupte SC, Bhatia HM. Increased incidence of haemolytic disease of the new-born caused by ABO-incompatibility when tetanus toxoid is given during pregnancy. *Vox Sang.* 1980;38(1):22–28.
30. Grove-Rasmussen M, Shaw RS, Marceau E. Hemolytic transfusion reaction in group-A patient receiving group-O blood containing immune anti-A antibodies in high titer. *Am J Clin Pathol.* 1953;23(8):828–832.
31. Dausset J, Vidal G. Accidents of transfusion in recipients of group A having received group O blood; role of vaccination with diphtheria and tetanus anatoxin. *Sang.* 1951;22(6):478–489.
32. Redman M, Malde R, Contreras M. Comparison of IgM and IgG anti-A and anti-B levels in Asian, Caucasian and Negro donors in the North West Thames Region. *Vox Sang.* 1990;59(2):89–91.
33. Worlledge S, Ogiemudia SE, Thomas CO, Ikoku BN, Luzzatto L. Blood group antigens and antibodies in Nigeria. *Ann Trop Med Parasitol.* 1974;68(3):249–264.
34. Grundbacher FJ. Genetics of anti-A and anti-B levels. *Transfusion.* 1976;16(1):48–55.
35. Miqdad AM, Abdelbasit OB, Shaheed MM, Seidahmed MZ, Abomelha AM, Arcala OP. Intravenous immunoglobulin G (IVIG) therapy for significant hyperbilirubinemia in ABO hemolytic disease of the newborn. *J Matern Fetal Neonatal Med.* 2004;16(3):163–166.
36. Greenough A. The role of immunoglobulins in neonatal Rhesus haemolytic disease. *BioDrugs.* 2001;15(8):533–541.
37. Li P, Pang LH, Liang HF, Chen HY, Fan XJ. Maternal IgG anti-A and anti-B titer levels screening in predicting ABO hemolytic disease of the newborn: a meta-analysis. *Fetal Pediatr Pathol.* 2015;34(6):341–350.
38. Bakkeheim E, Bergerud U, Schmidt-Melbye AC, et al. Maternal IgG anti-A and anti-B titres predict outcome in ABO-incompatibility in the neonate. *Acta Paediatr.* 2009;98(12):1896–1901.
39. Kaplan M, Hammerman C, Vreman HJ, Wong RJ, Stevenson DK. Hemolysis and hyperbilirubinemia in antiglobulin positive, direct ABO blood group heterospecific neonates. *J Pediatr.* 2010;157(5):772–777.
40. Matteocci A, De Rosa A, Buffone E, Pierelli L. Retrospective analysis of HDFN due to ABO incompatibility in a single institution over 6 years. *Transfus Med.* 2019;29(3):197–201.
41. Karafin MS, Glisch C, Souers RJ, et al.; College of American Pathologists Transfusion, Apheresis, and Cellular Therapy Committee. Use of fetal hemoglobin quantitation for Rh-positive pregnant females: a national survey and review of the literature. *Arch Pathol Lab Med.* 2019;143(12):1539–1544.

CASE STUDY

First Case of Bloodstream Infection Caused by *Ruminococcus gnavus* in an 85 Year Old Man in China

Xin Fan, MD[1] *Yejin Chen, MD,*[2] *Yanqing Liu, MD,*[3] *Liqing Hu, MD*[3,*]

[1]Department of Dermatology, Ningbo First Hospital, Ningbo, Zhejiang, China; [2]Department of Clinical Laboratory, No. 9 Hospital of Ningbo, Zhejiang, China; [3]Department of Clinical Laboratory, Ningbo First Hospital, Ningbo, Zhejiang, China; *To whom correspondence should be addressed. 13605887858@163.com

Keywords: *Ruminococcus gnavus*, anaerobe, bloodstream infection, target DNA sequencing, meropenem, ceftriaxone

Abbreviations: R. gnavus, *Ruminococcus gnavus*; T2DM, type 2 diabetes mellitus; WBC, white blood cells; CRP, C-reactive protein; PCT, procalcitonin; MIC, minimum inhibitory concentration; MALDI-TOF MS, matrix-assisted laser desorption ionization–time-of-flight mass spectrometry.

Laboratory Medicine 2022;53:e36–e39; https://doi.org/10.1093/labmed/lmab070

ABSTRACT

Ruminococcus gnavus (*R. gnavus*) is a gram positive anaerobe and a member of the normal intestinal flora of humans. Here, we present a case study of bloodstream infection caused by *R. gnavus* in an 85 year old man. We identified *R. gnavus* using target DNA sequencing. The patient was treated with intravenous meropenem and ceftriaxone based on antimicrobial susceptibility tests. He recovered well and was discharged.

Ruminococcus gnavus (*R. gnavus*) is an anaerobic, gram positive diplococcus found in the human gut microbiome.[1] A member of the Firmicutes division, *R. gnavus* is an early colonizer of the human gut and has been detected in more than 90% of human fecal specimens by metagenomic sequencing.[1,2] Several studies have indicated that an increased relative abundance of *R. gnavus* is linked to inflammatory bowel diseases, such as Crohn disease.[3,4] Recently, Henke et al[5] found that *R. gnavus* synthesizes and secretes a complex glucorhamnan polysaccharide, which induces the secretion of inflammatory cytokines (tumor necrosis factor-α) by dendritic cells and is dependent on Toll-like receptor 4. Previously, colonized sites of *R. gnavus* were also reported in the blood, urogenital tract, genital tract, and joint fluid.[6-9] Here, we report a case study of bloodstream infection caused by *R. gnavus* in an older adult male patient without an underlying gastrointestinal disease.

Case Study Presentation

An 85 year old male patient was referred to our hospital with fever. He had a history of hypertension for 20 years and type 2 diabetes mellitus (T2DM) for 16 years. One year earlier, he was treated for tuberculosis of the lumbar spine at the local hospital, but the specific course of treatment was unknown. The patient had no history of coronary heart disease; hepatitis; malaria; or lung, liver, kidney, brain, or any organ diseases.

On admission, the patient had a temperature of 38.4°C, multiple herpes around the mouth, and chills. He had no chest distress, shortness of breath, palpitations, nausea, vomiting, or abdominal pain. Blood tests revealed an elevated white blood cell (WBC) count of 18.3×10^9/L with 85.7% neutrophils and a decreased lymphocyte count of 1.5×10^9/L. The hemoglobin level was 111 g/L, and the platelet count was 151×10^9/L. The levels of C-reactive protein (CRP) and procalcitonin (PCT) were increased to 111.6 mg/L and 59.162 ng/L, respectively. The levels of alanine aminotransferase (15 U/L), aspartate aminotransferase (22 U/L), and albumin (36 g/L) were normal. He did not have hepatitis virus infections (hepatitis A, B, C, D, and E), HIV, or syphilis. Abdominal ultrasonography showed a slightly coarse gallbladder wall, a strong echo in gallbladder cavity, and a gallbladder length diameter of approximately 10 nm. The patient had gallstones but no cholecystitis. He was diagnosed with infectious fever and gallstones, accompanied by hypertension and T2DM.

Having presented with severe symptoms of infection with an unspecified site of infection, the patient was empirically treated with intravenous piperacillin/tazobactam (4.5 g/quaque die 8 hours). In addition, 2 sets of blood cultures were collected and cultured at 35°C for aerobic and anaerobic cultures (BD BACTEC, Becton Dickinson) before empiric treatment. Two anaerobic bottles tested positive after a 25-hour incubation, and specimens were then transferred to a blood plate and cultured at 35°C for 48 hours under anaerobic conditions. The cultured colonies were gray and small in size (**FIGURE 1A**). Gram stain revealed gram positive diplococci (**FIGURE 1B**). Nevertheless, we failed to identify the unknown pathogen using the French Meriere automatic microbiological analysis system (VITEK2-*Compact*).

The target DNA sequences showed 99.89% homology with sequences of *R. gnavus* isolates (GenBank accession number: NR_036800.1) compared with the NCBI GenBank using the BLAST server. Antimicrobial susceptibility tests in vitro for the clinical isolate were performed using a microbial drug sensitivity analyzer (ATB-EXPRESSION, bioMerieux, Ltd., France). The clinical isolate was susceptible to amoxicillin/clavulanic acid (minimum inhibitory concentration [MIC] ≤1 μg/mL), piperacillin

FIGURE 1. Cultured colonies and cultured microscopic morphology. A. Colony morphology cultured on anaerobic agar at 35°C for 48 hours. B. Gram stain morphology of bacteria under oil objective (×1000).

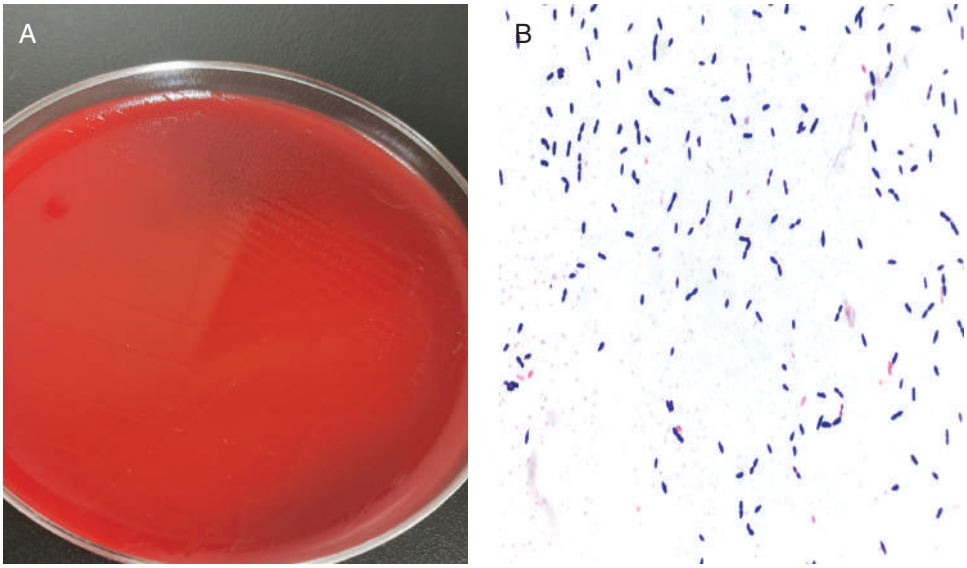

TABLE 1. Results of Laboratory Examination During 11 Days of Disease Course

	December 4	December 5	December 8	December 11	December 14
WBC ($\times 10^9$/L)	18.3	12	4.3	4.3	4.2
Neu ($\times 10^9$/L)	15.7	10.0	2.4	2.1	2.1
CRP (mg/L)	111.6	76.8	6.2	3.2	1.5
PCT (ng/L)	59.162	22.500	4.459	0.708	0.157

CRP, C-reactive protein; Neu, neutrophil; PCT, procalcitonin; WBC, white blood cell.

(MIC ≤32 μg/mL), piperacillin/tazobactam (MIC ≤32 μg/mL), ticarcillin (MIC ≤64 μg/mL), ticarcillin/clavulanic acid (MIC ≤32 μg/mL), cefoxitin (MIC ≤16 μg/mL), cefotetan (MIC ≤16 μg/mL), imipenem (MIC ≤4 μg/mL), meropenem (MIC ≤4 μg/mL), clindamycin (MIC ≤2 μg/mL), chloramphenicol (MIC ≤8 μg/mL), and penicillin (MIC 1 μg/mL, intermediate), and resistance to trimethoprim-sulfamethoxazole, levofloxacin (MIC ≥16 μg/mL), and metronidazole (MIC ≥ 8 μg/mL).

Based on the results of antimicrobial susceptibility tests, the patient was switched to intravenous meropenem (1 g/quaque die 8 hours) and ceftriaxone (1 g/quaque die) for anti-infection treatment, accompanied by symptomatic supportive treatment for hypertension and diabetes mellitus. The WBC, CRP, and PCT levels returned to normal after 11 days of intake of the anti-infection treatment (**TABLE 1**). The patient's condition improved and he was discharged. The patient did not relapse during the subsequent 3-month follow-up.

Discussion

After 2 infections with *R. gnavus* in humans were first reported by Hansen et al in 2013,[10] there have been 11 patients with *R. gnavus* infection reported. Of the 11 patients, 6 had bloodstream infections.[6,10–13] Here, we report the seventh patient with bloodstream infection attributed to *R. gnavus* and the first reported patient in China. **TABLE 2** shows a comparison between our patient and previous patients with bloodstream infection caused by *R. gnavus*. The mean age of the patients with bloodstream infection caused by *R. gnavus* was 77.5 years. Fever and abdominal pain were the most common initial symptoms; however, the patient in the study carried out by Gren et al[13] was asymptomatic. *R. gnavus* was susceptible to most antibiotics, and no natural resistance was observed. The effect of anti-infection treatment was relatively good; however, 2 patients died, which may have been related to their underlying disease, immune function, and timely and accurate diagnosis of the pathogen.

In our patient, *R. gnavus* was isolated from his bloodstream without any injury to the gastrointestinal tract. Our patient was similar to a patient reported by Kim et al[6] who had no gastrointestinal damage and/or tumor. However, *R. gnavus* infection had occurred in these 2 patients likely because of a weakened immune system resulting from old age and long-term underlying diseases. The other previously reported 5 patients with bloodstream infection also presented with an immunocompromised state, indicating that weakened immunity may be a risk factor for bloodstream infection by *R. gnavus*.[10-13]

Several studies have suggested an increased relative abundance of *R. gnavus* and decreased richness of Bacteroides and Faecalibacterium in patients with T2DM.[14,15] The mechanism underlying the increased relative abundance of *R. gnavus* may be involved in the production of an inflammatory polysaccharide with a resultant increase in tumor necrosis factor-α.[5] The intestinal ecology of patients with T2DM has been significantly altered. Similar to findings in most previously reported case studies, our clinical isolate was susceptible to most types of antibiotics. The

TABLE 2. Literature on Patients with Bloodstream Infection Caused by *R. gnavus*

Year	Country	Age (y)	Sex	Comorbidity	Initial Symptoms	Treatments	Outcome	Reference
2020	China	85	Male	Gallstone, hypertension, T2DM	Fever, multiple herpes around the mouth, chills	Piperacillin/tazobactam (4.5 g/q8h), meropenem (1 g/q8h), and ceftriaxone (1 g/qd)	Alive	our case
2019	Denmark	76	Female	MM and MDS	Asymptomatic	Ciprofloxacin (0.5 g/q12h), amoxicillin/clavulanic acid (0.5/q8h, 0.125/q8h), piperacillin/tazobactam (14 g/24 h), vancomycin (1 g), metronidazole (0.5 g/q8h)	Alive	13
2019	Belgium	66	Female	Fecal peritonitis, small bowel herniation and perforation	Abdominal pain, anorexia, vomiting	Levofloxacin (0.5 g/q12h), ornidazole (1 g/qd), meropenem (1 g/q8h)	Alive	11
2018	Spain	77	Male	MM, sigmoid colon cancer, acute respiratory failure, oliguria with acute kidney injury	Bone pain, low-grade fever	Piperacillin/tazobactam (4 g/6 h), levofloxacin (0.5 g/24 h), surgery	Died	12
2017	South Korea	82	Female	T2DM, cholecystitis, CBD stone treated with ERCP and stent	Fever, cough, sputum production, abdominal pain	Piperacillin/tazobactam (4.5 g/q8h)	Alive	6
2013	Denmark	67	Male	Disseminated lung carcinoma	Abdominal pain	Piperacillin/tazobactam (4 g/q8h) and metronidazole (0.5 g/q8h)	Died	10
2013	Denmark	90	Male	Diverticular disease	Abdominal pain, vomiting, and fever	Cefuroxime (1.5 g/q8h) and metronidazole (0.5 g/q8h)	Alive	10

CBD, common bile duct; ERCP, endoscopic retrograde cholangiopancreatography; MDS, myelodysplastic syndrome; MM, multiple myeloma; qd, quaque die; q8h, quaque die 8 hours; q12h, quaque die 12 hours; R. gnavus, Ruminococcus gravus; T2DM, type 2 diabetes mellitus.

patient was treated based on the results of antimicrobial susceptibility tests. Initial empirical anti-infective therapy is insufficient for the treatment of unknown pathogens. If the treatment is not adjusted in time, then it may lead to an imbalance of the flora in the patient, resulting in secondary infections and consequences.

Because traditional culture and automatic microbiological analysis cannot cover all bacteria and fungi, especially several rare pathogens, new technologies such as target DNA sequencing and matrix-assisted laser desorption ionization–time-of-flight mass spectrometry (MALDI-TOF MS) have revolutionized the accuracy and timeliness of the identification of unknown pathogens. Previous studies have indicated that MALDI-TOF MS may be an alternative method for identifying *R. gnavus*[9-13,16] and that it is accurate for direct pathogen identification from positive blood cultures and may reduce the turnaround time to identification.[17] An index score of 2 obtained in the above analysis indicated definite identification of the pathogens.[17] Moreover, target DNA sequencing is recommended because it is very fast and accurate in identifying rare pathogens, although it is considerably more expensive. Our patient was diagnosed promptly and had a better prognosis using this technology.

In conclusion, we report the first patient with a bloodstream infection caused by *R. gnavus* in China. Clinicians should be able to suspect infections with rare pathogens, even in unconventional colonization sites. Clinical laboratories should comprehensively use various methods to help clinicians accurately identify pathogens, especially rare pathogens.

Acknowledgments

This study was supported by the Medical Health Science and Technology Project of Zhejiang Provincial Health Commission (number 2019KY164). XF analyzed the data and wrote the manuscript. YC and YL collected the data. YL and LH carried out the experiment and revised the manuscript. All authors have read and approved the final manuscript.

REFERENCES

1. Kraal L, Abubucker S, Kota K, Fischbach MA, Mitreva M. The prevalence of species and strains in the human microbiome: a resource for experimental efforts. *PLoS One.* 2014;9(5):e97279.
2. Qin J, Li R, Raes J, et al.; MetaHIT Consortium. A human gut microbial gene catalogue established by metagenomic sequencing. *Nature.* 2010;464(7285):59–65.
3. Joossens M, Huys G, Cnockaert M, et al. Dysbiosis of the faecal microbiota in patients with Crohn's disease and their unaffected relatives. *Gut.* 2011;60(5):631–637.
4. Nishino K, Nishida A, Inoue R, et al. Analysis of endoscopic brush samples identified mucosa-associated dysbiosis in inflammatory bowel disease. *J Gastroenterol.* 2018;53(1):95–106.
5. Henke MT, Kenny DJ, Cassilly CD, Vlamakis H, Xavier RJ, Clardy J. Ruminococcus gnavus, a member of the human gut microbiome associated with Crohn's disease, produces an inflammatory polysaccharide. *Proc Natl Acad Sci U S A.* 2019;116(26):12672–12677.
6. Kim YJ, Kang HY, Han Y, Lee MS, Lee HJ. A bloodstream infection by Ruminococcus gnavus in a patient with a gall bladder perforation. *Anaerobe.* 2017;47:129–131.
7. Ceccarani C, Foschi C, Parolin C, et al. Diversity of vaginal microbiome and metabolome during genital infections. *Sci Rep.* 2019;9(1):14095.
8. Veale R, Hughes C, Woolley I. A novel case of bilateral tubo-ovarian abscesses attributed to Ruminococcus gnavus without gastrointestinal involvement. *Anaerobe.* 2021;67:102312.
9. Titécat M, Wallet F, Vieillard MH, Courcol RJ, Loïez C. Ruminococcus gnavus: an unusual pathogen in septic arthritis. *Anaerobe.* 2014;30:159–160.
10. Hansen SG, Skov MN, Justesen US. Two cases of Ruminococcus gnavus bacteremia associated with diverticulitis. *J Clin Microbiol.* 2013;51(4):1334–1336.
11. Lefever S, Van Den Bossche D, Van Moerkercke W, et al. Ruminococcus gnavus bacteremia, an uncommon presentation of a common member of the human gut microbiota: case report and literature review. *Acta Clin Belg.* 2019;74(6):435–438.
12. Fontanals D, Larruzea A, Sanfeliu I. Direct identification of Ruminococcus gnavus by matrix-assisted laser desorption/ionization time-of-flight mass spectrometry (MALDI-TOF MS) on a positive anaerobic blood culture bottle. *Anaerobe.* 2018;54:264–266.

13. Gren C, Spiegelhauer MR, Rotbain EC, Ehmsen BK, Kampmann P, Andersen LP. Ruminococcus gnavus bacteraemia in a patient with multiple haematological malignancies. *Access Microbiol.* 2019;1(8):e000048.
14. Wang Y, Ye X, Ding D, Lu Y. Characteristics of the intestinal flora in patients with peripheral neuropathy associated with type 2 diabetes. *J Int Med Res.* 2020;48(9):300060520936806.
15. Toya T, Ozcan I, Corban MT, et al. Compositional change of gut microbiome and osteocalcin expressing endothelial progenitor cells in patients with coronary artery disease. *PLoS One.* 2021;16(3):e0249187.
16. Fernández-Caso B, Domingo García D, Domingo LC, Ampuero JC. Ruminococcus gnavus infection of a metal-on-metal hip arthroplasty resembling a pseudo-tumour in a 72 year-old woman with no intestinal symptoms. *Enferm Infecc Microbiol Clin.* 2017;35(8):542–543.
17. Lagacé-Wiens PR, Adam HJ, Karlowsky JA, et al. Identification of blood culture isolates directly from positive blood cultures by use of matrix-assisted laser desorption ionization-time of flight mass spectrometry and a commercial extraction system: analysis of performance, cost, and turnaround time. *J Clin Microbiol.* 2012;50(10):3324–3328.

CASE STUDY

Use of Selective Arterial Calcium Stimulation Testing in Identification of Insulinoma in a Patient After Bariatric Surgery

Julianne M. Szczepanski, MD,[1,] Erika Hissong, MD,[1] David M. Manthei, MD, PhD[1]*

[1]Department of Pathology, University of Michigan, Ann Arbor, Michigan, US; *To whom correspondence should be addressed. Email: jmboyle@umich.edu

Keywords: pancreatic dysfunction, beta cell, selective arterial calcium stimulation, insulinoma, hypoglycemia, bariatric surgery, gastric bypass

Abbreviations: SACST, selective, arterial calcium stimulation; NIPHS, noninsulinoma pancreatogenous hypoglycemia syndrome; CT, computed tomography.

Laboratory Medicine 2022;53:e40–e43; https://doi.org/10.1093/labmed/lmab071

ABSTRACT

Objective: Insulinomas are rare in the post-bariatric surgery setting. The differential diagnosis for hypoglycemia is broad, requiring laboratory testing to verify endogenous hyperinsulinemic hypoglycemia. Selective arterial calcium stimulation testing (SACST) can help localize abnormal insulin production. We describe a patient with histologically confirmed insulinoma after bariatric surgery diagnosed with the aid of SACST.

Methods: We present a 67 year old woman with a history of Roux-en-Y bypass surgery who presented with endogenous hyperinsulinemic hypoglycemia. Initially, no pancreatic lesion was identified radiologically. We pursued SACST to localize the source of insulin production.

Results: The SACST successfully localized the source of hyperfunctioning islet cells to the pancreatic tail with absolute insulin values in a range consistent with insulinoma. Additional radiologic studies showed a small tumor in the pancreatic tail. Pathology showed a well-differentiated neuroendocrine tumor, compatible with insulinoma.

Conclusion: This case study illustrates the usefulness of SACST for the diagnosis and localization of insulinoma.

Clinical History

A 67 year old woman with a history of Roux-en-Y bypass surgery approximately 15 years earlier without complications presented with year-long episodes of severe hypoglycemia. She experienced autonomic and neuroglycopenic symptoms, including fatigue, weakness, mental fog, headaches, and diaphoresis; the patient also experienced episodes of confusion and syncope associated with hypoglycemia. Her overall pattern of hypoglycemia was predominantly postprandial, although fasting hypoglycemia was also observed. She ate frequently to prevent these symptoms and experienced an almost 50-pound weight gain over a year. Her glucose levels were monitored with a home blood glucose meter before formal endocrinology evaluation. Her hypoglycemia progressively worsened to daily values as low as 30 to 40 mg/dL. At values less than 30 mg/dL, the patient experienced tremors, headaches, and diaphoresis. She frequently took sugar tablets to increase her glucose with improvement of her symptoms. Based on the above clinical features, the patient met the criteria for Whipple's triad—symptoms of hypoglycemia, verification of low glucose at time of symptoms, and resolution of symptoms with elevation of glucose.

The patient's symptoms worsened to the point that she presented to the emergency department after an episode of unconsciousness that required glucagon injection. Spurred by this deterioration, she underwent multiple studies regarding her hypoglycemia. A 72-hour fast was notable for inappropriately high insulin (8.3 μU/mL) and proinsulin (111 pmol/L) with low blood glucose (29 mg/dL). Factitious causes of hypoglycemia were considered unlikely given a normal C-peptide (1.3 ng/mL) and negative sulfonylurea screen. In addition, insulin antibodies were negative and β-hydroxybutyrate levels were 1.7 mmol/L. In combination, these results highlighted the likelihood of endogenous hyperinsulinemic hypoglycemia and raised a differential diagnosis including insulinoma, noninsulinoma pancreatogenous hypoglycemia syndrome (NIPHS), and post–gastric bypass hypoglycemia.

Although insulinomas are rare in patients with a history of gastric bypass surgery, imaging studies were pursued to rule out this possibility, given her symptoms. Neither magnetic resonance cholangiopancreatography of the pancreas nor magnetic resonance imaging of the abdomen identified a localized process or mass to explain the symptoms. Given the lack of focal findings, increasing consideration was given to diffuse processes.

In an attempt to rule out an insulinoma, the patient underwent selective arterial calcium stimulation testing (SACST). The SACST findings suggested a localization of hyperfunctioning islet cells to the pancreatic tail (**TABLE 1** and **FIGURE 1**). With this additional information, alternative imaging studies were pursued, including computerized tomography (CT) with intravenous contrast, which showed a 0.8 cm nodular focus of hyperenhancement in the proximal pancreatic tail.

Given the SACST and CT results, surgical management was pursued for a suspected insulinoma. Intraoperative findings indicated a 1 cm tumor on the anterior-superior surface of the pancreatic tail. The tumor was enucleated, and intraoperative pathological examination confirmed the presence of a neoplasm.

Histologic sections revealed a well-circumscribed but unencapsulated proliferation of relatively monotonous epithelioid cells growing in trabecular cords and small nests separated by hyalinized stroma containing acellular, pale pink proteinaceous material and scattered microcalcifications. The neoplastic cells were characterized by ample eosinophilic and slightly granular cytoplasm. The nuclei were round and contained stippled chromatin, inconspicuous nucleoli, and frequent pseudonuclear inclusions (**FIGURE 2A** and **2B**). No mitotic figures were identified. Immunohistochemical stains showed diffuse positivity for synaptophysin and insulinoma-associated protein 1 (INSM1) (**FIGURE 2C** and **2D**), supporting neuroendocrine cell origin. In addition, the pink proteinaceous material was positive by Congo Red, confirming the presence of amyloid deposition. The estimated proliferation index based on a manual count of the Ki-67 immunostain was <2%. These findings were consistent with a well-differentiated neuroendocrine tumor, World Health Organization grade 1, and given the patient's clinical symptoms was compatible with an insulinoma. However, because the specimen was an enucleation of the tumor, there was little nonneoplastic pancreatic tissue to evaluate background islet density or features of nesidioblastosis.

Discussion

Evaluation of potential hypoglycemia in a patient with history of bariatric surgery may be more complicated compared to routine evaluations but still includes initial verification that symptoms are truly linked to hypoglycemia. If glucose values are normal at the time of symptoms, then hypoglycemia is unlikely, and dumping syndrome or cardiovascular causes of symptoms should be considered. Once a hypoglycemic disorder has been confirmed, the differential diagnosis may be broad and includes endogenous hyperinsulinemia, cortisol deficiency, drug or alcohol effects, illness, malnourishment, or tumor production of insulin-like growth factor.[1] Investigation of a suspected imbalance of insulin and glucose may use a mixed-meal test or 72-hour fasting study, which can aid in the establishment of endogenous hyperinsulinemia as the cause of hypoglycemia. The etiology of endogenous hyperinsulinemia includes a β-cell tumor (insulinoma), use of a β-cell secretagogue (sufonylurea), insulin autoimmune hypoglycemia, NIPHS, and post–gastric bypass hypoglycemia.[1]

Research has shown that NIPHS is a rare syndrome that shows diffuse histologic features of nesidioblastosis including β-cell hypertrophy, islets with enlarged and hyperchromatic nuclei, and increased islets budding from the periductular epithelium. Patients with NIPHS never have insulinomas but do have postprandial hypoglycemia (2–4 hours after a meal) with virtually no episodes of fasting hypoglycemia.[2] The histologic finding of nesidioblastosis has also been seen in patients with a history of gastric bypass surgery; although it shares similar features with NIPHS, it is considered a separate clinical entity.[3-6] The hypoglycemic pattern in those with the clinical syndrome of post–gastric bypass hypoglycemia is also typically postprandial. However, in contrast to NIPHS, patients with post–gastric bypass hypoglycemia may rarely have fasting hypoglycemia and can also have associated insulinoma, as seen in this patient.[2] Both post–gastric bypass hypoglycemia and NIPHS should have postprandial hyperinsulinemic hypoglycemia, negative radiologic localization, positive (multifocal) SACST, and histologic findings of nesidioblastosis. These pancreatic findings may be diffuse, in contrast to a single insulinoma.

Notably, insulinomas in patients with a history of gastric bypass surgery are rare.[7] Presentations and patterns of hypoglycemia are mixed, including some patients with hypoglycemia that occurs exclusively during fasting periods (56%), some with hypoglycemia that occurs exclusively during postprandial periods (22%), and some with hypoglycemia during both periods (22%).[7] Although these mixed patterns may not provide a specific diagnostic clue, note that the presence of fasting hypoglycemia in a patient after bariatric surgery is atypical. This tendency should raise suspicion for autonomous secretion by an insulinoma or other tumor.

TABLE 1. Hepatic Vein Insulin Levels Measured After Selective Arterial Calcium Stimulation of Indicated Pancreatic Arterial Supplies

	Insulin (μU/mL)				
	0 Sec	30 Sec	60 Sec	90 Sec	120 Sec
Specimen site					
GDA	15.9	22.2	19.7	20.0	21.6
PHA	28.8	21.0	22.1	22.3	21.7
SMA	24.1	18.8	19.6	18.1	18.2
Proximal SA	21.2	35.0	63.0	47.2	63.0
Distal SA	18.1	62.5	96.6	109	97.7

GDA, gastroduodenal artery; PHA, proper hepatic artery; SA, splenic artery; SMA, superior mesenteric artery.

Laboratory Role in Diagnosis

A diagnosis of endogenous hyperinsulinemia is established by showing inappropriately high serum insulin concentrations during a spontaneous or induced episode of hypoglycemia. In hyperinsulinemia, the prolonged fast results in hypoglycemia because of a defect in a patient's ability to maintain normoglycemia secondary to an excess of insulin. This finding is confirmed with measurements of low blood glucose (<55 mg/dL) and inappropriately high insulin (>3 μU/mL) and proinsulin (>5 pmol/L) levels. Insulin also has antiketogenic effects and causes plasma β-hydroxybutyrate values to be lower (<2.7 mmol/L). In patients with exogenous insulin, C-peptide levels will be low (<0.2 nmol/L) and proinsulin will be <5 pmol/L. Insulin antibodies are measured to exclude insulin autoimmune disease, and a sulfonurea screen is performed to exclude factitious disease resulting from oral hypoglycemic agents.[1]

After endogenous hyperinsulinemia is established, noninvasive imaging studies such as abdominal ultrasound and CT with intravenous contrast can identify an insulinoma in many patients. However, a negative imaging study does not exclude insulinoma and additional studies such as endoscopic ultrasonography or SACST may be useful.

FIGURE 1. Insulin values normalized to prestimulation (0 seconds) value for each arterial stimulation. Testing was considered positive at a 2- to 3-fold increase over baseline. GDA, gastroduodenal artery; PHA, proper hepatic artery; SA, splenic artery; SMA, superior mesenteric artery.

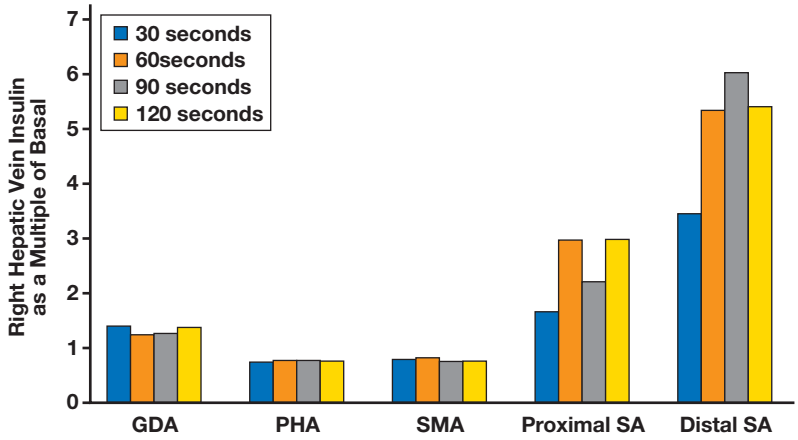

FIGURE 2. Histologic examination of the tumor revealed a monotonous proliferation of epithelioid cells growing in trabecular cords and ill-defined nests separated by hyalinized stroma containing acellular, pale pink proteinaceous material with scattered microcalcifications (A). The tumor cells contained round nuclei with stippled chromatin, inconspicuous nucleoli, and frequent nuclear pseudoinclusions (B). Immunohistochemical stains showed diffuse positivity for synaptophysin (C) and insulinoma-associated protein 1 (INSM1) (D) (hematoxylin-eosin, original magnification × 100 [A] and × 400 [B]; original magnification × 200 [C, D]).

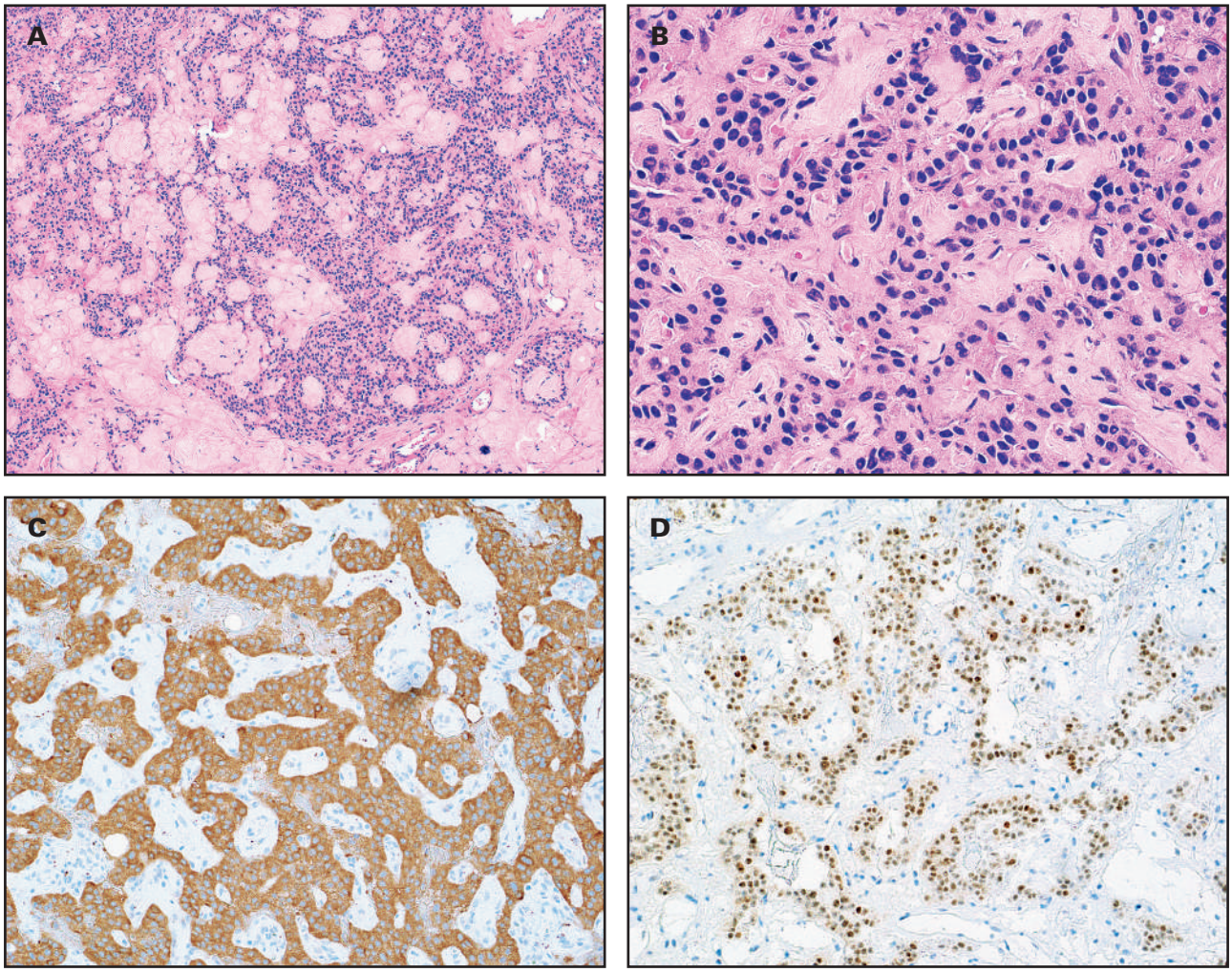

A SACST entails cannulation of the femoral vein and artery with a sampling catheter to the right hepatic vein for measurement of insulin and an injection catheter to introduce a calcium gluconate solution sequentially into different pancreatic arterial supplies.[8,9] Calcium gluconate is an insulin secretagogue and stimulates insulin release from insulinomas or islet hypertrophy, but notably not from normal β cells. An increase in venous insulin over baseline occurs when calcium gluconate is introduced to the arterial supply of the region of hyperfunctioning islets.[10] An increase of at least 2 to 3 times the basal hepatic venous insulin concentration is considered positive.[11] If the result is positive in a single artery or region, then a focal abnormality (insulinoma or focal nesidioblastosis) is likely; if the increase occurs in multiple arteries, then the patient more likely has a diffuse process (NIPHS or post–gastric bypass hypoglycemia), multiple insulinomas, or an insulinoma in a watershed area fed by 2 arteries.[12] In 1 series of 237 patients with an insulinoma, the sensitivity of SACST for the localization of insulinoma was 93%.[13] However, because nesidioblastosis may be concentrated in 1 region of the pancreas or, conversely, multiple insulinomas in a single patient can occur, correlation is still required. The absolute magnitude of insulin measurements may also be informative; higher peak insulin is observed with insulinoma compared to NIPHS or post–gastric bypass hypoglycemia. One report concluded that a maximum hepatic venous insulin concentration cutoff of >91.5 μU/mL was 95% specific for insulinoma.[11]

This current case study illustrates the usefulness of the SACST, with both the presence and localization of the insulinoma correlating to other laboratory and radiologic findings. The location of the tumor correlated with the distal (watershed) positivity of the SACST and the peak insulin concentration was 109 μU/mL, consistent with an insulinoma. Note that insulin levels (in our institution, plasma insulin is measured on a Siemens Immulite 2000 XPi) are susceptible to enzymatic degradation if hemolysis is present and can potentially hinder interpretation if specimens are poorly collected.

As described above, the surgical enucleation specimen revealed a well-differentiated neuroendocrine tumor, World Health Organization grade 1, consistent with an insulinoma. Although not pursued for this patient, in some scenarios a partial pancreatectomy may be considered instead of enucleation in patients with a history of gastric bypass to permit the evaluation of diffuse β-cell hyperplasia or the histologic features of nesidioblastosis.

Patient Follow-Up

The patient experienced overall improvement but not complete resolution of symptoms after tumor enucleation. She gradually developed predominantly postprandial hypoglycemia, with glucose values usually in the range of 60 mg/dL (compared to 40 mg/dL preoperatively), but with some fasting hypoglycemia as well. Proinsulin levels showed partial normalization at 44 pmol/L. Residual insulinoma is a diagnostic possibility, because the tumor was removed via laparoscopic enucleation without margin assessment. In addition, a more diffuse pancreatic dysfunction such as post–gastric bypass hypoglycemia may now be unmasked. The patient is continuing monitoring with a plan for a repeat 72-hour fast and possible second surgery.

As seen in this case study, hypoglycemia evaluation in patients with a history of bariatric surgery may be particularly complex. In conjunction with other testing, SACST is a useful laboratory method to evaluate for insulinoma, and it provides information regarding localization of hyperfunctioning islets; the magnitude of insulin values may augment the distinction between focal and diffuse processes.

REFERENCES

1. Cryer PE, Axelrod L, Grossman AB, et al.; Endocrine Society. Evaluation and management of adult hypoglycemic disorders: an Endocrine Society clinical practice guideline. *J Clin Endocrinol Metab.* 2009;94(3):709–728.
2. Ritz P, Hanaire H. Post-bypass hypoglycaemia: a review of current findings. *Diabetes Metab.* 2011;37(4):274–281.
3. Rumilla KM, Erickson LA, Service FJ, et al. Hyperinsulinemic hypoglycemia with nesidioblastosis: histologic features and growth factor expression. *Mod Pathol.* 2009;22(2):239–245.
4. Patti ME, McMahon G, Mun EC, et al. Severe hypoglycaemia post-gastric bypass requiring partial pancreatectomy: evidence for inappropriate insulin secretion and pancreatic islet hyperplasia. *Diabetologia.* 2005;48(11):2236–2240.
5. Yaqub A, Smith E, Salehi M. Hyperinsulinemic hypoglycemia after gastric bypass surgery: what's up and what's down? *Int J Obes (Lond)*. Published online ahead of print October 13, 2017. doi: 10.1038/ijo.2017.257.
6. Clancy TE, Moore FD Jr, Zinner MJ. Post-gastric bypass hyperinsulinism with nesidioblastosis: subtotal or total pancreatectomy may be needed to prevent recurrent hypoglycemia. *J Gastrointest Surg.* 2006;10(8):1116–1119.
7. Mulla CM, Storino A, Yee EU, et al. Insulinoma after bariatric surgery: diagnostic dilemma and therapeutic approaches. *Obes Surg.* 2016;26(4):874–881.
8. Doppman JL, Chang R, Fraker DL, et al. Localization of insulinomas to regions of the pancreas by intra-arterial stimulation with calcium. *Ann Intern Med.* 1995;123(4):269–273.
9. O'Shea D, Rohrer-Theurs AW, Lynn JA, Jackson JE, Bloom SR. Localization of insulinomas by selective intraarterial calcium injection. *J Clin Endocrinol Metab.* 1996;81(4):1623–1627.
10. Thompson SM, Vella A, Service FJ, Grant CS, Thompson GB, Andrews JC. Impact of variant pancreatic arterial anatomy and overlap in regional perfusion on the interpretation of selective arterial calcium stimulation with hepatic venous sampling for preoperative localization of occult insulinoma. *Surgery.* 2015;158(1):162–172.
11. Thompson SM, Vella A, Thompson GB, et al. Selective arterial calcium stimulation with hepatic venous sampling differentiates insulinoma from nesidioblastosis. *J Clin Endocrinol Metab.* 2015;100(11):4189–4197.
12. Service FJ, Natt N, Thompson GB, et al. Noninsulinoma pancreatogenous hypoglycemia: a novel syndrome of hyperinsulinemic hypoglycemia in adults independent of mutations in Kir6.2 and SUR1 genes. *J Clin Endocrinol Metab.* 1999;84(5):1582–1589.
13. Placzkowski KA, Vella A, Thompson GB, et al. Secular trends in the presentation and management of functioning insulinoma at the Mayo Clinic, 1987-2007. *J Clin Endocrinol Metab.* 2009;94(4):1069–1073.

CASE STUDY

HbA1c Below the Reportable Range

Vivek Pant, MD

Department of Clinical Biochemistry, Samyak Diagnostic Pvt Ltd., Jawalakhel, Kathmandu, Nepal; *To whom correspondence should be addressed. drvpant@gmail.com

Keywords: false low HbA1c, high-performance liquid chromatography, cold agglutinin, complete blood count, fructosamine, systemic lupus erythematosus

Abbreviations: HbA1c, glycosylated hemoglobin; RBC, red blood cell; CBC, complete blood count; PBS, peripheral blood smear; MCHC, mean corpuscular hemoglobin concentration; MCV, mean corpuscular volume; MCH, mean corpuscular hemoglobin; SLE, systemic lupus erythematosus; DAT, direct antibody test; HPLC, high-performance liquid chromatography.

Laboratory Medicine 2022;53:e44–e47; https://doi.org/10.1093/labmed/lmab082

ABSTRACT

This case report concerns a 71 year old female patient who had a very low glycosylated hemoglobin (HbA1c) despite having a high level of fasting blood glucose. The patient had a decreased erythrocyte count, elevated red blood cell indices, and a reticulocyte count with no evidence of hemoglobinopathy. She reported receiving hydroxychloroquine treatment for systemic lupus erythematosus. Subsequent laboratory investigations revealed hemolysis with formation of cold agglutinin. Because cold agglutinins can interfere with HbA1c assays, the specimens were reanalyzed after warming. The complete blood count results improved, but the HbA1c result did not change. In patients in whom medications and/or medical conditions may interfere with HbA1c levels, alternative measures of glycemic control, such as fructosamine, could be beneficial.

Glycosylated hemoglobin (HbA1c) is extensively used for the screening, diagnosis, and monitoring of diabetes mellitus. It reflects an individual's glycemic control over the past 8 to 12 weeks and correlates with the development of diabetic complications. The measurement of HbA1c does not require patients to be fasting, and it has high preanalytical stability. In addition, it is more convenient in clinical practice than other measures such as fasting blood glucose or a glucose tolerance test.

Research has shown that HbA1c is formed from the posttranslational addition of glucose to the N-terminal valine of the beta chain of hemoglobin A through an Amadori rearrangement.[1] Application of HbA1c as a glycemic control indicator relies on glycation efficiency, which is determined by the integrity of globin chains and the life span of erythrocytes. Therefore, HbA1c may give false results in certain conditions (**TABLE 1**), thus warranting alternative methods to diagnose and monitor diabetes.

Apart from the hematologic and genetic conditions mentioned in **TABLE 1**, the use of certain drugs affecting the red blood cells (RBCs) may also cause a false HbA1c result (**TABLE 2**). This report highlights the limitations of using HbA1c as a diagnostic tool in a patient with hemolytic anemia further complicated by the formation of cold agglutinin. Furthermore, this report indicates that an HbA1c finding needs to be interpreted in the context of a clinical situation.

Case Presentation

We received a blood specimen from a 71 year old female patient to investigate the HbA1c level and found it to be 3.4% as printed in a chromatogram (**FIGURE 1**). The fasting blood glucose was 5.8 mmol/L

TABLE 1. Conditions in Which HbA1c Is Not A Reliable Indicator of Glycemic Status

Scenario	Conditions	Mechanism
False decrease in HbA1c level	Pregnancy	Increased erythropoietin/ decreased RBC survival[2,3]
	Erythropoietin use	Reticulocytosis[4]
	Hemolytic anemia	Decreased erythrocyte survival[5]
	Chronic kidney disease	Anemia, use of erythropoietin, uremia, and transfusion[6]
	Liver cirrhosis/chronic hepatitis and alcoholic liver disease	Anemia of chronic disease, low albumin, gastrointestinal bleed, and hypersplenism[7]
	Acute/chronic blood loss	Reduction in life span of RBCs
	Hemoglobinopathies	Reduction in life span of RBCs
	Myelodysplastic syndrome	Reduction in life span of RBCs, frequent blood transfusion[8]
False increase in HbA1c level	IDA	Malondialdehyde (increased in IDA) enhances glycation of hemoglobin[9,10]
	Folate/vitamin B_{12} deficiency	Prolonged life span of erythrocytes[11]
	Postsplenectomy	Prolonged life span of erythrocytes[11]
	Chronic alcohol consumption	Formation of HbA1-AcH compound[12]

HbA1-AcH , hemoglobin-acetaldehyde; HbA1c, glycosylated hemoglobin; IDA, iron deficiency anemia; RBCs, red blood cells.

TABLE 2. Drugs Affecting RBCs Where HbA1c Is Not A Reliable Indicator of Glycemic Status

Scenario	Name of Drugs	Mechanism
False decrease in HbA1c level	Dapsone	Oxidation of hemoglobin to methemoglobin, reduced erythrocyte survival, and increased erythrocyte destruction[13]
	Ribavirin/interferon-α	Shortened survival of erythrocytes[14,15]
	Nucleoside analogue antiretroviral agents	Subclinical hemolysis[16]
	High dose of vitamins C and E	Competitive inhibition of glycosylation[17]
	Hydroxyurea	Shift in hemoglobin pattern from HbA to HbF[18]

HbA, hemoglobin A; HbA1c, glycosylated hemoglobin; HbF, hemoglobin F; RBCs, red blood cells.

FIGURE 1. HPLC chromatogram. HPLC, high-performance liquid chromatography.

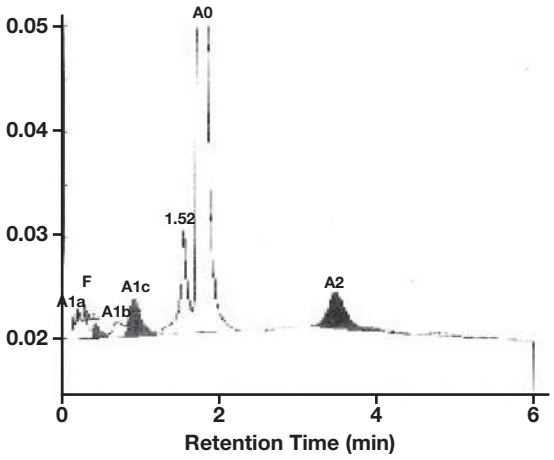

Peak	R. Time	Height	Area	Area %
Unknown	0.14	2,791	6,238	0.3
A1a	0.20	2,920	11,413	0.6
A1b	0.28	3,277	10,705	0.6
F	0.42	1,327	8,767	<0.8*
LA1c/CHb-1	0.69	1,403	12,261	0.6
A1c	0.90	3,492	34,843	3.4*
P3	1.52	10,027	66,178	3.4
A0	1.70	392,579	1,730,745	89.5
A2	3.45	3,371	56,265	3.2
Total Area		1,937,415		

Concentration	%
F	<0.8*
A1c	3.4+
A2	3.2

(3.89–5.55 mmol/L). The blood specimen was analyzed in a Bio-Rad D-10 variant II Beta Thalassemia Short Program mode for the percentage determination of hemoglobin A2, F, and A1c and for the detection of any abnormal hemoglobin. Hemoglobinopathy was not detected. The specimen was also investigated using alternative methods for HbA1c analysis. The result was 3.1% and 3.3% using nephelometry (MISPA i3, Agappe Diagnostic, Switzerland) and the boronate affinity chromatography method, respectively (NycoCard HbA1c test, Axis-Shield, Oslo, Norway).

Because the patient's HbA1c was very low and was discordant with the plasma blood glucose in 3 different assay platforms, a reason for the false low HbA1c was investigated. The complete blood count (CBC) test and examination of the peripheral blood smear (PBS) was done as per the established laboratory protocol. The patient had decreased hemoglobin, a reduced RBC count, and an increased mean corpuscular hemoglobin concentration (MCHC), mean corpuscular volume (MCV), and mean corpuscular hemoglobin (MCH) (**TABLE 3**). A PBS examination revealed clusters of RBCs. The presence of cold agglutinin was suspected and the tube was incubated at 37°C for 30 minutes. The MCHC and MCH results after incubation were corrected, but the RBC and MCV results were only slightly corrected (**TABLE 3**). The repeat PBS examination after incubation revealed ansiopoikilocytosis and mild hypochromia along with few macrocytes and microspherocytes. Considering the possibility of hemolysis, a detailed patient history was taken.

The patient was diagnosed with systemic lupus erythematosus (SLE). She received hydroxychloroquine and steroid treatment. She also had a hemolytic picture in the PBS; therefore, the other markers of hemolysis were assessed. High levels of lactate dehydrogenase, reticulocyte count, and total and indirect bilirubin along with a positive direct antiglobulin test (DAT) confirmed the presence of hemolysis (**TABLE 3**). Her renal function test, glucose-6-phosphate dehydrogenase activity, and thyroid

TABLE 3. Laboratory Results

Parameters	Result		Reference Interval/ Unit
	Before Incubation	After Incubation	
Hemoglobin	8	8.4	13.5–16.9 g, %
RBC count	190	220	440–560 G/L
MCV	115.5	110.9	81.8–95.5 fL
MCH	43.3	37.6	27–32.3 pg
MCHC	37.5	33.9	32.4–35 g/dL
Platelet count	161	161	150–450 G/L
Reticulocyte count	…	4.8	Up to 2%
PCV	22.4	25.4	42%–52%
ESR	6		0–22 mm/h
Total bilirubin	39.33		5.13–32.49 μmol/L
Direct bilirubin	4.68		0.0–5.13 μmol/L
AST	25		17–59 U/L
ALT	32		10–45 U/L
ALP	348		98–279 U/L
LDH	393		100–210 U/L
FBG	5.8		3.89–5.55 mmol/L
Fructosamine	311		205–285 μmol/L
Vitamin B_{12}	301.2		138.01–614.75 pmol/L
Vitamin D	56.41		74.88–249.6 nmol/L
Iron	16.3		13–31 μmol/L
Ferritin	269.2		21.81–274.66 μg/L
Serum folate	22.66		6.25–45.32 nmol/L

ALP, alkaline phosphatase; ALT, alanine transaminase; AST, aspartate transaminase; BG, fasting blood glucose; ESR, erythrocyte sedimentation rate; LDH, lactate dehydrogenase; MCH, mean corpuscular hemoglobin; MCHC, mean corpuscular hemoglobin concentration; MCV, mean corpuscular volume; PCV, packed cell volume; RBC, red blood cell.

function test were normal. The patient's family history did not include hematologic disorders.

Studies have shown that HbA1c monitoring in patients with hemolytic anemia may be unreliable. Therefore, other markers such as plasma glucose and the fructosamine level should be used as an alternative measure in such patients. The serum fructosamine level was found to be higher in our patient (**TABLE 3**). Interpretive comments about the unreliability of HbA1c for monitoring glycemic status and advice on testing for plasma glucose or the serum fructosamine level were added in the report for this patient.

Discussion

Patients with undetectable HbA1c are rarely reported. Patients with hemoglobinopathy, shortened erythrocyte life span, and rapid RBC turnover may have a low HbA1c level because of an inefficient and lowered degree of glycation. However, this lower HbA1c does not indicate good glycemic control.

In hemoglobinopathy, the hemoglobin variants and increased fetal hemoglobin concentration affect the quantification of HbA1c according to high-performance liquid chromatography (HPLC). The separation of hemoglobin fragments in HPLC is based on molecular charge; thus, a hemoglobin variant molecule can migrate with HbA1c and create a false reading, making an estimation of the fraction of HbA1c unreliable. In addition, some forms of hemoglobinopathy make RBCs more susceptible to hemolysis, which decreases their life span. Consequently, the time available for the glycosylation of hemoglobin chains is decreased. Thus, hemoglobinopathies should be ruled out in patients with a very low HbA1c. Hemoglobinopathy in our patient was ruled out by analyzing the blood specimen in a Bio-Rad D-10 variant II Beta Thalassemia Short Program mode.

There are several case reports of falsely low HbA1c levels in patients with hemolytic anemia.[19,20] Cold agglutinin as a cause of false low HbA1c in hemolytic anemia is rarely reported.[21]

The CBC test using automated hematology analyzers may show a low RBC count but high RBC indices if the specimen contains cold agglutinins. When the tube was incubated at 37°C for 30 minutes, the CBC results seemed to be corrected (**TABLE 3**). However, HbA1c was undetectable even after the specimen was warmed. Note that our patient had SLE and was receiving hydroxychloroquine treatment; the formation of cold agglutinins in individuals with autoimmune disorders such as SLE and rheumatoid arthritis has been observed.[22,23] Cold agglutinin-induced hemolytic anemia as a primary presentation in SLE has also been reported.[24]

These cold agglutinins form secondary to the underlying disease, such as SLE-caused RBC agglutination and extravascular hemolysis, the pathophysiology of which is based on the molecular mimicry of foreign antigens. Cold agglutinin activates the classical complement pathway, leading to complement component (C3b) deposition on the surface of RBCs, which are later phagocytosed. Autoimmune hemolytic anemia may occur in 10% of patients with SLE.[25] However, cold antibody–mediated hemolytic anemia is rare in SLE.[26,27] Our patient had features of hemolytic anemia, such as high lactate dehydrogenase, reticulocytosis, a positive DAT, and unconjugated hyperbilirubinemia. Thus, we attributed the hemolysis secondary to cold agglutinin syndrome resulting from SLE to a false low HbA1c in this patient.

In hemolysis, hemoglobin exposed to glycation has a lower percentage and causes a false decrease in test results regardless of the method. Our patient had similar results in her HbA1c when it was analyzed using the ion exchange-HPLC, nephelometry, and boronate affinity chromatography platforms. All these methods are National Glycohemoglobin Standardization Program–certified methods traceable to the Diabetes Control and Complications Trial reference method.

Fructosamine refers to proteins that are nonenzymatically glycated via ketoamine linkages at the N-amino terminal. Albumin is a major plasma protein; therefore, fructosamine primarily reflects glycated albumin. In addition, fructosamine indicates recent glycemic status because the half-life of albumin is 2 to 3 weeks. The index patient had a higher fructosamine level (**TABLE 3**).

Hemolytic disorders should be considered when evaluating an incompatible HbA1c result. Clinicians need to be aware of the limitations of HbA1c testing. Relying heavily on the results of HbA1c testing without cautious interpretation in light of the relevant clinical context may cause over- or undertreatment of diabetes. It is advisable to evaluate all laboratory findings and communicate with laboratory personnel when an HbA1c result is found to be misleading.

Conclusion

Levels of HbA1c below the lower limit of the reference range should accompany interpretive comments that such a measurement could result from the breakdown of erythrocytes or the presence of abnormal hemoglobin.

Acknowledgments

Written consent was obtained from the patient for the publication of this case report.

REFERENCES

1. Dybkær R. Recommendation for term and measurement unit for "HbA1c." *Clin Chem Lab Med.* 2007;45(8):1081–1082.
2. Lurie S, Mamet Y. Red blood cell survival and kinetics during pregnancy. *Eur J Obstet Gynecol Reprod Biol.* 2000;93(2):185–192.
3. Lind T, Cheyne GA. Effect of normal pregnancy upon the glycosylated haemoglobins. *Br J Obstet Gynaecol.* 1979;86(3):210–213.
4. Nakao T, Matsumoto H, Okada T, et al. Influence of erythropoietin treatment on hemoglobin A1c levels in patients with chronic renal failure on hemodialysis. *Intern Med.* 1998;37(10):826–830.
5. Herranz L, Grande C, Janez M, Pallardo F. Red blood cell autoantibodies with a shortened erythrocyte life span as a cause of lack of relation between glycosylated hemoglobin and mean blood glucose levels in a woman with type 1 diabetes. *Diabetes Care.* 1999;22(12):2085–2086.
6. Speeckaert M, Van Biesen W, Delanghe J, et al; European Renal Best Practice Guideline Development Group on Diabetes in Advanced CKD. Are there better alternatives than haemoglobin A1c to estimate glycaemic control in the chronic kidney disease population? *Nephrol Dial Transplant.* 2014;29(12):2167–2177.
7. Clarke M, Benmoussa J, Penmetsa A, Otterbeck P, Ebrahimi F, Nfonoyim J. Inaccuracies of hemoglobin A1c in liver cirrhosis: a case report. *J Endocr Metab.* 2016;6(1):30–32.
8. Okawa T, Tsunekawa S, Seino Y, Hamada Y, Oiso Y. Deceptive HbA1c in a patient with pure red cell aplasia. *Lancet.* 2013;382(9889):366.

9. Selvaraj N, Bobby Z, Sathiyapriya V. Effect of lipid peroxides and antioxidants on glycation of hemoglobin: an in vitro study on human erythrocytes. *Clin Chim Acta.* 2006;366(1–2):190–195.
10. Hardikar PS, Joshi SM, Bhat DS, et al. Spuriously high prevalence of prediabetes diagnosed by HbA(1c) in young Indians partly explained by hematological factors and iron deficiency anemia. *Diabetes Care.* 2012;35(4):797–802.
11. Gallagher EJ, Le Roith D, Bloomgarden Z. Review of hemoglobin A(1c) in the management of diabetes. *J Diabetes.* 2009;1(1):9–17.
12. Hoberman HD, Chiodo SM. Elevation of the hemoglobin Al fraction in alcoholism. *Alcoholism: Clin Exp Res.* 1982;6(2):260–266.
13. Aljenaee K, Hakami O, Davenport C, et al. Spurious HbA1c results in patients with diabetes treated with dapsone. *Endocrinol Diab Metab Case Rep.* 2019;2019:19–0027.
14. Robertson M. Artificially low HbA1c associated with treatment with ribavirin. *BMJ.* 2008;336(7642):505.
15. Virtue MA, Furne JK, Ho SB, Levitt MD. Use of alveolar carbon monoxide to measure the effect of ribavirin on red blood cell survival. *Am J Hematol.* 2004;76(2):107–113.
16. Diop ME, Bastard JP, Meunier N, et al. Inappropriately low glycated hemoglobin values and hemolysis in HIV-infected patients. *AIDS Res Hum Retroviruses.* 2006;22(12):1242–1247.
17. Davie SJ, Gould BJ, Yudkin JS. Effect of vitamin C on glycosylation of proteins. *Diabetes.* 1992;41(2):167–173.
18. Karsegard J, Wicky J, Mensi N, Caulfield A, Philippe J. Spurious glycohemoglobin values associated with hydroxyurea treatment. *Diabetes Care.* 1997;20(7):1211–1212.
19. Lum G. Artefactually low hemoglobin A1c in a patient with hemolytic anemia. *Lab Med.* 2010;41(5):267–270.
20. Aggarwal N, Rai AK, Kupfer Y, Tessler S. Immeasurable glycosylated haemoglobin: a marker for severe haemolysis. *Case Rep.* 2013;2013:bcr2013200307.
21. Yasar NE, Ozgenc A, Bolayirli IM, Adiguzel M, Konukoglu D. Unexpected laboratory results in cold agglutinin disease. *Int J Med Biochem.* 2018;1(1):40–43.
22. Oshima M, Maeda H, Morimoto K, Doi M, Kuwabara M. Low-titer cold agglutinin disease with systemic sclerosis. *Intern Med.* 2004;43(2):139–142.
23. Honne K, Nagashima T, Iwamoto M, Kamesaki T, Minota S. Glucocorticoid-responsive cold agglutinin disease in a patient with rheumatoid arthritis. *Case Rep Rheumatol.* 2015;2015:823563.
24. Mohanty B, Ansari MZ, Kumari P, Sunder A. Cold agglutinin-induced hemolytic anemia as the primary presentation in SLE—a case report. *J Family Med Prim Care.* 2019;8(5):1807–1808.
25. Keeling DM, Isenberg DA. Haematological manifestations of systemic lupus erythematosus. *Blood Rev.* 1993;7(4):199–207.
26. Chaubey VK, Chhabra L. Cold agglutinin-induced haemolysis in association with antinuclear antibody-negative SLE. *Case Rep.* 2013;2013:bcr2013009337.
27. Srinivasan N, Oswal A, Garg S, Nahar J, Gosmonova A, Nahar R. Cold agglutinin induced hemolysis in a newly diagnosed systemic lupus erythematosus. *Am J Med Sci.* 2010;339(3):270–273.

CORRECTION

Due to a production error, an outdated list of the board of editors was placed in the January 2022 issue of Laboratory Medicine. The current board of editors appears in the March 2022 issue and can also be accessed online at https://academic.oup.com/labmed/pages/Editorial_Board. We regret the error.